WARWICK
THE UNIVERSITY OF WARWICK

A Thesis Submitted for the Degree of PhD at the University of Warwick

Permanent WRAP URL:
http://wrap.warwick.ac.uk/140316

Copyright and reuse:
This thesis is made available online and is protected by original copyright.
Please scroll down to view the document itself.
Please refer to the repository record for this item for information to help you to cite it.
Our policy information is available from the repository home page.

For more information, please contact the WRAP Team at: wrap@warwick.ac.uk

warwick.ac.uk/lib-publications

NUCLEAR MAGNETIC RESONANCE

IN

METALS AND ALLOYS

BY

Graham Tranfield B.Sc.

A thesis submitted for the degree of

Doctor of Philosophy of the

University of Warwick

Department of Physics,

University of Warwick.

October 1975.

Acknowledgements

I am indebted to Dr. G. A. Styles for the help and advice which he has given me throughout this work, and during the preparation of this thesis. I would like to thank Prof. E.F.W. Seymour and Dr.R.Dupree who gave me useful advice about NMR and many theoretical aspects of liquid metals; and Robert Pettifer who, amongst other things, allowed me to use his computer graph plotting procedure. Furthermore, I would like to thank Prof. A. J. Forty for allowing me to use the facilities of the Physics Department. Finally, I would like to thank those who helped me prepare this manuscript; Julie Smith, Vicki Ryder, Roy McLeod, and my wife.

Declaration

This Thesis is submitted to the University of Warwick in support of my application for admission to the degree of Doctor of Philosophy. It contains an account of my own work performed at the Department of Physics of the University of Warwick in the period October 1971 to 1975 under the supervision of Dr. G. A. Styles. No part of it has been used previously in a degree thesis submitted to this, or any other University. The work described in this thesis is the result of my own independent research, except where specifically acknowledged in the text. An account of the work on the Knight Shift of barium has been published in Phys. Letts., 48 A, 471, (1971). It is anticipated that the results of the measurements on cadmium alloys and thallium, and the results of the alloy calculations of Chapter 5 will be published presently.

G. Tranfield

September, 1975.

Abstract

This thesis reports experimental and theoretical work on the NMR Knight shift in simple liquid metals.

Measurements have been made of the ^{113}Cd Knight shift in a series of binary alloys involving zinc, indium, tin, mercury, lead, thallium, bismuth, copper, silver and antimony. Generally there is a small variation of the Knight shift with concentration, as with other simple liquid metals.

The main theoretical work has been the development of a formalism for evaluating the Knight shift to include nonlocal pseudopotentials. Calculations have been performed for all simple metals and many binary alloys, using this formalism. The pure metal results generally show agreement with experiment to within 20%, which is a great improvement on other calculations of this type which have used local potentials. Elements in the 5th row of the periodic table are exceptions, where it is necessary to make significant relativistic corrections to core electron wave function. There is a similar agreement between theory and experiment for alloy, however, in the majority of alloy systems studied there are very small changes of Knight shift, and this method is insufficiently sensitive to predict these small variations. In the alkali metal alloys, the Knight shift changes quite significantly with concentration, and the general pattern of these large changes is predicted.

The Knight shifts of both elements in Hg-In alloys have been measured as a function of temperature, and pseudopotential calculations have also been performed for this system. A significant improvement is found from the use of a pseudopotential which takes account of the influence of the mercury 5d core level.

The Knight shift of barium has been measured at temperatures between 4.2. and 750K. The unusually large, nonlinear variation is thought to be due to the influence of an unfilled d-core level, and the very small Knight shift of this metal is predicted by calculations which include s-d hybridisation.

Finally, the Knight shift of thallium has been measured as a function of temperature. This completes previous measurements which ignored the α to β phase change in the solid.

CONTENTS

CHAPTER 1

Introduction

1.1. Liquid Metals

The properties of liquid metals have been examined extensively over the last 20 years. They have been the subject of several review articles (e.g. 1,2,3), the topic of two international conferences (4,5) and have recently been surveyed in detail in the book 'The Theory of Liquid Metals' by T.E.Faber (6). Only a brief review is therefore given here.

The study is devided broadly into two fields; the study of the electronic behaviour, with which this thesis will be principally concerned, and the study of the ionic arrangements. The latter has been mainly studied by X-ray and neutron scattering experiments, and most simple* metals have been studied by one or other of these techniques. This has been supplemented by extensive surveys of compressibility, viscosity, density and various thermodynamic properties. In general the results are consistent with a model of rapidly moving, randomly arranged ions packed closely together. The X-ray and neutron structure factors have been quite successfully predicted by the hard sphere model, where the ions are assumed to interact only on collision. However there are significant discrepancies and a lot of theoretical work has concentrated on evaluating a more realistic pair potential. The ionic interactions are, of course, largely via the conduction electrons, so that a proper understanding of the electronic behaviour is required for this work.

* Transition metals are to be considered beyond the scope of this work and all subsequent reference to metals refer to simple metals.

Conversely, the ionic positions clearly effect the electronic behaviour. However, there has been some success for the Free Electron theory in predicting the electronic properties. Here the conduction electrons are assumed to be entirely free except that they are constrained to lie within the metal. As a result, they form a degenerate Fermi gas with a spherical Fermi surface and a parabolic density of states curve, and the individual electron wave functions are plane waves. The Hall coefficient and Optical constants of all pure liquid metals can be explained by this model although it is clear that such a model would suggest an infinite conductivity.

This theory has therefore been modified to the Nearly Free Electron (NFE) theory, where it is assumed that the ions possess very weak potentials that scatter the electrons and therefore provide a limit to the conductivity, but do not significantly modify the electron wave functions or the density of states curve. In order to get quantitative agreement with experimental conductivities it is of course necessary to evaluate the ion potential, and the most recent calculations (13) obtain agreement to within 20% for most metals. Agreement between calculated and experimental thermopower is less good, although for both of these properties the discrepancies appear to be due to uncertainties in the input parameters or approximations in the calculations, rather than a fundamental error in the NFE theory.

However, the calculations of Hall effect, optical properties, resistivity and thermopower are very insensitive to the details of the electron wave functions or density of states curve, and therefore do not provide a rigorous test of the assumption of this theory. In solid metals the de Haas-van Alphen effect provides valuable information related to these quantities, but these experiments require very long mean free paths which are not available in liquids.

One property that is directly proportional to the Fermi surface

density of states is the conduction electron spin susceptibility, χ_s. In principle this can be measured by conduction electron spin resonance, CESR, however the experiment requires the accurate measurement of the area under a Lorentzian curve, and can only be performed when the CESR signal is very strong. As a result, χ_s has only been found for sodium and lithium in this way. Unfortunately these are the metals where it is hardest to calculate the exchange enhancement to χ_s, and it has not been possible to extract reliable values for the Fermi surface density of states from these results, although they are not inconsistent with the NFE theory.

Dupree and Seymour (48) have suggested a method for evaluating χ_s by subtracting the calculated values of the ionic and orbital contributions from the total measured susceptibility. For divalent and polyvalent metals they find that these values of χ_s are generally in agreement with the values calculated from the NFE theory using an appropriate exchange enhancement factor. In view of the differences between these methods, this is strong evidence that at least the Fermi surface density of states is near the NFE value for these metals. The results for the alkali metals, obtained by these two methods do not agree very well, however, this is almost certainly due to the difficulties in calculating the exchange enhancement and certain other contributions to the total susceptibility, since the scattering in these metals is known to be weaker than in the divalent and polyvalent metals. Consequently one would expect the density of states in the alkali metal to lie closer to the NFE values than for other metals.

The NMR Knight shift also provides evidence that the density of state at the Fermi surface is generally near the NFE value. This quantity is directly proportional to χ_s (see Sec.1.2.2.), and for metals where the Fermi surface density of states is near the NFE value in the

solid, there is little change of this quantity on melting. In other metals, eg. cadmium and bismuth, the change of Knight shift is consistent with a return of the density of states to the NFE value. The Knight shift varies monotonically and slowly with temperature in the liquid which also suggests that the density of states is NFE like. Otherwise, any dips would be reflected by noticable changes of Knight shift with temperature as the Fermi surface passed through these regions. However the Knight shift is also proportional to the electron contact density at the nuclear site and it has not so far been possible to evaluate this sufficiently accurately to obtain χ_s from measured Knight shifts.

Measurement of the angular distribution of photons given off as a result of positron annihilation in the liquid metal, in principle, provides a method of measuring the momentum distribution of the conduction electrons, which would be a very good test of the free electron theory. However, only very few experiments have been performed and it has not been possible to interpret the data reliably, largely because of the difficulty of evaluating the positron wave function in the metal. It is also not certain how the existence of the positron in the metal effects its local environment. Measurement of the Compton profile should give similar information without these complications, but the experimental techniques that have been used so far are insufficiently accurate, although recent improvements(46) may mean that this technique will provide useful information in the future.

A similar situation exists in binary alloys. Measurements have been made of a wide range of electrical and structural properties in many alloy systems. In general the results are consistent with the NFE theory, although there are more exceptions than for pure metals.

However, although the NFE theory is very successful in predicting electrical properties of liquid metals, it cannot be regarded as realistic

since it is well known that the ion cores produce a strongly attractive potential which varies rapidly in space. A more sophisticated theory is therefore required and in Sec.1.1.1., it is shown how a more realistic model of the metal can still produce the behaviour of nearly free electrons. The remainder of this section is then concerned with how quantitative results can be obtained from this theory.

1.1.1. The Concept of Neutral Pseudoatoms

This idea is based on four main assumptions. Firstly it is assumed that the behaviour of the conduction electrons can be understood in terms of the behaviour of single electrons moving in a self consistent field due to the ions and all the other electrons. Secondly it is assumed that the ionic cores do not overlap in a liquid metal so that the potential due to the ions is simply a linear combination of the single ion potentials. The conduction electrons spread throughout the metal, but are of course attracted into the ion cores and thus screen the ionic charges. The third assumption is that the density of screening charge, that is the density of conduction electron charge at the ion sites greater than the average throughout the metal, depends only on the nature of the ion and is not affected by the relative positions of the ions. We can thus think of the metal as consisting of a number of "neutral atoms" where one "atom" is an ion core together with the associated screening charge. The potential of such an atom has a very short range, because the screening is very effective and the total potential experienced by a conduction electron will be generally flat, although there will be deep wells at the centre of the ion cores where the conduction electrons will not be able to screen the dense nuclear charge.

We may consider what happens to an electron as it arrives at an ion site. In the flat potential region its wave function will be a plane

wave, initially. On entering the ion core, this will be completely distorted and finally a transmitted wave will leave the core region and interfere with the incoming wave. The nature of this transmitted wave in the flat region can be found using partial wave analysis, in which the effect of the potential is described in terms of the phase shifts of each angular momentum component of the outgoing wave with respect to the incident wave. The deeper the potential the larger the phase shifts.

The final assumption is that, although these phase shifts may be large, they are all close to an integral number of π. Thus the potential of the "atom" has the same effect as any small potential whose phase shifts differ from those of the "atom" by an integral number of π. The smallest of these potentials is called the effective potential or pseudopotential.

There will be great similarities between the properties of the real metal and a material made of neutral pseudoatoms, ie. particles whose potential is the effective potential, since the scattering properties of the two materials are identical. In particular, the wave functions of the electrons outside the ion core regions will be the same for the two materials and as a consequence the electronic transport properties will also be the same.

Since the effective potential is weak it will be seen that the electronic properties will be those of a gas of nearly free electrons. To a first approximation the electron wave functions will be plane waves and the energy given by

$$E = \frac{\hbar^2 k^2}{2m} \quad , \qquad (1.1)$$

where k is the wave vector, m is the electronic mass and $\hbar$, Planck's constant. The density of states curve will be the free electron parabola.

Thus the fact that the electronic properties of a real metal are free electron like can be explained qualitatively. However, this theory is much more powerful. Because the effective potential is weak, the properties of the metal can be evaluated quantitatively using perturbation theory once this potential has been found.

1.1.2. Evaluation of the Effective Potential -

In principle, phase shift of the effective potential could be evaluated by first calculating the phase shifts of the true potential and subtracting the required number of π. However, this requires an accurate knowledge of the true potential which is not generally available and only a few calculations have been performed in this way (8).

A somewhat different approach to evaluating the effective potential is based on the O.P.W. method (9). Here it is argued that, in order to obey the Pauli exclusion principle, the conduction electron wave functions must be orthogonal to the core wave functions. A fairly realistic approximation to the conduction electron wave functions should therefore be plane waves, $e^{i\underline{k}.\underline{r}}$, with a proportion of core wave functions $\Psi_\alpha(r)$ mixed in ie.,

$$\Psi_k^{OPW}(\underline{r}) = e^{i\underline{k}.\underline{r}} + \sum_\alpha b_\alpha(\underline{k})\, \Psi_\alpha(\underline{r}), \qquad (1.2)$$

where the summation runs over all core states of all ions labelled, α, and $b_\alpha(\underline{k})$ chosen so as to make the OPW othogonal to the core states. Between the ionic cores, these functions are plane waves, and are thus consistent with the concepts of the last section. If these functions are substituted into Schrödingers Equation we get

$$(\nabla + U(r))\, \Psi_k^{OPW}(\underline{r}) = E_k\, \Psi_k^{OPW}(\underline{r}) \quad , \qquad (1.3)$$

where U(r) is the true metal potential, and E_k the energy of the electron.

This can be rearranged to give:-

$$(\nabla + V)\, e^{i\underline{k}\cdot\underline{r}} = E_k\, e^{i\underline{k}\cdot\underline{r}} \quad ,$$

where $V = U(r) - U(r)\hat{P} - E\hat{P}$ (1.4)

and $\hat{P} = \sum_{\alpha} b_\alpha(k)\, \Psi_\alpha(r)\, e^{-i\underline{k}\cdot\underline{r}}$.

The terms $-U\hat{P}$ and $-E\hat{P}$ tend to cancel out much of U so equation 1.3. describes essentially free electrons moving in the field of a small potential V, referred to as the pseudopotential. The plane waves will only be eigenfunctions when V=0, but if we write equation 1.3 as

$$(\nabla + V)\, \Phi_k(r) = E\Phi_k(r) \qquad (1.5)$$

the $\Phi_k(r)$, referred to as pseudowaves will be represented by a linear combination of plane waves whose coefficients can hopefully be found by the use of perturbation theory. The scattering matrix elements can also be found using perturbation theory and the true wave function found from the pseudowave function by the relationship

$$\Psi_k(r) = \Phi_k(r) - \sum_{\alpha} b_\alpha(k).\Psi_\alpha(r).\Phi^*_\alpha(r) \quad . \qquad (1.6)$$

However there is still the problem of evaluating the pseudopotential, which requires an accurate knowledge of the core wave functions and several authors have developed models to replace the pseudopotential, which have parameters adjusted to fit some property of the metal. The simplest is the Ashcroft potential (10) where the model potential is taken to be zero within some core radius, R_c, and is replaced by the true, coulombic potential outside this region. He has found that realistic core radii can be found to fit the resistivity data for most liquid metals, and the band gaps in many solid metals can be predicted using these potentials.

In constructing a model of the pseudopotential in this way two very

important aspects of the potential have been ignored. Firstly the pseudopotential, as defined in eq.1.3., is non-local, that is, it is not a simple function of $\underline{r}$. It contains the operator $\hat{P}$ which involves integrals over all space; and secondly it is energy-dependent and thus varies with the energy of the conduction electron considered. A model which takes both of these aspects into account was proposed by Heine and Aberenkov (11). Outside a core radius R_c the potential is again taken to be coulombic, but inside the potential is taken to have a depth A_ℓ which is different for the different angular momentum components of the incident electrons, and furthermore, depends on the energy of the incident electron. The well depths and core radius are chosen by reference to spectroscopic data so that the potential is more fundamental than that of Ashcroft although the method does leave an arbitrariness in the choice of R_c. This model is fairly successful in predicting the electrical properties of many simple metals, but the results do depend on the choice of R_c.

An improvement has consequently been made by Shaw (12) who points out that the smoothest pseudowave function, and therefore the one most rapidly arrived at using perturbation theory, is found if R_c is chosen so that the potential is continuous. This entails using a different R_ℓ for the different angular momentum components and the model is referred to as the Optimised Model Potential (OMP). The screening of this potential has been improved by Appapillai and Williams (13) who have found that the resistivity of most liquid metals can be predicted by to OMP to within 20%. Notable exceptions are cesium, barium and mercury, and they do not attempt the calculation for the noble metals where the proximity of d-bands to the Fermi surface is thought to play a significant part in the calculations. In other cases the errors may be due to inaccuracies in the structure, although the whole concept of linear screening is suspect

for metals with valency greater than 3.

1.1.3. Effects of d-bands

Where there are core states near the Fermi surface (in practice these are usually d-states) the single OPW seems inappropriate as a zero order approximation to the conduction electron wave functions. They are more accurately described by a mixture of the OPW and the ionic d-states. A considerable amount of work on this topic has been done by Moriarty (14,15,16) who has calculated the amount of mixing, referred to as hybridisation, for most liquid metals. The pseudopotential can then be calculated according to equation 1.3, except that extra terms must be included to take account of the hybridisation. For metals where the hybridisation is considerable, that is in the noble metals, barium and cesium, the method gives more accurate predictions of the liquid resistivity than the OMP, however where there is less hybridisation, the inaccuracies in the knowledge of the wave function cause this method to be considerably less reliable.

The proximity of d-states to the Fermi surface effects the model potential calculations somewhat differently. Here the A_ℓ are found for Fermi surface electrons by a linear interpolation of the A_ℓ found at free ion Fermi values. If there is a core state at the Fermi level, the well depth for angular momentum component corresponding to this state will be very deep, and the linear interpolation quite inappropriate. In less severe cases, where the Fermi level lies only near a core state, this is still a source of error. Evans (17) has tried to avoid this error by relating the well depths to the quantum defects which can be interpolated more reliably. He has constructed a model potential in this way for Hg which predicts its resistivity and thermopower very accurately. For the Noble metals and heavy Alkaline Earth metals this method is not appropriate

the potentials constructed in this way are not expected to be small enough to allow the use of perturbation theory. More recent calculations for these metals have reverted to evaluating the phase shifts of the true potentials and evaluating the resistivity according to the T-matrix method (47).

1.1.4. Electronic States in Liquid Metals

The pseudoatom concept has been reasonably successful in predicting many of the electronic properties of liquid metals: resistivity, Hall effect, optical constants, and to a lesser extent thermopower. However, this success is only indirect evidence that this model can yield the true nature of the electronic states in a liquid metal. All of these properties are very insensitive to the exact shape of the density of states curve or the details of the electron wave functions.

It has been argued by Edwards (18) that it is incorrect to assume that the electron pseudowave functions are approximately plane waves, even though the pseudopotential is weak. If first order perturbation theory is used to construct a pseudowavefunction of wavevector k_o it is given by

$$\Phi(k_o) = e^{i\underline{k}_o \cdot \underline{r}} + \sum_k \frac{\langle k|V|k_o\rangle}{E_k - E_{k_o}} e^{i\underline{k}\cdot\underline{r}} , \qquad (1.7)$$

where V is the pseudopotential and E_k is the energy of the state of wave vector k. This description is adequate provided

$$\left| \frac{\langle k|V|k_o\rangle}{E_k - E_{k_o}} \right| \ll 1 , \qquad (1.8)$$

which will be the case for a weak potential except where

$$E_k \approx E_{k_o} . \qquad (1.9)$$

For these terms perturbation theory is clearly inadequate. Edwards

therefore argues that the wavefunctions should be given by wave packets containing a spread of wave vectors around a central wave vector, k_o. It is then no longer certain that the energy of such a state is given by

$$E_{k_o} = \frac{\hbar^2 k_o^2}{2m} \quad , \qquad (1.10)$$

so that there may be considerable deviations from a parabolic density of states curve.

He suggests that the wavefunctions should be constructed using Green's functions, and Ballentine and Chan (19) have used this method to evaluate the density of states curve for a few metals. However, even for mercury, which shows large deviation from the NFE behaviour, they find that the density of states curve is very similar to the free electron parabola. Shaw and Smith (20) have also argued that the perturbation approach is quite adequate for density of states calculations.

Unfortunately it is not easy to obtain information of a microscopic nature about the conduction electrons in a liquid metal experimentally. In the solid such information has come mainly from the de Haas-van Alphen effect, but this requires very long mean paths which do not exist in liquids. The NMR Knight shift does, however, in principle, provide such information and is in fact measured more easily in the liquid than in a solid metal. The Knight shift, which is discussed in more detail in the next section, is proportional to both the Fermi surface density of states and the electronic wavefunction at the nuclear site. An evaluation of this quantity therefore provides a rigorous test of any microscopic theory of electron behaviour. However the calculations are very sensitive to the details of the effective potential and as yet there have been few reliable calculations even using the perturbation approach. The main aim of this work is then to extend the range of

materials in which the Knight shift has been measured, and to perform calculations of this quantity as accurately as possible within this perturbation approach.

1.2. Nuclear Magnetic Resonance

1.2.1. Basic Principles

Since its discovery in 1945, the phenomena of nuclear magnetic resonance, NMR, has been the subject of many books (21,22,23) and therefore only a brief description is given here.

Nuclei with non-zero spin, $\underline{I}$, possess a magnetic moment, $\underline{\mu}$, related to the spin by

$$\underline{\mu} = \gamma_n \hbar \underline{I} \quad , \tag{1.11}$$

where γ_n is known as the gyromagnetic ratio and is a property of a particular nucleus. In a magnetic field, $\underline{B}_o$, an isolated nuclear magnetic moment has an interaction energy $-\underline{\mu}.\underline{B}_o$ which results in the nucleus having $2I + 1$ quantised Zeeman states, separated in energy by $\gamma_n \hbar B_o$. Transitions between these states can be produced by circularly polarised electromagnetic radiation of the resonance frequency ν given by

$$\nu = \frac{\gamma_n B_o}{2\pi} \quad , \tag{1.12}$$

with its magnetic vector perpendicular to the plane of B_o.

For any macroscopic sample in a magnetic field the nuclear states will be populated according to the Boltzmann factor

$$\exp\left(\frac{\gamma_n \hbar B_o}{kT}\right) \quad ,$$

where k is Boltzmann's constant and T is the absolute temperature, giving a nett magnetisation in the z-direction (defined to lie along the magnetic field). A rotating r.f. magnetic field of the resonant

frequency, will then cause transitions between these states. Upward and downward transition probabilities are equal, however, while the lower energy levels are more highly populated, there will be more upward transitions. Thus energy is taken from the r.f. field until the populations of the states are equal. At the same time, the spin system interacts with the lattice which tends to maintain thermal equilibrium, so that a steady state may be set up with energy being absorbed from the r.f. field by the nuclei and then dissipated in the lattice via the spin-lattice interaction. The strength of the spin-lattice interaction is characterised by T_1, the time constant for the exponential return of the z-magnetisation to its equilibrium value, after it has been disturbed. In materials with a long T_1, steady state NMR experiments can only be performed with very weak r.f. magnetic fields, otherwise saturation occurs. This is when the population of the spin states equalise and no more energy can thus be absorbed from the r.f. field.

The rotating magnetic field also produces a rotating component of magnetisation in the x-y plane. However there are various interactions which tend to destroy this and their strength is characterised by T_2, the time constant for the decay of this component of magnetisation when the r.f. field is turned off. It is these T_2 processes which give the width of the steady state NMR line, as the rate at which the magnetisation decays is entirely dependent on the spread of resonance frequencies of the individual nuclei. T_2 processes can be caused by the mutual interaction between the spins as well as the interaction of the spins with the lattice. In the first case, the spin-spin interaction causes different nuclei to sit in slightly different magnetic fields, and thus have slightly different resonance frequencies. This can also cause mutual spin flipping between nuclei, which changes their phase with respect to the x-y magnetisation,

and therefore alters their average precession rate. The transitions caused by the spin-lattice interaction have a similar effect.

In liquids or in solids, where there is some thermal motion taking place, the local field fluctuations will be averaged to a very small value, and the resonance line will be narrowed. Under these conditions it may be shown that

$$\frac{1}{T_2} = \frac{1}{T_2'} + \frac{1}{T_2''} = \frac{1}{T_2'} + \frac{1}{2T_1} \quad . \tag{1.13}$$

$(T_2')^{-1}$ is called the secular broadening and is the contribution due to the local field fluctuations and $(T_2'')^{-1}$, the life-time broadening, is that due to the finite spin-lattice relaxation time. In the limit of extremely rapid motion, which is the case in all liquid metals, it can be shown that

$$\frac{1}{T_2} = \frac{1}{T_1} \quad . \tag{1.14}$$

Here the line width is determined entirely by the spin-lattice relaxation rate and the line is Lorentzian in shape.

1.2.2. NMR in Metals

In certain respects the NMR of metals differs from that of non-metallic materials principally because of the strong interaction between the nuclear and electron spins.

Firstly, the resonance frequency for a given nucleus is different in a metal from that of a nonmetal. The shift, K, may be defined by

$$K = \frac{\nu_{metal} - \nu_{ref}}{\nu_{metal}} \quad , \tag{1.15}$$

where ν_{metal} and ν_{ref} are the resonant frequencies of the nucleus in the metal, and in some nonmetallic reference compound respectively. This is found to be independent of magnetic field. It is called the Knight shift,

after its discoverer, Professor Walter Knight and is in the range 0.1 to 1.5% for most simple metals which is an order of magnitude larger than the chemical shifts observed is other compounds.

In the majority of metals the dominant contribution to the Knight shift comes from the contact interaction between the nuclear and conduction electron spins, which has the effect of producing an extra magnetic field at the nuclear site given by

$$\Delta B = \frac{8\pi}{3} \chi_s \cdot \Omega P_F \cdot B_o \qquad (1.16)$$

where $P_F = \left\langle |\Psi_{k_F}(0)|^2 \right\rangle$,

Ω is the atomic volume, χ_s is the conduction volume susceptibility of the electron spins, Ψ_{k_F} is the wave function of an electron at the Fermi surface and an average is taken over all such electrons.

Thus we see that the Knight shift is a direct measure of the conduction electron density at the nuclear site and can therefore provide a check on any microscopic theory of electron behaviour. Furthermore, it is directly related to the density of states at the Fermi surface since χ_s is directly proportional to this quantity.

However, there may be other contributions to the shift not given by equation 1.16 . Firstly there is exchange core polarisation (E.C.P) which arises from the contact density due to the core electrons. These cannot by themselves give rise to a nett spin density at the nuclear site, since the core electrons exist in pairs with the same spacial wave function, but opposite spin. However the exchange interaction between these electrons and the conduction electrons will depend on spin orientation of the core electrons so that the two spin states of the core electrons will be perturbed differently. As a consequence there may be some nett spin density due to the core electrons at the nuclear site. It is also possible that the orbital motion of the conduction

electrons is not entirely quenched in a strong magnetic field and this will give rise to a further contribution to the Knight shift. Both these mechanisms are important in the Knight shifts of transition elements, but they have not been shown to be significant in the simple metals studied here, although some estimates of ECP have suggested that it may contribute up to 20% of the direct contact interaction. In the present work it is assumed that both ECP and orbital effects may be neglected.

A second consequence of the contact interaction is that metals have a very short spin lattice relaxation time, T_1. The expression for T_1 due to this mechanism is

$$\frac{1}{T_1} = \frac{64}{9}\ \pi^3 \hbar^3 \gamma_e^2 \gamma_n^2 P_F^2 \rho^2(E_F)\ kT \qquad (1.17)$$

where $\rho(E_F)$ is the Fermi surface density of states, γ_e and γ_n are the gyromagnetic ratios of the electron and nucleus respectively, k is Boltzmann's constant and T is the absolute temperature. T_1 may thus be related to the direct contribution to the Knight shift, K_D, by the equation

$$T_1\ T\ K_D^2 = \frac{\chi_P}{\rho(E_F)} \cdot \frac{1}{\pi k} \cdot \frac{1}{\gamma_e^2 \gamma_n^2 \hbar^2} \cdot \qquad (1.18)$$

This is the well known Korringa relation which reduces to

$$T_1 \cdot T \cdot K_D^2 = \frac{\hbar}{4\pi k} \left[\frac{\gamma_e}{\gamma_n}\right]^2 \qquad (1.19)$$

for non-interacting electrons. Unfortunately the corrections to this final equation to take account of the electron-electron interactions cannot be evaluated with sufficient accuracy to predict K from measurements of T_1 and thus test whether the other contributions to the Knight shift are significant. However one practical consequence of the rapid T_1 process is that strong r.f. fields can be used to get good NMR signals.

One other important practical difference between NMR of metals and of nonmetals is that the r.f. skin effect in metals means that experiments must be performed on finely divided particles.

1.2.3. Knight Shift in Pure Liquid Metals

The Knight shifts of almost all simple liquid metals have been measured (26,27) near the melting point, although Zn and the alkaline earth metals are exceptions. In general, there is an increase of Knight shift, K, with atomic number. Metals in the same row of the periodic table have similar K, and in most cases there is little change of K on melting (27). K also tends to vary very little with temperature and $\frac{1}{K}\frac{dK}{dT}$ is less than $10^{-4}K^{-1}$ for most metals (27).

Since the Knight shift is proportional to the density of states at the Fermi surface, the lack of change of K on melting was originally taken to indicate that band structure existed in the liquid as in the solid. This is no longer believed to be the case. Subsequent band structure calculations have shown that in many cases the Fermi surface density of states in the solid is equal to the free electron value. In other metals eg. cadmium and bismuth, large changes of K have been observed on melting and it is now believed that the density of states in liquid metals is very much like that for free electrons. The fact that K varies very slowly and regularly with temperature in liquid metals also supports this view. Otherwise any irregularities in the density of states curve would cause changes in the Knight shift as the Fermi surface moved through these regions.

It has not, however, been possible to calculate the contact density in liquid metals with sufficient accuracy to obtain the spin susceptibility, and hence density of states, from the measured Knight shift. Instead, calculations of the contact density have been compared with

experimental Knight shifts using values of the spin susceptibilities from other sources. (See discussion of Chapter 5.)

Most successful calculations of the contact density, $\mathcal{P}_F$, have been based on the OPW method. Heighway and Seymour (30) have shown that calculations based on a single OPW give agreement with measured Knight shifts to within 20% for most metals. Their values depend slightly on the spin susceptibility used. Kasowski (31), who obtains values of the spin susceptibility of cadmium by a careful analysis of low temperature data in the solid is able to calculate the Knight shift in the liquid almost exactly using a single OPW, although this may be somewhat fortuitous.

Because of the success of the single OPW approach one would hope to be able to improve the agreement between theory and experiment by constructing more realistic wavefunctions from many OPW's. Perdew and Wilkins (32) have therefore developed an expression for the contact density for electron wavefunctions constructed from many OPW's by first order perturbation theory. Their results for the alkali metals are, however, slightly further from the experimental values than the single OPW results, and they attribute this descrepency to exchange core polarisation terms. However, subsequent calculations, using this method, for the divalent and polyvalent metals (33,34) do not agree with experiment and it seems likely that the values of the calculated contact densities are incorrect.

The source of the error appears to be the choice of input parameters, in particular the pseudopotential, rather than the basic formalism. In the above work the Ashcroft model potential is used when the OMP was used in a similar calculation for sodium (35), quite different results were obtained which were a small improvement on the single OPW calculation. In particular it is shown that it is essential to include the nonlocality of the potential when performing this calculation. There have been a few

experimental Knight shifts using values of the spin susceptibilities from other sources. (See discussion of Chapter 5.)

Most successful calculations of the contact density, $\mathcal{P}_F$, have been based on the OPW method. Heighway and Seymour (30) have shown that calculations based on a single OPW give agreement with measured Knight shifts to within 20% for most metals. Their values depend slightly on the spin susceptibility used. Kasowski (31), who obtains values of the spin susceptibility of cadmium by a careful analysis of low temperature data in the solid is able to calculate the Knight shift in the liquid almost exactly using a single OPW, although this may be somewhat fortuitous.

Because of the success of the single OPW approach one would hope to be able to improve the agreement between theory and experiment by constructing more realistic wavefunctions from many OPW's. Perdew and Wilkins (32) have therefore developed an expression for the contact density for electron wavefunctions constructed from many OPW's by first order perturbation theory. Their results for the alkali metals are, however, slightly further from the experimental values than the single OPW results, and they attribute this descrepency to exchange core polarisation terms. However, subsequent calculations, using this method, for the divalent and polyvalent metals (33,34) do not agree with experiment and it seems likely that the values of the calculated contact densities are incorrect.

The source of the error appears to be the choice of input parameters, in particular the pseudopotential, rather than the basic formalism. In the above work the Ashcroft model potential is used when the OMP was used in a similar calculation for sodium (35), quite different results were obtained which were a small improvement on the single OPW calculation. In particular it is shown that it is essential to include the nonlocality of the potential when performing this calculation. There have been a few

other calculations (37,38,39) of this type which have included nonlocal pseudopotentials, although, here the Stark and Falicon potentials (45) were used which have not been shown to be as accurate as the OMP at predicting other electronic properties of liquid metals, and no exact agreement with experiment was obtained for the Knight shift results. Some estimates of core polarisation have also been made, mainly for the alkali metals (39), but as yet these results seem rather uncertain.

1.2.4. Knight Shifts in Liquid Alloys

The Knight shifts of the constituents of many binary liquid alloys have been measured. In those formed by the alkali metals, K varies linearly with concentration, lines of $\Delta K/K$ are roughly parallel for the two elements, and the value of $1/K\ dK/dc$ depends in a consistent way with the difference of size of the ions. This general behaviour is also seen in the polyvalent alloys made from metals of the same valency, although where differences of valency exist, there are some large deviations from linearity eg. In-Bi. The data on alloys involving divalent metals is less complete. The zinc resonance and those of the alkaline earth metals have not been seen in the liquid, and the cadmium resonance only reported in one alloy (34), Cd-Sn, where a small but noticably non-linear variation of the Knight shift is observed. The Knight shift of mercury has been measured in many alloys where the variation is again non-linear. However, the behaviour of Hg alloys differs from the N.F.E. predictions in many properties, so one would not expect the Knight shift to be "well behaved". The spectacular dip in the indium Knight shift in Hg-In near the Hg end has been attributed to a dip in the density of state of Hg, which was first proposed by Mott, (41), in order to explain its resistivity. The mercury Knight shift, however, varies in quite the opposite way and a more thorough discussion of mercury properties are given in Chap. 6.

In many ways calculations of the relative variation of the contact density in alloys present an easier task than calculating the absolute magnitude in the pure metals. Bladin, Daniel and Friedel (42) have suggested a method calculating the initial slope of such curves, based on the NFE model. If a charge is introduced into a free electron gas, there is a build up of electron density around the charge, which causes its potential to decay very rapidly in space. However, the screening does require oscillations in the electron density which extend to a distance, large compared with the ionic separation in a metal. They attribute changes of K on alloying to the changes of the local electron density brought about in this way. In his initial calculations Friedel evaluated the size of these fluctuations by assuming that the impurity potential well could be represented by a square whose depth was chosen by reference to resistivity data. In subsequent calculations authors have used more realistic potentials based on the free atom potential, but in neither case is there particularly good agreement with experiment.

This method has been shown to be equivalent to a simplified version of a formulation based on pseudopotential theory due to Faber (43). He develops the expression

$$\frac{1}{K}\frac{\partial K}{\partial c_1} = \frac{-2m^*}{(2\pi)^2\hbar^2 k_F}\int\left[U_o(a_{oo}-1) - U_o(a_{o1}-1)\right] x \frac{1}{2}\ell n\left|\frac{(2k_F+q)^2 + (k_F/2\ell q)^2}{(2k_F-q)^2 + (k_F/2\ell q)^2}\right| qdq \qquad (1.20)$$

for the concentration dependance of K. Here U_o and U_1 are the pseudopotentials of the two pure metals, a_{oo} and a_{o1} are the partial structure factors and ℓ is the coherence length of the electron wavefunctions. This assumes that the pseudopotential is local and energy independent and that the change in k_F does not directly effect either the pseudowave, nor the ratio of the

pseudo-to real wave function at the nuclear site. The expression also ignores the variation of the spin susceptibility, but even when this is included as in the calculations by Moulson and Seymour (44) for some alloy systems, the agreement obtained between theory and experiment is rather poor.

The most successful calculations of the variation of Knight shift in liquid alloys has been made by Perdew and Wilkins. They have derived an expression for the contact density which is exact to first order in the pseudopotential. They have assumed that any other contributions to the Knight shift, for example from core polarisation, can be included as a simple correction factor, Λ, which is a constant for an element throughout any alloy system. They have thus been able to derive an expression for the relative change of Knight shift in an alloy which is independent of Λ. Their results for some alkali metal alloys are in good agreement with experiment.

They use their calculated values of the contact density, with the measured Knight shift to evaluate the spin susceptibility of potassium, rubidium and cesium. These results do however disagree with the values from other sources and it seems that the inaccuracies of their calculations arise from the choice of input parameters, in particular the local pseudopotential. Nevertheless their calculations of the Knight shift variations in the alkali alloys are the most reliable to date. Similar calculations by Host and Styles (33), Ford and Styles (34) on polyvalent alloys have, however, been less successful but again this does seem due to the rather approximate pseudopotential used.

1.3. Present Work

The work described in this thesis is as follows. Firstly the ^{113}Cd Knight shift has been measured in a number of liquid metal alloys. The

methods used to prepare the samples and to take the measurements, are given in Chapter 2, and the results presented in Chapter 3. This is the only comprehensive series of measurements of a divalent metal's Knight shift in a range of alloys, except for mercury which cannot be regarded as a typical simple metal.

Secondly, the pseudopotential method for calculating the contact densities in metals and alloys is examined. In Chapter 4 the formalism of Perdew and Wilkins is extended to include the use of nonlocal pseudopotentials, and the results of such calculations, for a wide range of metals and alloys, is presented and discussed in Chapter 5.

The Knight shifts of both elements in Hg-In alloys are examined in Chapter 6. Their variation with temperature is measured in order to investigate the pseudogap hypothesis of Mott (49) and calculations of the contact density, as described in Chapter 4 are performed using a pseudopotential that is modified to take account of the d-core levels just below the Fermi surface.

Experimental results for the temperature dependence of the Knight shift in barium is given in Chapter 7, and the importance of s-d hybridisation in evaluating this quantity is investigated.

The final chapter describes the measurement of the ^{205}Tl Knight shift in the solid and the liquid. This completes previous measurements that had ignored the α to β phase change in the solid.

References

1. Cusack N.E., Rep.Prog.Phys., 36, 361, (1963).
2. Mott N.F., Liquids:Structure, Properties and Solid Interactions, (ed. Hugel 1965), Elserier, 152.
3. Wilson J.R., Met.Rev., 10, 381, (1965).
4. Properties of Liquid Metals, Proc.Int.Conf. at Brookhaven, (1967), Taylor and Francis.
5. Properties of Liquid Metals, Proc.Int.Conf. at Tokyo, (1972), Taylor and Francis.
6. Faber T.E., Theory of Liquid Metals, (1972), C.U.P.
7. Ziman J.M., Adv.Phys., 13, (89), (1964).
8. Meyer A. et al, Proc. Phys.Soc., 92, 446, (1967).
9. Harrison W.A., Pseudopotentials in the Theory of Metals, (1966), Benjamin.
10. Ashcroft N.W., J.Phys.C, 1, 232, (1968).
11. Heine V. and Aberenkov I.V., Phil.Mag., 9, 451, (1964).
12. Shaw, R.W., Ph.D.Thesis, Univ. of Stanford, (1968).
13. Appapillai M. and Williams A.R., J.Phys.F., 3, 759, (1973).
14. Moriarty J.A., Phys.Rev.B., 1, 1363, (1970).
15. Moriarty J.A., Phys.Rev.B., 6, 4445, (1972).
16. Moriarty J.A., Phys.Rev.B., 10, 3075, (1974).
17. Evans R., J.Phys.C., 3, 5137, (1970).
18. Edwards S.F., Proc.Roy.Soc.A., 267, 518, (1962).
19. Chan T.and Ballentine L.E., Con.J.Phys., 50, 813, (1972).
20. Shaw R.W. and Smith N.V., Phys.Rev., 178, 985, (1969).
21. Abragam A., The Principles of Nuclear Magnetism (1961) O.U.P.
22. Andrew E.R., Nuclear Magnetic Resonance (1958) C.U.P.
23. Slitcher C.P., Principles of Magnetic Resonance (1963), Harper and Row.

24. Knight W.D., Solid State Physics 2, 93, (1956).

25. Korringa J., Physica, 16, 601, (1950).

26. Drain L.E., Met.Rev., 12, 195, (1967).

27. Faber T.E., ref. 6 p. 304.

28. Devine R.A.B. and Dupree R., Phil.Mag., 22, 1069, (1970).

29. Enderby J.E. et al, Phil.Mag., 10, 633, (1964).

30. Heighway J. and Seymour E.F.W., Phys.Kondens.Mat., 13, 1, (1971).

31. Kasowski R.V., Phys.Rev., 187, 891, (1969).

32. Perdew J.P. and Wilkins J.W., Phys.Rev.B., 7, 2461, (1973).

33. Host I.P. and Styles G.A., J.Mag.Res., 6, 475, (1972).

34. Ford C.J. and Styles G.A., Properties of Liquid Metals:Proc.Int. Conference at Tokyo, 189, (1972), Taylor and Francis.

35. Ritter A.L. and Gardner J.A., Phys.Rev.B., 3, 46, (1971).

36. Jena P. et al, Phys.Rev.B., 3, 2158, (1971).

37. Jena P. et al, Phys.Rev.B., 1, 432, (1972).

38. Wei Mei Shyu et al, Phys.Rev.B., 152, 7, (1966).

39. Mahanti S.D. et al, Magnetic Resonance (ed. Coogan et al, 1970) Plenum.

40. Faber T.E., ref. 6 p. 499.

41. Mott N.F., Phil.Mag., 13, 989, (1966).

42. Blandin A. et al, Phil.Mag., 4, 180, 1959).

43. Faber T.E., ref. 6 p. 502.

44. Moulsen P. and Seymour E.F.W., Adv.Phys., 16, 449, (1967).

45. Stark R.W. and Falicov L.M., Phys. Rev. Lett., 19, 795, (1967).

46. Pattison P., Ph.D.Thesis, Univ. of Warwick, (1975).

47. Ratti V.K. and Evans R., J.Phys.F., 3, L238, (1973).

48. Dupree R. and Seymour E.F.W., Phys.Kondens.Mater., 12, 97, (1970).

49. Mott N.F., Phil.Mag., 13, 989, (1966).

CHAPTER 2

Experimental Methods

2.1. Introduction

Measurements were made of the Knight shift in metals and alloys at temperatures up to 750K. Since a commercially available NMR spectrometer was used, only an outline of its design is given here. This, together with a description of the measuring technique and of the modifications made in order to heat and cool the sample, is given in section 2.2. All samples were prepared in the laboratory and the methods are described in section 2.3.

2.2 NMR Measurements

2.2.1 NMR Apparatus

The apparatus consisted principally of a Varian VF16 Wide Line Spectrometer and a Varian 12" Low Impedance Electromagnet A block diagram of the whole experimental set up is shown in Fig 2.01.

The spectrometer works on the nuclear induction principle which is described by Andrew (1). The sample is placed in a probe, between the magnet poles, which houses two coils, wound so as to be very nearly orthogonal. At resonance an r.f. voltage in the transmitter coil induces a precessing magnetic moment in the sample which in turn produces a voltage in the receiver coil. By means of adjustment paddles, a voltage leakage between the two coils is introduced which is either exactly in phase, or at 90° to the driving voltage; then the additional voltage produced in the receiver coil by the sample is proportional to χ' or χ'', the real or imaginary parts respectively, of the frequency dependent magnetic susceptibility.

There are also two Helmholtz coils in the probe body, driven by an audio-frequency oscillator which modulates the magnetic field. The detected signal emerging from the r.f. receiver is then an a.f. voltage and, provided the modulation is small compared with the NMR line width, the amplitude of this signal is proportional to the derivative of χ'(or χ'') with respect to the magnetic field. See Fig 2.02.

In general nuclear resonance signals are very weak due to the small differences in energy between the nuclear magnetic energy levels. To improve the signal to noise ratio this a.f. signal is fed to a phase sensitive detector whose reference signal comes from the modulation oscillator. The output from this stage is a D.C. voltage proportional

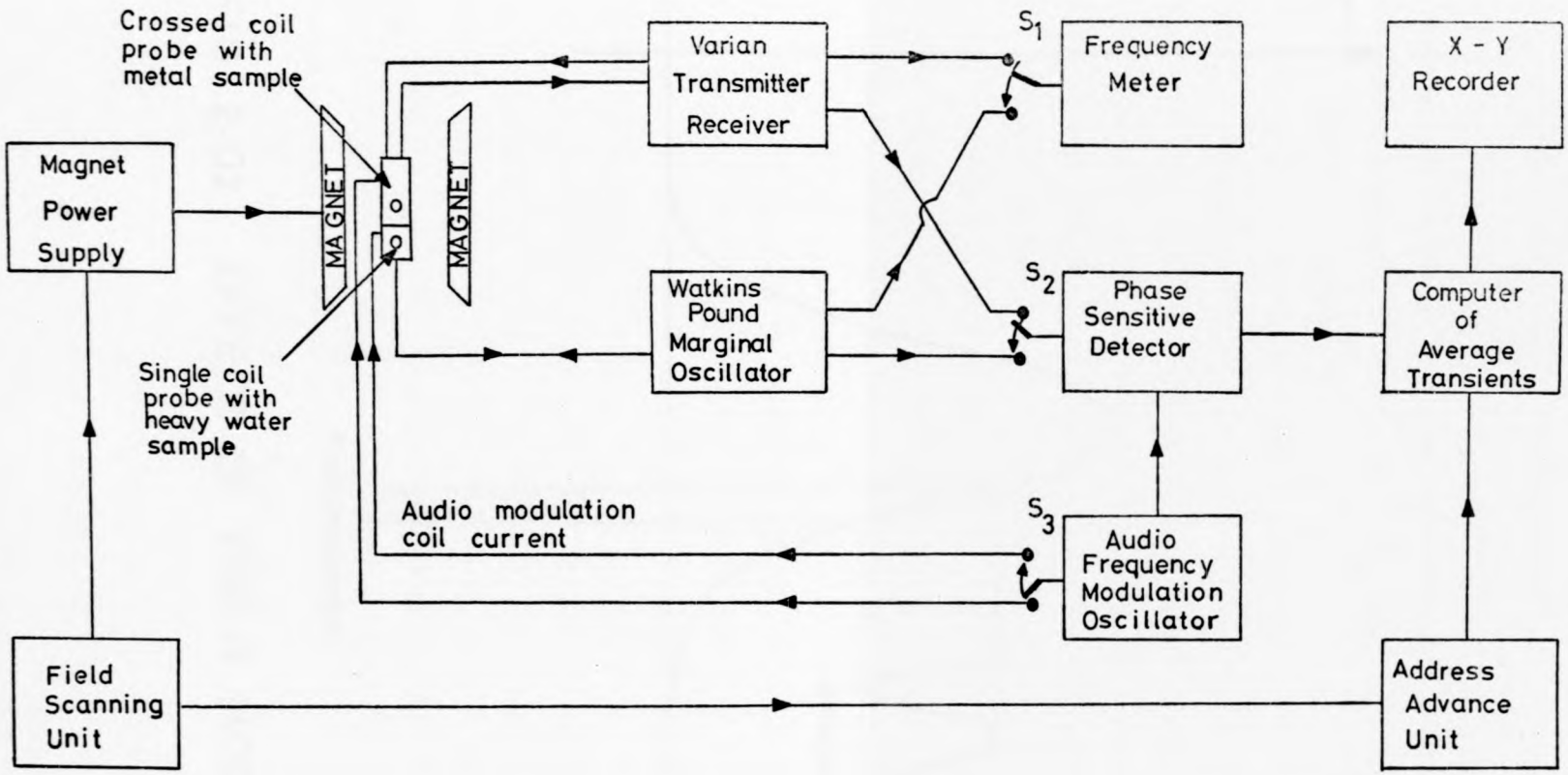

FIG 2·01 BLOCK DIAGRAM OF N·M·R· APPARATUS·

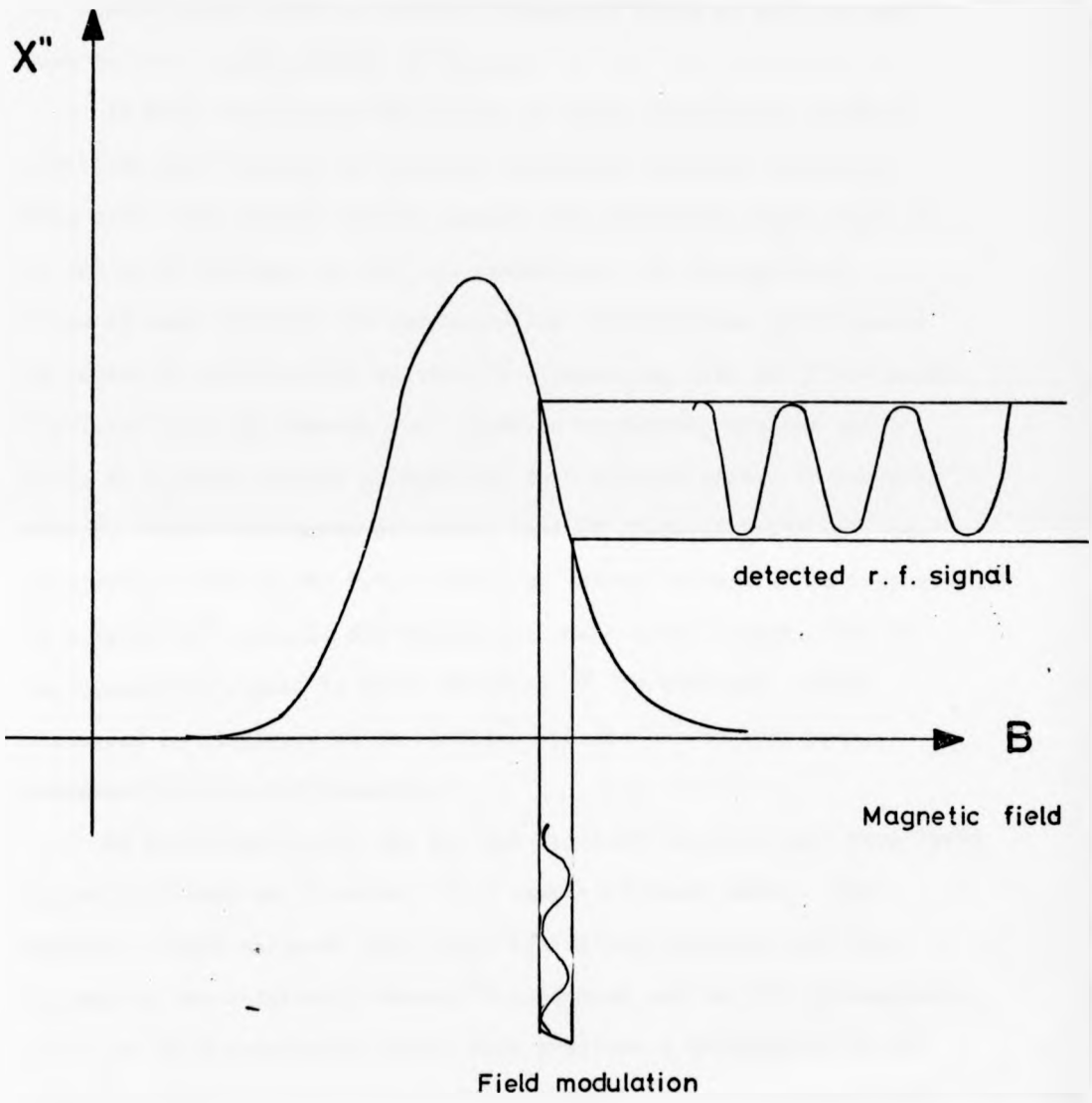

FIG 2·02 EFFECT OF FIELD MODULATION

to the slope of the resonance line. The field is then gradually scanned so that the whole of the resonance line can be observed. The apparatus was able to produce a magnetic field up to 1.4T and work in the frequency range 2-16 MHz.

In order to improve the signal to noise ratio still further, a Nicolet 1072 Computer of Average Transients (C.A.T.) was used. This device has a 1023 channel memory into which the signal may be fed after analogue to digital conversion. As the magnetic field is swept through the resonance the output of the spectrometer is routed to each channel in turn in synchronism with the field sweep. The field is swept through the resonance repeatedly and the signal going to a given channel is added to that already stored in previous sweeps. Thus a histogram of signal against field is built up. On completing N sweeps, the r.m.s. value of random noise will be increased by a factor $\sqrt{N}$, whereas any signal will be N times larger, thus an improvement in signal to noise ratio of $\sqrt{N}$ is obtained. This histogram is displayed on an oscilloscope and can be recorded permenantly on an X-Y recorder.

By switching S_1, S_2 and S_3 (see Fig 2.01) an auxiliary experiment can be performed on ^2D nuclei in a sample of heavy water. The Watkins - Pound marginal oscillator (2) is sufficiently sensitive to observe the relatively strong ^2D resonance and, as the gyromagnetic ratio of ^2D is accurately known, this provides a calibration of the magnetic field. For both of the experiments the radio frequency is measured with a Venner TSA 346 frequency counter used in conjunction with a Venner frequency divider.

2.2.2 Measuring Technique

In all of the measurements, the frequency of the r.f. oscillator

was kept constant and the field sweep adjusted to pass through the whole of the resonance line in either 30 or 60s. Measurements were usually made with the spectrometer operating in the adsorption mode and at the highest possible field in order to obtain maximum sensitivity. Saturation is not a serious problem in NMR of metals because of the very fast spin-lattice relaxation times, so the highest available r.f. level was used throughout. At 12 MHz this corresponded to a rotating H_1 field of 20μT.

The values of the audio frequency modulation and P.S.D. time constant were genererally set to maximise the signal. This was achieved by setting the modulation equal to the line width and the response time of the P.S.D. approximately equal to the time taken to scan between the two peaks of the derivative of the resonance line. With these settings the signal was considerably distorted so,where details of the line shape or width were required, or where a strong signal was being studied a smaller value of each of these two parameters was set.

The field was swept through the resonance repeatedly until a sufficiently good signal to noise ratio was obtained as shown on the C.A.T. oscilloscope. The histogram was then fed onto the X-Y recorder. Throughout this process the frequency was monitored and its value recorded.

Calibration of the field sweep was performed by subsequent measurements on the ^2D resonance in the D_2O which could be observed by switching S_1, S_2 and S_3 (Fig 2.01). The frequency of the marginal oscillator was adjusted so that resonance occurred near the beginning of the field sweep, and the modulation and P.S.D. time constant reduced to values suitable for the narrow ^2D resonance. This resonance was recorded on the C.A.T. and the radio frequency noted. The measurement was then repeated with the oscillator frequency ajusted so that resonance occurred near the end of the field sweep, and the final signal read onto the X-Y

recorder to give a trace as shown in Fig 2.03. From the known gyromagnetic ratio for deuterium and the measured frequencies, the fields at the centres of these two resonances on the recorder chart could be calculated, and that of any point between found by interpolation.

For a symmetrical resonance line, the centre can be taken to be the point where the derivative curve passes through zero. This was found by interpolating the baseline on either side of the resonance. However, where the signal was weak, the baseline was instead taken to be a horizontal line passing half way between the derivative peaks, A and B. This enabled a smaller sweep to be used, which permitted a longer time constant for P.S.D. and so resulted in an improvement in the signal to noise ratio.

In both of these methods a systematic error is introduced because the finite response time of the P.S.D. causes the metal resonance to be displaced towards the end of the sweep, and also produces an asymmetric distortion of the line. To overcome this, the experiment was repeated sweeping the field in the opposite direction. With a symmetric line the line shift was thus equal and opposite in the two cases and the true position obtained by averaging. In practice six readings were taken for each resonance, three in each direction of the field sweep. Two asymmetric lines were studied, barium and thallium. In these cases only relative changes of position as a function of temperature were required and the above method was still valid since the line shape did not change with temperature.

A further slight error was introduced because the deuterium and metal samples were not at the same point in the magnetic field. This has no effect on measurements of relative changes of position, but

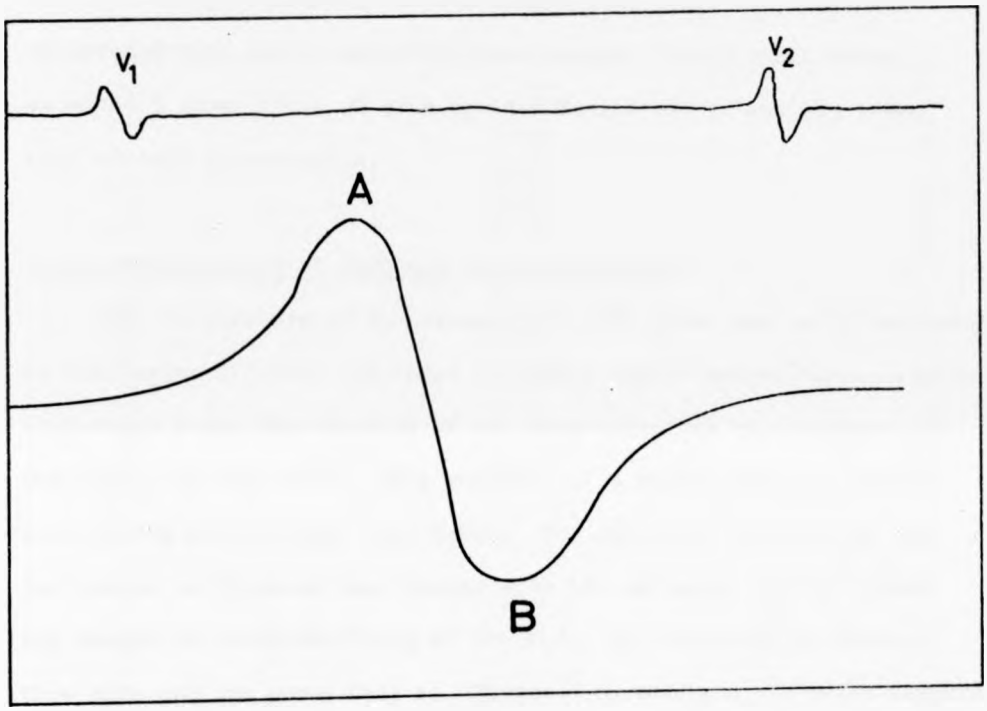

FIG 2·03 DIAGRAM OF SIGNAL TRACE

where an absolute valve was required, the field was calibrated by observation of the ^{2}D resonance in a sample of heavy water in the Varian probe itself.

The poorest signals studied could be measured after 1 hr of time averaging, and where it took longer than $\frac{1}{2}$ hr, the field was calibrated both before and after measurement. Field drift never exceeded 1 gauss (1 or 2% of a typical Knight shift) and was taken into account by averaging.

2.2.3. Measurements at High and Low Temperatures

The temperature of the crossed coil NMR probe has to be maintained in the region 273-340K. In order to obtain sample temperatures outside this range a gas flow furnace of the type described by Schreiber (3) was used. See Fig 2.04. This consists of a double walled L-shaped tube having an evacuated interspace. The walls are silvered on the the inside to minimise heat losses with the silvering scored around the sample to avoid shielding of the r.f. Air is sucked up between this tube and the probe body at 10ℓ min^{-1} to maintain the probe temperature as near to that of the room as possible. The sample is contained inside the furnace and its temperature changed by gas flowing through the tube.

To lower the temperature of the sample the gas flow is provided by connecting the L-shaped tube to a dewar of liquid nitrogen and boiling with an immersed heating coil. Temperatures down to 140K were obtained with a gas flow of 25ℓ min^{-1}. No improvement was found using liquid helium since although much cooler, this has a very low specific heat.

Elevated temperatures are obtained by placing a heating coil in the horizontal part of the tube and sucking air over the coil by means of a pump attached to the gas flow exit. The heating coil is powered

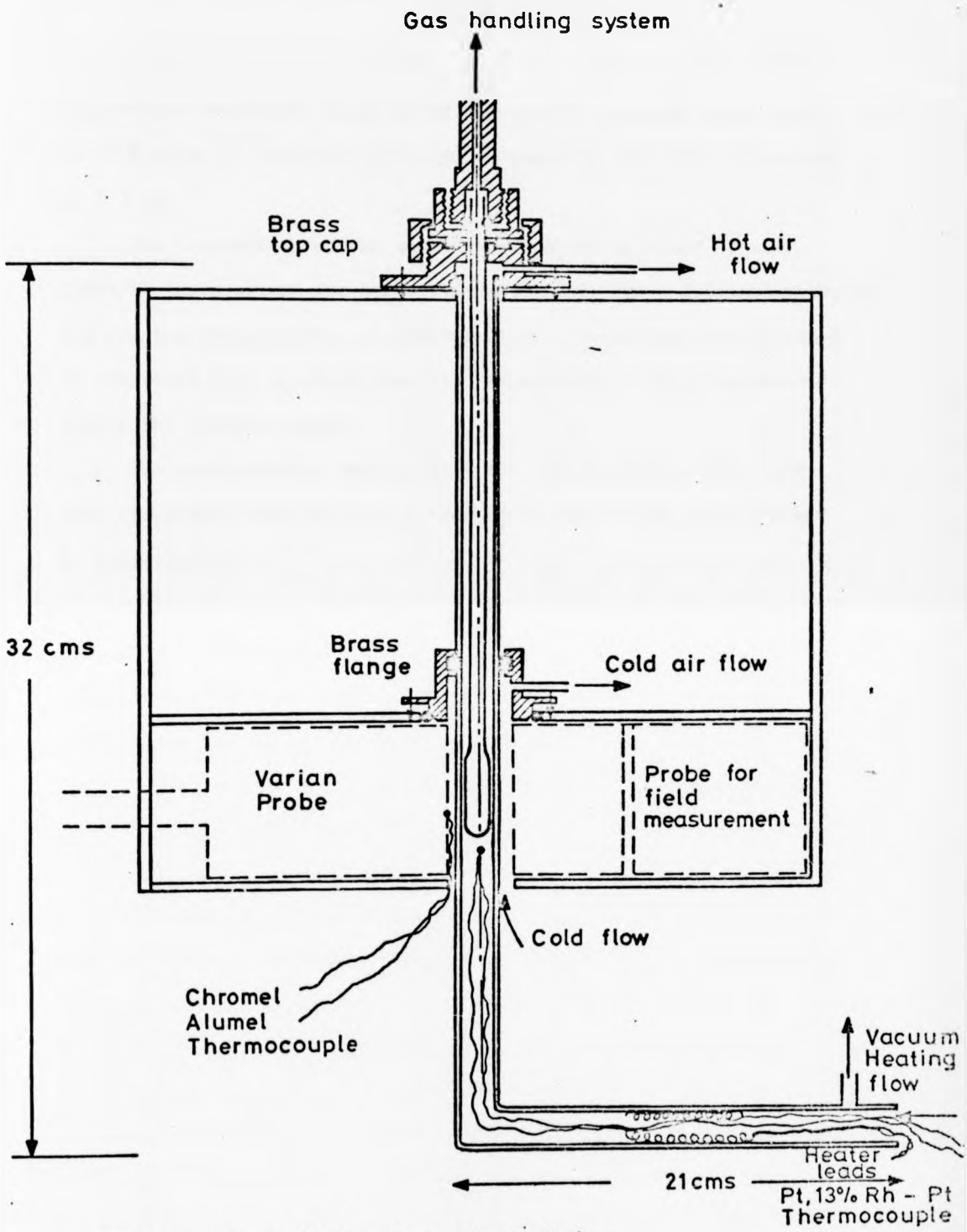

Sample tubes : 24 cms. long, the bulb is 2 cms. long and 1 cm. diameter.

FIG. 2.04 THE FURNACE SYSTEM USED FOR MEASUREMENTS OF LIQUID METALS.

by a direct current to avoid pick up in the r.f. coil. The maximum temperature obtainable (limited by the need to keep the probe cool) is 750K which is achieved with a power input of 150W and a flow rate of 8 ℓ min^{-1}.

The temperature of the sample is recorded by means of a Pt, 13%Pt/Rh thermocouple for high temperature work and a Copper-Constantin one for low temperatures. A Chromel-Alumel thermocouple is attached to the probe body to check that its temperature is being maintained within the required range.

Two measurements, made at 4.2K and 77K on Barium, were made with the sample immersed in a finger dewar containing liquid He and N_2 respectively.

2.3 Sample Preparation

2.3.1 Introduction

One of the problems of NMR of metals is the r.f. skin effect. This prevents the r.f. penetrating to the nuclei within a bulk sample, thus reducing the signal intensity, and causes a distortion of the line shape by mixing adsorption and dispersion signals from nuclei in different parts of the sample. This has been discussed by Chapman, Rhodes and Seymour (4) who show that this effect is virtually eliminated for electrically isolated particles of diameter less then the r.f. skin depth. This is of the order of 100μm for the metals studied.

In principle particles of this size can be produced by grinding or filing, however considerable care has to be taken when dealing with reactive elements because of the very large surface area of the resulting samples. Details of the methods used to overcome these difficulties for barium and thallium are given in section 2.3.2.

In the case of alloys it is also important that each particle has the nominal composition of the sample. On casting binary alloys, large scale phase separation may occur, so that subsequent filing may lead to a wide variation of composition between particles. To overcome this, alloy samples were prepared either by directly dispersing the liquid metal in oil with an ultrasonic drill or by spraying from the solid as described in sections 2.3.3 and 2.3.4 respectively.

In some cases an oxide layer ensures electrical isolation of the particles, but generally a dispersing agent must be mixed with the powder. For the samples prepared by dispersion, the oil keeps the particles apart while for the other samples the particles were separated by mixing with an equal volume of finely ground quartz powder.

2.3.2 Preparation of Barium and Thallium Samples

Samples of barium powder were prepared from barium rod of 99.5% purity obtained from Koch Light Laboratories. This is, unfortunately, the highest purity commercially available.

Initially the rods were powdered using a fine grinding wheel. However, using this method it was impossible to avoid getting small particles of the grinding wheel mixed with the sample and it was thought that these may have been responsible for sample oxidising at higher temperatures.

As an alternative the samples were prepared by filing under carbon tetrachloride. This method, however, is not to be recommended as it was discovered that the barium reacted violently with the carbon tetrachloride when the filing produced sufficient heat. However, the samples used were prepared this way before this was realised. A new file was used to ensure ferromagnetic contamination did not occur from previous use and it was thought that barium was sufficiently soft not to break any particles from the file. This was checked by passing a magnet over the finished samples. The sample, still immersed in carbon tetrachloride, was then transfered to a glove box filled with dry nitrogen gas. The carbon tetrachloride was allowed to evaporate and the dried powder poured through a 100μm sieve, before transfering to a tube in which the sample was finally sealed, under vacuum.

Samples produced in this way gave a reasonable room temperature resonance but were destroyed by heating over 100°C. This was attributed to reaction with the glass walls of the tube or an adsorbed layer of oxygen or water which was not removed even by heating the tube under vaccum. Samples were then prepared and mixed with silicone oil MS550 to form a buffer to reaction. By this method measurements were able to be made upto 580°K, the temperature at which the oil started to decompose.

Thallium is considerably less reactive although it is oxidised readily when exposed to the atmosphere. This was prepared from Koch Light 5N pure rod by filing under liquid N_2 as it was impossibly soft at room temperature. Again this was seived under a nitrogen atmosphere, mixed with quartz powder and sealed into a glass tube.

2.3.3 Spraying from the Solid

In this method (5) the alloy, in the form of a $^3/_{16}$" diameter rod, was sprayed into water using a Mk 45 metal spraying gun from Metallisation Ltd., Dudley, Worcs. An oxygen propane flame melted the tip of the rod which was gradually fed forwards at about 2 inches per second. The liquid was immediately sprayed into droplets by compressed air. On reaching the water the droplets were quenched and a fine powder of spherical particles was allowed to settle. Most of the water was decanted and the sample washed with acetone and ether. Finally the sample was sieved to obtain particles of the required size and mixed with quartz powder.

For Cd-Tℓ alloys these last processes were carried out in a glove box containing a nitrogen atmosphere and the samples sealed into glass tubes to avoid oxidation. The spraying process itself did not appear to cause significant oxidation since the powder produced had a grey colour characteristic of the metal rather than the brown colour of thallium oxide.

In order to produce the alloy rods, the components were melted together in a silica glass tube under an argon atmosphere, and then quenched into a copper mould. It was not possible to cast $^3/_{16}$" rods in this way because the metal tended to solidify near the top of the mould thus preventing the mould from being filled, so an ingot $^3/_8$" in diameter and about 2" long was cast and the diameter reduced, where possible, by swaging.

Alloys which were too brittle to swage were recast into a 3/16" split mould which was heated to a temperature above the alloy melting point and the mould then quenched by dropping into cold water. Care was taken to heat the mould before the alloy was placed in it, otherwise during a gradual heating process, firstly the constituent with the lower melting point would melt out of the alloy and run to the bottom of the mould followed by the other constituent at its melting point. It would then be unlikely that the two liquids would mix very thoroughly in such a narrow tube.

2.3.4 Dispersing by Ultrasonic Drill

This method was used to produce powders or droplets of alloys with melting points lower than 200°C.

The constituents were melted together in a glass phial, 1 cm in diameter under 3 or 4 mm of Silicone oil (MS550) using a Bunsen burner. While still heating, the tip of an ultrasonic drill was introduced just below the surface of the liquid and switched on to vibrate at 20kHz. By adjusting the position of the phial a violent disturbance was produced in the liquid and the alloy split up into droplets. The drill used was an L667 supplied by M.E.L. Equipment Co.

The particles of Hg-In produced in this way all had a diameter less than the r.f. skin depth, as shown by the symmetry of the indium resonance in these samples. With Hg-Cd alloys, however, there always remained some larger particles so the dispersion was washed with acetone and sieved to produce the final sample.

2.3.5 Summary of Methods of Alloy Preparation

The method used for the production of each of the alloys is summarised in table 2.1. All were prepared from pure metals of at least 5N purity

supplied by Koch Light Laboratories and which, except for Mercury, were in the form of shot, rod, or sheet. Except in the case of Hg-Cd alloys it was assumed that the final composition of the alloy samples were determined by the initial weight of the constituents. Some evaporation of mercury during spraying was suspected for Hg-Cd alloys and they were therefore analysed by X-ray florescence technique at the Centre for Material Science at the University of Birmingham. The compositions quoted are those given by analysis.

TABLE 2.1 SAMPLE PREPARATION

SAMPLE	METHOD OF DISPERSION	SEPARATING MEDIUM
all Cd-Cu	recasting and spraying	quartz powder
all Cd-Zn	swaging and spraying	
all Cd-Ag		
all Cd-In		
Cd90% Sn10%	swaging and spraying	
Cd80% Sn20%		
Cd70% Sn30%		
Cd60% Sn40%	recasting and spraying	
Cd50% Sn50%	swaging and spraying	
Cd40% Sn60%	recasting and spraying	
Cd30% Sn70%	swaging and spraying	
all Cd-Sb	recasting and spraying	
Cd85% Hg15%	swaging and spraying	
Cd73% Hg27%		
Cd67% Hg33%		
Cd60% Hg40%	ultrasonic drill	
Cd50% Hg50%		
Cd38% Hg62%		
Cd29% Hg71%		
Cd23% Hg77%		
all Cd-Tℓ	swaging and spraying	
all Cd-Pb		
all Cd-Bi	recasting and spraying	
all Hg-In	ultrasonic drill	silicone oil

References

1. Andrew E.R., Nuclear Magnetic Resonance, C.U.P., (1958).

2. Styles G.A., Ph.D. Thesis, Leeds (1964).

3. Schreiber D.S., Rev.Sci.Instr., 35, (1964), 1582.

4. Chapman A.C., Rhodes P., and Seymour E.F.W., Proc.Phys.Sco. B70, (1959), 343.

5. Heighway J., Host I.P., and Styles G.A., J.Phys.E, 3, (1970), 391.

CHAPTER 3

Experimental Results

The experimental results for the ^{113}Cd Knight shift in a wide range of cadmium alloys are presented in this chapter. The discussion of these, and other, experimental results is given in Chapter 5 after a framework for Knight shift calculations has been discussed in Chapter 4. The results of observation of NMR in mercury, barium and thallium are given separately in Chapters 6, 7 and 8.

The Knight shift K is defined by the equation

$$K = \frac{\nu_{metal} - \nu_{ref}}{\nu_{ref}} \qquad (3.1)$$

where ν_{metal} and ν_{ref} are the NMR frequencies of a given nucleus in a metal and in a non-metallic reference compound respectively in the same applied magnetic field. It is not possible, however, to keep the magnetic field exactly constant throughout a set of measurements and an equivalent and more useful expression is

$$K = \frac{\left(\frac{B}{\nu}\right)_{ref} - \left(\frac{B}{\nu}\right)_{metal}}{\left(\frac{B}{\nu}\right)_{metal}} \qquad (3.2)$$

where $(B/\nu)_{metal}$ and $(B/\nu)_{ref}$ are the ratios of magnetic field to frequency at resonance in the metal and in the reference compound respectively.

Since the value of the Knight shift in pure cadmium is well known, and the main aim of these experiments was to observe the change in Knight shift in alloys, no measurements were made on a reference compound. Instead the reference value of the field to frequency ratio was calculated to be

$$\left(\frac{B}{\nu}\right)_{ref} = 1.058873 \text{ gauss/kHz}$$

using the data published in the Varian tables and this value was used throughout.

Measurements were made of the field to frequency ratio of the ^{113}Cd resonance in alloys of cadmium and, zinc, indium, tin, mercury, thallium, lead, bismuth, silver, copper and antimony. The Knight shift, and the relative change of this quantity with concentration have thus been evaluated and the results are given in Tables 3.1. to 3.10. All concentrations are given in atomic per cent. Each value given is the result of six measurements, and the error quoted is the r.m.s deviation of these values from the mean. A steady temperature was maintained for all readings in any alloy system and in all cases the maximum available magnetic field of 1.4T was used. The results for the relative change of Knight shift as a function of concentration in the alloy systems is given in Figs.3.1. to 8. and as a function of electron density in Fig.3.9.

Alloy Conc. Cd%	Zn%	Field / Frequency (gauss / kHz)	Knight Shift K%	Relative Change of K: $\frac{\Delta K}{K}$
100	0	1.050 634 ± 0.000 005	0.7843 ± 0.0005	0
89	11	1.050 752 ± 0.000 010	0.7738 ± 0.001	-0.014 ± 0.001
78	22	1.050 888 ± 0.000 010	0.7698 ± 0.001	-0.033 ± 0.001
66	34	1.050 991 ± 0.000 010	0.7500 ± 0.001	-0.045 ± 0.001
57	43	1.050 105 ± 0.000 020	0.7390 ± 0.002	-0.060 ± 0.002
47	53	1.051 208 ± 0.000 020	0.7291 ± 0.002	-0.075 ± 0.002
39	61	1.051 258 ± 0.000 030	0.7244 ± 0.003	-0.082 ± 0.003
30	70	1.051 389 ± 0.000 030	0.7126 ± 0.003	-0.099 ± 0.003

Table 3.1. ^{113}Cd Knight Shift in Liquid Cd-Zn Alloys at 670K.

Alloy Conc. Cd%	In%	Field / Frequency gauss / kHz	Knight Shift K%	Relative Change of K: $\frac{\Delta K}{K}$
100	0	1.050 631 ± 0.000 005	0.7846 ± 0.0005	0
90	10	1.050 566 ± 0.000 010	0.7907 ± 0.001	0.009 ± 0.001
80	20	1.050 528 ± 0.000 010	0.7944 ± 0.001	0.013 ± 0.001
70	30	1.050 530 ± 0.000 010	0.7942 ± 0.001	0.013 ± 0.001
60	40	1.050 538 ± 0.000 010	0.7934 ± 0.001	0.011 ± 0.001
40	60	1.050 536 ± 0.000 020	0.7936 ± 0.002	0.013 ± 0.002
30	70	1.050 561 ± 0.000 010	0.7912 ± 0.001	0.009 ± 0.001
20	80	1.050 569 ± 0.000 020	0.7904 ± 0.002	0.008 ± 0.002
10	90	1.050 594 ± 0.000 030	0.7880 ± 0.003	0.005 ± 0.003

Table 3.2. ^{113}Cd Knight Shift in Liquid Cd-In Alloys at 620K.

Alloy Conc. Cd	Sn	Field / Frequency (gauss / kHz)	Knight Shift K%	Relative Change of K: $\frac{\Delta K}{K}$
100	0	1.050 631 ± 0.000 005	0.7846 ± 0.0005	
90	10	1.050 525 ± 0.000 010	0.795 ± 0.001	0.014 ± 0.001
80	20	1.050 485 ± 0.000 010	0.798 ± 0.001	0.018 ± 0.001
70	30	1.050 486 ± 0.000 010	0.798 ± 0.001	0.018 ± 0.001
60	40	1.050 490 ± 0.000 010	0.7980 ± 0.001	0.018 ± 0.001
50	50	1.050 499 ± 0.000 010	0.7971 ± 0.001	0.017 ± 0.001
40	60	1.050 540 ± 0.000 020	0.7924 ± 0.002	0.011 ± 0.002
30	70	1.050 564 ± 0.000 020	0.7909 ± 0.002	0.009 ± 0.002
20	80	1.050 573 ± 0.000 030	0.7901 ± 0.003	0.008 ± 0.003

Table 3.3. ^{113}Cd Knight Shift in Liquid Cd-Sn Alloys at 620K.

Alloy Conc. Cd	Hg	Field / Frequency (gauss / kHz)	Knight Shift K%	Relative Change of K: $\frac{\Delta K}{K}$
100	0	1.050 630 ± 0.000 005	0.7847 ± 0.0005	0
85	15	1.050 454 ± 0.000 010	0.8015 ± 0.001	0.022 ± 0.001
73	27	1.050 275 ± 0.000 010	0.8186 ± 0.001	0.043 ± 0.001
67	33	1.050 201 ± 0.000 020	0.8257 ± 0.002	0.051 ± 0.002
61	39	1.050 154 ± 0.000 020	0.8302 ± 0.002	0.056 ± 0.002
49	51	1.049 837 ± 0.000 030	0.8607 ± 0.003	0.089 ± 0.003
37	63	1.049 457 ± 0.000 030	0.8972 ± 0.003	0.127 ± 0.003
29	71	1.049 108 ± 0.000 040	0.9308 ± 0.004	0.158 ± 0.004
23	77	1.048 749 ± 0.000 040	0.9653 ± 0.004	0.188 ± 0.004

Table 3.4. ^{113}Cd Knight Shift in Liquid Cd-Hg Alloys at 570K.

Alloy Conc. Cd	Tℓ	Field / Frequency (gauss / kHz)	Knight Shift K%	Relative Change of K: $\frac{\Delta K}{K}$
100	0	1.050 631 ± 0.000 005	0.7846 ± 0.0005	0
90	10	1.050 588 ± 0.000 010	0.7886 ± 0.001	0.006 ± 0.001
80	20	1.050 568 ± 0.000 010	0.7906 ± 0.001	0.009 ± 0.001
70	30	1.050 564 ± 0.000 010	0.7909 ± 0.001	0.008 ± 0.001
60	40	1.050 611 ± 0.000 020	0.7864 ± 0.001	0.004 ± 0.002
50	50	1.050 646 ± 0.000 020	0.7830 ± 0.001	-0.002 ± 0.002

Table 3.5. ^{113}Cd Knight Shift in Liquid Cd-Tℓ Alloys at 620K.

Alloy Conc. Cd	Pb	Field / Frequency (gauss / kHz)	Knight Shift K%	Relative Change of K: $\frac{\Delta K}{K}$
100	0	1.050 631 ± 0.000 005	0.7846 ± 0.0005	0
90	10	1.050 671 ± 0.000 010	0.7806 ± 0.001	-0.004 ± 0.001
80	20	1.050 695 ± 0.000 010	0.7783 ± 0.001	-0.007 ± 0.001
70	30	1.050 784 ± 0.000 020	0.7698 ± 0.002	-0.018 ± 0.002
60	40	1.051 045 ± 0.000 020	0.7448 ± 0.002	-0.052 ± 0.002
50	50	1.051 206 ± 0.000 030	0.7294 ± 0.003	-0.074 ± 0.003

Table 3.6. ^{113}Cd Knight Shift in Liquid Cd-Pb Alloys at 620K.

Alloy Conc. Cd	Bi	Field / Frequency (gauss / kHz)	Knight Shift K%	Relative Change of K: $\frac{\Delta K}{K}$
100	0	1.050 631 ± 0.000 005	0.7846 ± 0.0005	0
97	3	1.050 539 ± 0.000 010	0.7933 ± 0.001	0.011 ± 0.001
95	5	1.050 529 ± 0.000 010	0.7943 ± 0.001	0.012 ± 0.001
93	7	1.050 472 ± 0.000 010	0.7997 ± 0.001	0.019 ± 0.001
90	10	1.050 401 ± 0.000 010	0.8065 ± 0.001	0.029 ± 0.001
80	20	1.050 609 ± 0.000 020	0.7863 ± 0.002	0.003 ± 0.002
70	30	1.050 998 ± 0.000 020	0.7493 ± 0.002	-0.046 ± 0.002
60	40	1.051 498 ± 0.000 020	0.7014 ± 0.002	-0.117 ± 0.002
40	60	1.052 045 ± 0.000 040	0.6490 ± 0.004	-0.207 ± 0.004

Table 3.7. ^{113}Cd Knight Shift in Liquid Cd-Bi Alloys at 620K.

Alloy Conc. Cd	Cu	Field / Frequency (gauss / kHz)	Knight Shift K%	Relative Change of K: $\frac{\Delta K}{K}$
100	0	1.050 634 ± 0.000 005	0.7843 ± 0.0005	
95	5	1.050 949 ± 0.000 010	0.7540 ± 0.001	-0.040 ± 0.001
90	10	1.051 180 ± 0.000 010	0.7319 ± 0.001	-0.071 ± 0.001
85	15	1.051 296 ± 0.000 010	0.7207 ± 0.001	-0.088 ± 0.001

Table 3.8. ^{113}Cd Knight Shift in Liquid Cd-Cu Alloys at 670K.

Alloy Conc. Cd	Ag	Field / Frequency (gauss / kHz)	Knight Shift K%	Relstive Change of K: $\frac{\Delta K}{K}$
100	0	1.050 634 ± 0.000 005	0.7843 ± 0.0005	0
95	5	1.050 833 ± 0.000 010	0.7651 ± 0.001	-0.025 ± 0.001
90	10	1.050 907 ± 0.000 010	0.7599 ± 0.001	-0.034 ± 0.001

Table 3.9. ^{113}Cd Knight Shift in Liquid Cd-Ag Alloys at 670K.

Alloy Conc. Cd	Sb	Field / Frequency (gauss / kHz)	Knight Shift K%	Relative Change of K: $\frac{\Delta K}{K}$
100	0	1.050 634 ± 0.000 005	0.7843 ± 0.0005	
95	5	1.050 496 ± 0.000 010	0.7974 ± 0.001	0.017 ± 0.001
90	10	1.056 438 ± 0.000 010	0.8030 ± 0.001	0.024 ± 0.001

Table 3.10. ^{113}Cd Knight Shift in Liquid Cd-Sb Alloys at 670K.

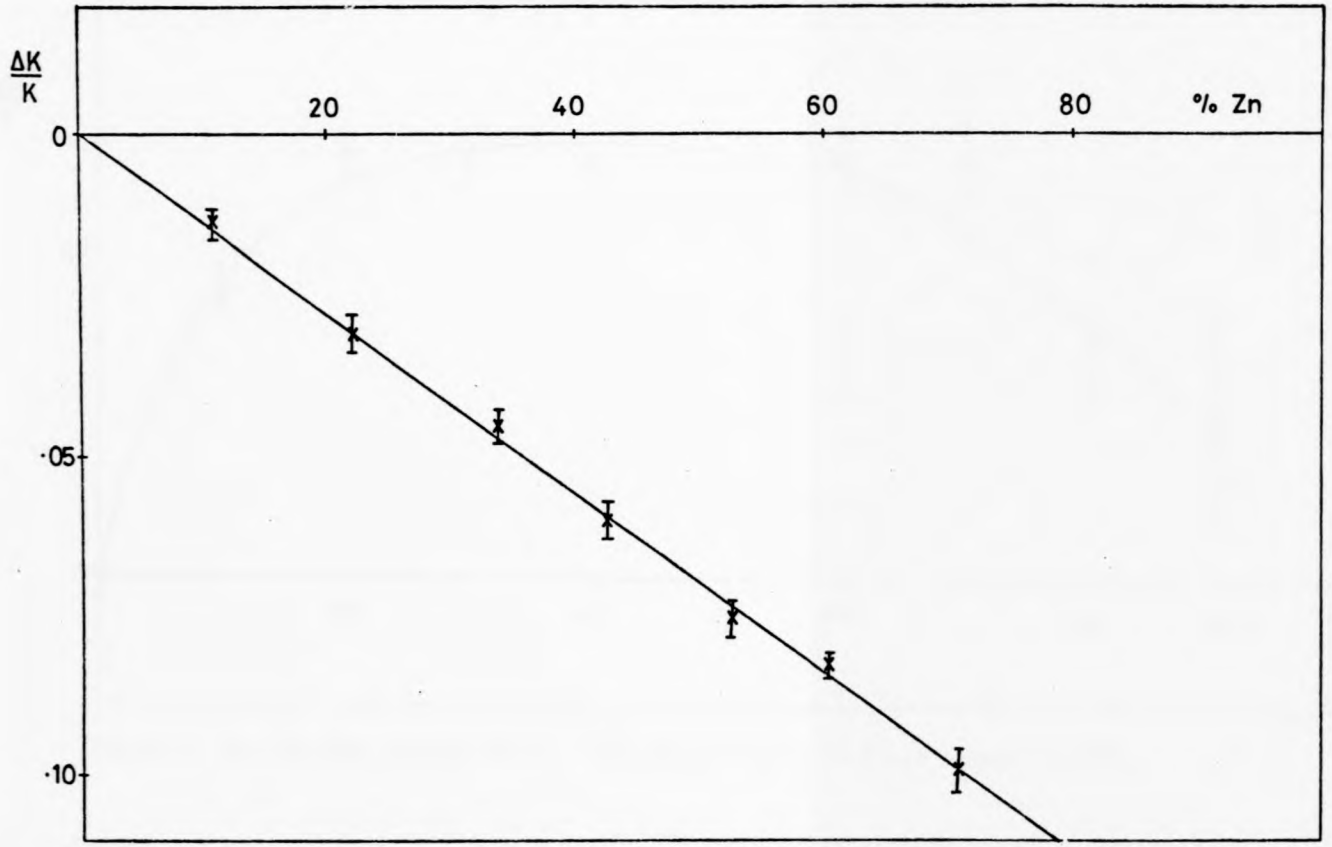

Fig.3.1. The Relative Change of the ^{113}Cd Knight Shift in Cd-Zn Alloys at 67OK.

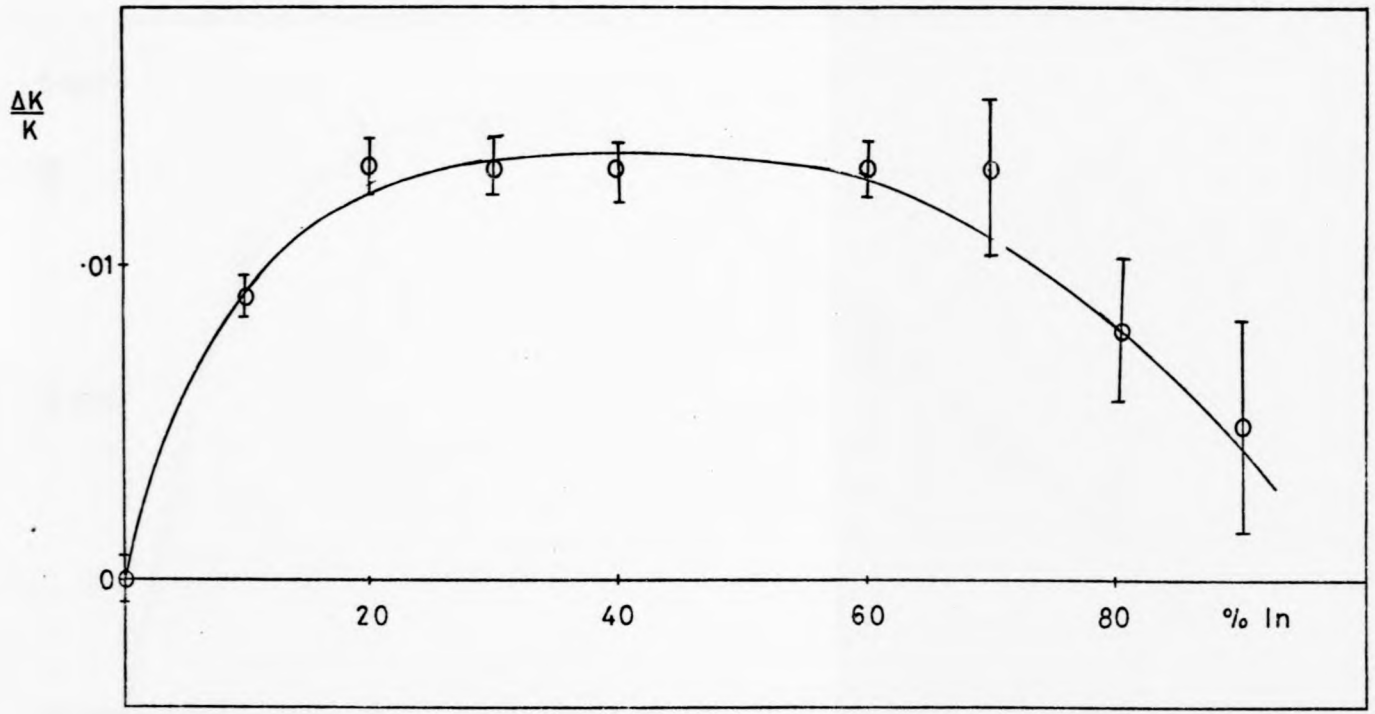

Fig.3.2. The Relative Change of the ^{113}Cd Knight Shift in Cd-In Alloys at 620K.

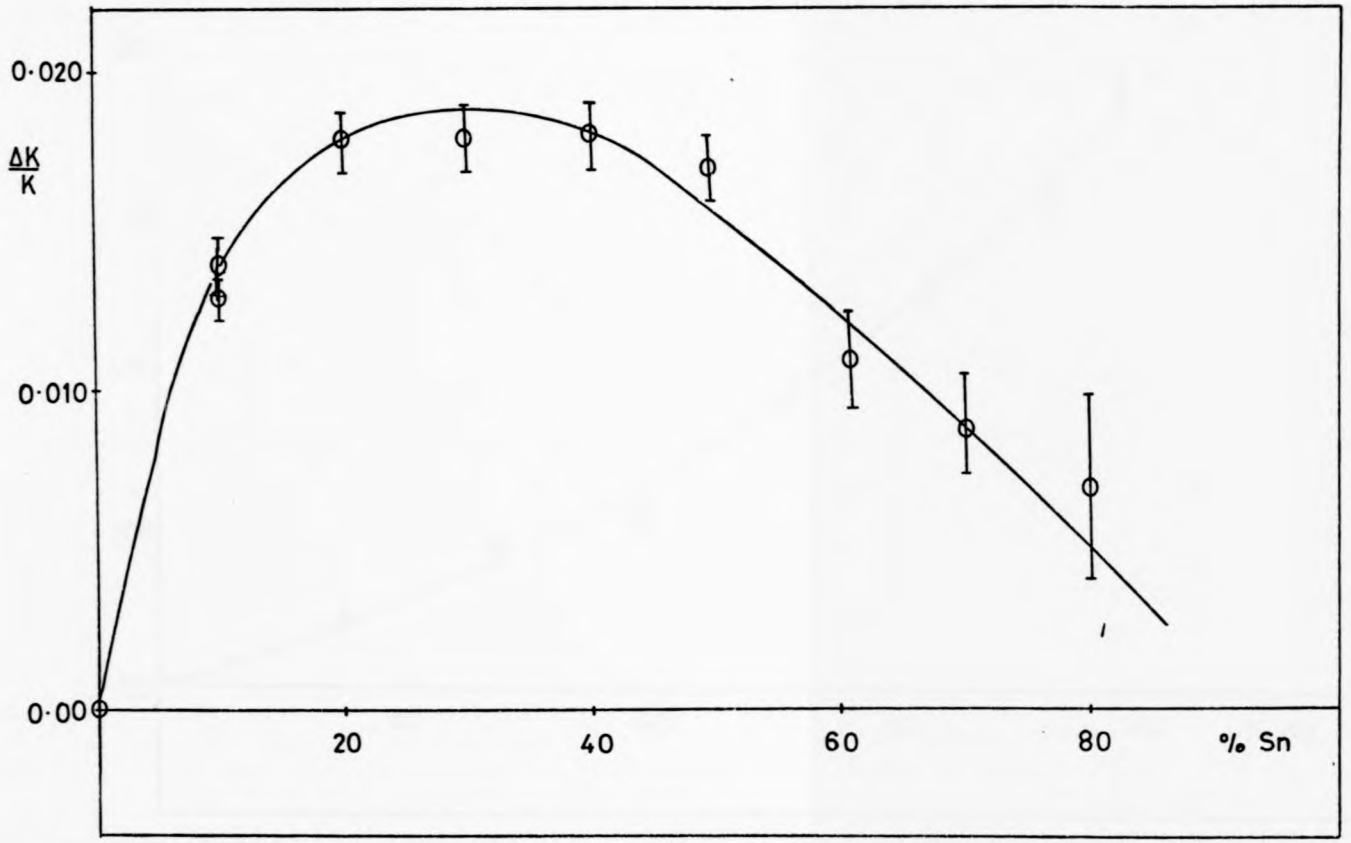

Fig.3.3. The Relative Change of the ^{113}Cd Knight Shift in Cd-Sn Alloys at 620K.

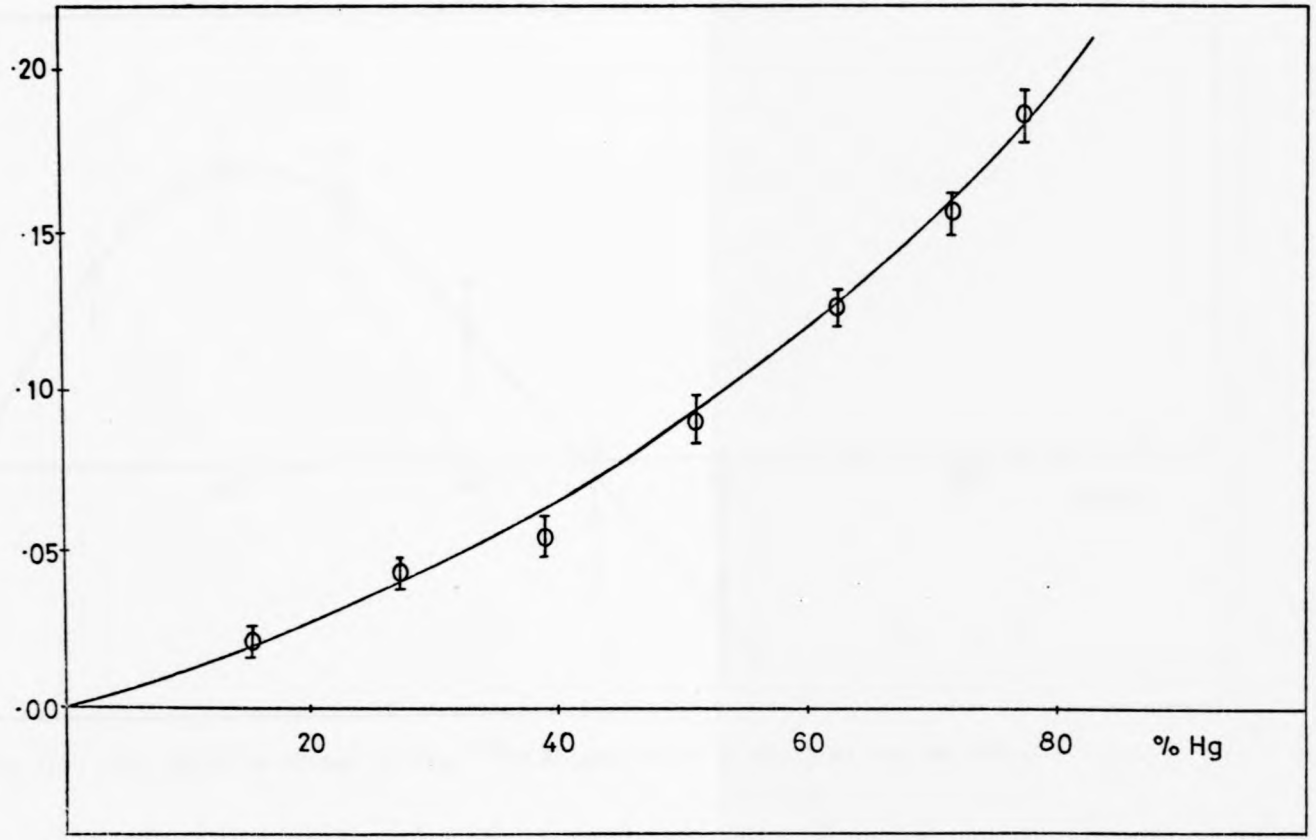

Fig.3.4. The Relative Change of the ^{113}Cd Knight Shift in Cd-Hg Alloys at 570K.

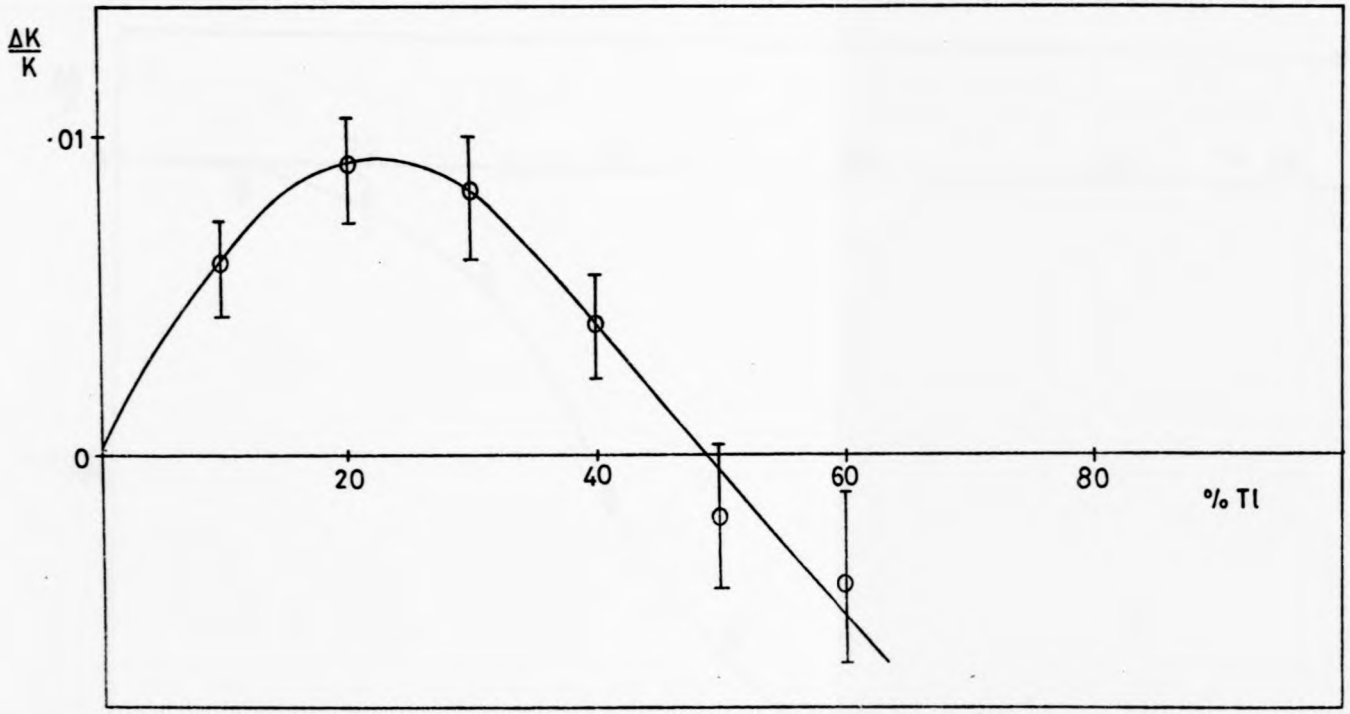

Fig.3.5. The Relative Change of the ^{113}Cd Knight Shift in Cd-Tl Alloys at 620K.

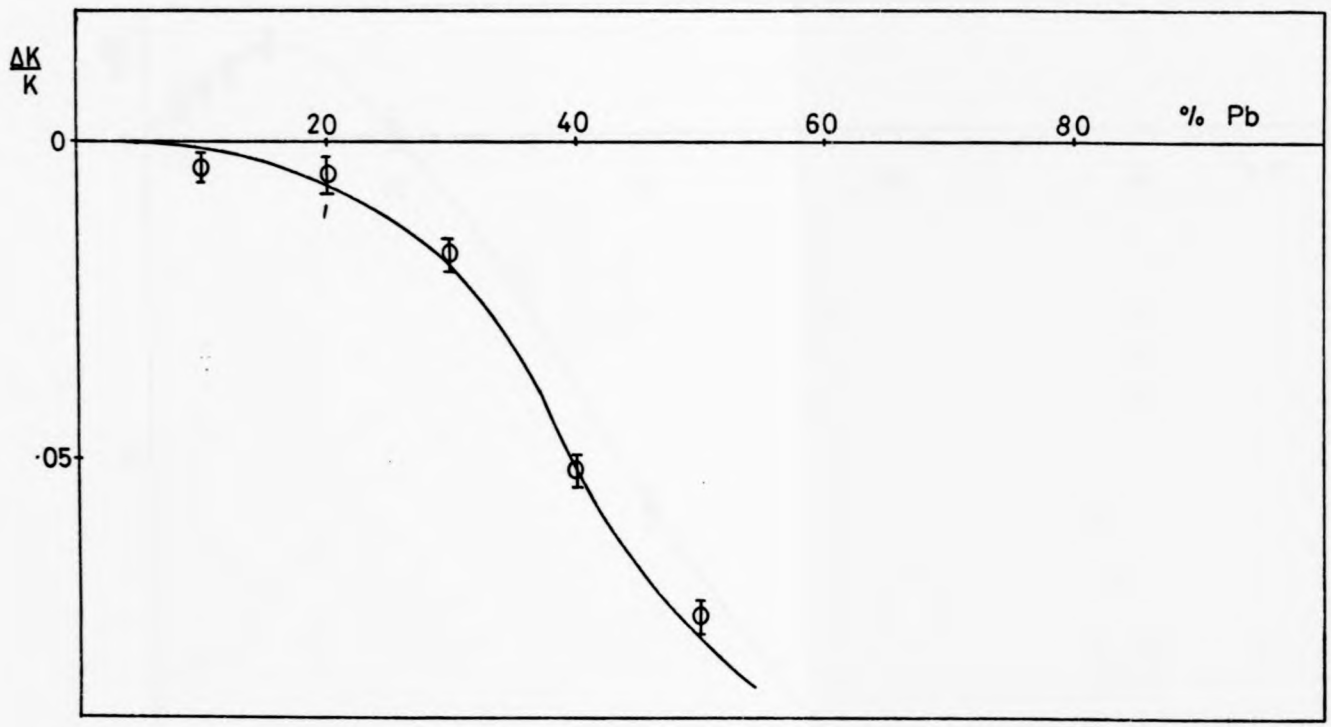

Fig.3.6. The Relative Change of the ^{113}Cd Knight Shift in Cd-Pb Alloys at 620K.

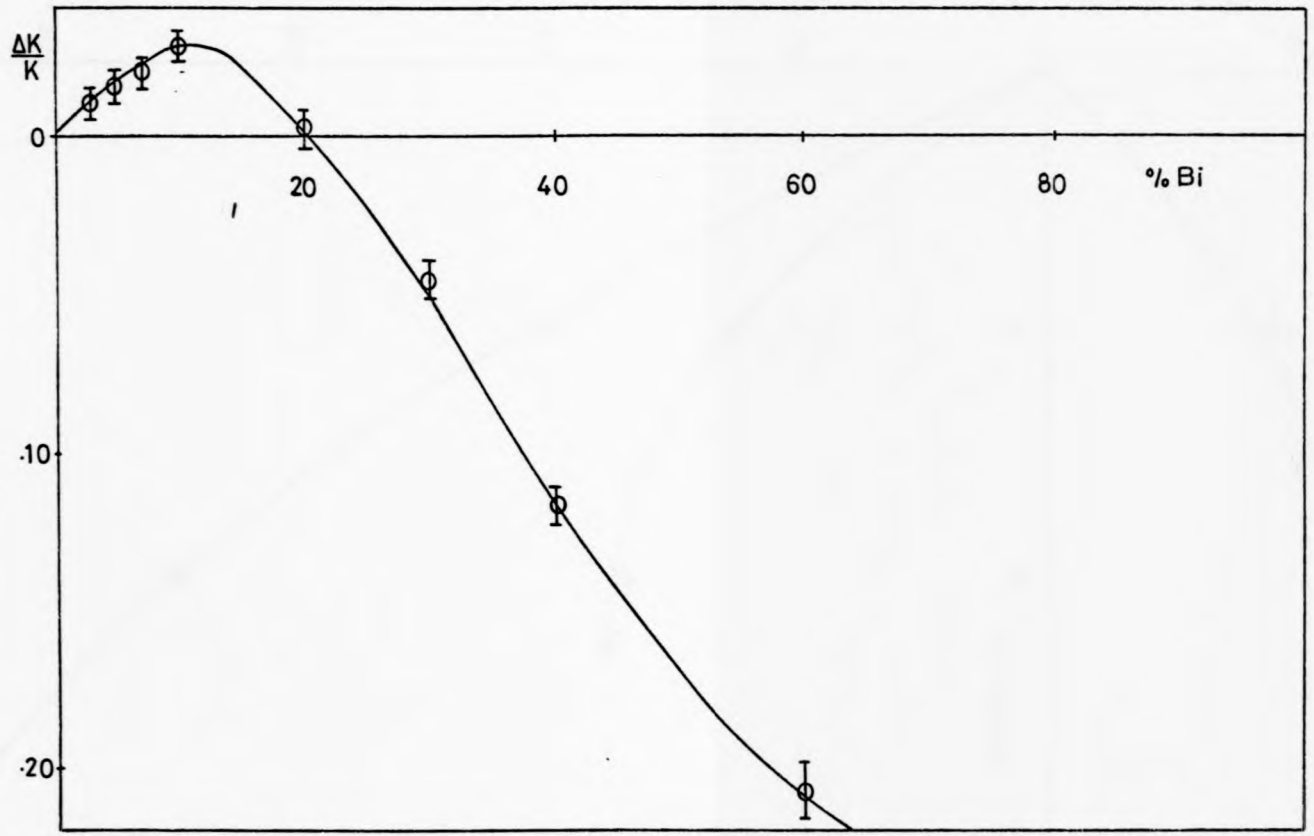

Fig.3.7. The Relative Change of the ^{113}Cd Knight Shift in Cd-Bi Alloys at 620K.

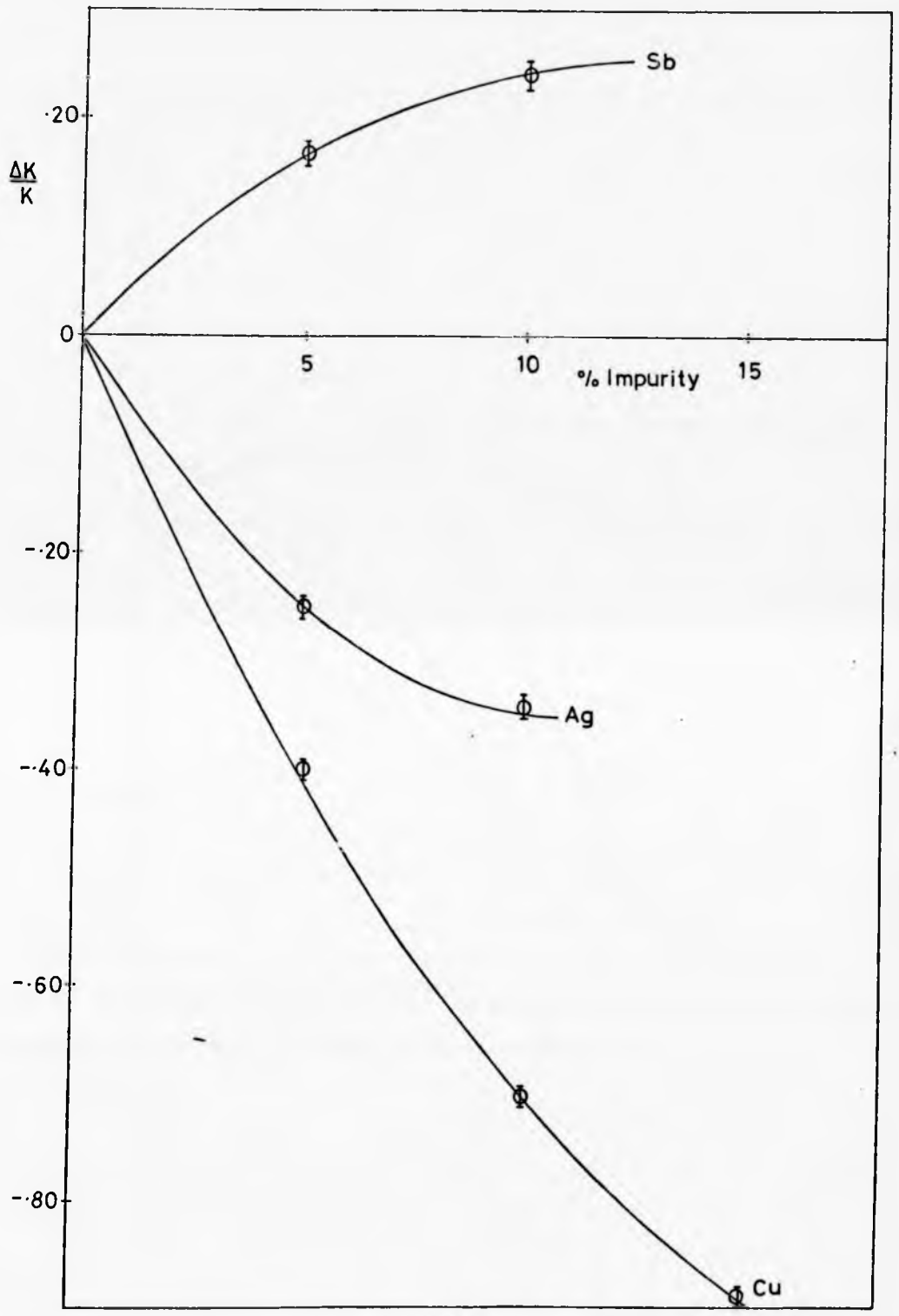

Fig.3.8. The Relative Change of the ^{113}Cd Knight Shift in Cd-Cu, Cd-Ag, and Cd-Sb Alloys at 670K.

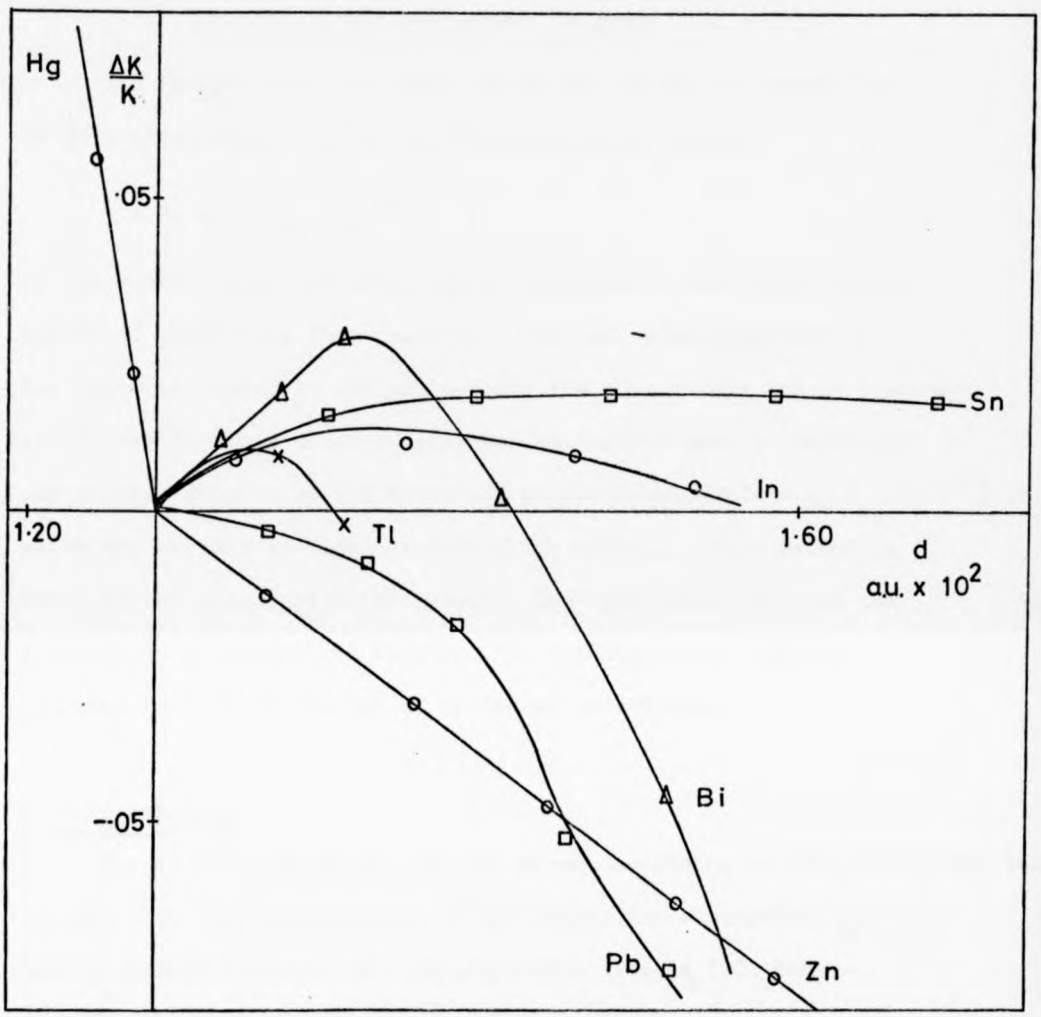

Fig.3.9. The Relative Change of the ^{113}Cd Knight Shift in Alloys with various Elements, as a Function of Conduction Electron Density, d.

CHAPTER 4

The Calculation of Contact Density

The Knight shift in simple metals and alloys is thought to be due, principally, to the contact interaction giving

$$K = \frac{8\pi}{3} \chi \left\langle |\psi_{k_F}(R_s)|^2 \right\rangle \quad , \tag{4.1}$$

so any quantitative understanding of the subject must start with a method of evaluating this quantity. The spin susceptibility, χ, has been calculated by various authors for most metals and is discussed in Chapter 5. This chapter describes the method used to calculate the contact density of the electrons at the Fermi surface, $\left\langle |\psi_{k_F}(R_s)|^2 \right\rangle$, where the average is taken over all like nuclei. This method is based on the pseudopotential concept, and essentially follows the formulation of Perdew and Wilkins (1), although their work is extended to include the use of non-local potentials.

4.1. Formulation

For an alloy of A- and B- type atoms, according to the pseudopotential concept (2), the wavefunctions of the conduction electrons, $\psi_k(r)$, can be written in terms of a pseudowavefunction, $\phi_k(r)$, thus:-

$$\psi_k(r) = \frac{1}{N^{\frac{1}{2}}} \left[\phi_k(\underline{r}) - \sum_{i,\alpha} \left\langle \alpha | \phi \right\rangle \psi_\alpha(\underline{r} - \underline{R}_i) \right] \quad , \tag{4.2}$$

where the ψ_α are the ionic core states of the particular ion at R_i and the summation is taken over all states of all ions. The Dirac notation is used for the overlap integrals between the pseudowavefunction and core state and the function normalised by the factor $N^{\frac{1}{2}}$.

As a first approximation the pseudowavefunction is taken to be a plane wave with wave vector k,

$$\phi_k(\underline{r}) = e^{i\underline{k}.\underline{r}} = \left\langle \underline{r} | \underline{k} \right\rangle \quad , \tag{4.3}$$

and the expression for the contact density at an A type ion at site $\underline{R}_s$ then becomes

$$|\Psi_k^A(\underline{R}_s)|^2 = \frac{1}{N_o}\left[1 - 2Re\sum_{i,\alpha}\langle\alpha|\underline{k}\rangle e^{i\underline{k}.\underline{R}_s}\,\Psi_\alpha(\underline{R}_s-\underline{R}_i) + \sum_{i,j}\sum_{\alpha\alpha'}\langle\alpha|\underline{k}\rangle\langle\underline{k}|\alpha'\rangle\Psi^*_\alpha(\underline{R}_s-\underline{R}_i)\,\Psi_{\alpha'}(\underline{R}_s-\underline{R}_i)\right]. \quad (4.4)$$

N_o is the normalisation factor appropriate to this approximation, and is made to unit volume, so that

$$N_o = 1 - \sum_{i,\alpha}|\langle\alpha|\underline{k}\rangle|^2 = 1 - \frac{1}{\Omega}\sum_{\alpha}|\langle\alpha|\underline{k}\rangle|^2 . \quad (4.5)$$

Ω is the ionic volume, so there are $1/\Omega$ ions to orthogonalise to.

The ion cores are assumed not too overlap so that $\Psi_\alpha(\underline{R}_s-\underline{R}_i)$ is zero for all ions not at R_s and the expression 4.4 reduces to

$$|\Psi^A(R_s)|^2 = \frac{1}{N_o}\left[1 - \sum_\alpha\langle\alpha^A|\underline{k}\rangle\Psi_\alpha(0)\right]^2 \equiv \frac{\gamma^2(k)}{N_o}$$

where (4.6)

$$\langle\alpha^A|\underline{k}\rangle = \int\Psi^{A*}_\alpha(\underline{r}-\underline{R}_s).e^{i\underline{k}.(\underline{r}-\underline{R}_s)}d(\underline{r}-\underline{R}_s)$$

which will be the same for all A-type ions. It may also be noted that the summation need only extend over s-states as $\Psi_\alpha(0)$ is zero otherwise.

More realistically the pseudowavefunction is given as a sum of plane wave states, and in a liquid, where there are no symmetry restrictions, this sum must extend throughout phase space. This mixing of states is regarded as being due to a small perturbing potential, the pseudopotential U, and the using first order perturbation theory we obtain

$$\Phi_k(\underline{r}) = e^{i\underline{k}.\underline{r}} + \sum_{k'}\frac{\langle\underline{k}|U|\underline{k}'\rangle}{E_{\underline{k}} - E_{\underline{k}'}}\,e^{i\underline{k}'.\underline{r}} . \quad (4.7)$$

Because of the high density of states in any macroscopic sample, the sum can be reduced to an integral throughout phase space so that

$$\Phi_k(\underline{r}) = e^{i\underline{k}.\underline{r}} + \int f(\underline{q}) e^{i(\underline{k}+\underline{q}).\underline{r}} d\underline{q} \qquad (4.8)$$

where $\underline{q} = \underline{k}' - \underline{k}$ (4.9)

and $$f(\underline{q}) = \frac{1}{(2\pi)^3} \frac{\langle \underline{k}+\underline{q}|U|\underline{k}\rangle}{E_{\underline{k}} - E_{\underline{k}+\underline{q}}} \qquad (4.10)$$

which leads to an expression for the contact density for an A-type ion at site R_s of the form

$$|\Psi_k^A(R_s)|^2 = \frac{1}{N}\left[\gamma_A^2(k) + 2\gamma_A(k)\,\mathrm{Re}\int f(\underline{q})\, e^{i\underline{q}.\underline{R}_s}\, \gamma(\underline{k}+\underline{q}).d\underline{q}\right]. \qquad (4.11)$$

To calculate the Knight shift, it is the contact density for electrons at the Fermi surface averaged over all like nuclei that is required i.e.

$$\left\langle |\Psi^A_{k_F}(\underline{R}_s)|^2 \right\rangle = \frac{1}{N_A}\sum_s^A |\Psi^A_{k_F}(\underline{R}_s)|^2 \qquad (4.12)$$

where the summation is carried out over the N_A sites of the A-type ions. In theory a further average should be made over all Fermi surface electrons but as the Fermi surface in a liquid is spherical this is unnecessary and our expression becomes

$$\left\langle |\Psi_A(\underline{R}_s)|^2 \right\rangle = \frac{1}{N}|\gamma_A(k)|^2 + \frac{2\gamma_A(k)}{N_A.N}\sum_s^A \mathrm{Re}\int f(\underline{q})\, e^{i\underline{q}.\underline{R}_s}\, \gamma(\underline{k}+\underline{q})d\underline{q}\ . \qquad (4.13)$$

A basic assumption of pseudopotential theory is that the pseudopotential, U, can be represented by a sum of the pseudopotentials, U_i, of the individual ions i.e.,

$$U = \sum_i U_i \qquad (4.14)$$

Because of the high density of states in any macroscopic sample, the sum can be reduced to an integral throughout phase space so that

$$\Psi_k(\underline{r}) = e^{i\underline{k}.\underline{r}} + \int f(\underline{q}) e^{i(\underline{k}+\underline{q}).\underline{r}} d\underline{q} \qquad (4.8)$$

where $\underline{q} = \underline{k}' - \underline{k}$ (4.9)

and $$f(\underline{q}) = \frac{1}{(2\pi)^3} \frac{\langle \underline{k}+\underline{q}|U|\underline{k}\rangle}{E_{\underline{k}} - E_{\underline{k}+\underline{q}}} \qquad (4.10)$$

which leads to an expression for the contact density for an A-type ion at site R_s of the form

$$|\Psi_k^A(R_s)|^2 = \frac{1}{N}\left[\gamma_A^2(k) + 2\gamma_A(k)\,\mathrm{Re}\int f(\underline{q})\, e^{i\underline{q}.\underline{R}_s}\, \gamma(\underline{k}+\underline{q}).d\underline{q}\right]. \qquad (4.11)$$

To calculate the Knight shift, it is the contact density for electrons at the Fermi surface averaged over all like nuclei that is required i.e.

$$\left\langle |\Psi^A_{k_F}(\underline{R}_s)|^2 \right\rangle = \frac{1}{N_A}\sum_s^A |\Psi^A_{k_F}(\underline{R}_s)|^2 \qquad (4.12)$$

where the summation is carried out over the N_A sites of the A-type ions. In theory a further average should be made over all Fermi surface electrons but as the Fermi surface in a liquid is spherical this is unnecessary and our expression becomes

$$\left\langle |\Psi_A(\underline{R}_s)|^2 \right\rangle = \frac{1}{N}|\gamma_A(k)|^2 + \frac{2\gamma_A(k)}{N_A.N}\sum_s^A \mathrm{Re}\int f(\underline{q})\, e^{i\underline{q}.\underline{R}_s}\, \gamma(\underline{k}+\underline{q})d\underline{q}\ . \qquad (4.13)$$

A basic assumption of pseudopotential theory is that the pseudopotential, U, can be represented by a sum of the pseudopotentials, U_i, of the individual ions i.e.,

$$U = \sum_i U_i \qquad (4.14)$$

Because of the high density of states in any macroscopic sample, the sum can be reduced to an integral throughout phase space so that

$$\Phi_k(\underline{r}) = e^{i\underline{k}.\underline{r}} + \int f(\underline{q}) e^{i(\underline{k}+\underline{q}).\underline{r}} d\underline{q} \qquad (4.8)$$

where $\underline{q} = \underline{k}' - \underline{k}$ (4.9)

and $$f(\underline{q}) = \frac{1}{(2\pi)^3} \frac{\langle \underline{k} + \underline{q} | U | \underline{k} \rangle}{E_{\underline{k}} - E_{\underline{k}+\underline{q}}} \qquad (4.10)$$

which leads to an expression for the contact density for an A-type ion at site R_s of the form

$$|\Psi_k^A(R_s)|^2 = \frac{1}{N} \left[\gamma_A^2(k) + 2\,\gamma_A(k)\,\mathrm{Re} \int f(\underline{q})\, e^{i\underline{q}.\underline{R}_s}\, \gamma(\underline{k}+\underline{q}).d\underline{q} \right] . \qquad (4.11)$$

To calculate the Knight shift, it is the contact density for electrons at the Fermi surface averaged over all like nuclei that is required i.e.

$$\left\langle |\Psi_{k_F}^A (\underline{R}_s)|^2 \right\rangle = \frac{1}{N_A} \sum_s^A |\Psi_{k_F}^A (\underline{R}_s)|^2 \qquad (4.12)$$

where the summation is carried out over the N_A sites of the A-type ions. In theory a further average should be made over all Fermi surface electrons but as the Fermi surface in a liquid is spherical this is unnecessary and our expression becomes

$$\left\langle |\Psi_A(\underline{R}_s)|^2 \right\rangle = \frac{1}{N} |\gamma_A(k)|^2 + \frac{2\gamma_A(k)}{N_A.N} \sum_s^A \mathrm{Re} \int f(\underline{q})\, e^{i\underline{q}.\underline{R}_s}\, \gamma(\underline{k}+\underline{q}) d\underline{q} \; . \qquad (4.13)$$

A basic assumption of pseudopotential theory is that the pseudopotential, U, can be represented by a sum of the pseudopotentials, U_i, of the individual ions i.e.,

$$U = \sum_i U_i \qquad (4.14)$$

so that

$$\left\langle \underline{k+q} \middle| U \middle| \underline{k} \right\rangle = \int d\underline{r}\; e^{i(\underline{k}+\underline{q})\cdot\underline{r}} \sum_i U_i\; e^{i\underline{k}\cdot\underline{r}}$$

$$= \sum_i e^{-i\underline{q}\cdot\underline{R}_i} \int d\underline{r} \left[e^{i(\underline{k}+\underline{q})\cdot(\underline{r}-\underline{R}_i)}\; U_i\; e^{i\underline{k}\cdot(\underline{r}-\underline{R}_i)} \right]$$

$$= \sum_i e^{-i\underline{q}\cdot\underline{R}_i} \left\langle \underline{k+q} \middle| U_i \middle| \underline{k} \right\rangle \qquad (4.16)$$

The single ion matrix elements are functions of both $\underline{q}$ and $\underline{k}$. However, in an isotropic medium, such as a liquid metal, we may define the angular part of $\underline{q}$ with respect to $\underline{k}$ and the value of the matrix element will be entirely independent of the direction of $\underline{k}$. The matrix elements for all electrons with Fermi wave vector k_F are then described by a single function of $\underline{q}$ referred to as the form factor, $U_i(\underline{q})$.

$$U_i(\underline{q}) = \left\langle \underline{k_F+q} \middle| U_i \middle| \underline{k_F} \right\rangle \qquad (4.17)$$

This is true whatever form the quantum mechanical operator may take. If U_i is a local potential, i.e. described by a simple function of position,

$$\left\langle \underline{k+q} \middle| U_i \middle| \underline{k} \right\rangle = \int e^{-i(\underline{k}+\underline{q})\cdot(\underline{r}-\underline{R}_i)}\; U_i\; e^{i\underline{k}\cdot(\underline{r}-\underline{R}_i)}\; d\underline{r}$$

$$= \int e^{-i\underline{q}\cdot(\underline{r}-\underline{R}_i)}\; U_i\; d\underline{r} \qquad (4.18)$$

which is entirely independent of $\underline{k}$, and in an isotropic medium is a function of the magnitude of $\underline{q}$ only. This approximation was used by Perdew and Wilkins (1) and in similar calculation for the polyvalent metals by Host, and Ford and Styles (6,7). However, this local approximation is not used here and substitution of the form factor into eq.4.13 yields

$$\left\langle \left| \Psi_A(\underline{R}_s) \right|^2 \right\rangle = \frac{1}{N} \left| \gamma_A(k) \right|^2 + \frac{1}{N_A} \cdot \frac{1}{N} \frac{2\gamma_A(k)}{(2\pi)^3} \sum_s^A \mathrm{Re} \int d\underline{q} \sum_i \frac{e^{i\underline{q}(\underline{R}_s-\underline{R}_i)} U_i(\underline{q}) \gamma(\underline{k+q})}{E_{\underline{k}} - E_{\underline{k+q}}} \qquad (4.19)$$

For a binary alloy containing A-type and B-type ions the double sum,

$$\frac{1}{N_A} \sum_s \sum_i e^{i\underline{q}.(\underline{R}_s - \underline{R}_i)} U_i(\underline{q}),$$

can be divided into three parts. The first part involves the A-type ion at the site R_s, the second involves all other A-type ions, and the third involves the B-type ions. Thus

$$\frac{1}{N_A} \sum_s^A \sum_i e^{i\underline{q}.(\underline{R}_s - \underline{R}_i)} U_i(\underline{q}) = \frac{1}{N_A} \sum_s^A U_A(\underline{q}) + \frac{1}{N_A} \sum_s^A U_A(\underline{q}) \sum_i^A e^{i\underline{q}.(\underline{R}_s - \underline{R}_i)} + \frac{1}{N_A} \sum_s^A U_B(\underline{q}) \sum_i^B e^{i\underline{q}.(\underline{R}_s - \underline{R}_i)} \qquad (4.20)$$

The sums over i are precisely those which appear in the partial structure factors S_{AB} where

$$S_{AB}(q) = \frac{N_A N_B}{N_A + N_B} \sum_i e^{i(\underline{R}_s - \underline{R}_i).q}$$

so that the expression 4.20 can be written as

$$U_A(\underline{q}) + C_A \left[S_{AA}(q) - 1 \right] U_A(\underline{q}) + C_B S_{AB}(q) U_B(\underline{q}) \qquad (4.21)$$

where C_A and C_B are the concentrations of the constituents. If we assume that the alloy is perfectly substitutional, it may be described by a single structure factor S(q) where

$$S(q) = S_{AA}(q) = S_{BB}(q) = S_{AB}(q) + 1 = S_{BA}(q) + 1 \qquad (4.22)$$

and in this approximation eq. 4.19 can be written

$$\left\langle |\Psi_A(R_s)|^2 \right\rangle = \frac{|\gamma_A(k)|^2}{N_o} \left[\frac{1 + \Sigma + \Delta}{1 + \frac{\delta N}{N_o}} \right] \qquad (4.23)$$

where

$$\Sigma = \frac{2}{\gamma_A(k).(2\pi)^3} \int \frac{U_A(\underline{q}).\gamma_A(\underline{k}+\underline{q}).d\underline{q}}{E_{\underline{k}} - E_{\underline{k}+\underline{q}}} \qquad (4.24)$$

and

$$\Delta = \frac{2}{\gamma_A(k).(2\pi)^3} \int \frac{d\underline{q}\left(C_A U_A(\underline{q}) + C_B U_B(\underline{q})\right)(S(q)-1).\gamma(\underline{k}+\underline{q})}{E_{\underline{k}} - E_{\underline{k}+\underline{q}}} \qquad (4.25)$$

The normalisation has been written in terms of the normalisation of a single O.P.W., N_o, and a small correction δN.

For a pure metal

$$\delta N = \frac{1}{\Omega} \frac{2}{(2\pi)^3} \int \frac{s(q).U(\underline{q}) \sum_\alpha \langle \alpha | k \rangle \langle k+q | \alpha \rangle}{E_{\underline{k}} - E_{\underline{k}+\underline{q}}} \qquad (4.26)$$

and as this is a very small correction. Perdew and Wilkins assumed that the normalisation for an alloy could be obtained by a linear interpolation between the pure metal values and this procedure has been carried out in the present calculations.

The expressions 4.22 to 4.26 are exactly the same as Perdew and Wilkin's. The self term, Σ, is the first order correction to the contract density of a particular ion due to its own pseudopotential while Δ, (the distinct term) is the correction due to all other ions. In the present calculations the terms are further divided into local and nonlocal terms. This is possible because the pseudopotential used can be written simply as a sum of two terms

$$U_A(\underline{q}) = U_A^L(q) + U_A^{NL}(\underline{q}) \qquad (4.27)$$

Thus we can write

$$\Sigma = \Sigma_{\text{local}} + \Sigma_{\text{nonlocal}} \qquad (4.28)$$

where

$$\Sigma_{\text{local}} = \frac{2}{\gamma_A(k).(2\pi)^3} \int \frac{U_A^L(q).\gamma(\underline{k}+\underline{q})\ d\underline{q}}{E_{\underline{k}} - E_{\underline{k}+\underline{q}}} \qquad (4.29)$$

and

$$\Sigma_{\text{nonlocal}} = \frac{2}{\gamma_A(k).(2\pi)^3} \int \frac{U_A^{NL}(q).\gamma(\underline{k}+\underline{q})\, d\underline{q}}{E_{\underline{k}} - E_{\underline{k}+\underline{q}}} \qquad (4.30)$$

and similar equations exist for the distinct term.

This is particularly useful as the local part of the pseudopotential can be taken out as a constant factor when the angular integrals of eq.4.29 are performed. Of course the angular contributions to the pseudopotential still have to be calculated when performing the angular integration of eq.4.30 but since calculation of the nonlocal contribution requires very much less computer time than the calculation of the local part this is less important.

4.2. Model Potential

The principal quantity required in the above formalism is the single ion pseudopotential U_i which can be shown to be related to the true potential, V(r),

$$U_i(r) = V(r) + \sum_{\alpha} (E - E_\alpha) \, |\alpha\rangle\langle\alpha| \qquad (4.31)$$

where E_α are the energies of the core states $|\alpha\rangle$, and E is the energy of the conduction electron state. It is immediately apparent that this is energy dependant, as E appears on the R.H.S. of this equation, and it is also non-local as the second term is a quantum mechanical operator envolving an integral over all space. As discussed in Chapter 1 there are difficulties in solving this equation and there are various alternative methods used to obtain U_i.

4.2.1. Optimised Model Potential

In this work the optimised model potential (OMP) as proposed by Shaw (4) is used for U_i. This has the advantage over the Ashcroft potential (3) used by Perdew and Wilkins (1), Host and Styles (5) and,

Ford and Styles (7), in that it is intrinsically both nonlocal and energy dependent and is more fundamental than many other model potentials as it is not determined from any experimentally observed property of the solid or liquid state. Furthermore it has been found reliable for calculating other electronic properties of metals (8).

As in all model potential theories, the potential is regarded as being due to a combination of the bare ion potential and the self consistent potential of all the other other electrons. Here the bare ion potential is defined by the equation

$$U_o(r) = -\frac{Z}{r} - \sum_{\ell=0}^{\ell_o} \Theta(R_\ell - r)(A_\ell - \frac{Z}{r})\hat{P}_\ell$$

$$\Theta(r) = 1 \quad r > 0$$

$$= 0 \quad r < 0 \ . \qquad (4.32)$$

$\hat{P}_\ell$ is an operator which picks out the ℓ^{th} angular momentum component of the conduction electron wave function, thus this component experiences a potential of constant depth, A_ℓ, inside a radius R_ℓ, and the true, Coulombic, potential outside this region. The second term is nonlocal because it is a function of ℓ as well as r and it should be noted that the summation only extends to ℓ_o, the highest value of the angular momentum of the core states. Shaw (4) argues that for higher angular momentum components no nodes exist in the true wave function of the conduction electron, so there is no necessity to model the true potential.

In general both A_ℓ and R_ℓ depend on ℓ but they are related by the optimisation condition,

$$A_\ell = \frac{Z}{R_\ell} \ . \qquad (4.33)$$

Z is the ion valency. This ensures that the potential is continuous, which was not done for previous model potentials (3,9,10). Consequently they exhibited non-physical oscillations in their form factors at large q. This condition also ensures the smoothest possible model wavefunction, which should therefore be readily calculated by a perturbation expansion of plane waves. The evaluation of these parameters is discussed in section 4.2.2. The evaluation of the self consistent electron potential is discussed in section 4.2.3.

The formalism of section 4.1. relies on the real wavefunction and pseudowavefunction being related by the expression

$$\Psi(r) = (1 - \hat{P})\, \Phi_p(r)$$

which allows the Schroedinger equation to be rewritten in terms of the pseudowavefunction (2)

$$(H + U_p) \left| \Phi_p \right\rangle = E \left| \Phi_p \right\rangle \quad , \tag{4.34}$$

thus defining the pseudopotential, U_p. The derivation of the model potential method is rather different, starting with the model potential U_m and so defining the model wave function by

$$(H + U_m) \left| \Phi_m \right\rangle = E \left| \Phi_m \right\rangle \quad . \tag{4.35}$$

The relationship between these two methods has been thoroughly discussed by Shaw (4) who shows one cannot rigorously go on to relate the true and model wavefunctions by

$$\Psi(r) = (1 - \hat{P})\, \Phi_m(r) \quad . \tag{4.36}$$

However, outside the core, both the model and pseudowave functions are equal to the true wave functions. If we then compare the model and pseudowave functions we have two smoothly varying functions which are equal between the cores. It therefore seems we shall not make any great error by approximating the pseudowave by the model wave and thus applying the projection operator to find the true wavefunction.

4.2.2. Determination of Model Potential Parameters

A full description of the procedure for determining the model potential parameters is given in Shaw's thesis (4). They are chosen in order to obtain the smoothest possible model wavefunction, which when substituted into equation 4.35,

$$(H + U_m) \left| \Phi_m \right\rangle = E \left| \Phi_m \right\rangle \quad ,$$

will give the true energy of the state associated with $\left| \Phi_m \right\rangle$.

For the free ion the $A_\ell(E)$ can be found exactly at the term values. The electron-wave functions are Whittaker functions outside the core region and Bessel functions inside, so the A_ℓ and R_ℓ are adjusted until the logarithmic derivatives of the solutions in the two regions match at the boundary. With A_ℓ and R_ℓ related by the optimisation condition there are still several possible A_ℓ corresponding to the internal solutions having different numbers of nodes. The solution with no nodes is chosen. The points on a graph of A_ℓ against E for different term values are found to lie on a straight line and the A_ℓ for intermediate values are assumed to lie on this line.

The extension of this method to metals is shown by Shaw to be valid as long as the real potential, due to the electrons and other ions, is constant over the ionic volume. For calculations of Knight shifts we require the values of A_ℓ at the Fermi level, E_F, so these are obtained by interpolation, (or in some cases extrapolation) between the free ion $A_\ell(E)$. The potential is thus intrinsically energy dependent as required.

Model potential parameters, for a large number of metals have been calculated in this way by Ese and Reissland (11). The Fermi level is calculated to take account of electron-electron and electron-ion effects, the latter being dependent on R_ℓ .They have therefore applied

an iterative process until a consistent R_ℓ , A_ℓ and E_F, have been found and these were used in the present calculations. The values $\partial A_\ell/\partial E$ are also given in the above paper and the values of A_ℓ in the present alloys were calculated by assuming that changes of E_F with alloy concentration were entirely due to changes in $\hbar k_F^2/2m$, where k_F is calculated using the free electron model.

4.2.3. Screening of the Model Potential

In order to evaluate the form factors, $U_i(q)$, we must now include the self consistent field of the electrons, and again following Shaw (4) we first find an expression for the electron density n(r). Outside the cores, the model and the real wavefunction are equal so we can write

$$n(r) = |\Phi(r)|^2 \quad R_A - r > 0. \tag{4.37}$$

Inside the core there will generally be some difference between n(r) and $|\Phi(r)|^2$ and this will be referred to as the depletion hole. Shaw shows that if this difference is considered to be entirely concentrated at points at the ion centres, this depletion hole, ρ, can be found in terms of the model wavefunction and model potential only.

Specifically

$$\rho = \sum_{k<k_F} \int d^3r \, \Phi_k^*(r) \, \frac{\partial U(E_k)}{\partial E_k} \, \Phi_k(r) \, . \tag{4.38}$$

The complete expression for the charge density in the metal is then

$$n(r) = |\Phi(r)|^2 + \rho \sum_i \delta(r - R_i) \tag{4.39}$$

where R_i specifies the centre of an ion. With the model wavefunction expressed to first order, the Fourier transform of the charge density n_q is found to be

$$n_{\underline{q}} = \frac{2}{\Omega} \sum_{\underline{k}<\underline{k}_F} \frac{\langle \underline{k}+\underline{q}| U|\underline{k}\rangle}{E_{\underline{k}} - E_{\underline{k}+\underline{q}}} + \frac{\rho}{\Omega} \; S(q). \tag{4.40}$$

S(q) is the structure factor introduced in equation 4.21 and Ω is the crystal volume. The self consistent potential V_{eq} can be related to this expression using Poissons equation which in the Fourier representation is

$$V_{eq} = \frac{4\pi n_{\underline{q}}}{q^2} \; . \tag{4.41}$$

The expression $\langle \underline{k}+q| U|\underline{k}\rangle$ in equation 4.40 which of course contains V_{eq}, may be written simply as $\langle \underline{k}+\underline{q}| U_o|\underline{k}\rangle + V_{eq}$, where U_o is the bare ion potential discussed in section 4.2.1., so that an explicit expression for V_{eq} can be obtained. The sum over states can be changed to an integral and in particular we note that

$$\sum_{k<k_F} \frac{1}{k^2 - |\underline{k}+\underline{q}|^2} \simeq P \int \frac{d^3k}{\underline{k}^2 - |\underline{k}+\underline{q}|^2} = \frac{\pi^2 q^4}{4} .(1-\epsilon(q)) \tag{4.42}$$

where the dielectric function

$$\epsilon(q) = 1 + \frac{1}{2\pi k_F \eta} \left[\frac{1-\eta^2}{2\eta} \log \left| \frac{1+\eta}{1-\eta} \right| + 1 \right] \tag{4.43}$$

and $\eta = q/2k_F$

giving

$$V_{eq} = \frac{S(q)}{\epsilon(q)} \left[\frac{4}{\pi^2 q^2} \int_{k<k_F} d^2k \; \frac{N\langle \underline{k}+\underline{q}| U_o|\underline{k}\rangle + \frac{4\pi\rho}{\Omega q^2}}{k^2 - |\underline{k}+\underline{q}|^2} \right] \tag{4.44}$$

Thus we can factor out the structure dependent term as was assumed in section 4.1. and the expression for the form factor becomes

$$U(\underline{q}) = N\langle \underline{k}+\underline{q}| U_o|\underline{k}\rangle + \frac{4\pi\rho}{\Omega q^2 \epsilon(q)} + \frac{4}{\pi^2 q^2 \epsilon(q)} \int \frac{d^3k \; N\langle \underline{k}+\underline{q}| U_o|\underline{k}\rangle}{k^2 - |\underline{k}+\underline{q}|^2} \; . \tag{4.45}$$

The bare ion potential can be expressed as two terms (eq.4.42)

$$N\langle \underline{k}+\underline{q}| U_o|\underline{k}\rangle = V_q + f(\underline{k},\underline{q}) \tag{4.46}$$

where

$$V_q = N \left\langle \underline{k}+\underline{q} \right| V_b \left| \underline{k} \right\rangle \tag{4.47}$$

is the local contribution and

$$f(\underline{k},\underline{q}) = -N \sum_{\ell=0}^{\ell_o} \left\langle \underline{k}+\underline{q} \right| \left[A_\ell(E)+V_b \right] P_\ell \left| \underline{k} \right\rangle \tag{4.48}$$

is the non-local contribution. Thus

$$U(\underline{q}) = \frac{V_q + V_{dq}}{\epsilon(q)} + f(k,q) + g(q) \tag{4.49}$$

where

$$V_{dq} = \frac{4\pi\rho}{\Omega q^2} \tag{4.50}$$

is the local potential due to the depletion hole and

$$g(q) = \frac{4}{\pi^2 q^2 \epsilon(q)} \int_{k<k_F} d^3k \quad \frac{f(\underline{k},\underline{q})}{k^2 - |\underline{k}+\underline{q}|^2} \tag{4.51}$$

is the screening of the nonlocal part of the bare potential.

It is important to realise, however, that g(q) is itself a local contribution to the form factor. This requires the major part of the computing time in calculating the form factor, and in the integrals involved in the calculation of the contact density it can be factored out of the angular part of the integration leaving only $f(\underline{k},\underline{q})$ to be evaluated as a function of angle. Without this simplification the calculations would have been intractable.

In this derivation no attempt has been made to take account of exchange or correlation. However, following Evans (13) this can be included in the Hubbard-Sham approximation to give,

$$U(\underline{q}) = \frac{V_q + \left(1 + \frac{q^2 \chi_q}{4\pi}\right) V_{dq}}{\epsilon^*(q)} + f(\underline{k},\underline{q}) + \left\{ 1 + \frac{q^2 \chi_q}{4\pi\epsilon^*(q)} \right\} g(q) \tag{4.52}$$

where

$$\chi_q = \frac{-2\pi}{q^2 + k_F^2 + k_{FT}^2} \quad ,$$

$$\epsilon^x(q) = \{\epsilon(q)-1\}\left(1+ \frac{q^2 \chi_q}{4\pi}\right) + 1,$$

and $$k_{FT} = \frac{12\pi Z}{\Omega k_F^2} \quad .$$

This expression for the model potential was used in all calculations.

4.3. Details of the Calculations

The basic expression to be evaluated is 4.23 with the correction terms divided into their local and non-local contributions

i.e. $$\left\langle \left| \psi_{k_F}(R_s) \right|^2 \right\rangle_A = \frac{|\gamma_A(k)|^2}{N_o} \left[\frac{1 + \Sigma_L + \Sigma_{NL} + \Delta_L + \Delta_{NL}}{(1 + \delta N/N_o)} \right] . \qquad (4.53)$$

The orthogonalisation factors $\gamma_A(k)$ can be expressed in terms of the wave functions of the ionic s-states and the plane wave states as

$$\gamma_A(k) = 1 - \sum_{ns} \psi^A_{ns}(0) \left\langle \psi^A_{ns} \middle| k \right\rangle . \qquad (4.54)$$

Similarly the normalisation coefficient is given by

$$N_o = \left(1 - \frac{1}{\Omega} \sum_{\alpha} \left| \left\langle \psi_\alpha \middle| k \right\rangle \right|^2 \right) , \qquad (4.55)$$

except that here the sum extends over all core states.

To evaluate the correction terms it is convenient to separate them into radial and angular integrals. For the local contributions we write

$$\Sigma_L = \frac{4}{(2\pi)^2} \int U_A^L(q) \quad \Gamma_A(k,q)\, dq \qquad (4.56)$$

and

$$\Delta_L = \frac{4}{(2\pi)^2} \int (C_A\, U_A^L(q) + C_B\, U_B^L(q))\, \Gamma_A(k,q)\, (S(q)-1)\, dq \qquad (4.57)$$

where

$$\Gamma_A(k,\underline{q}) = \frac{q^2}{2} \frac{1}{2\pi\, \gamma_A(k)} \; P \int \frac{d\hat{q}\, \gamma\, (\underline{k} + \underline{q})}{E_{\underline{k}} - E_{\underline{k}} + \underline{q}} \qquad (4.58)$$

and $d\hat{q}$ refers to an integration over the angular part of q only. Both of these radial integrals have a weak singularity at $q = 2\, k_F$, and, in order to treat this in a consistent way, the integration is performed over a dimensionless variable $x = q/2k_F$. Thus we write

$$\Sigma_L = 2 \int V_A^L(q)\, \Gamma_A(k,q)\, dx. \qquad (4.59)$$

$$\Delta_L = 2 \int (C_A\, V_A^L + C_B\, V_B^L)\, \Gamma_A(k,q)(S(q)-1)\, dx \qquad (4.60)$$

where

$$V_A^L = \frac{k_F\, U_A^L(q)}{\pi^2} = \frac{Z^*\, U_A^L(q)}{2/3\, E_F\, \Omega} \qquad (4.61)$$

is a dimensionless pseudopotential and Z* is the average valency of the ions in the alloy.

For the non local terms the pseudopotential must be included in the angular integrals. Functions Λ_A and Λ_B are defined such that

$$\Lambda_A = \frac{q^2}{2} \frac{1}{2\pi\, \gamma_A(k)} \; P \int \frac{d\hat{q}\, V_A^{NL}(\underline{q})\, \gamma_A\, (\underline{k} + \underline{q})}{E_{\underline{k}} - E_{\underline{k}} + \underline{q}} \qquad (4.62)$$

and

$$\Lambda_B = \frac{q^2}{2} \frac{1}{2\pi\, \gamma_A(k)} \; P \int \frac{d\hat{q}\, V_B^{NL}(\underline{q})\, \gamma_A\, (\underline{k} + \underline{q})}{E_{\underline{k}} - E_{\underline{k}} + \underline{q}} \qquad (4.63)$$

giving

$$\Sigma_{NL} = 2x \int \Lambda_A\, dx \qquad (4.64)$$

and

$$\Delta_{NL} = 2x \int (C_A \Lambda_A + C_B \Lambda_B)\ (S(q)-1)\ dx \qquad (4.65)$$

The evaluation of each of these functions is discussed in detail in the following sections.

4.3.1. Overlap Integrals

These are evaluated by expressing both the ionic core states and the plane wave states in terms of spherical harmonics, i.e.

$$\Psi_{n\ell m} = \frac{P_{n\ell}}{r} Y_{\ell m}(\theta,\Phi) \qquad (4.66)$$

and

$$e^{i\underline{k}.\underline{r}} = 4\pi \sum_{\ell,m} i^{\ell}\ j_{\ell}(kr)\ Y^{*}_{\ell m}(\hat{k})\ Y_{\ell m}(\hat{r}). \qquad (4.67)$$

The overlap integral can then be expressed as

$$\left\langle \Psi_{n\ell m} \middle| \underline{k} \right\rangle = \int \frac{P^{*}_{n\ell}}{r}(r)\ Y^{*}_{\ell m}(\theta,\Phi).4\pi \sum_{\ell',m'} i^{\ell'}\ j_{\ell'}(kr)\ Y^{*}_{\ell' m'}(\hat{k})\ Y_{\ell' m'}(\hat{r})\ d^3r. \qquad (4.68)$$

The orthogonality of the spherical harmonics causes the angular integrals of all terms where $\ell \neq \ell'$ or $m \neq m'$ to be zero and the integral can be written in the form

$$\left\langle \Psi_{n\ell m} \middle| k \right\rangle = i^{\ell}\ Y^{*}_{\ell m}(\hat{k})\ B_{n\ell}(k). \qquad (4.69)$$

where

$$B_{n\ell}(k) = \int_0^{\infty} P_{n\ell}(r)\ 4\pi r\ j_{\ell}(kr)\ dr. \qquad (4.70)$$

4.3.2. Othogonalisation Factors

Using the above expression for the overlap integrals and again dividing the core wave-function into angular and radial parts equation 4.54 becomes

$$Y_A(k) = 1 - \sum_{n\ell} Rn_{n\ell}(0)\ Y_{\ell m}(\theta,\Phi)\ i^{\ell}\ Y^{*}_{\ell m}(\hat{k})\ B_{n\ell}(k)\ . \qquad (4.71)$$

Since $$R_{n\ell}(r) = \frac{P_{n\ell}(r)}{r} \qquad (4.72)$$

is only non-zero for s-states ($\ell=0$), the expression finally becomes

$$\gamma_A(k) = 1 - \frac{1}{4\pi} \sum_n R_{no}(0)\, B_{no}(k). \qquad (4.73)$$

4.3.3. Angular Integrals: Local terms

With the above expression (4.73) for the orthogonalisation factors, substituted into the expression for the local angular integral (4.58) we obtain

$$\Gamma_A(k,q) = \frac{q^2}{2\pi} \cdot \frac{1}{2\gamma_A(k)} \; P \int \frac{1 - \frac{1}{4\pi} \sum_n R_{no}(0)\, B_{no}(|\underline{k}+\underline{q}|)}{E_{\underline{k}} - E_{\underline{k}+\underline{q}}} \, d\hat{q} \; . \qquad (4.74)$$

Since

$$|\underline{k} + \underline{q}|^2 = k^2 + q^2 - 2kqy \qquad (4.75)$$

where

$$y = -\hat{k}.\hat{q} = \cos\theta \; , \qquad (4.76)$$

we can write

$$E_{\underline{k}+\underline{q}} = (k^2 + q^2 - 2kqy)/2 \qquad (4.77)$$

and

$$\Gamma_A(k,q) = \frac{-q^2}{2\pi\, \gamma(k)} \; P \int \frac{d\hat{q} \left[1 - 1/4\pi \sum_n R_{no}(0)\, B_{no}\left((k^2 + q^2 - 2kqy)^{\frac{1}{2}}\right)\right]}{q^2 - 2kqy} \qquad (4.78)$$

The right hand side of this equation may be divided into two integrals;

$$I_1 = \frac{-q^2}{2\pi\, \gamma(k)} \; P \int \frac{d\hat{q}}{q - 2kqy} \qquad (4.79)$$

and

$$I_2 = \frac{+q^2}{2\pi\, \gamma(k)} \; P \int \frac{\sum_n \frac{1}{4\pi} R_{no}(0)\, B_{no}\left((k^2 + q^2 - 2kqy)^{\frac{1}{2}}\right)}{q^2 - 2kqy} \, d\hat{q} \qquad (4.80)$$

The first integral can be evaluated analytically to give

$$I_1 = \frac{-1}{\gamma(k)} \; \frac{q}{2k} \; \ell n \left| \frac{1 - q/2k}{1 + q/2k} \right| \qquad (4.81)$$

Since $$R_{n\ell}(r) = \frac{P_{n\ell}(r)}{r} \qquad (4.72)$$

is only non-zero for s-states ($\ell=0$), the expression finally becomes

$$\gamma_A(k) = 1 - \frac{1}{4\pi} \sum_n R_{no}(0)\, B_{no}(k). \qquad (4.73)$$

4.3.3. Angular Integrals: Local terms

With the above expression (4.73) for the orthogonalisation factors, substituted into the expression for the local angular integral (4.58) we obtain

$$\Gamma_A(k,q) = \frac{q^2}{2\pi} \cdot \frac{1}{2\gamma_A(k)} \; P \int \frac{1 - \frac{1}{4\pi} \sum_n R_{no}(0)\, B_{no}(|\underline{k}+\underline{q}|)}{E_{\underline{k}} - E_{\underline{k}+\underline{q}}} \, d\hat{q} \, . \qquad (4.74)$$

Since

$$|\underline{k} + \underline{q}|^2 = k^2 + q^2 - 2kqy \qquad (4.75)$$

where

$$y = -\hat{k}.\hat{q} = \cos\theta \, , \qquad (4.76)$$

we can write

$$E_{\underline{k}+\underline{q}} = (k^2 + q^2 - 2kqy)/2 \qquad (4.77)$$

and

$$\Gamma_A(k,q) = \frac{-q^2}{2\pi\, \gamma(k)} \; P \int \frac{d\hat{q} \left[1 - 1/4\pi \sum_n R_{no}(0)\, B_{no}((k^2 + q^2 - 2kqy)^{\frac{1}{2}})\right]}{q^2 - 2kqy} \qquad (4.78)$$

The right hand side of this equation may be divided into two integrals;

$$I_1 = \frac{-q^2}{2\pi\, \gamma(k)} \; P \int \frac{d\hat{q}}{q - 2kqy} \qquad (4.79)$$

and

$$I_2 = \frac{+q^2}{2\pi\, \gamma(k)} \; P \int \frac{\sum_n \frac{1}{4\pi} R_{no}(0)\, B_{no}((k^2 + q^2 - 2kqy)^{\frac{1}{2}})}{q^2 - 2kqy} \, d\hat{q} \qquad (4.80)$$

The first integral can be evaluated analytically to give

$$I_1 = \frac{-1}{\gamma(k)} \; \frac{q}{2k} \; \ell n \left| \frac{1 - q/2k}{1 + q/2k} \right| \qquad (4.81)$$

However, with the second integral expressed in spherical polar coordinates, with the z-axis defined along the vector $\underline{k}$, only the integral over Φ can be performed analytically giving

$$I_2 = \frac{1}{\gamma(k)} \; P \int \frac{1/4\pi \sum_n R_{no}(0)\; B_{no}\; ((k^2 + q^2 - 2kqy)^{\frac{1}{2}})}{\frac{2k}{q}\, y - 1}\, dy, \qquad (4.82)$$

where $\quad \mathrm{Sin}\theta \; d\theta = dy \qquad (4.83)$

follows immediately from the definition of y (4.76). This may be expressed in terms of an integral $C_o(n,k,q)$ so that

$$I_2 = - \frac{1}{\gamma(k)} \frac{1}{4\pi} \sum_n R_{no}(0).C_o(n,q,k) \qquad (4.84)$$

where

$$C_o = P \int_{-1}^{+1} \frac{dy \;\; B_{no}((k^2 + q^2 - 2kqy)^{\frac{1}{2}})}{\frac{2k}{q}\, y - 1} \qquad (4.85)$$

Thus

$$\Gamma_A(k,q) = \frac{1}{\gamma_A(k)} \left[\frac{q}{2k} \ell n \left| \frac{1 - q/2k}{1 + q/2k} \right| - \frac{1}{4\pi} \sum_n R_{no}(0).C_o(n,k,q) \right] \qquad (4.86)$$

The integral $C_o(n,k,q)$ must be evaluated numerically.

4.3.4. Angular Integrals: Non local Case

These differ from the local integrals in that the pseudo-potentials are included in the integrand, and using the definition of y given in the last section

$$\Lambda_A\,(k,q) = \frac{-q^2}{2\pi\gamma(k)} \; P \int \frac{d\hat{q}\; V_A^{NL}(\underline{q}) \left[1 - 1/4\pi \sum_n R_{no}(0)\; B_{no}\; ((k^2+q^2-2kqy)^{\frac{1}{2}}) \right]}{q^2 - 2kqy} \qquad (4.87)$$

Again splitting this up into two integrals and performing the integration over Φ we have

$$I_1 = \frac{-q^2}{\gamma(k)} \int \frac{dy \; V_A^{NL}\,(\underline{q})}{q^2 - 2kqy}$$

$$= \frac{1}{\gamma(k)} \; D_o^A\,(k,q) \qquad (4.88)$$

and

$$I_2 = \frac{-q^2}{\gamma(k)} \frac{1}{4\pi} \sum_n R_{no}(0)\, V_A^{NL}(\underline{q})\, B_{no}((k^2 + q^2 - 2kqy)^{\frac{1}{2}}) \Big/ q^2 - 2kqy$$

$$= \frac{-1}{\gamma(k)} \frac{1}{4\pi} \sum_n R_{no}(0)\, G_o^A(n,k,q) \quad , \tag{4.89}$$

where

$$D_o^A(k,q) = P \int_{-1}^{+1} \frac{dy\, V_A^{NL}(\underline{q})}{\frac{2ky}{q} - 1} \tag{4.90}$$

and

$$G_o^A(n,k,q) = P \int_{-1}^{+1} \frac{dy\, V_A^{NL}(\underline{q})\, B_{no}((k^2 + q^2 - 2kqy)^{\frac{1}{2}})}{\frac{2ky}{q} - 1} \quad . \tag{4.91}$$

Thus

$$\Lambda_A(k,q) = \frac{1}{\gamma(k)} \left(D_o^A(k,q) - \frac{1}{4\pi} \sum_n^A R_n(0)\, G_o^A(n,k,q) \right) \tag{4.92}$$

4.3.5. Normalisation Factor

In evaluating expression 4.55 we note that the second term contains a sum over i, which in a binary alloy, will contain N_A identical terms from overlap with A-type ion cores, and N_B identical terms from the overlap with the B-type ions. Writing the number of atoms in terms of the concentration of the species and the mean ionic volume of the alloy the second term becomes

$$\frac{1}{\Omega} \sum_{i\alpha} \left| \langle \psi_\alpha^i | \underline{k} \rangle \right|^2 = \frac{C_A}{\Omega} \sum_\alpha \left| \langle \psi_\alpha^A | \underline{k} \rangle \right|^2 + \frac{C_B}{\Omega} \sum_\alpha \left| \langle \psi_\alpha^B | \underline{k} \rangle \right|^2 \quad . \tag{4.93}$$

These can be expressed in terms of the integral $B_{n\ell}(k)$ defined in section 4.3.1 to give an expression for the normalisation factor

$$N_o = 1 - \frac{C_A}{\Omega} \sum_{n\ell}^A \frac{2\ell+1}{4\pi} B_{n\ell}^2(k) - \frac{C_B}{\Omega} \sum_{n\ell}^B \frac{2\ell+1}{4\pi} B_{n\ell}^2(k). \tag{4.94}$$

4.3.6. Normalisation Correction

As discussed in section 4.1 the normalisation correction is only evaluated for pure metals. Following the method used for the other correction terms, this is written in terms of a dimensionless pseudopotential and the integration divided into a radial and angular part to give

$$\delta N = -2P \int dx\ \Pi\ (k,q)\ S(q) \tag{4.95}$$

where

$$\Pi(k,q) = \frac{1}{\Omega} \sum_{n\ell m} \frac{1}{2\pi} \int V_A(\underline{q})\ \frac{\left\langle \underline{k}' \middle| \Psi_{n\ell m} \right\rangle \left\langle \Psi_{n\ell m} \middle| k \right\rangle}{E_{\underline{k}'} - E_{\underline{k}}}\ d\hat{q} \ . \tag{4.96}$$

Here we have written

$$\underline{k}' = \underline{k} + \underline{q} \ .$$

By expanding the wave functions as spherical harmonics as in section 4.3.3 this angular integral can be expressed in the form

$$\Pi(k,q) = \frac{1}{\Omega} \sum_{n\ell} \frac{2\ell+1}{4\pi}\ B_{n\ell}(k)\ C_\ell(n,k,q) \tag{4.97}$$

where

$$C_\ell(n,k,q) = P \int_{-1}^{+1} dy\ P_\ell\left(\frac{k-qy}{k'}\right) \frac{B_{n\ell}(k')}{\frac{2k}{q}\, y-1}\ V_A(\underline{q}) \ . \tag{4.98}$$

The P_ℓ are Legendre polynomials, and the $B_{n\ell}$ are the integrals defined in section 4.3.1.

4.3.7. Structure Factors

The structure factors are evaluated using the method put forward by Ashcroft and Lekner (14), which has been successful in describing other electronic properties of liquid metals. This is based on a hard sphere model, where the hard sphere diameter, σ, is related to the ionic density, n, by a packing fraction η, thus,

$$\sigma = \left(\frac{6\eta}{n\pi}\right)^{\frac{1}{3}} \equiv \frac{(18\pi\eta Z)^{\frac{1}{3}}}{k_F} \quad . \tag{4.99}$$

The structure factor is given as a function of $q\sigma$ by

$$S(q\sigma) = \left[1 - nc(q\sigma)\right]^{-1} \tag{4.100}$$

where

$$C(q\sigma) = -4\pi\sigma^3 \int_0^1 ds\, s^2 \, \frac{\sin(sq\sigma)}{sq\sigma} \, (\alpha + \beta s + \gamma s^3) \tag{4.101}$$

$$\alpha = (1 + 2\eta)^2/(1 - \eta)^4 \tag{4.102}$$

$$\beta = -6\eta(1 + \eta/2)^2/(1 - \eta)^4 \tag{4.103}$$

and

$$\gamma = \tfrac{1}{2}\eta(1 + 2\eta)^2/(1 - \eta)^4. \tag{4.104}$$

Ashcroft and Lekner found that a value of η=0.45 was appropriate for all liquid metals near the melting point, and this has been used throughout these calculations. This yields

$$S(q\sigma) = \left[1 + \frac{10.8}{(k\sigma)^3}\left(-13.59 - \frac{213.0}{(q\sigma)^2}\right)\right.$$

$$+ \left. -4.05q\sigma + \frac{17.96}{q\sigma} - \frac{213.0}{(q\sigma)^3}\right)\cos(q\sigma)$$

$$\left. + \frac{88.55}{q\sigma} + \frac{213.0}{(q\sigma)^3}\right]^{-1} \tag{4.105}$$

4.3.8. Form Factors

In evaluating the screened form factors equation 4.52 is written in a slightly different form.

$$U(\underline{q}) = \frac{Z^*}{\varepsilon^*(q)} - \frac{4\pi}{\Omega} F(\underline{k},\underline{q}) + \left(1 + \frac{q^2\chi_q}{4\pi e^*(q)}\right)\frac{\partial\varepsilon}{\partial e(q)} \, G(q) \tag{4.106}$$

where

$$Z^* = Z + \left(1 + \frac{q^2\chi_q}{4\pi}\right)\rho \tag{4.107}$$

$$G(q) = + \frac{\Omega}{32} q^2 \, \epsilon(q) \, g(q) \tag{4.108}$$

and the non local contribution

$$F(\underline{k},\underline{q}) = - \frac{\Omega}{4\pi} \, f(\underline{k},\underline{q}) \; . \tag{4.109}$$

ρ is the depletion hole given by equation 4.38 as

$$\rho = \sum_{k<k_F} \int d^3r \; \Phi_k^*(\underline{r}) \; \frac{\partial U(E_k)}{\partial E_k} \; \Phi_k(\underline{r}) \; . \tag{4.110}$$

Shaw shows that the energy derivative of the optimised potential can be written as

$$\frac{\partial U}{\partial E}(E) = \sum_{\ell=0}^{\ell_o} \frac{\partial A_\ell}{\partial E} \; \theta \, (R_\ell - r_i) \, \hat{P}_\ell \tag{4.111}$$

so if the pseudowave functions are treated as plane waves and expanded in spherical harmonics, and the summation over states converted to an integral in the usual way, we may obtain

$$\rho = \frac{4}{\pi} \sum_{\ell=0}^{\ell_o} (2\ell+1) \; \frac{\partial A_\ell}{\partial E} \int_o^1 x^2 \, dx \int_o^1 y^2 \, dy \left[k_F R_\ell(x)\right]^3 \; j_\ell{}^2 \left[k_F R_\ell(x) xy\right] . \tag{4.112}$$

The integration over y can be done exactly to yield

$$\rho = \frac{2}{\pi} \sum_{\ell=0}^{\ell_o} (2\ell+1) \; \frac{\partial A_\ell}{\partial E} \int_o^1 dx \; x^2 (k_F R_\ell)^3 \left[j_\ell^2(k_F R_\ell x) - j_{\ell-1}(k_F R_\ell x) \; j_{\ell+1}(k_F R_\ell x) \right] \tag{4.113}$$

which contains 1,2 or 3 integrals depending on the value of ℓ_o and may be written as

$$\rho = \frac{2}{\pi} \left(\frac{\partial A_o}{\partial E} \; I_o(k_F) + 3 \; \frac{\partial A_1}{\partial E} \; I_1(k_F) + 5 \; \frac{\partial A_2}{\partial E} \; I_2 \, (k_F) \right) \tag{4.114}$$

An expression for F can also be obtained by expanding the plane waves to give

$$F(\underline{k},\underline{q}) = \sum_{\ell=0}^{\ell_o} (2\ell+1) \; P_\ell \, (\mathrm{Cos}\theta) \; A_\ell(E) \; R_\ell^3 \, (E) \int_o^1 dx \; (x-1) \; j_\ell(kR_\ell x) \; j_\ell(kR_\ell x) \tag{4.115}$$

where $\underline{k}' = \underline{k} + \underline{q}$

and $\text{Cos}\theta = \dfrac{\underline{k}.\underline{k}'}{kk'}$.

From equation 4.51 we can deduce that

$$G(q) = \int_0^1 dx \int_0^{k_F} \frac{k^2\, dk\, F(k,q)}{q^2 + 2kqx} \,. \tag{4.116}$$

However it is convenient to evaluate this expression in terms of the deminsionless parameters

$$\eta = q/2k_F, \; z = \frac{k_Z}{k_F}, \; u = \frac{k_P}{k_F} \,, \tag{4.117}$$

where k_Z and k_P are the components of $\underline{k}$ along, and perpendicular to, $\underline{q}$ respectively. We can thus write

$$G(\eta) = \frac{k_F}{4\eta} \int_{-1}^{+1} \frac{dz}{z + \eta/2} \; g(z,\eta) \tag{4.118}$$

with

$$g(z,\eta) = \int_0^{1-z^2} du \;\; F(u,z,\eta) \tag{4.119}$$

The first of these integrals has a singularity at $z = -\eta/2$ where η is less than 2, and Shaw has developed a method of evaluating the principal part. The integral is calculated using Simpson's rule, ensuring that the singularity lies on the integration mesh. At the singular point, the integrand is replaced by a function

$$F\left(1 - \frac{\eta}{2}^2, -\frac{\eta}{2}, \eta\right) \int_0^{1-(\frac{\eta}{2})^2} du \;\; \frac{\partial F}{\partial z}\left(u, -\frac{\eta}{2}, \eta\right) \tag{4.120}$$

which gives the value of the integral to within one part in 10^6.

4.4. Organisation of Computing

Three computer programs were used to perform the calculations outlined above. Firstly the local contributions to the form factors

were evaluated and stored on disc file. The main program then used these to calculate the contact density, assuming the normalisation correction was negligible. A third program calculated this normalisation correction for the pure metals. The listing of each of these programs, together with a list of their identifiers and outline of their structure is given in appendices A, B and C.

In order to save computing time, the local contribution to the form factors for a particular element, was only calculated for a limited number of alloys and the values for other found by interpolation. This is possible as $\Omega\, U^{L}(q)$ is a function of k_F only. The interpolation was carried out by the evaluation of a 3rd order polynomial fitted to at least 5 calculated values.

References

1) Perdew J.P. and Wilkins J.W., Phys.Rev., B7, 2461, (1973) and Solid State Commun., 8, 2041, 1970).

2) Harrison W.A., Pseudopotentials in the Theory of Metals, Benjamin Inc. (1966).

3) Ashcroft N.W., J.Phys.,C 1, 232, (1968).

4) Shaw R.W., Ph.D. Thesis, University of Stanford (1968).

5) Host I.P. and Styles G.A., J.Mag.Res., 6, 472, (1972).

6) Host I.P., Ph.D. Thesis, University of Warwick, (1971).

7) Ford C.J. and Styles G.A., The Properties of Liquid Metals; Proceedings of the 2nd International Conference, 189, Taylor and Francis (1972).

8) Shaw R.W. and Smith N.V., Phys.Rev.B, 178, 985, (1969).

9) Heine V. and Aberenkov I.V., Phil.Mag., 9, 451, (1964).

10) Animalu A.O.E. and Heine V., Phil.Mag.12, 1249, (1965).

11) Ese O. and Reissland J.A., J.Phys.F,3, 2066, (1973).

12) Evans R., J.Phys.C: Metal Phys.Supp., 2, 5137, (1970).

13) Mann J.B., Los Alamos Scientific Laboratory of University of California Report, (1967).

14) Ashcroft N.W. and Lekner J., Phys.Rev. 145, 83, (1966).

CHAPTER 5

Calculation of the Knight Shift in Metals and Alloys

Chapter 4 describes a method of calculating the contact density in liquid metals and alloys, which is exact to first order in the pseudopotential and the results of such calculations are presented here. In Sec.5.1. the results for pure metals are combined with spin susceptibilities to obtain the values of the direct contact contribution to the Knight shift. These are compared with the measured Knight shifts, and the sensitivity of the results to the input parameters is examined. Sec.5.2. is devoted to the calculation of the relative changes of Knight shifts with concentration in alloys.

5.1. Pure Metals

The direct contact density has been calculated for most simple metals using the formalism of the last chapter. The input parameters used in the calculations are given in Table 5.1. The atomic volumes, Ω, were calculated from the density just above the melting point given in the Liquid Metals Handbook (2) and the Fermi wavevector, k_F, found using the free electron formula. The values quoted for beryllium and barium are, however, for the solid at room temperature as no liquid data was available, but this should not be a large source of error as the Knight shift does not vary significantly with volume in liquid. Except for lead, the model potential parameters are taken from Ese and Reissland (3). These have been evaluated according to Shaw's procedure (11) except that an iterative process is used to obtain a consistent set of parameters and Fermi energies. The values for lead were taken from Evans (4) since Ese and Reissland do not present a complete set of parameters for this metal. The column labelled $R_s(0)$ contains the values

Metal	k_F	Ω	MODEL POTENTIAL PARAMETERS						$R_s(0)$				
			A_o	A_1	A_2	DA_o	DA_1	DA_2	1_s	2_s	3_s	4_s	5_s
Li	0.5773	153.9	0.329			-.186			9.26				
Be*	0.9957	60	1.046			-.147			14.67				
Na	0.4742	277.5	.313	.358		-.187	-.117		70.29	17.16			
Mg	0.6993	173.5	0.806	0.907		-.237	-.168		80.28	20.28			
Aℓ	0.8871	127.3	1.432	1.654		-.266	-.049		90.71	23.58			
K	0.3812	534.8	.249	.249		-.240	-.287		161.63	46.43	15.30		
Zn	0.8240	105.8	1.032	1.413	.661	-.300	-.900	+.352	323.22	99.81	37.69		
Ga	0.8850	128.2	1.589	1.831	1.377	-.297	-.215	+.186	339.67	105.27	40.15		
Rb	0.3573	649.2	.234	.228	.306	-.280	-.177	+1.66	443.92	140.05	56.71	19.15	
Cd	0.7222	157.2	.942	1.187	.658	-.407	-.603	+.090	657.80	212.09	92.42	39.04	
In	0.7816	186.0	1.422	1.538	1.185	-.379	-.281	-.057	678.60	219.13	95.95	41.10	
Su	0.8476	194.5	1.839	2.056	1.798	-.487	-.246	-.183	699.61	226.26	99.51	43.21	
Cs	0.3261	835	.214	.202	.390	-.335	+.223	+.525	807.82	262.99	118.1	54.43	20.23
Ba*	0.5053	460	.456	.459	2.523	-.467	-.200	-2.231	830.08	270.56	121.89	56.79	22.16
Hg	0.7018	171.3	1.207	1.448	.568	-.306	-2.538	+.218	1421.1	473.49	224.78	112.0	47.49
Tℓ	0.7594	202.8	1.515	1.637	1.060	-.405	-.465	-.096	1447.9	482.7	229.5	114.8	49.86
Pb	0.8170	217.2	1.94	2.00	1.38	-.44	-.20	+.28	1474.0	492.0	234.2	117.6	51.82
Bi	0.8593	233.3	2.387	2.610	2.504	-.547	-.518	-.846	1502.1	504.4	239.0	120.4	53.83

Table 5.1. Input Parameters for Contact Density Calculation. The atomic volume, Ω, and Fermi wavevector, k_F are calculated from the density just above the melting point except for those marked * where values for solid room temperature are used. The Model potential parameters are taken from Ese and Reissland (2) except for lead which are taken from Evans (4). The core electron wavefunctions at the nuclear site, $R_s(0)$, are from Mann (13).

of the wavefunction at the nucleus for the s-electrons in the atomic core taken from Mann (13).

The results of the calculations are summarised in Table 5.2., where the best available values of the spin susceptibility (see discussion in Sec.5.1.4.) have been combined with the calculated contact density to evaluate the Knight shift. A comparison is made between these and the experimental values in Figs.5.1. and 5.2. Also given in Fig.5.2. are the theoretical results obtained by other authors. In general there is good agreement between the results of the present calculations and experiment, which supports the assumption that the direct contact term gives the major contribution to the Knight shift. It can be seen, however, that these results differ from the results obtained using a similar formalism by Perdew and Wilkins (1) for Na, K & Rb, Jena and Halder (5) for Mg, Jena et al (6) for Cd, Ritter and Gardner (7) for Na, and Ford and Styles (8) for Ga, Cd, In, Sn, Pb and Bi. This indicates that the results are very sensitive to the choice of input parameters and the importance of each of the parameters will now be examined.

5.1.1. Pseudopotential

The major difference between the present calculation and most previous calculations is the nature of the pseudopotential that is employed. Here a properly nonlocal, energy-dependent potential is used. In order to investigate how this effects the results, calculations have been made using less sophisticated potentials for comparison purposes. They are:-

a) Ashcroft potential. This is the potential used by both Perdew and Wilkins, and Ford and Styles. The bare potential is assumed to be zero within a core radius, R_c, and Coulombic outside this

Element	OPW	$1+\Sigma+\Delta$	$1+\frac{\delta N}{N_o}$	$\mathcal{P}_F$	$\chi \times 10^6$	K_{TH}%	K_{EXPT}%	$\frac{K_{TH}}{K_{EXPT}}$
Li	55.67	0.529	1.033	28.51	1.176	0.028	0.026	1.077
Be	45.02	0.529	1.028	23.16	1.747	0.034	0.000	-
Na	152.4	0.933	1.004	141.6	1.056	0.125	0.116	1.078
Mg	116.2	0.829	1.002	96.14	1.340	0.108	(0.110)*	0.982
Aℓ	93.26	0.884	0.994	82.98	1.592	0.111	0.164	0.677
K	441.1	1.101	0.995	488.1	0.874	0.357	0.265	1.347
Zn	376.0	1.084	0.989	402.2	1.525	0.514	-	-
Ga	331.8	1.114	1.001	369.5	1.588	0.492	0.449	1.096
Rb	803.4	1.045	0.992	846.7	0.829	0.588	0.662	0.888
Cd	551.3	1.165	0.967	664.2	1.375	0.765	0.795	0.962
In	467.2	1.149	0.964	567.6	1.465	0.697	0.786	0.887
Sn	425.0	0.921	0.965	405.6	1.556	0.529	0.73	0.725
Cs	1662.	1.043	0.997	1738.	0.776	1.13	1.44	0.784
Ba	1056.	0.691	1.048	696.2	1.001	0.583	(0.403)*	1.447
Hg	1185.	1.793	0.903	2353.	1.345	2.65	2.42	1.095
Tℓ	992.0	1.357	0.939	1433.	1.425	1.71	1.48	1.155
Pb	876.9	1.133	0.956	1039.	1.522	1.32	1.49	0.886
Bi	805.6	0.852	0.941	729.4	1.554	0.950	1.41	0.674

Table 5.2. Calculation of Knight Shifts.

The results of the zero order calculation of the contact density are given in the column labelled OPW. $1+\Sigma+\Delta$ is the first order correction term, and $1+\delta N/N_o$ is the correction to the normalisation, giving the first order contact density $\mathcal{P}_F$. K is the spin susceptibility used to calculate the Knight shift, K_{TH}. Experimental results, K_{EXPT}, are for the liquid just above the melting point except those labelled * which are for the solid at room temperature.

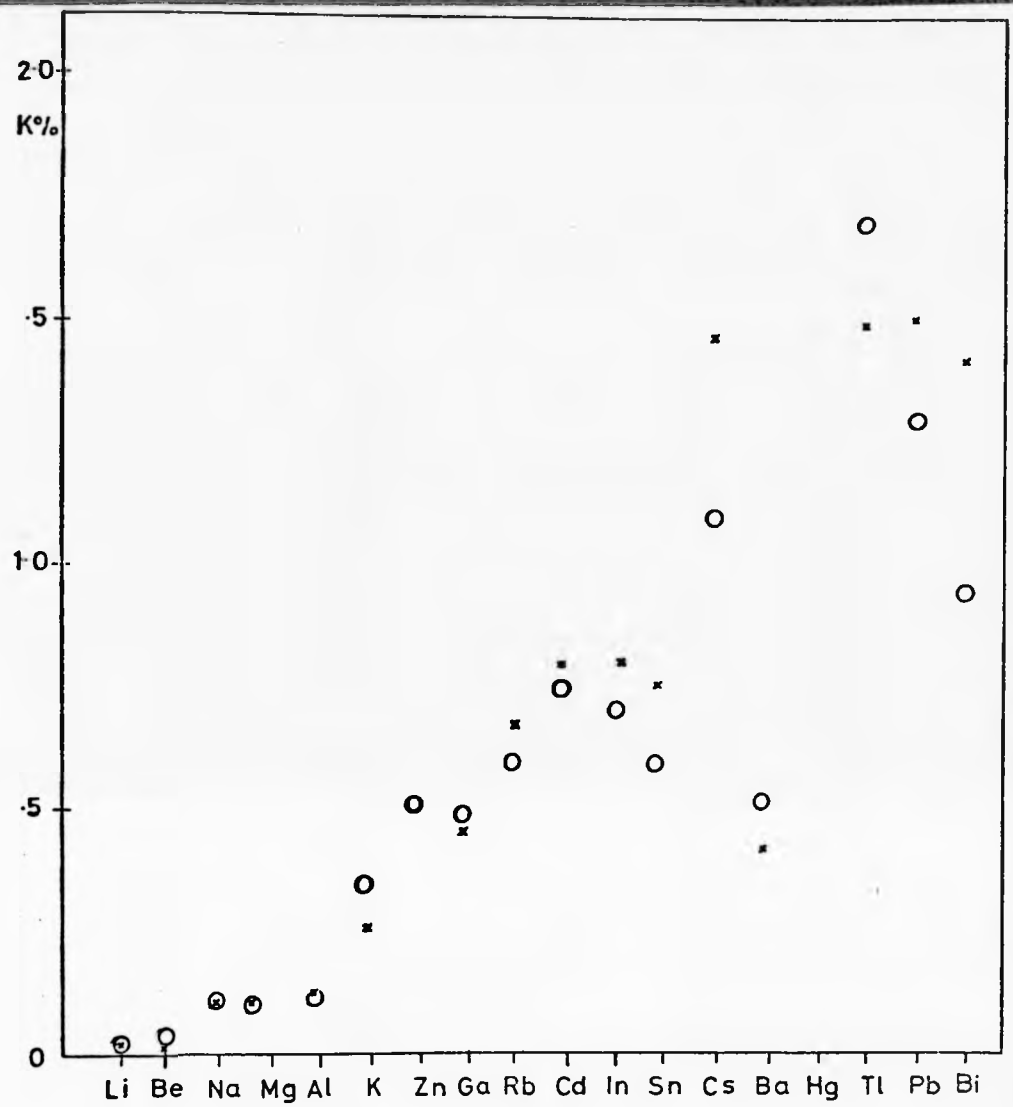

Fig. 5.1. Knight Shifts of Liquid Metals.

The experimental values of the Knight shift of liquid metals, arranged according to atomic number, are denoted by x. The calculated values are denoted by o. Experimental points for Be and Ba are for the solid as no liquid data are available.

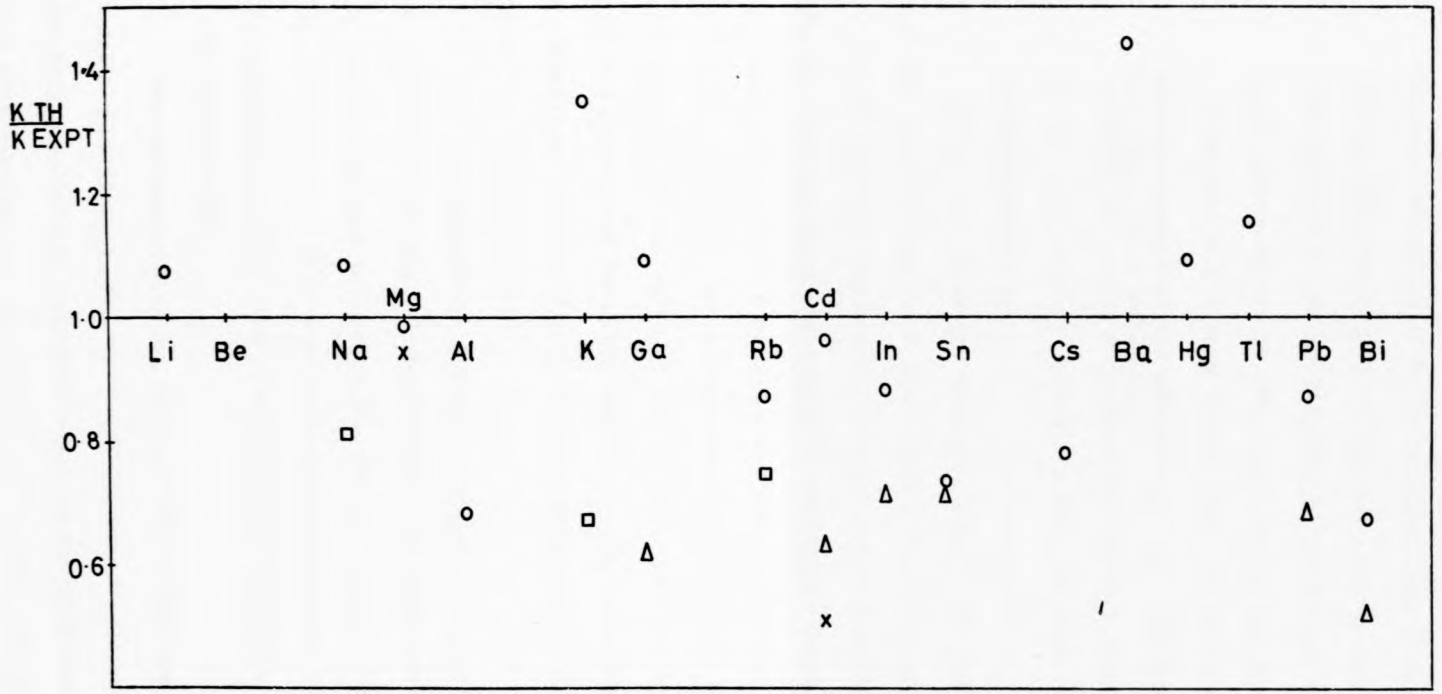

Fig.5.2. Calculations of Knight Shifts by Various Authors.

Calculated Knight shifts, K TH, are given relative to the experimental values, K EXPT, for pure liquid metals according to a) Present work o, b) Ford & Styles (6) Δ, c) Perdew & Wilkins (1) □, and d) others mentioned in Sec.5.1. ×.

region. The value of R_c is obtained from either Fermi surface data or from the liquid resistivity, but no attempt is made to take account of the nonlocality or the energy dependence.

b) Local Approximation to OMP. Here the potential is taken to be a local one with a form factor equal to the Fermi shell scattering matrix elements of the OMP for $q < 2k_F$, and q antiparallel to k_F for $q>2k_F$. These definitions coincide at $q = 2k_F$ and represent the most important contributions in the full nonlocal case since they are emphasised by the energy denominator.

It should be noted, however, that not only is the full nonlocal OMP somewhat more sophisticated then these other model potentials, but that it can in principle represent the scattering properties of the ions exactly, whereas these other potentials cannot. Calculations have also been performed using the single OPW method. Here the wavefunction of each conduction electron is represented by a single plane wave, orthogenalised to the ion cores. This is equivalent to using a uniformly zero pseudopotential and forms the zero order approximation for the other calculations. The results of each of these calculations is given in Table 5.3. and Fig.5.3.

What is immediately apparent is the diversity of the results. It is also clear that the results obtained using the Ashcroft potential are incorrect. In only two out of the twelve elements for which calculations have been made, is this result closer to experiment than the zero order approximation, and the negative results for gallium and bismuth are quite meaningless.

The difference between the Ashcroft results and the local OMP results show that, within the local approximation, these calculations are very sensitive to the exact shape of the form factors. To show this more clearly, the two factors for cadmium are plotted out in Fig.5.4. where it can be seen that their general form is very similar.

Element	SINGLE OPW			NON-LOCAL OMP			LOCAL OMP			ASHCROFT POT.		
	ΩP_F	$K_{TH}\%$	$\frac{K_{TH}}{K_{EXPT}}$	ΩP_F	$K_{TH}\%$	$\frac{K_{TH}}{K_{EXPT}}$	ΩP_F	$K_{TH}\%$	$\frac{K_{TH}}{K_{EXPT}}$	ΩP_T	$K_{TH}\%$	$\frac{K_{TH}}{K_{EXPT}}$
Li	55.67	0.055	2.115	28.51	0.028	1.077	-ve			64.64	0.063	2.42
Be	45.02	0.067		23.16	0.034		-ve					
Na	152.4	0.134	1.155	141.6	0.125	1.078	111.2	0.098	0.845	102.5	0.091	0.782
Mg	116.2	0.130	1.182	96.14	0.108	0.982	67.09	0.075	0.682			
Al	93.26	0.124	0.756	82.98	0.111	0.677	46.54	0.062	0.378	64.24	0.086	0.524
K	441.1	0.325	1.226	488.1	0.357	1.347	481.9	0.353	1.332	284.6	0.208	0.785
Zn	367.0	0.467		402.2	0.514		34.39	0.044		47.53	0.061	
Ga	331.8	0.441	0.982	369.5	0.492	1.096	237.8	0.316	0.704	-ve		
Rb	803.4	0.573	0.866	846.7	0.588	0.888	912.5	0.634	0.958	814.9	0.561	0.855
Cd	551.3	0.635	0.799	664.2	0.765	0.962	490.4	0.565	0.711	264.6	0.305	0.384
In	476.2	0.581	0.736	567.6	0.697	0.887	515.5	0.633	0.805	318.7	0.391	0.497
Sn	425.0	0.554	0.759	405.6	0.529	0.725	356.3	0.464	0.636	249.5	0.325	0.445
Cs	1662.	1.07	0.743	1738.	1.13	0.784	2016.	1.31	0.910			
Ba	1056.	0.885	2.20	696.2	0.583	1.447	695.5	0.583	1.447			
Hg	1185.	1.335	0.55	2353.	2.56	1.095	1622.	1.83	0.756	2231.	2.51	1.037
Tl	992.0	1.184	0.80	1433.	1.71	1.155	1248.	1.49	1.007			
Pb	876.9	1.118	0.75	1039.	1.32	0.886	860.6	1.10	0.738	217.8	0.278	0.187
Bi	805.6	1.049	0.74	729.4	0.95	0.674	608.8	0.723	0.513	-ve		

Fig.5.3. Calculations of Knight Shifts using Various Pseudopotentials. Calculated values of contact density, ΩP_F, Knight shift K_{TH} and the ratio K_{TH}/K_{EXPT} of the theoretical and experimental shifts are given for the four methods outlined in Sec.5.1.1.

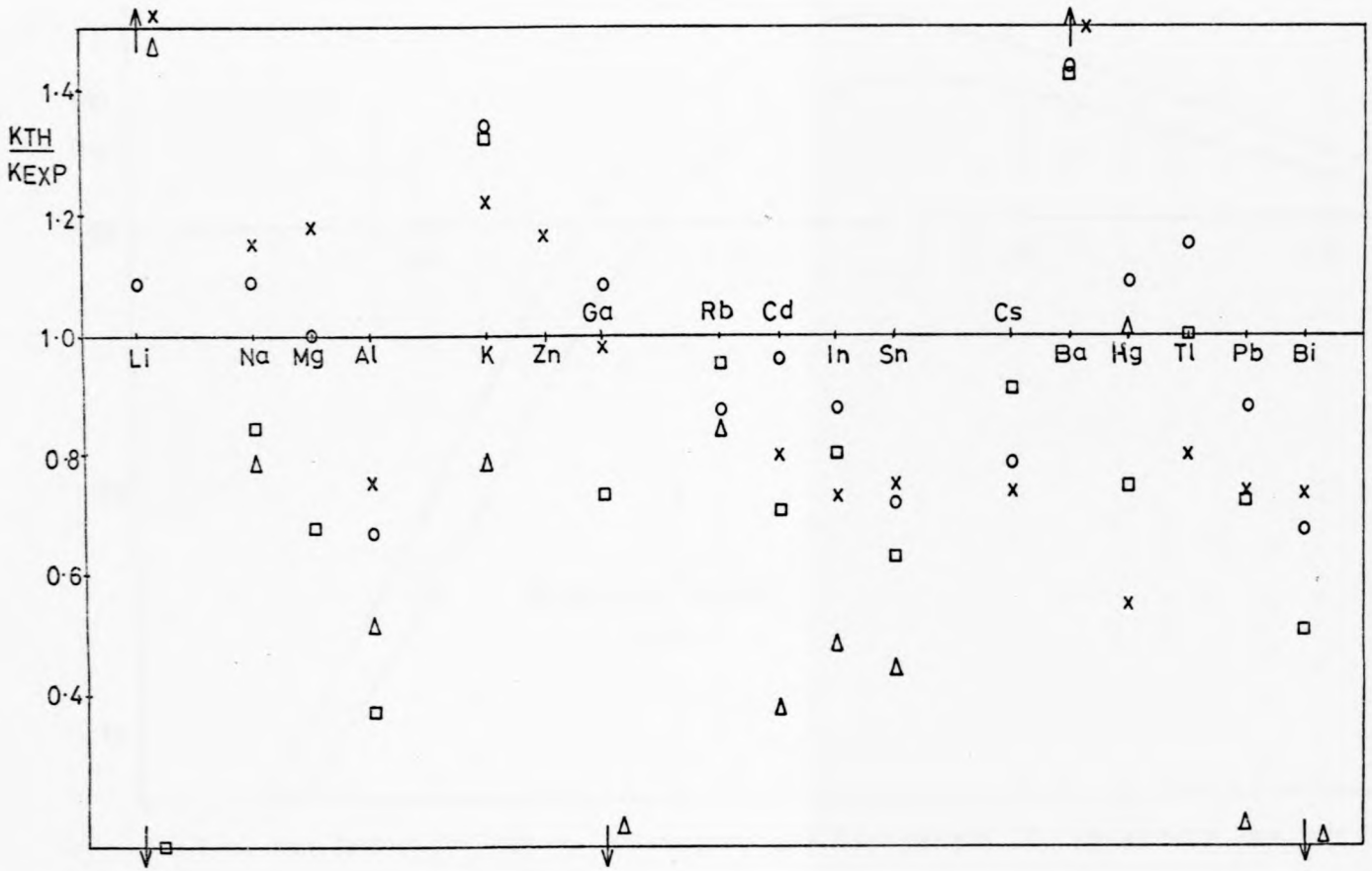

Fig.5.3. Calculations of the Knight Shift Using Various Pseudopotentials. Calculated ratios K TH/K EXP of the theoretical and experimental Knight shifts were obtained using a) nonlocal OMP o, b) local OMP □, c) Ashcroft model potential Δ. The zero order result is denoted by × .

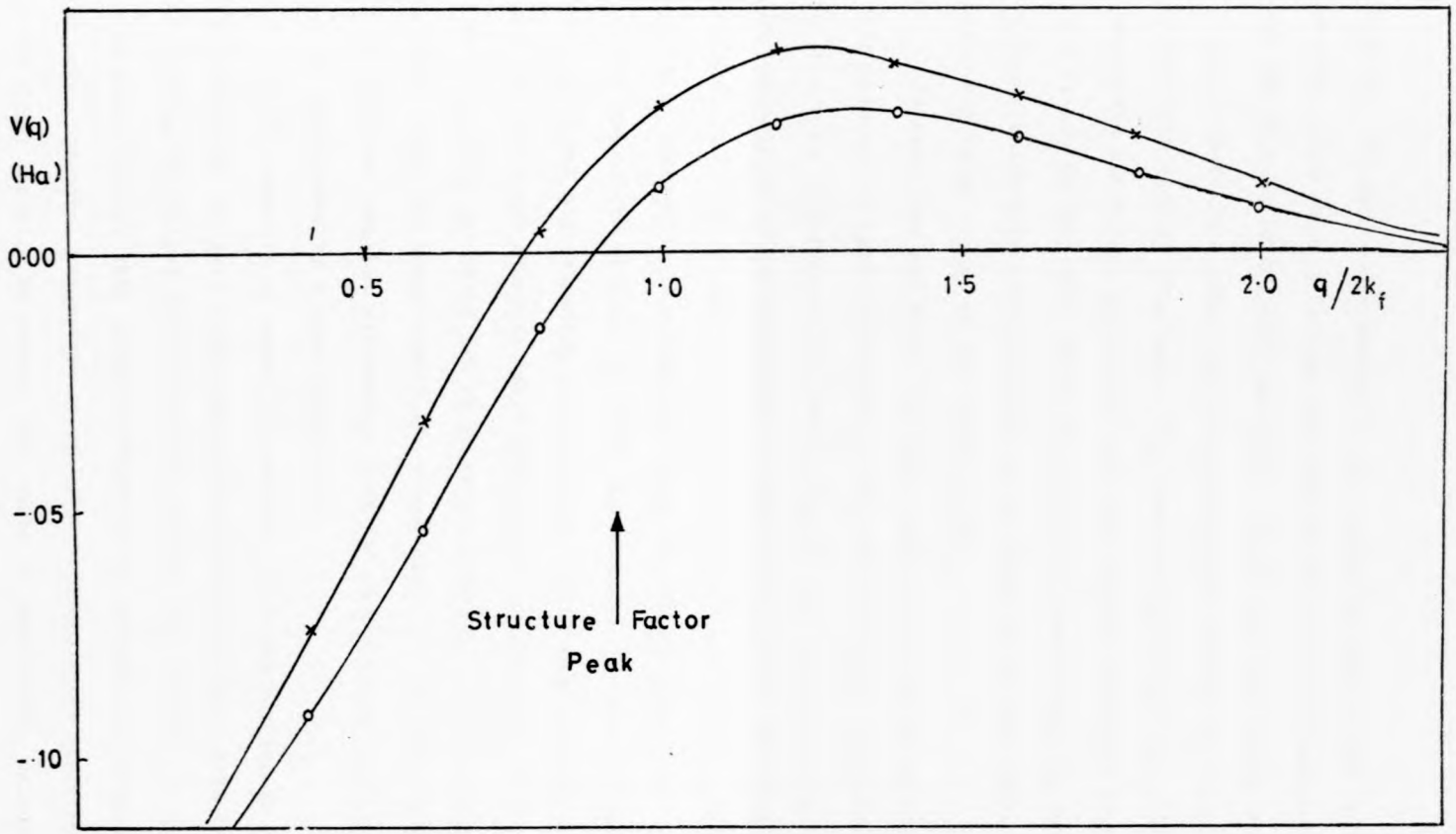

Fig.5.4. Form factors for Cadmium. Values given by x from Ashcroft (9). Values given by o from Ese and Reissland (3).

However, the main contribution to the correction term to the contact density comes where q is near the peak of the structure factor. For the OMP this coincides with the first node of the form factor and as a result, there is a great deal of cancellation between the contributions from either side of this node. This does not occur for Ashcroft's potentials which thus gives rise to a much larger correction term. Thus it can be seen that small inaccuracies in evaluating the form factors, which give rise to errors in the position of this node, can give very large errors in the final results.

However Shaw and Smith (10) have pointed out that in other calculations, in particular those of density of states, the results are no longer so sensitive to the exact shape of the form factors provided the nonlocality of the potential is properly included. The present calculations involve very similar integrals to those of Shaw and Smith's and it is reasonable to assume that this is also the case here.

A comparison between the local and nonlocal OMP results show clearly that the local approximation is inadequate. This seems particularly true for the light elements where there are no d-electrons, or in the case of lithium and beryllium no d- or p-electrons, in the atomic cores. In these cases one would expect the d-components of the conduction electrons to be affected somewhat differently from the s-components and this can not be represented by a local potential.

In the majority of cases the nonlocal calculation gives an improvement on the zero order approximation and provides a method of calculating the Knight shift to within 20% for most metals. It remains to be shown however that slight differences of procedure in determining the model potential parameters do not produce significant differences in the final result. To examine this cause of uncertainty, calculations of the contact density have been made for cadmium and indium using optimised model potential parameters from three different sources:-

Ese and Reissland (3), Shaw (11), and Evans (4). The results in Table 5.4. show very little difference (< 5%) between the results for indium but those for cadmium have a spread of almost 20%. All authors have pointed out the difficulties of obtaining A_2 for cadmium (and zinc) so one would expect the consistency obtained for indium to be more typical of the other metals.

The potentials for Bi, Pb and Sn are also somewhat suspect as for elements of valency greater than 3, the assumption of linear screening, which is basic to model potential theory, is in doubt. The very large corrections for mercury and barium suggest first order perturbation theory is not appropriate for these metals. With these reservations, it seems that for most metals the potential used is not only the best available, but that any errors that are introduced into the final result by inaccuracies in this potential are small compared with remaining differences between theory and experiment.

5.1.2. Structure Factor

The structure factors used were those, based on the hard sphere model, proposed by Ashcroft and Lekner (12) with a packing fraction of 0.45 for all metals. In their original paper the form of this factor is compared with the experimental results from scattering data. The packing fraction of 0.45 is found to give good agreement for the alkali metals and a value between 0.4 and 0.5 is appropriate for the other metals they studied. For all metals the agreement is good near the main peak of the structure factor but the oscillations tend to get out of step with the measured structure factor at higher q. Since it is found in the present calculations that the main contribution to the correction term comes from the region round the first peak, the use of the hard sphere structure factor should be adequate, but to examine the effect of these

	CADMIUM			INDIUM		
	SHAW	EVANS	ESE and REISSLAND	SHAW	EVANS	ESE and REISSLAND
A_o	0.892	0.90	0.942	1.341	1.35	1.422
A_1	1.144	1.10	1.187	1.494	1.48	1.538
A_2	0.924	0.75	0.658	1.089	0.99	1.185
DA_o	-.424	-.36	-.407	-.454	-.36	-.379
DA_1	-.513	-.30	-.603	-.224	-.086	-.281
DA_2	-.571	0.00	0.90	0.094	0.43	-.051
$\mathcal{P}_F$	541.1	566.5	642.3	531.6	562.6	546.6
K_{TH}%	0.623	0.653	0.740	0.649	0.686	0.667
K_{TH}/K_{EXPT}	0.78	0.82	0.93	0.83	0.87	0.85

Table 5.4. Calculations of Cadmium and Indium Knight shifts.

Model potential parameters, A's and DA's, for indium and cadmium given by three authors, Shaw (11), Evans (4), and Ese and Reissland (3), are listed together with the results for contact density $\mathcal{P}_F$ and Knight shift K_{TH}, calculated using these potentials. In the final row these results are compared with the experimental Knight shift K_{EXP}.

approximate structure factors, calculations were made for some metals using experimental values. The results are given in Table 5.5.

In general there is little difference between the two sets of results. The differences of 3% and 4% for gallium and tin respectively, are not surprising as both of these metals have somewhat unusual structure factors, with shoulders on the high q side of the main peak. The differences of 6% for sodium and 4% for potassium were somewhat unexpected and represent very significant changes in the correction terms. Fig.5.5. shows the final q integrand which makes up the correction term for sodium. It can be seen that the final result comes from a cancellation of terms on either side of the structure factor peak. The value of the Ashcroft and Lekner structure factor decreases far less rapidly than the experimental curve immediately after the main peak and thus it overemphasises the negative contribution. The difference between the potassium results seem to come from the rather large values of the experimental structure factor for low q. The experimental results for potassium are poorer than for any other of the alkali metals and it is possible that these are in error.

The results of these two sets of calculations do, however, generally agree even when the structure factors are slightly different. It can therefore be concluded that these calculations are not particularly sensitive to the exact values of the structure factors, and the remaining uncertainties in these structure factors cannot be held responsible for the existing differences between the present calculations, and the experimental values of the Knight shift.

5.1.3. Core Wavefunctions

Exact solutions for the core electron wavefunctions are not available and most authors have used some approximation to the corresponding

approximate structure factors, calculations were made for some metals using experimental values. The results are given in Table 5.5.

In general there is little difference between the two sets of results. The differences of 3% and 4% for gallium and tin respectively, are not surprising as both of these metals have somewhat unusual structure factors, with shoulders on the high q side of the main peak. The differences of 6% for sodium and 4% for potassium were somewhat unexpected and represent very significant changes in the correction terms. Fig.5.5. shows the final q integrand which makes up the correction term for sodium. It can be seen that the final result comes from a cancellation of terms on either side of the structure factor peak. The value of the Ashcroft and Lekner structure factor decreases far less rapidly than the experimental curve immediately after the main peak and thus it overemphasises the negative contribution. The difference between the potassium results seem to come from the rather large values of the experimental structure factor for low q. The experimental results for potassium are poorer than for any other of the alkali metals and it is possible that these are in error.

The results of these two sets of calculations do, however, generally agree even when the structure factors are slightly different. It can therefore be concluded that these calculations are not particularly sensitive to the exact values of the structure factors, and the remaining uncertainties in these structure factors cannot be held responsible for the existing differences between the present calculations, and the experimental values of the Knight shift.

5.1.3. Core Wavefunctions

Exact solutions for the core electron wavefunctions are not available and most authors have used some approximation to the corresponding

Element	Ashcroft Structure factor		Experimental Structure factor		Difference
	$\mathcal{P}_F$	K%	$\mathcal{P}_F$	K%	%
Na	134.3	0.119	142.2	0.126	+6
K	449.3	0.329	485.7	0.357	+4
Ga	379.2	0.602	369.5	0.492	-3
Rb	841.6	0.586	840.9	0.588	0
In	546.6	0.695	547.3	0.697	0
Sn	406.5	0.569	391.2	0.529	-4
Cs	1773	1.15	1734	1.13	-2
Pb	989.0	1.32	993.7	1.32	0
Bi	693.7	0.960	686.3	0.950	-1

Table 5.5. Effect of Different Structure Factors.

Contact density, $\mathcal{P}_F$, and Knight shift, k, is shown as a result of calculations using a) Ashcroft-Lekner, hard sphere structure factors and b) experimental structure factors.

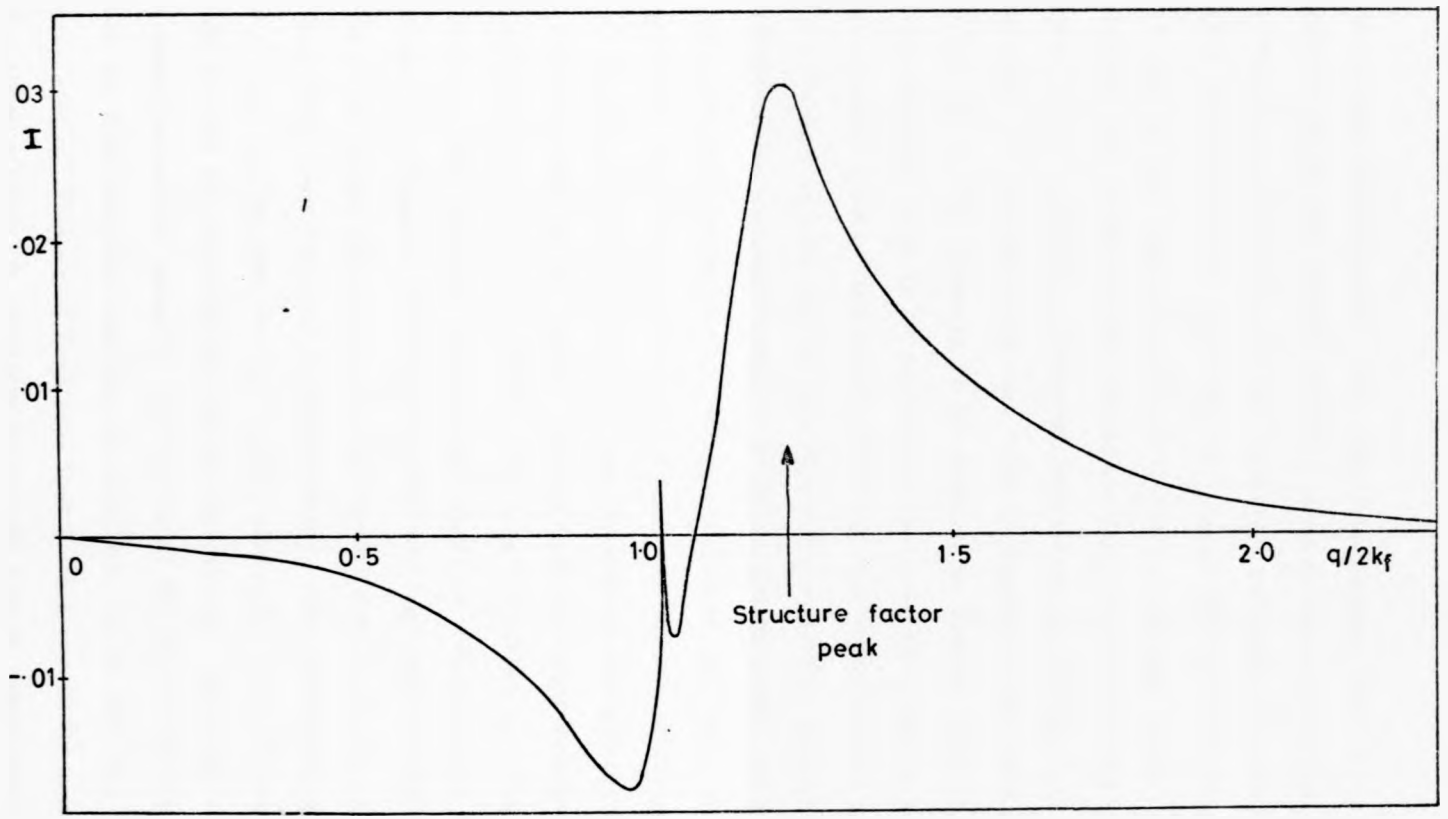

Fig.5.5. The First Order Correction to the Normalisation Coefficient fo Sodium as a Function of Scattering Vector.

neutral atom wavefunctions. For comparison purposes Table 5.6. shows the single OPW results obtained using different wavefunctions. The Mann functions (13), are exact numerical solutions for neutral atoms within the Hartree Fock approximation, whereas Herman and Skillman have used further approximations to obtain the exchange terms. The functions used by Perdew and Wilkins are analytic, and derived by Bagus (15) for sodium and potassium, and Watson and Freeman (16) for rubidium. It is to be noted that there is reasonable agreement between the results for the elements in the first three rows of the periodic table, although there is an increasing divergence for elements with higher atomic number. One would expect the Mann wavefunctions to be the most accurate, because they do not employ any additional assumptions in calculating the exchange terms, as do Herman and Skillman, and do not restrict their solutions to any analytical form as the other authors have done. However there are still a number of sources of error.

Firstly no account has been taken of relativistic effects which will be important in the heavier elements. Neutral atom wavefunctions which include relativistic effects have been calculated by Liebermann (26). He uses the free electron exchange approximation used by Herman and Skillman, and Mahanti, Tterlikkis and Das (17) have made a comparison between the single OPW results for the contact density of the alkali metals using these two sets of wavefunctions. They find that, although the results are the same for the lighter metals, there are differences of 8% and 30% for rubidium and cesium respectively. These may not be the exact correction terms for the results of the present calculation, where the Mann wavefunctions that are employed do not use this free electron approximation. However it does show that for 5th row of the periodic table these effects are considerable and may also be significant in the 4th row.

CONTACT DENSITY			
Source of core wave function / Element	Mann (13)	Herman and Skillman (14)	Perdew and Wilkins (1)
Li	55.67	57.03	
Be	45.02	45.93	
Na	152.4	165.7	150.7
Mg	116.2	121.9	
Aℓ	93.26	100.9	
K	441.1	462.6	433.9
Zn	367.0	379.7	
Ga	331.8	342.1	
Rb	803.4	842.6	773.7
Cd	551.3	577.3	
In	476.2	508.5	
Sn	425.0	492.2	
Cs	1662	1722	
Ba	1056	1145	
Hg	1185	1165	
Tℓ	992.0	1044	
Pb	876.9	1164	
Bi	805.6	934.6	

Table 5.6. Zero Order Calculations of Contact Density Using Various Core Wavefunctions.

It was also not entirely clear what error was introduced by use of the neutral atom wavefunctions to represent the core electrons. In the liquid it seems likely that the outer electron wavefunctions are somewhat modified and, although the inner s-electrons have the largest contact density, it is the overlap with the outer s-electrons which give the largest contributions to the conduction electron contact density. This is demonstrated in Table 5.7. where the single OPW calculation for lead is analysed into the components due to the overlap with the different core electrons.

It was suspected that the relatively disappointing results for aluminium, tin and bismuth may be due to the fact that, since a relatively high proportion of the electrons have been stripped from these atoms, the core functions are somewhat effected. In order to examine this hypothesis, a single OPW calculations of the contact density were made for a few elements, using free ion core wavefunctions (27), calculated in exactly the same way as the Mann, free atom wavefunctions (13). The results are given in Table 5.8. and it is clear that core wavefunction are very similar for the free ion and the free atom. In the metal the core wavefunctions will be even more like the free atom functions as although the conduction electrons are not localised, they have a very high density in the core region.

It is therefore concluded that no significant error is introduced into these calculations by the use of neutral atom core wavefunctions to represent the metal cores. However, for metals in the fifth row of the periodic table, these wavefunctions must certainly be in error due to the lack of relativistic corrections and a large part of of the discrepancy between the calculated and experimental results for elements in the 4th row of the periodic table may also be caused by this omission. For other metals, however, it seems that these core functions are quite adequate for this calculation.

It was also not entirely clear what error was introduced by use of the neutral atom wavefunctions to represent the core electrons. In the liquid it seems likely that the outer electron wavefunctions are somewhat modified and, although the inner s-electrons have the largest contact density, it is the overlap with the outer s-electrons which give the largest contributions to the conduction electron contact density. This is demonstrated in Table 5.7. where the single OPW calculation for lead is analysed into the components due to the overlap with the different core electrons.

It was suspected that the relatively disappointing results for aluminium, tin and bismuth may be due to the fact that, since a relatively high proportion of the electrons have been stripped from these atoms, the core functions are somewhat effected. In order to examine this hypothesis, a single OPW calculations of the contact density were made for a few elements, using free ion core wavefunctions (27), calculated in exactly the same way as the Mann, free atom wavefunctions (13). The results are given in Table 5.8. and it is clear that core wavefunction are very similar for the free ion and the free atom. In the metal the core wavefunctions will be even more like the free atom functions as although the conduction electrons are not localised, they have a very high density in the core region.

It is therefore concluded that no significant error is introduced into these calculations by the use of neutral atom core wavefunctions to represent the metal cores. However, for metals in the fifth row of the periodic table, these wavefunctions must certainly be in error due to the lack of relativistic corrections and a large part of of the discrepancy between the calculated and experimental results for elements in the 4th row of the periodic table may also be caused by this omission. For other metals, however, it seems that these core functions are quite adequate for this calculation.

Core Orbital	$R_s(0)$	B_L	γ_n
1s	1475	0.0690	8.10
2s	492.0	-.4294	-16.81
3s	234.2	1.454	27.10
4s	117.66	-4.251	-39.78
5s	51.53	12.13	50.03

Table 5.7. Contribution to Contact Density in Lead.

The single OPW calculation is analysed into the contributions from the overlap with each of the core s-electron wavefunctions. $R_s(0)$ is the value of the core wavefunction at nuclear site, B_L is the overlap integral between the core and conduction electron wavefunction and γ_n is related to the final contact density by

$$\Omega\rho_F = \frac{\Sigma\gamma_n^2}{N_o}$$

where N_o is the normalisation coefficient.

Core wave-function / Element	Free Atom (13)	Free Ion (27)
Li	55.67	55.14
Be	45.02	44.78
Na	152.4	151.4
Mg	116.2	115.3
Al	93.26	94.07
K	441.1	436.5
Sn	425.0	416.8

Table 5.8. Zero Order Calculation of Contact Density. Comparing results using free atom and free ion core wavefunctions.

5.1.4. Spin Susceptibility

The final quantity required to calculate the Knight shift is the spin suceptibility of the conduction electrons, χ_s. In principle this can be obtained directly from Conduction Electron Spin Resonance, CESR. However the experiment, which requires the accurate measurement of the area under the Lorentzian spectral line, can only be performed where the CESR signal is very strong, and results have only been obtained for lithium (18) and sodium (19) in this way.

A semi-empirical approach to evaluating the spin susceptibility has been proposed by Dupree and Seymour (24). They have calculated the Landau diamagnetic susceptibility and the susceptibility of the ion cores for a wide range of metals, and subtracted these from the total measured susceptibility to obtain χ_s. Other authors, Rice (20), Silverstein (21) and most recently Dupree and Geldhart (22), have calculated the spin susceptibility from the free electron value, with a suitable correction for exchange enhancement. Most recently,experiments have been performed to obtain this exchange enhancement (25), which consist of a measurement of the de Haas-van Alphen and CESR g-factors, but as yet these results are only available for the alkali metals.

The Knight shifts deduced, using different values for the susceptibility are compared in Fig.5.6. Except for the alkali metals the values deduced using different χ_s's are within 5% of one another which must be considered very satisfactory in view of the differences in the methods used to obtain the susceptibilities. Thus values of χ_s from Dupree and Geldhart (22) are considered adequate and have been used throughout these calculations except for the alkalis. The g-factor results for the alkali metals are considerably more accurate than for the other metals, and are believed to be within a few per cent of the true values. These have therefore been used for the alkali metals.

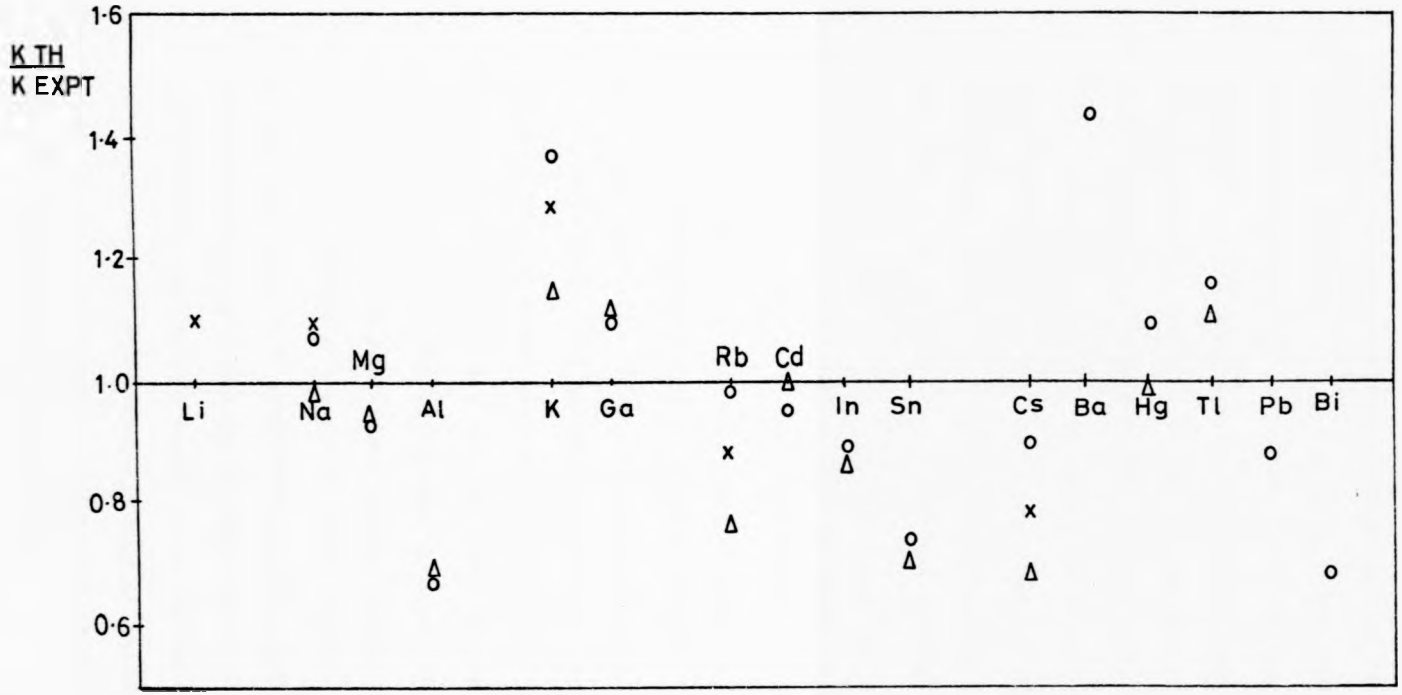

Fig.5.6. Knight Shifts Calculated Using Various Values of Spin Susceptibility.

The ratios K TH/ K EXPT of the theroretical and experimemtal Knight shifts shown are calculated using the spin susceptibilities given by a) Dupree & Geldhart (22) o , b)Dupree & Seymour (24) Δ , and c) Dupree (25) × .

5.1.5. Conclusion

The results presented here show that the calculation of the contact density by first order perturbation theory must include the nonlocal character of the pseudopotential. If the nonlocality is taken into account it is possible to evaluate the Knight shift for most simple metals, above the fifth row of the periodic table, to within 20% of their experimental value, and generally these calculations represent a significant improvement on the zero order approximation.

The uncertainties in the form factors and the core electron wavefunctions must account for some of the remaining descrepances between theory and experiment although it is possible that other contributions to the Knight shift such as core polarisation or orbital effects are present in these metals. The effect of core polarisation has been estimated by Mahanti et al for the alkali metals (17) and by Halder and Jena (23) for magnesium, and in all cases is found to be less than 20% of the direct contribution. These results are believed to be very sensitive to the exact form of the core electron wavefunctions which are not known with sufficient certainty, however a contribution of about 10% could bring most of these results into line with the experimental values. Orbital contributions, which are very important in transition metals, have not yet been shown to be significant in these simple metals.

The calculations for aluminium, tin and potassium are not so satisfactory. For aluminium and tin it seems likely that the discrepancy is associated with their high conduction electron density and large ionic charge which may mean that linear screening of their potentials is inadequate. No very satisfactory explanation can be given for the discrepancy between theory and experiment for potassium, although it is not inconceivable that this is due to an unfavourable combination of the several small cources of error inherent in this calculation.

For the heavy metals in the fifth row of the periodic table it is clear that the core wavefunctions must include relativistic effects to produce accurate results, although it seems likely that in pentavelent bismuth certainly, and possibly in lead, the linear screening of their potentials is also inadequate.

5.2. Knight Shifts of Alloys

The formalism of Chapter 4 allows the contact density of both pure metals and alloys to be calculated and the Knight shift may be evaluated using

$$K = \frac{8\pi}{3} \mathcal{P}_F \chi \ . \tag{5.1}$$

However, if there are additional contributions, for example from core polarisation, or the calculation of $\mathcal{P}_F$ has some systematic errors, these may be taken into account by using the expression

$$K = \frac{8\pi}{3} \mathcal{P}_F \chi \Lambda \ , \tag{5.2}$$

where Λ is a correction factor of order unity. If we assume that this correction factor is a constant for a given nuclear species indepenennt of its surroundings, in an alloy for example, we can calculate the relative change of the Knight shift with concentration without calculating the factor Λ. If K_o is the Knight shift in the pure metal and K the Knight shift in the alloy, the relative change of Knight shift is given by

$$\frac{K-K_o}{K_o} \cong \frac{\Delta K}{K_o} = \frac{\chi \mathcal{P}_F}{\chi_o (\mathcal{P}_F)_o} - 1 \ . \tag{5.3}$$

In all alloys that do not contain alkali metals $\Delta K/K_o$ is very small and given adequately by the differential relation

$$\frac{\Delta K}{K_o} = \frac{\Delta \chi}{\chi_o} + \frac{\Delta \mathcal{P}_F}{(\mathcal{P}_F)_o} \ . \tag{5.4}$$

Calculations of the contact density have been made for a large number of alloy systems. In all cases the spin susceptibility is taken to be a linear average of the two pure metal values in order to calculate the Knight shift. Those systems involving the alkali metals are discussed in Sec.5.2.1. and those involving the Knight shifts of cadmium, indium and gallium are discussed in Sec.5.2.2.

5.2.1. Alkali Metal Alloys

The relative changes of the Knight shift with concentration of the first named elements in the alloy systems Na-K, Na-Rb, Na-Cs, K-Na, Rb-Na have been calculated and the results are presented in Figs.5.7. to 11. Numerical results are given in Appendix D. The values of the spin susceptibilities have been found by a linear interpolation between the pure metal values but the contact density has been calculated in a number of different ways. Firstly the full nonlocal calculation has been performed using the structure factors proposed by Ashcroft and Lekner. A second similar calculation used structure factors obtained by adding the experimental structure factors of the two pure metals, each weighted by their concentration in the alloy. Thirdly the values of the contact density calculated by Perdew and Wilkins (1) were used; and finally the single OPW results have also been calculated.

As expected from the pure metal results, the first two methods of calculating the contact density give very similar $\Delta K/K_o$ curves (See Appendix D for comparison of these results). However, the fact that Perdew and Wilkin's contact densities also yield very similar results for $\Delta K/K_o$ is rather suprising. Not only do they use different values for the core functions and the pseudopotential, they also get quite different results for the absolute value of the contact densities they

KEY TO FIGS. 5.7. to 11.

× Denotes results of single OPW calculation.

Δ Denotes results of calculation using OMP.

□ Denotes results obtained from values $\mathcal{P}_F$ by Perdew and Wilkins (1).

Experimental curves are labelled EXP.

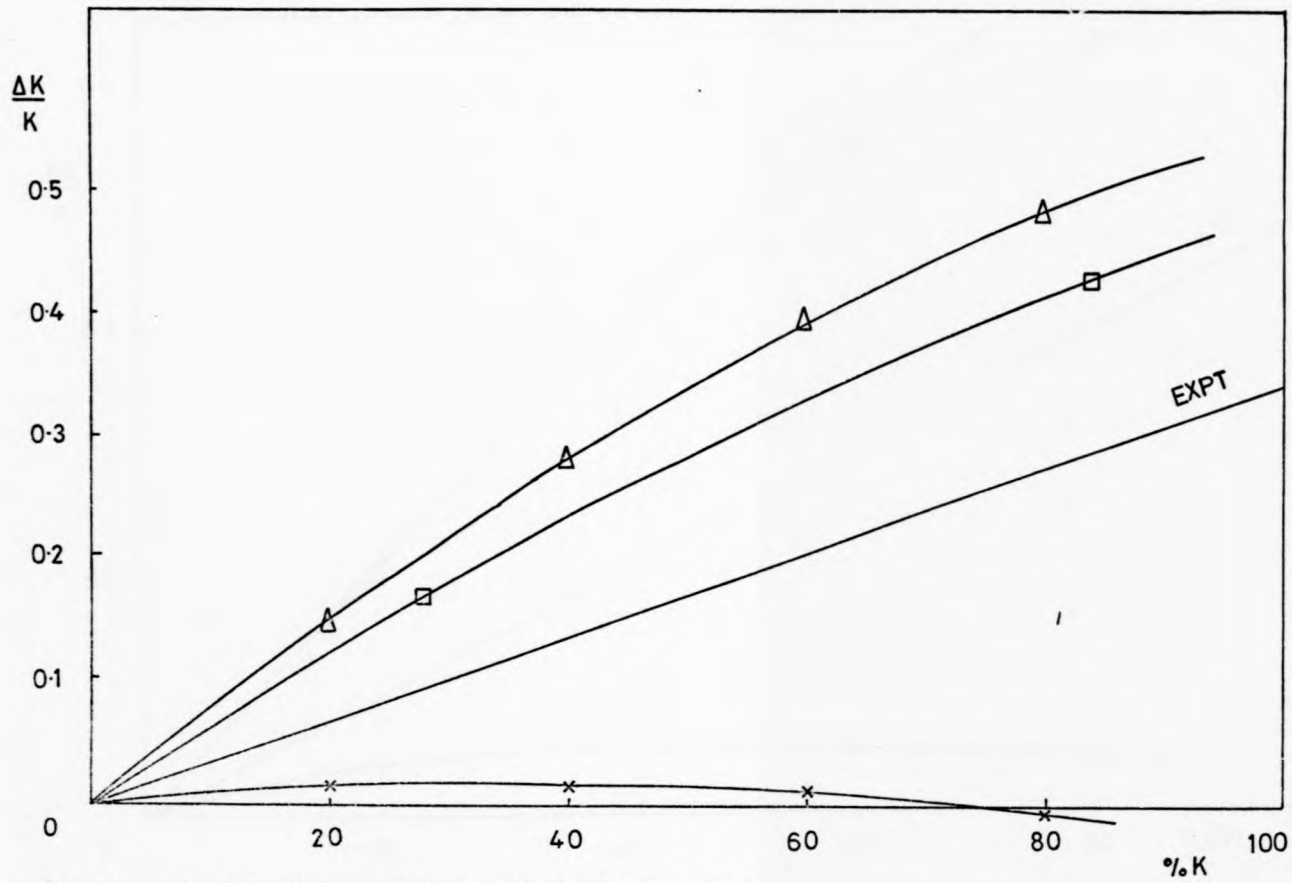

Fig. 5.7. Relative Change of Sodium Knight Shift in Na-K.
Key page 78.

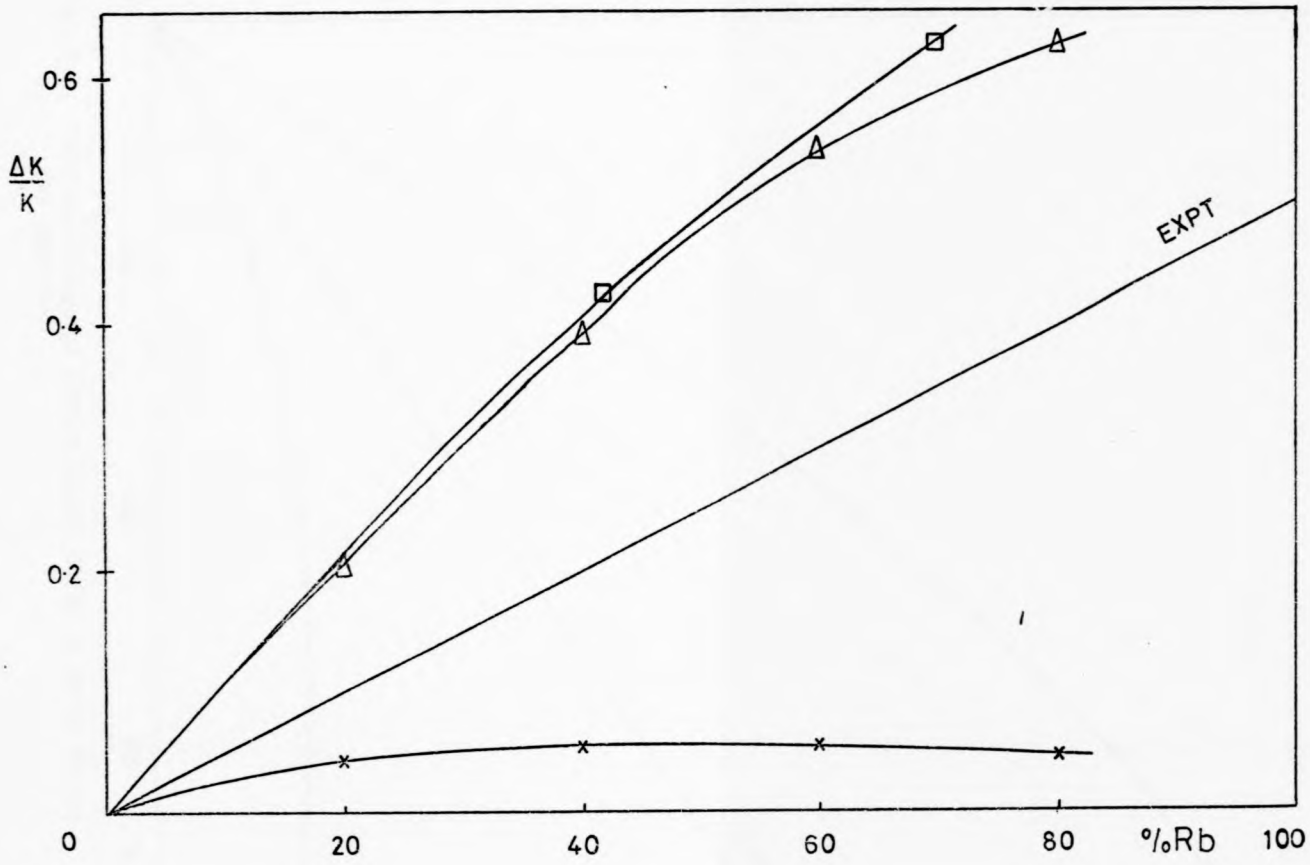

Fig. 5.8. Relative Change of Sodium Knight Shift in Na-Rb.
Key page 78.

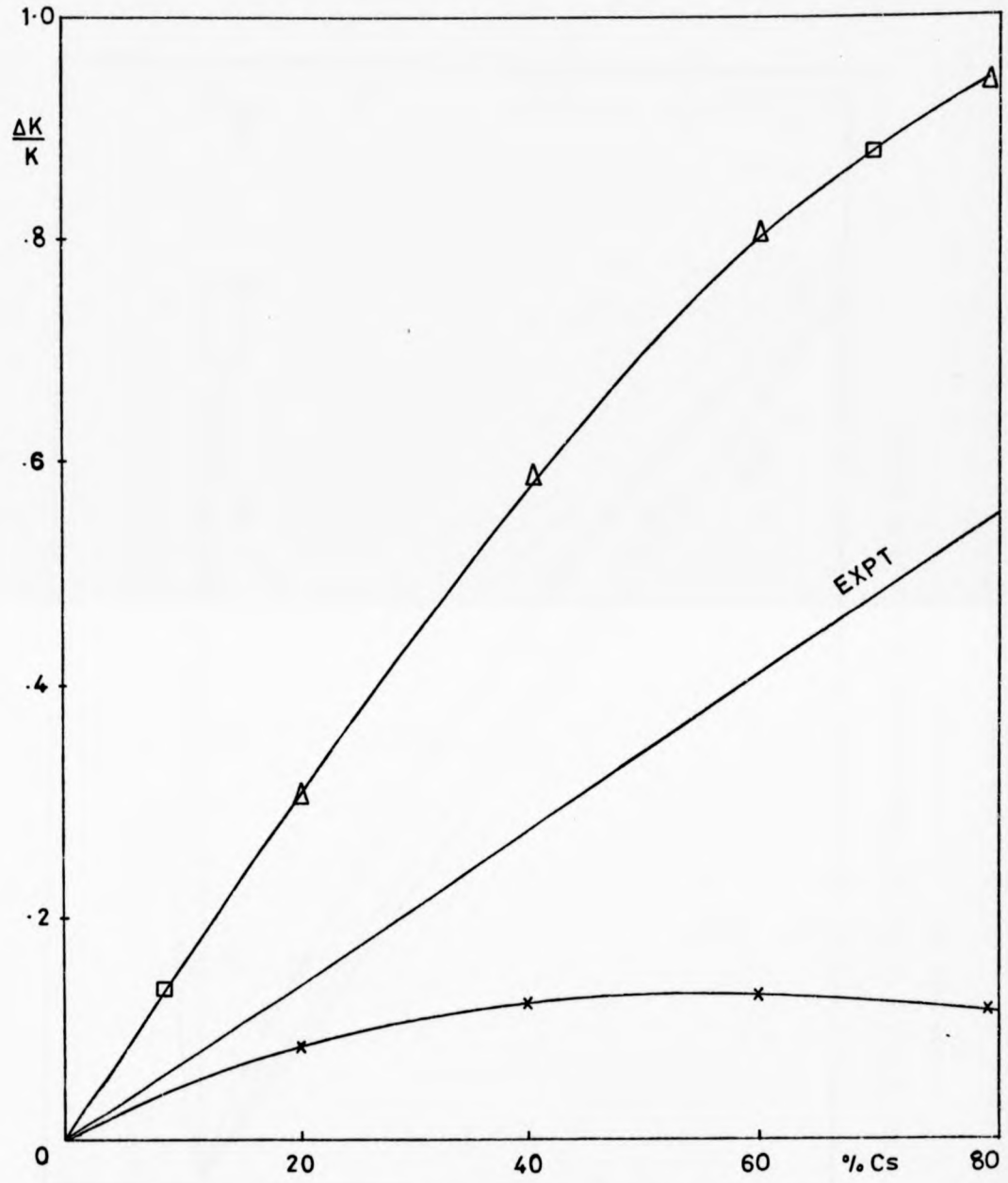

Fig. 5.9. Relative Change of Sodium Knight Shift in Na-Cs Alloys.
Key page 78.

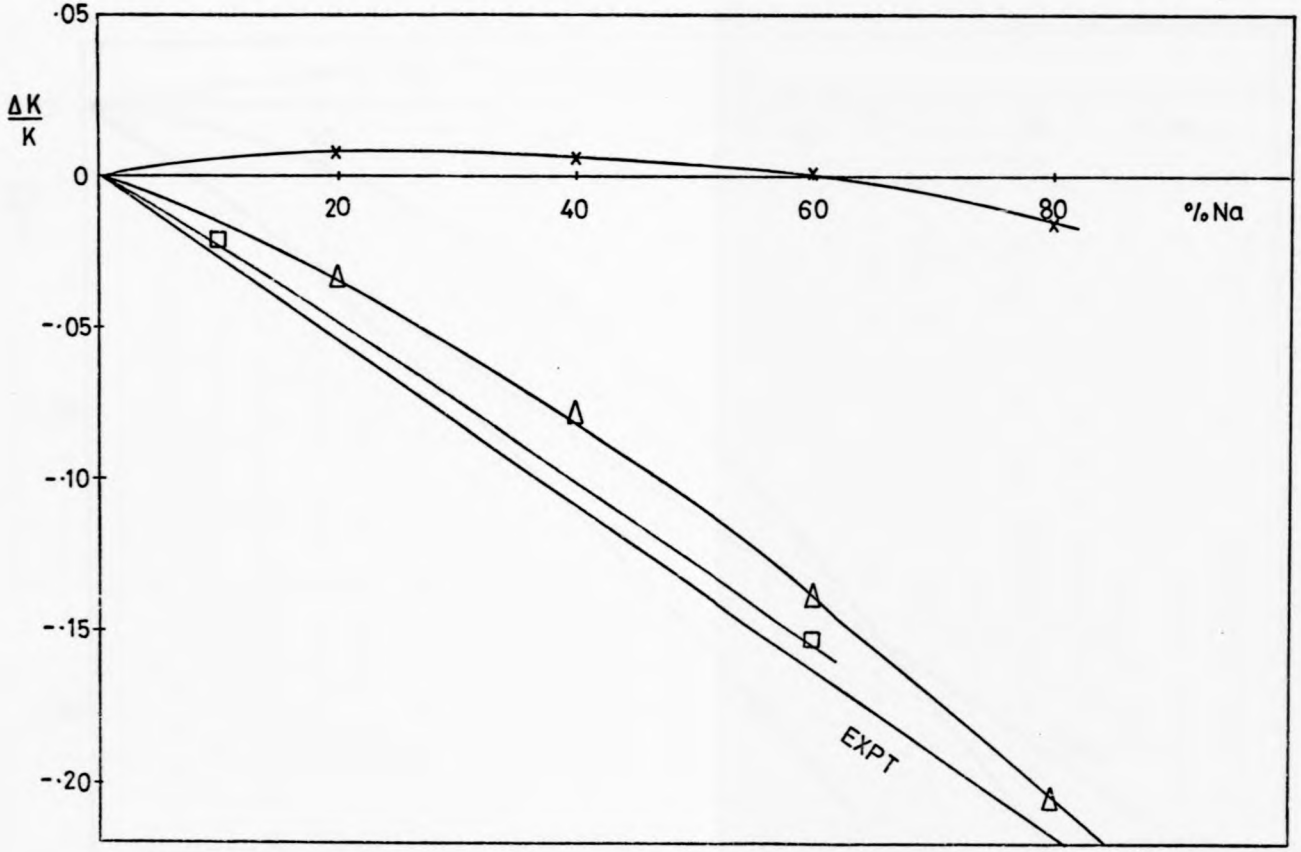

Fig. 5.10. Relative Change of Potassium Knight Shift in K-Na Alloys.

Key page 78.

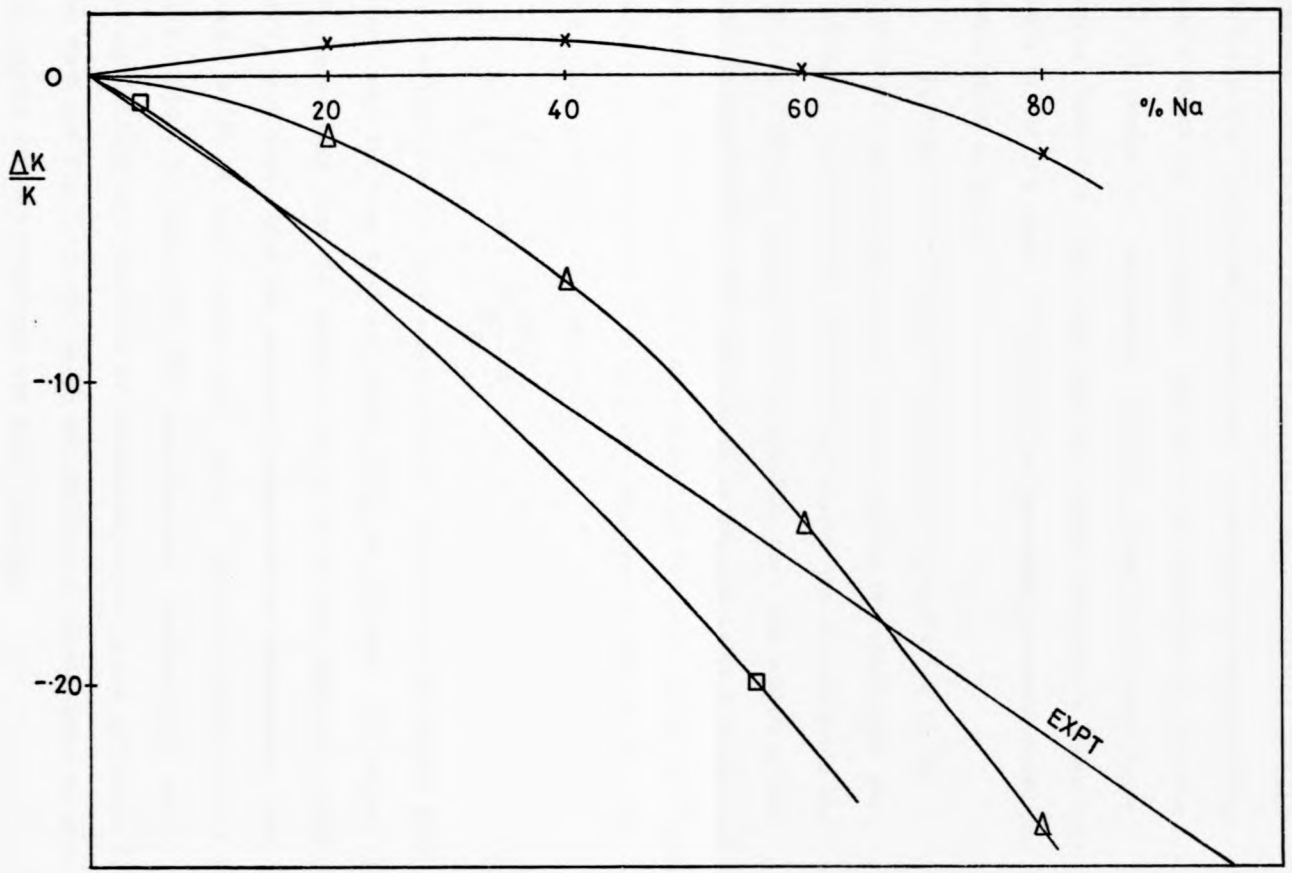

Fig. 5.11. Relative Change of Rubidium Knight Shift in Rb-Na Alloys.
Key page 78.

calculate. The main difference between their calculation and the present calculation is the choice of pseudopotential which only effects the first order correction. A similarity between Perdew and Wilkins and the present results would therefore be expected if the change in K was mainly due to a change in the zero order term. However a comparison with the single OPW results shows that this is not the case. In general the agreement between theory and experiment is good.

In view of the insensitivity of this calculation to the choice of input parameters it is interesting to investigate the causes of the remaining discrepancy between the calculations and the experimental results. It is possible that the values of the spin susceptibility used here are in error, and in fact Perdew and Wilkins originally proposed this formalism for calculating the contact density in the hope of finding χ from measured Knight shifts. By rearranging eq 5.3. the expression

$$\chi = \left(\frac{\Delta K}{K_o} + 1 \right) \frac{\chi_o (\Omega P_F)_o}{\Omega P_F} \qquad (5.5)$$

is obtained for the spin susceptibility of an alloy and values have been found for some Na-K and Na-Rb alloys as follows. The values of ΩP_F were taken from the calculations given in this chapter; values of $\Delta K/K_o$ were found from the measured concentration dependence of the Knight shift in these alloys (28); and χ_o, the spin susceptibility of pure sodium, is known from CESR measurements. Graphs of the spin susceptibility as a function of concentration are given in Fig.5.12 for Na-K and Fig.5.13 for Na-Rb and these were extrapolated to give the values for pure potassium and pure rubidium.

A second set of values for the alloy spin susceptibilities was

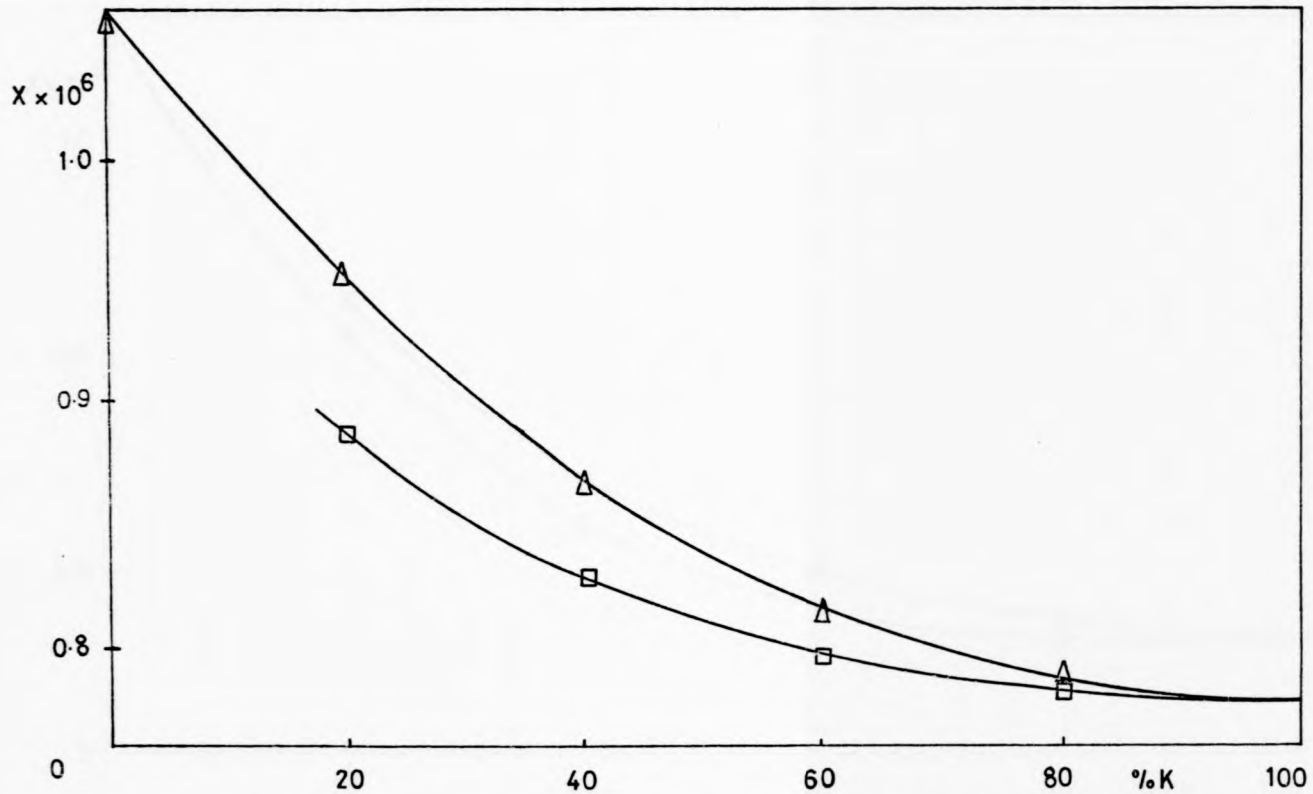

Fig. 5.12. Spin Susceptibility of Na-K Alloys. Points deduced from sodium Knight shift given by Δ. Points deduced from potassium Knight shift given by □.

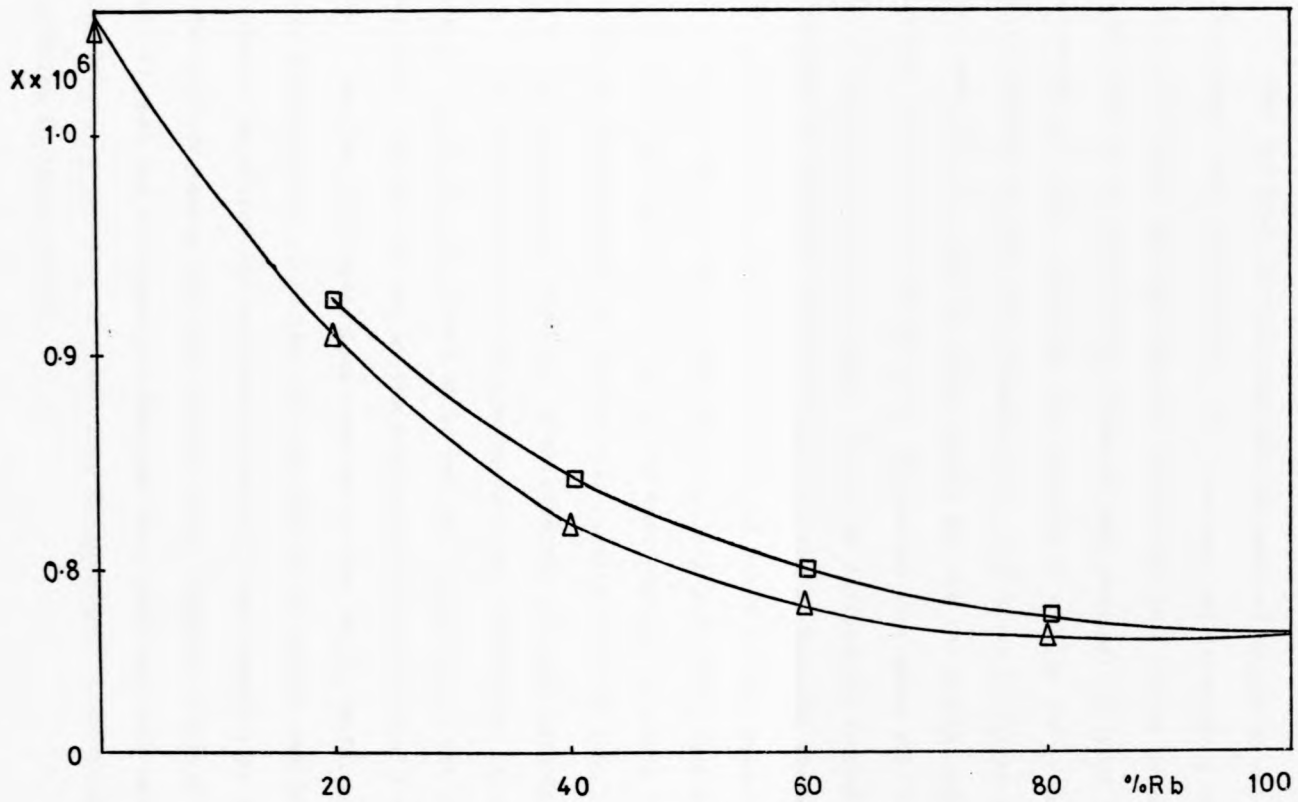

Fig. 5.13. Spin Susceptibility of Na-Rb Alloys. Points deduced from sodium Knight given by Δ. Points deduced from rubidium Knight shift given by □.

then found by repeating this process for the second element in the alloy system using this extrapolated value of pure metal spin susceptibilities.

For the Na-K we note that the two sets of values do not coincide. This shows that equation 5.3 is in error and the discrepancy between the theoretical and experimental results for $\Delta K/K$ cannot be merely explained by an error in the value of spin susceptibility of the elements involved. In Na-Rb the two sets of results for χ in the alloy system do coincide. However this will occur if Λ varies at the same rate through the alloy system for the two metals, but of course the correct value of χ for the second pure metal will only be obtained if Λ is a constant. The large differences between χ obtained in this way and χ obtained from the de Haas-Van Alphen g-factor experiments for both potassium and rubidium also suggests that this method is unreliable for obtaining pure metal spin susceptibilities. The values of χ for cesium that would be required to bring the experimental and theoretical results for $\Delta K/K$ into line is also very much larger than the value obtained by other methods.

The remaining discrepancies between the theoretical and experimental results for $\Delta K/K$ must therefore be due to a variation of the correction factor Λ. As pointed out at the beginning of this section, Λ may be due either to other mechanisms envolved in the Knight shift, such as core polarisation, or to the inaccuracies of the method used here to evaluate the direct contact density, and it is not possible to distinguish between these causes from the present work. However it should be noticed that the discrepancies here are very small and this method does provide a good way of predicting the magnitude of the Knight shift variation in these alloys.

5.2.2. Divalent and Polyvalent Metal Alloys

The variation of Knight shift has been calculated for gallium alloyed with zinc, indium and tin; for cadmium alloyed with indium, zinc, tin, mercury, thallium, lead and bismuth; and for indium alloyed with gallium, cadmium, tin, mercury, thallium, lead and bismuth. These results are shown graphically in Figs.5.14 to 30 and numerical results given in Appendix D.

As well as the full nonlocal calculation using Shaw's potential, Ashcroft and Lekner's structure factors and Mann's wavefunctions a number of other calculations have been made for comparison. Firstly, for gallium alloys, the effect of using more realistic structure factors than Ashcroft and Lekner's has been investigated. Structure factors for the alloys were obtained by taking a weighted average of the pure metal structure factors found by neutron or X-ray diffraction. The results obtained using these "experimental" structure factors are also shown in Fig.5.14 to 16 It can be seen that the values of $\Delta K/K_o$ differ very little from those derived using the hard sphere model. Since gallium was one of the pure metals for which changing the structure factor had the greatest effect, it seems likely that the concentration dependence of K will be insensitive to the choice of structure factor for all the other alloy systems.

On the contrary, there are large differences between the values of $\Delta K/K$ obtained using different pseudopotentials. For most alloy systems four calculations have been made:-

a) to zero order the pseudopotential (the single OPW calculation).

b) using the Ashcroft pseudopotential.

c) using the OMP - but in the local approximation discussed in Sec.5.1.

d) using the full nonlocal OMP.

As can be seen from Figs. 5.14. to 30.

KEY TO FIGS. 5.14. to 30.

o Denotes experimental results.

× Denotes results of single OPW calculation.

□ Denotes results of calculation using Ashcroft pseudopotential and Ashcroft and Lekner structure factor.

▽ Denotes results of calculation using OMP in local approximation and Ashcroft and Lekner structure factor.

△ Denotes results of calculations using OMP and Ashcroft and Lekner structure factor.

+ Denotes results of calculation using OMP and experimental structure factor.

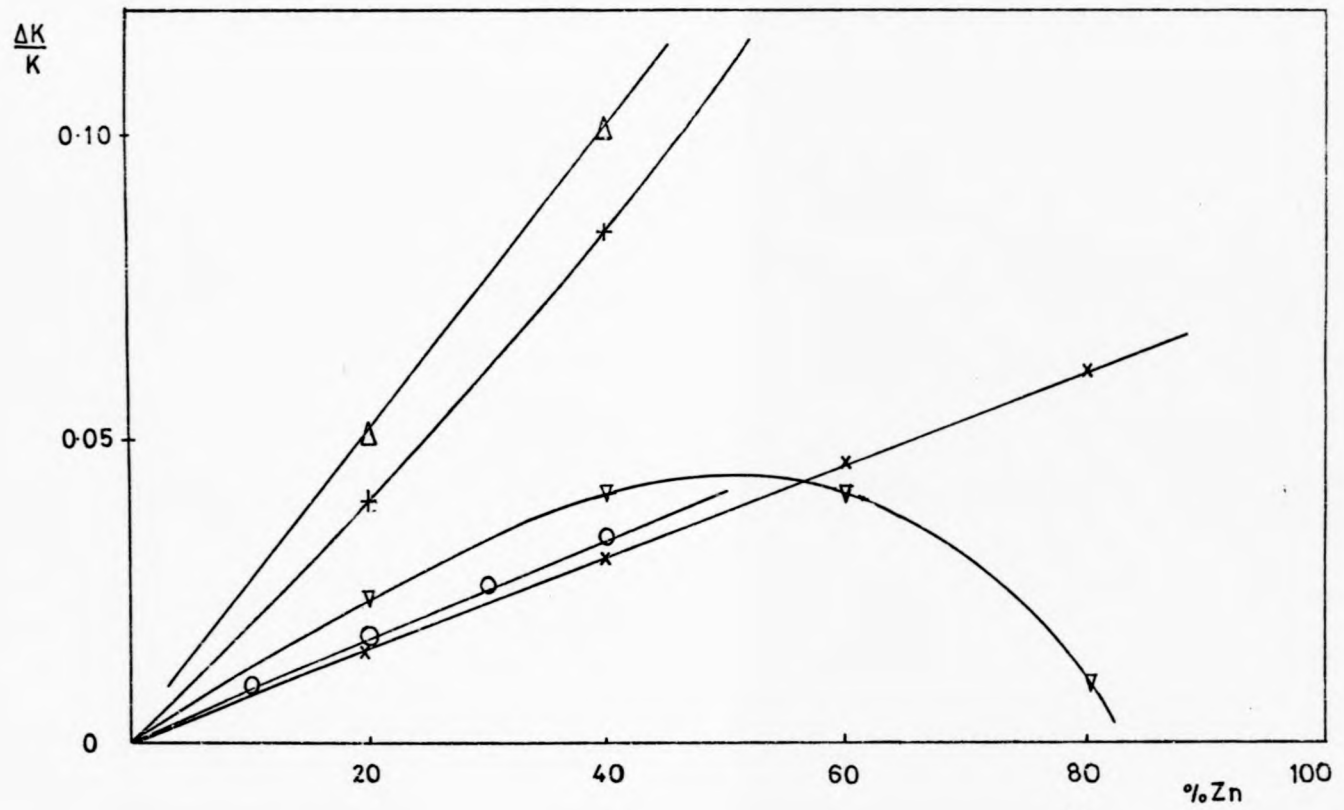

Fig. 5.14. Relative Change of Gallium Knight Shift in Ga-Zn Alloys. Key page 82.

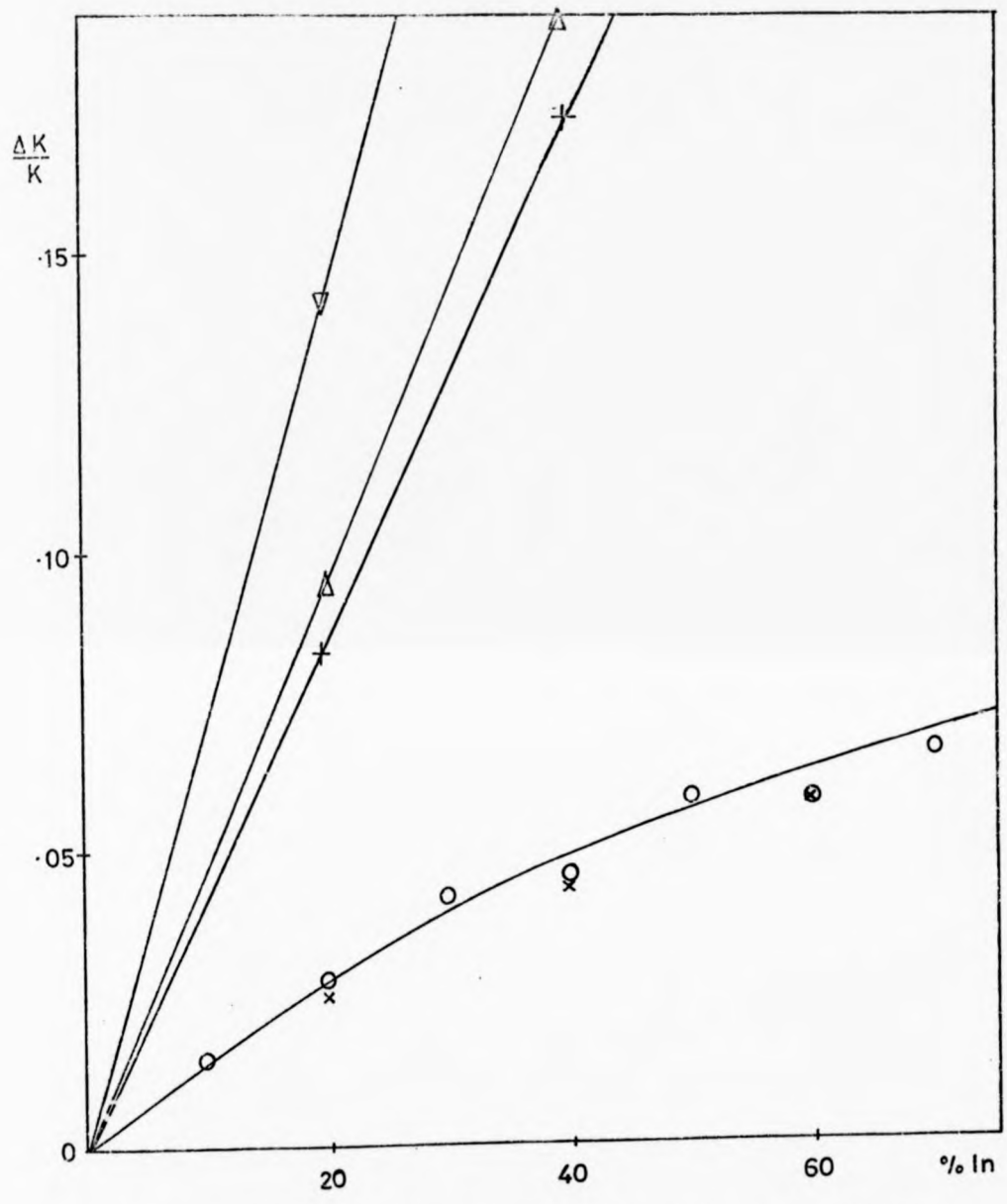

Fig. 5.15. Relative Change of Gallium Knight Shift in Ga-In Alloys.
Key page 82.

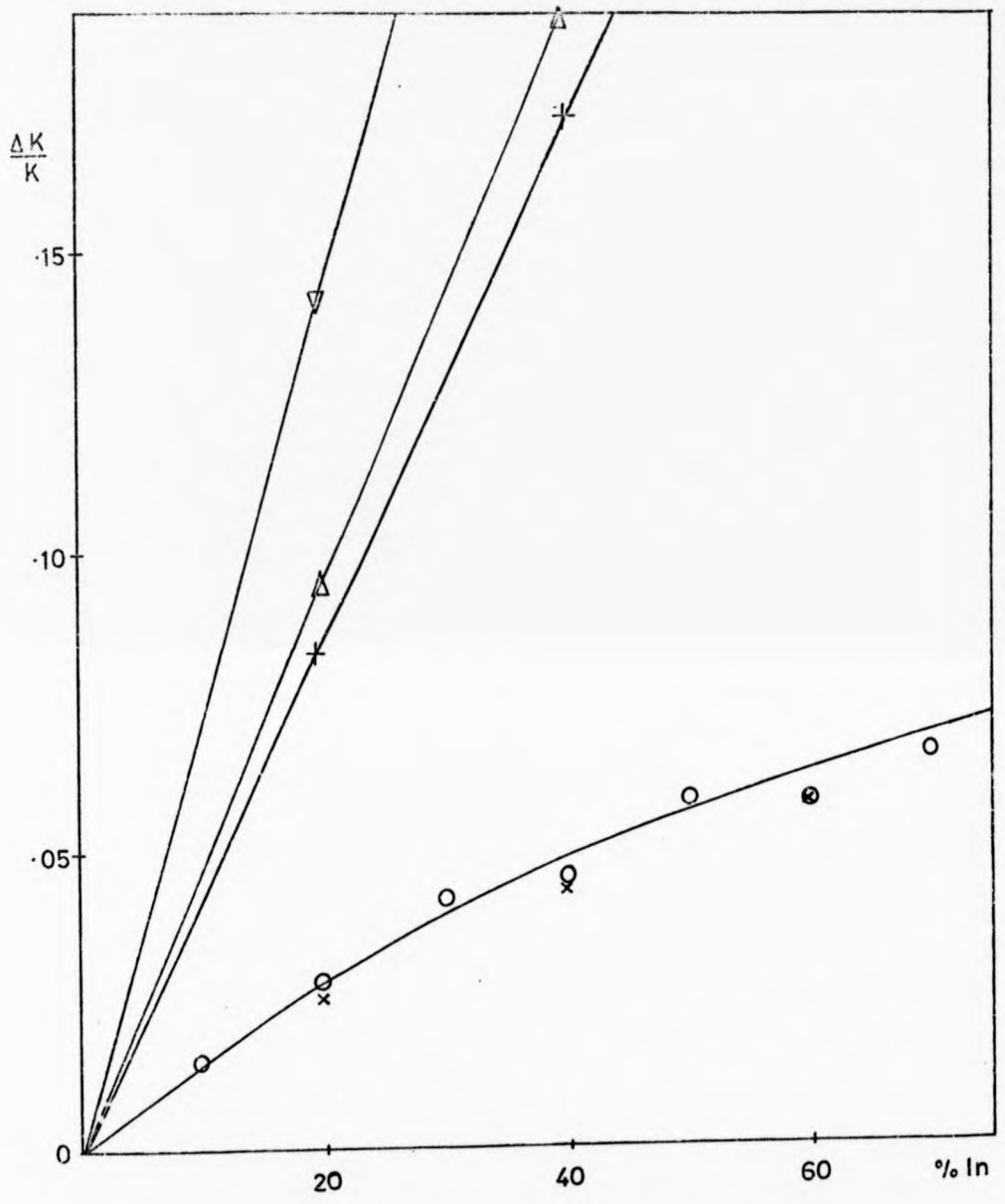

Fig. 5.15. Relative Change of Gallium Knight Shift in Ga-In Alloys.
Key page 82.

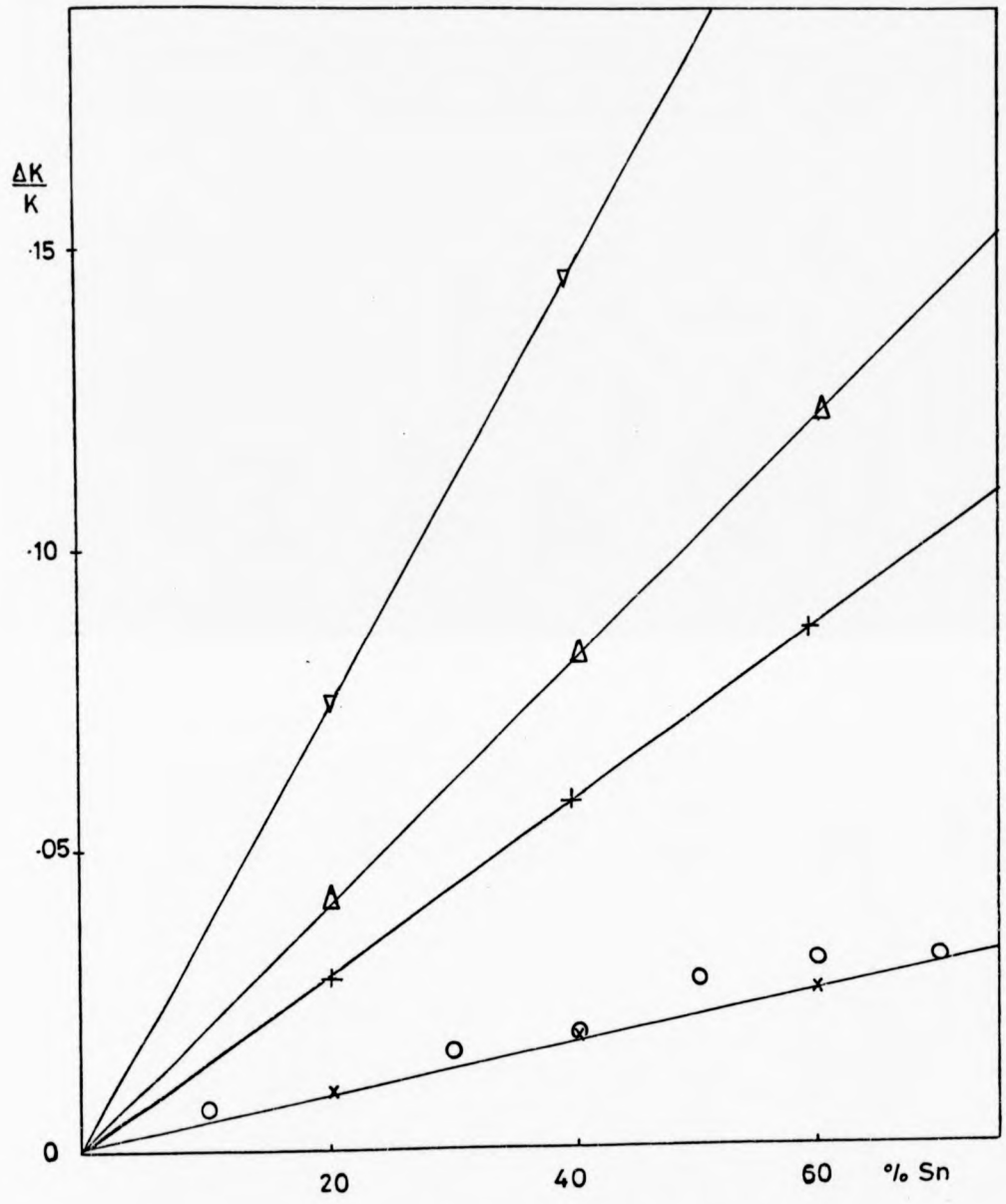

Fig. 5.16. Relative Change of Gallium Knight Shift in Ga-Sn Alloys.
Key page 82.

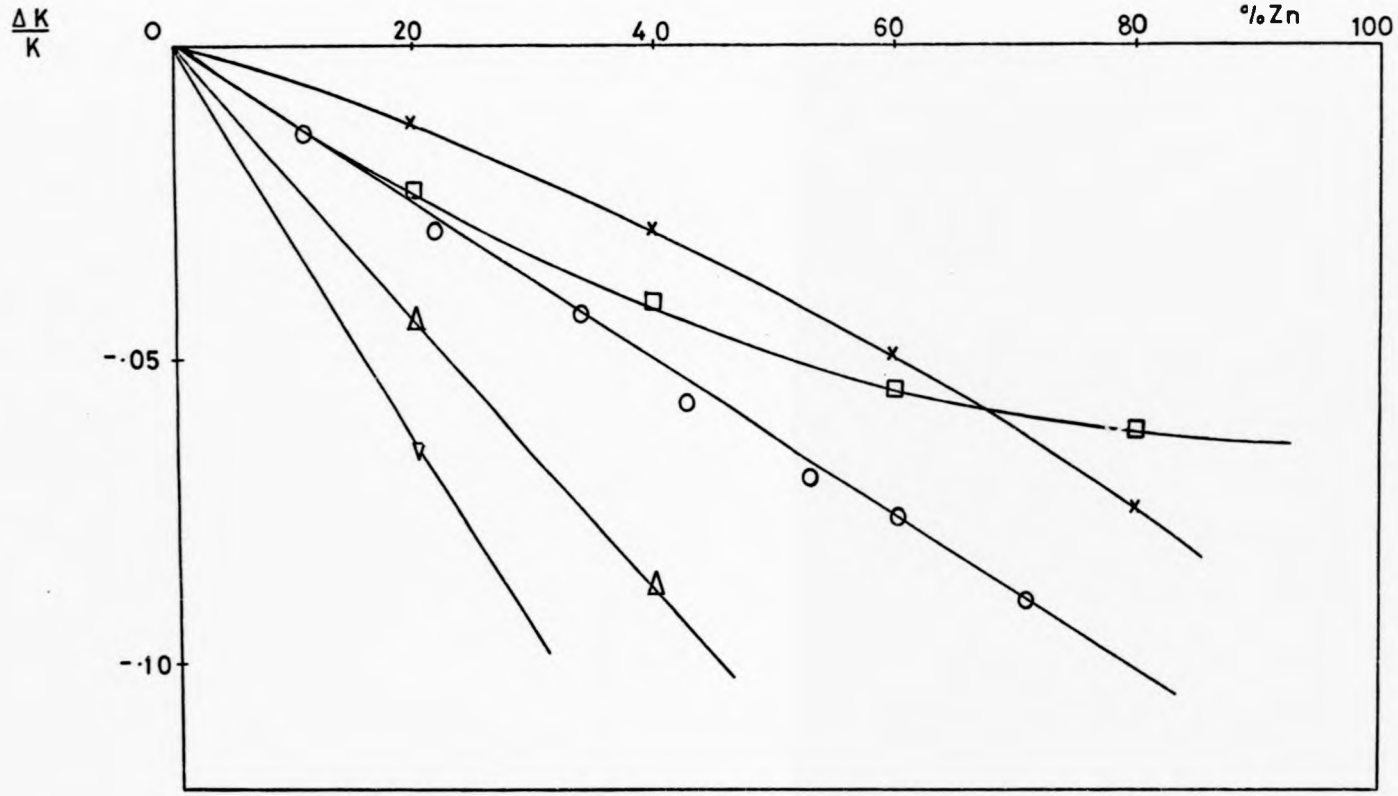

Fig. 5.17. Relative Change of Cadmium Knight Shift in Cd-Zn Alloys.
Key page 82.

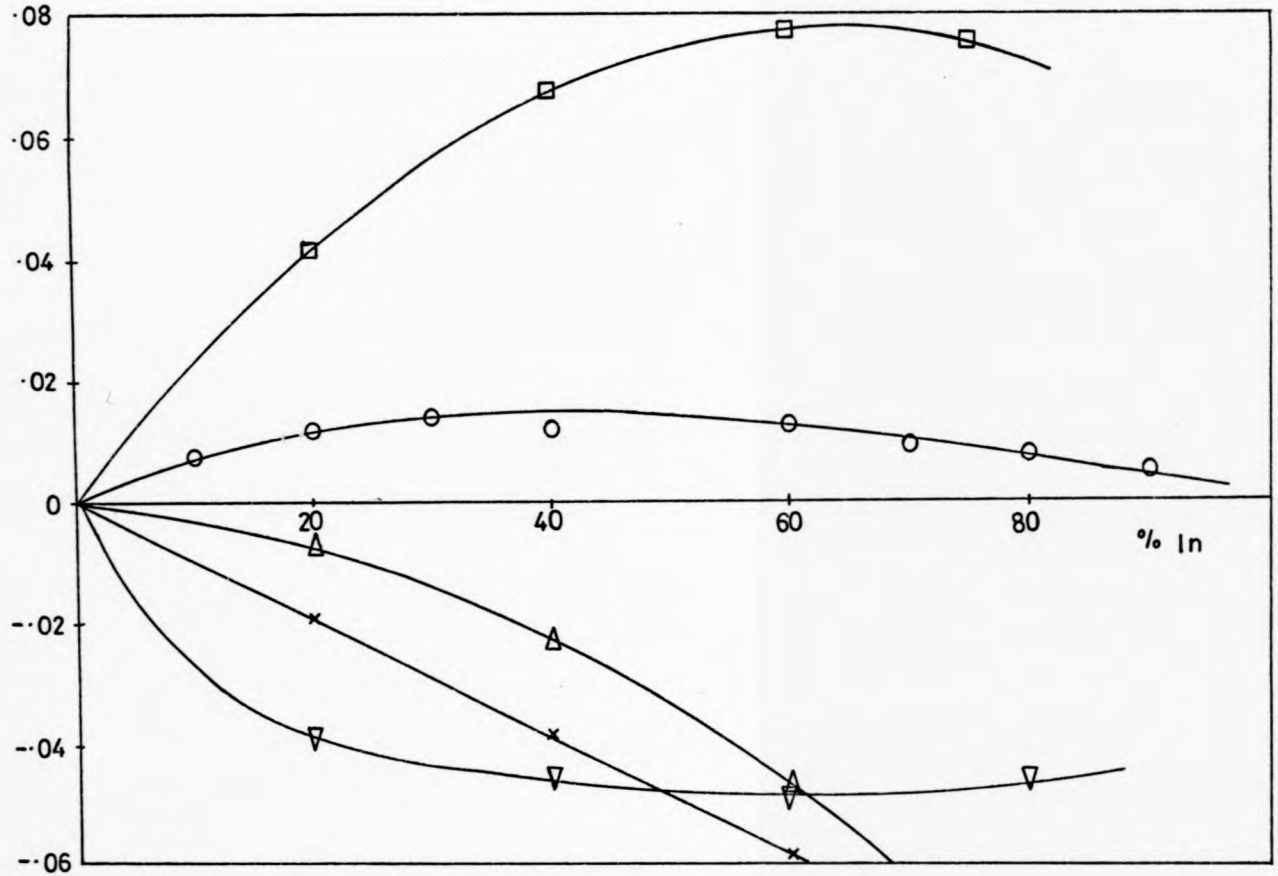

Fig. 5.18. Relative Change of Cadmium Knight Shift in Cd-In Alloys.
Key page 82.

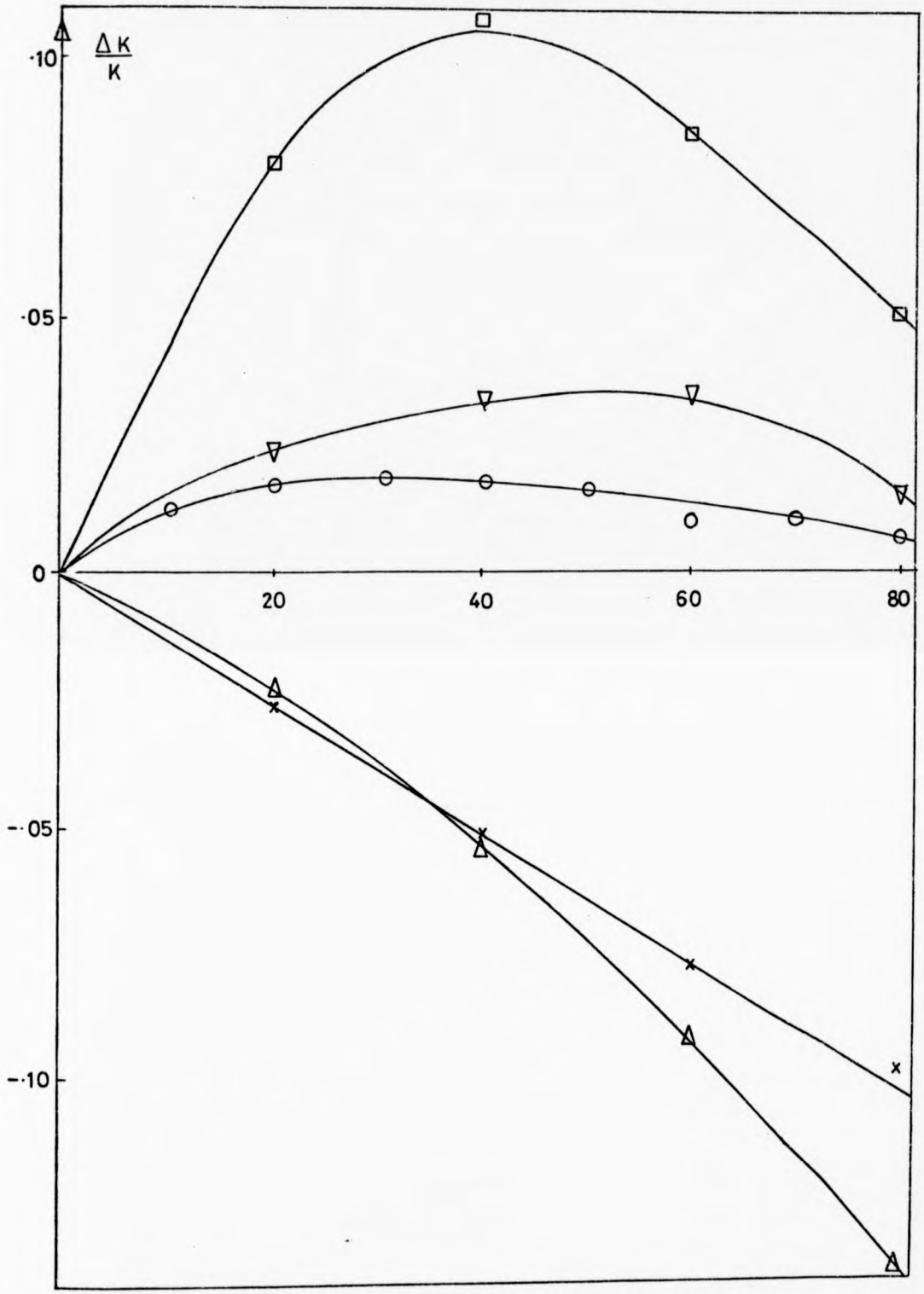

Fig. 5.19. Relative Change of Cadmium Knight Shift in Cd-Sn Alloys.
Key page 82.

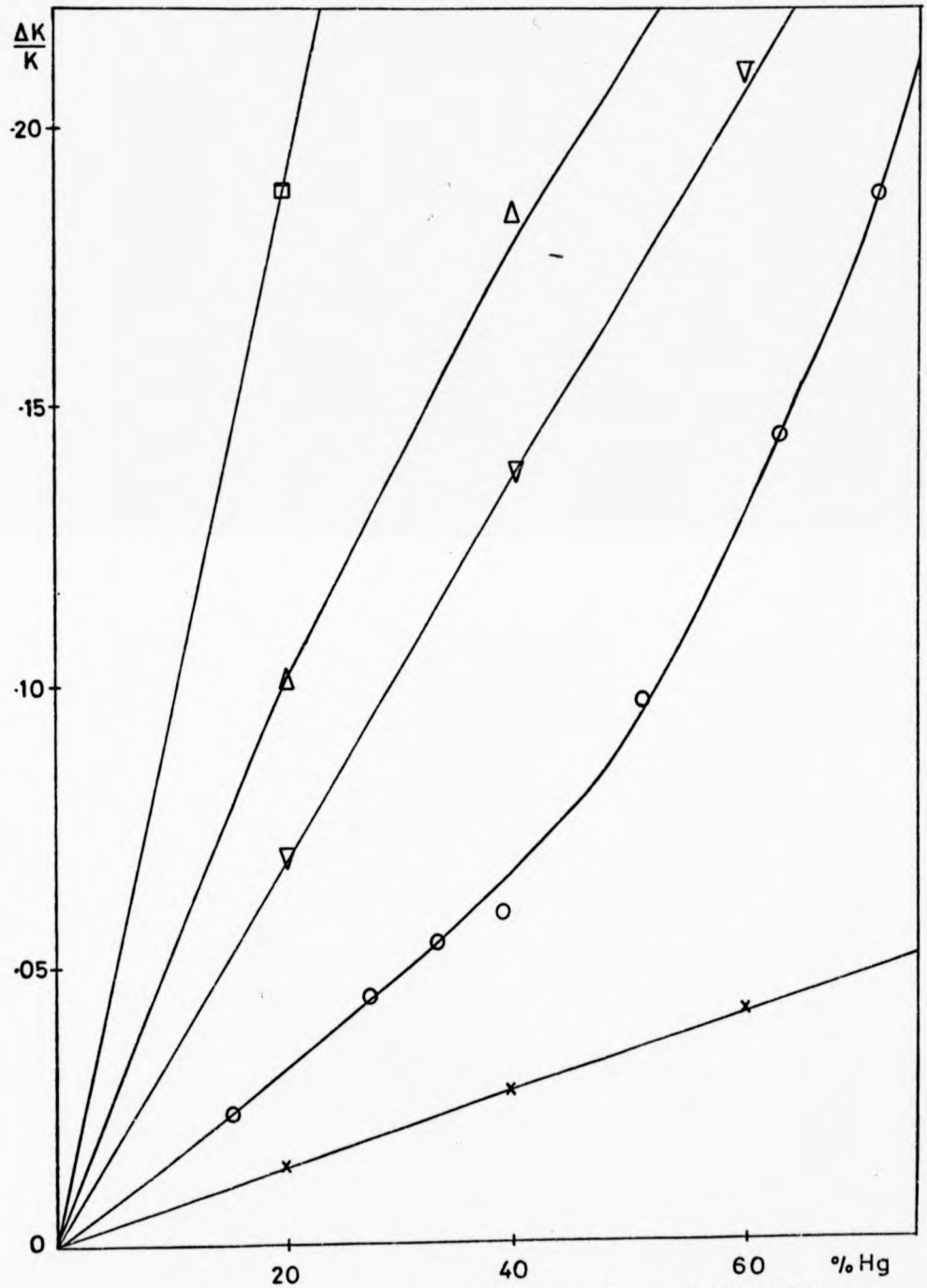

Fig. 5.20. Relative Change of Cadmium Knight Shift in Cd-Hg Alloys.

Key page 82.

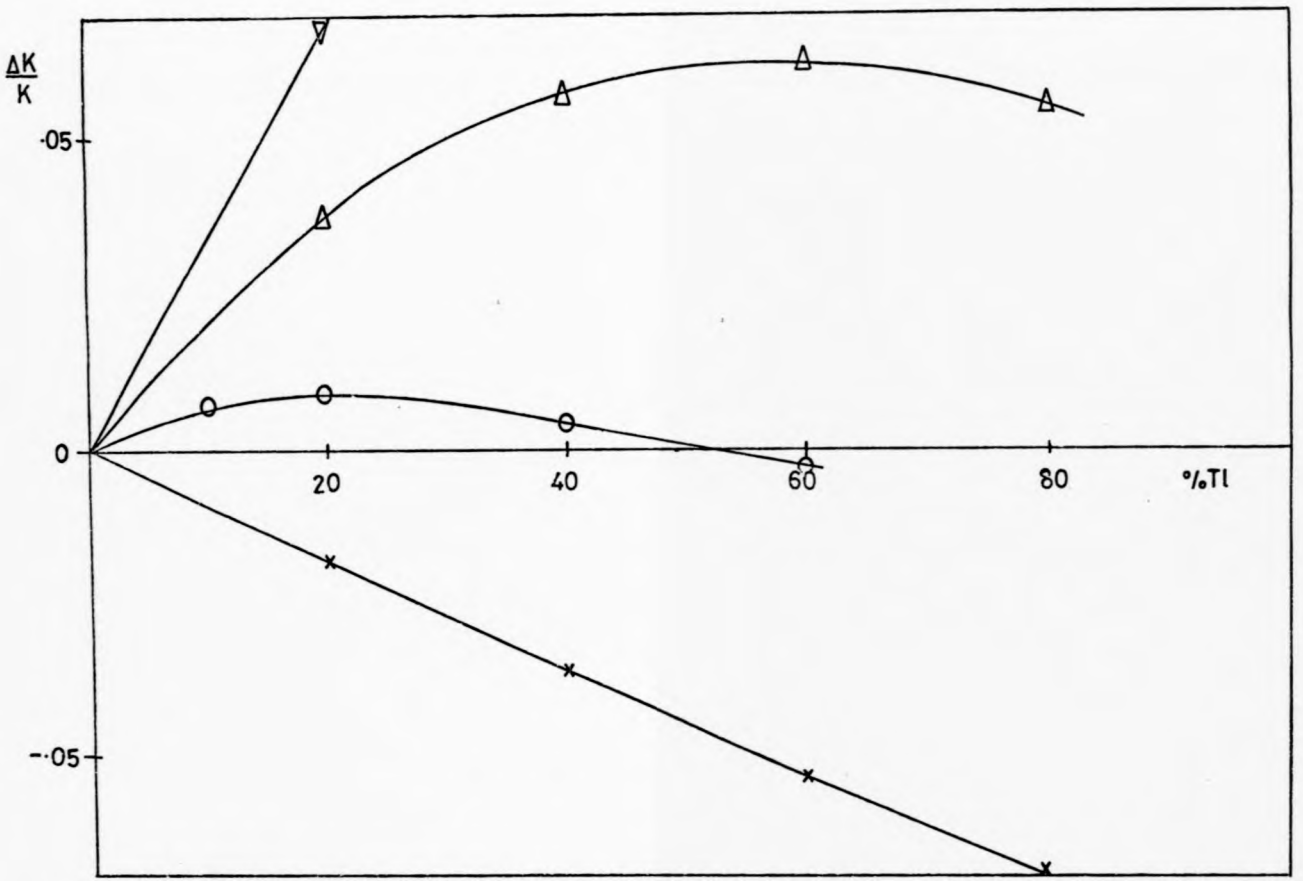

Fig. 5.21. Relative Change of Cadmium Knight Shift in Cd-Tl Alloys.
Key page 82.

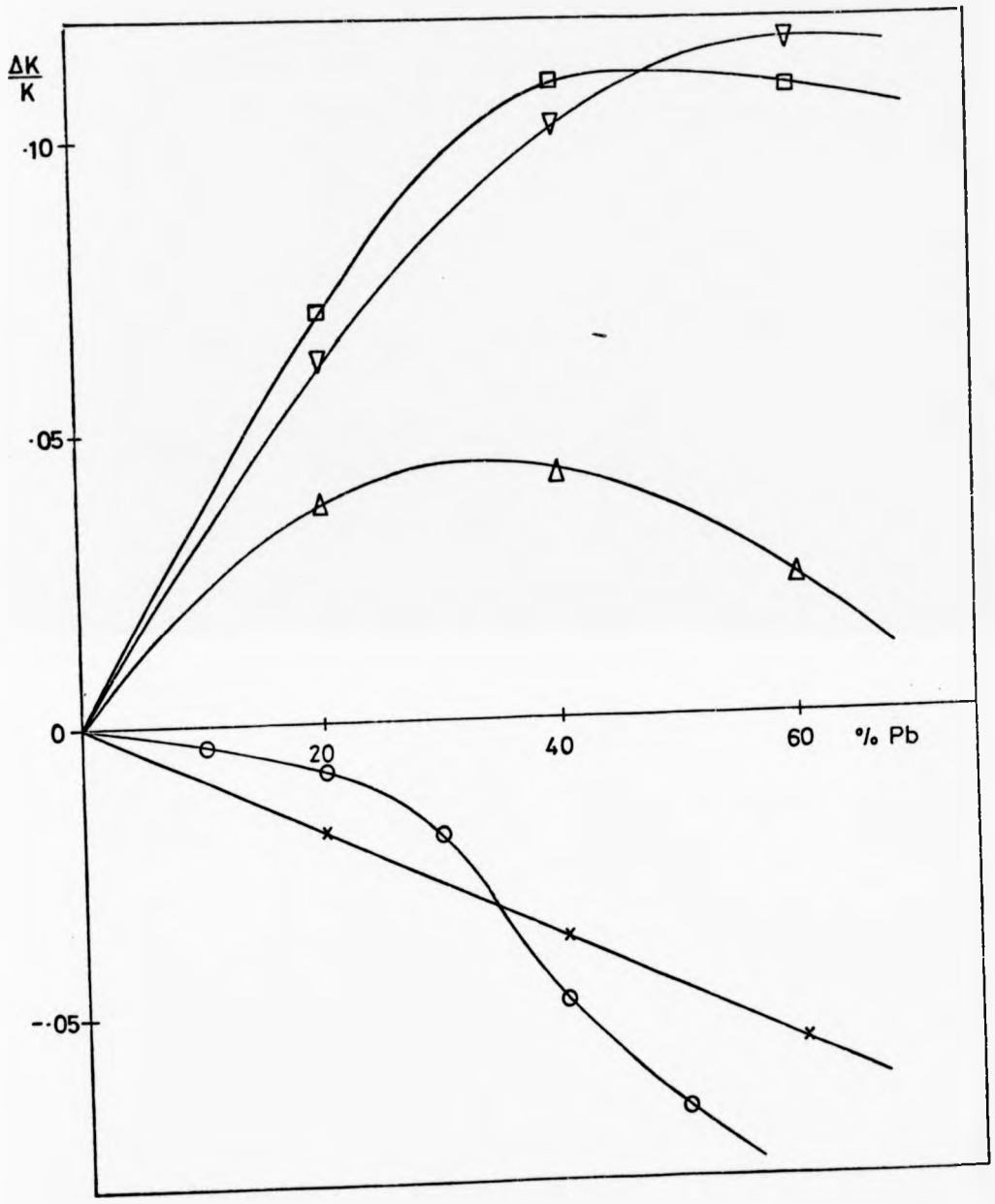

Fig. 5.22. Relative Change of Cadmium Knight Shift in Cd-Pb Alloys.
Key page 82.

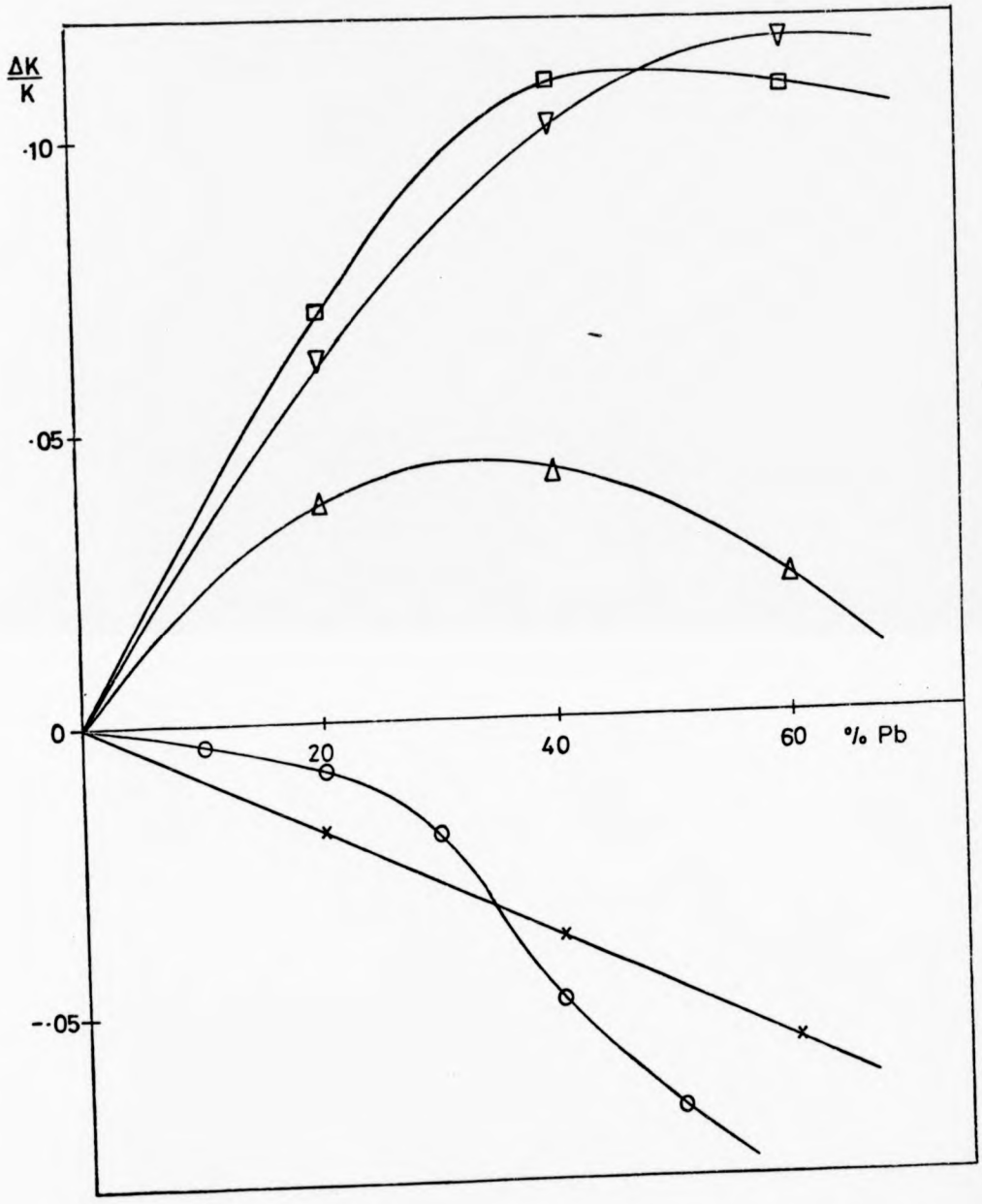

Fig. 5.22. Relative Change of Cadmium Knight Shift in Cd-Pb Alloys.
Key page 82.

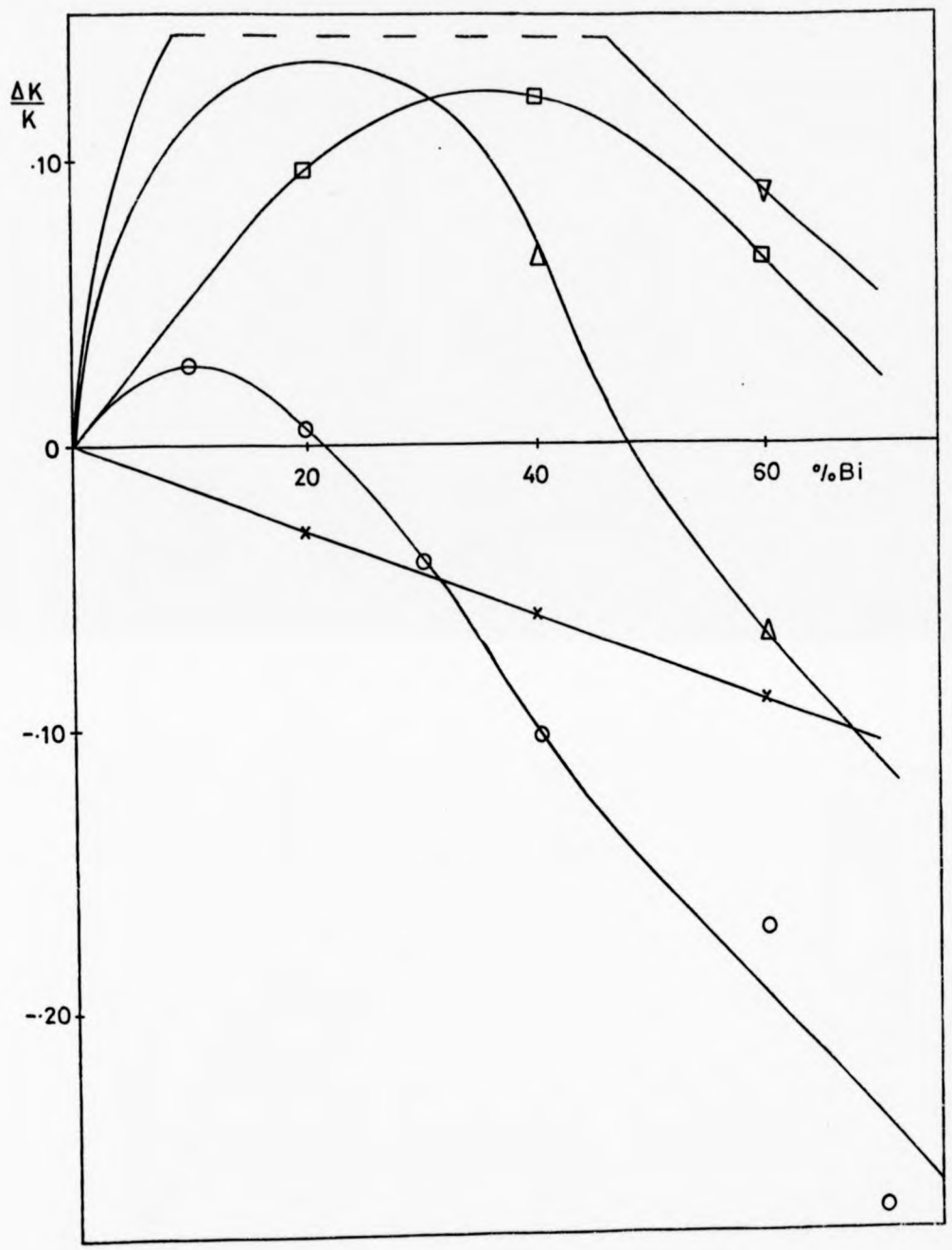

Fig. 5.23. Relative Change of Cadmium Knight Shift in Cd-Bi Alloys.
Key page 82.

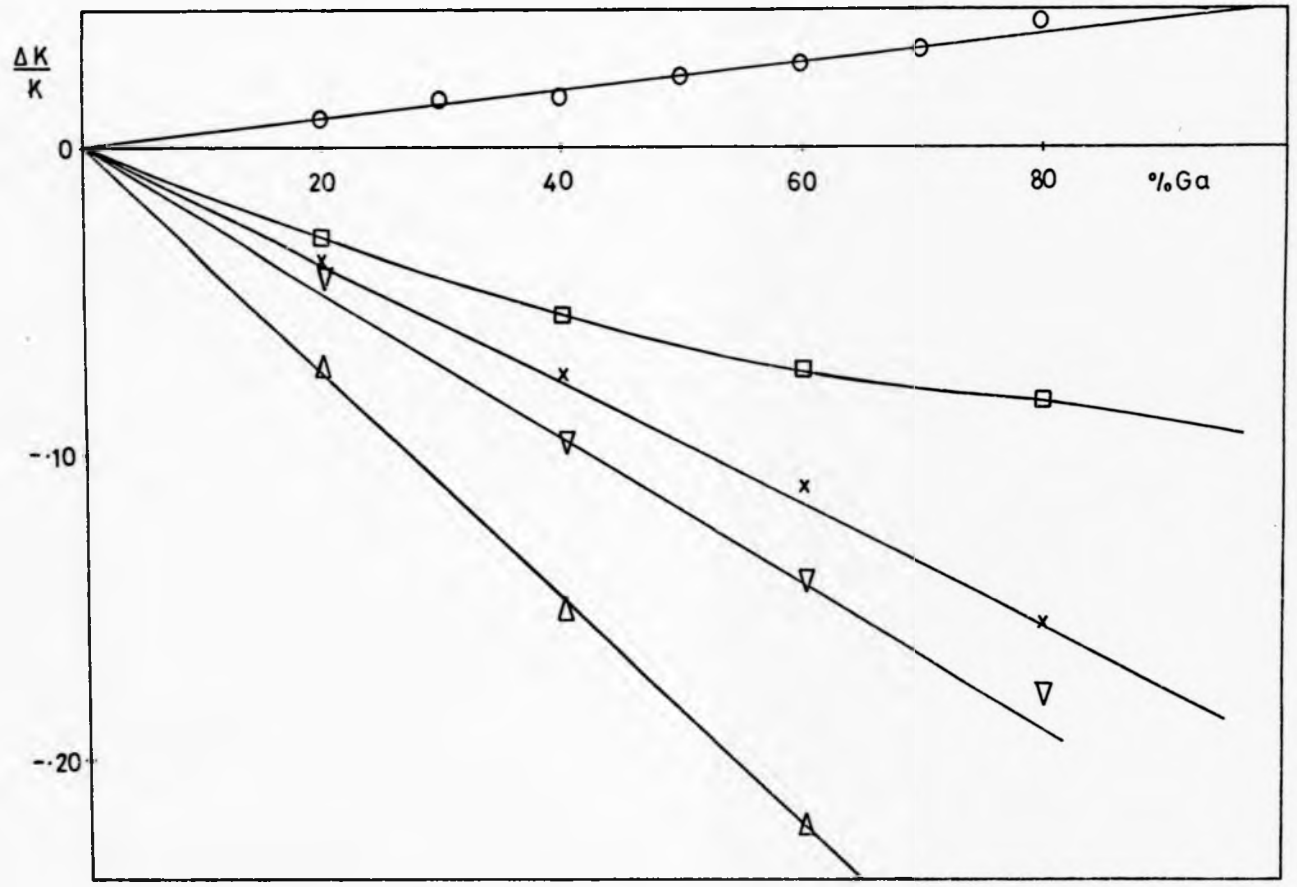

Fig. 5.24. Relative Change of Indium Knight Shift in In-Ga Alloys.
Key page 82.

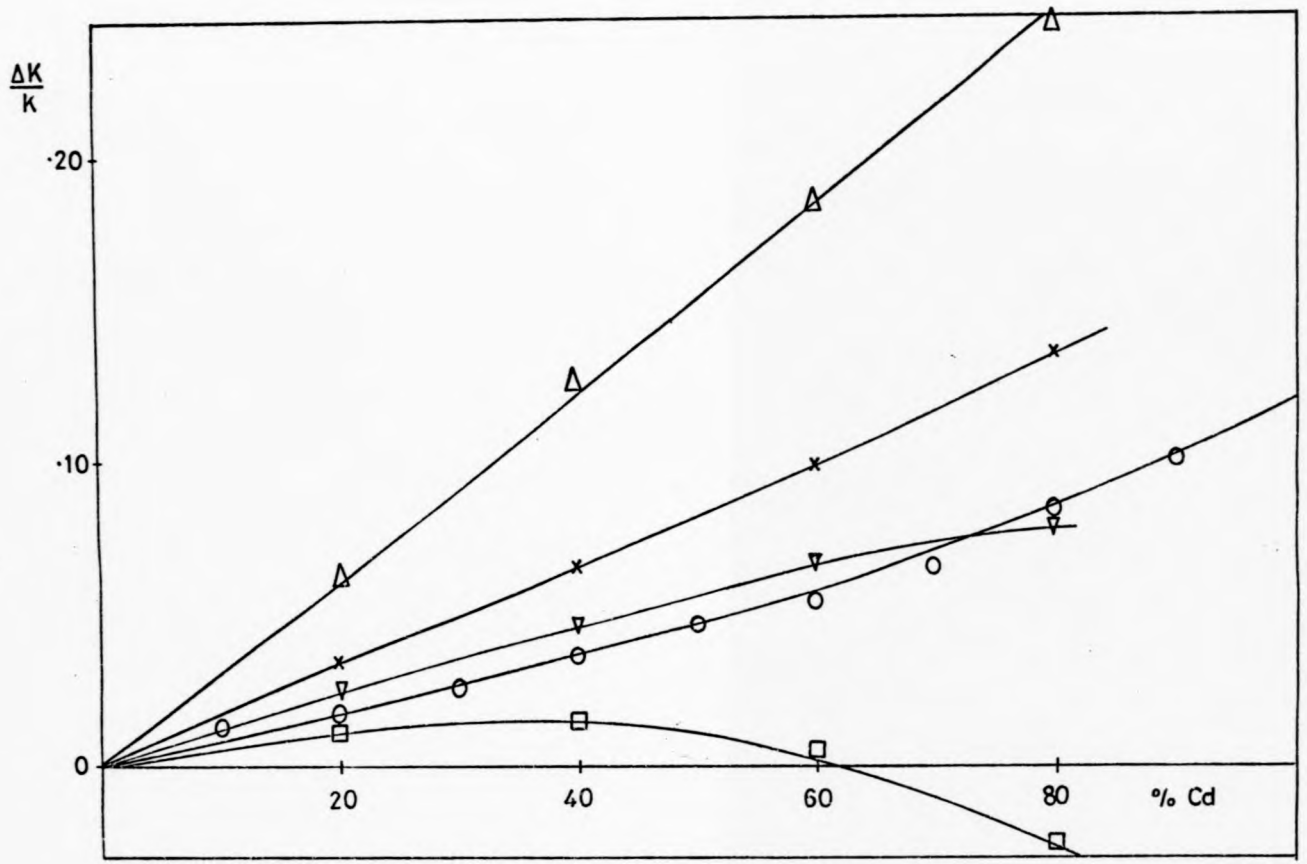

Fig. 5.25. Relative Change of Indium Knight Shift in In-Cd Alloys.
Key page 82.

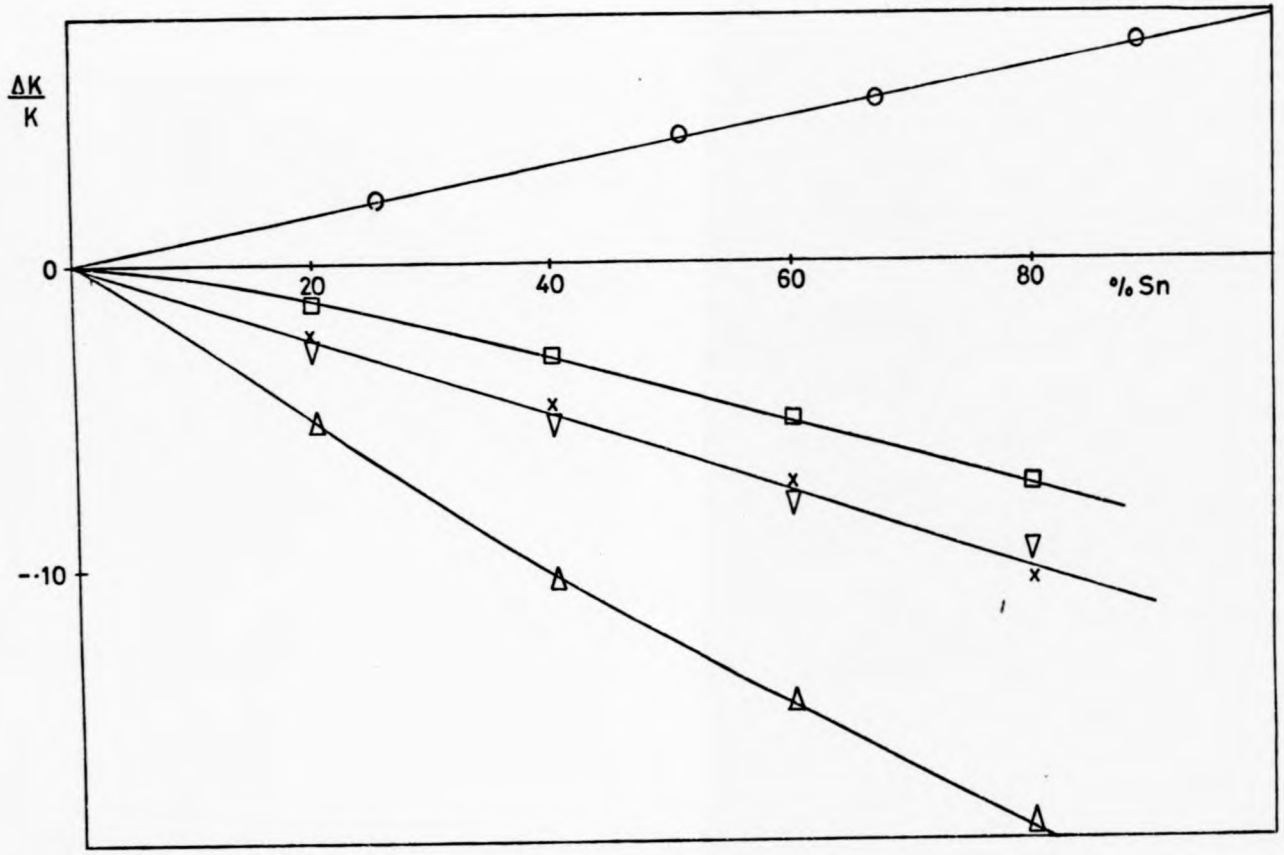

Fig. 5.26. Relative Change of Indium Knight Shift in In-Sn Alloys..
Key page 82.

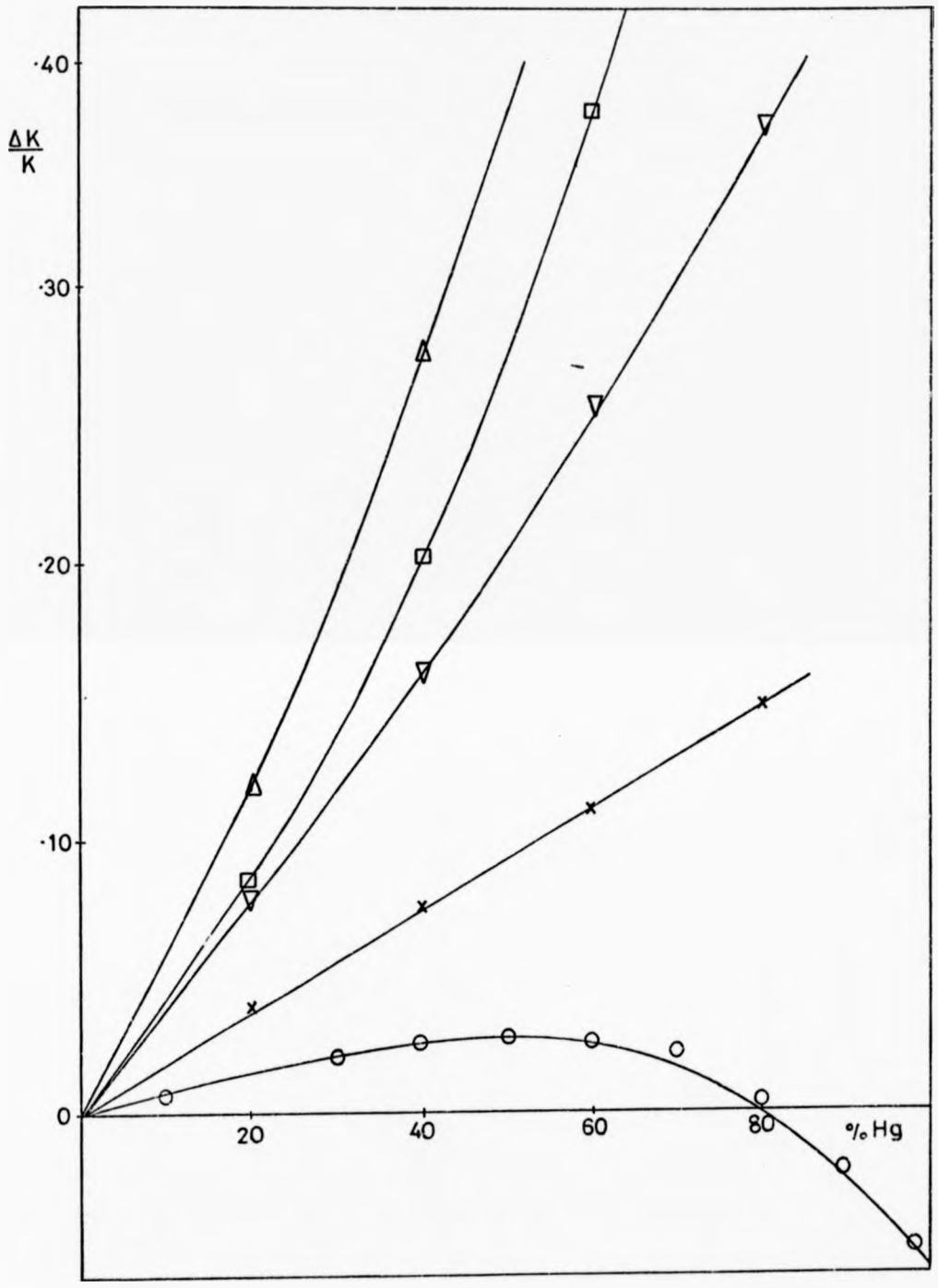

Fig. 5.27. Relative Change of Indium Knight Shift in In-Hg Alloys.
Key page 82.

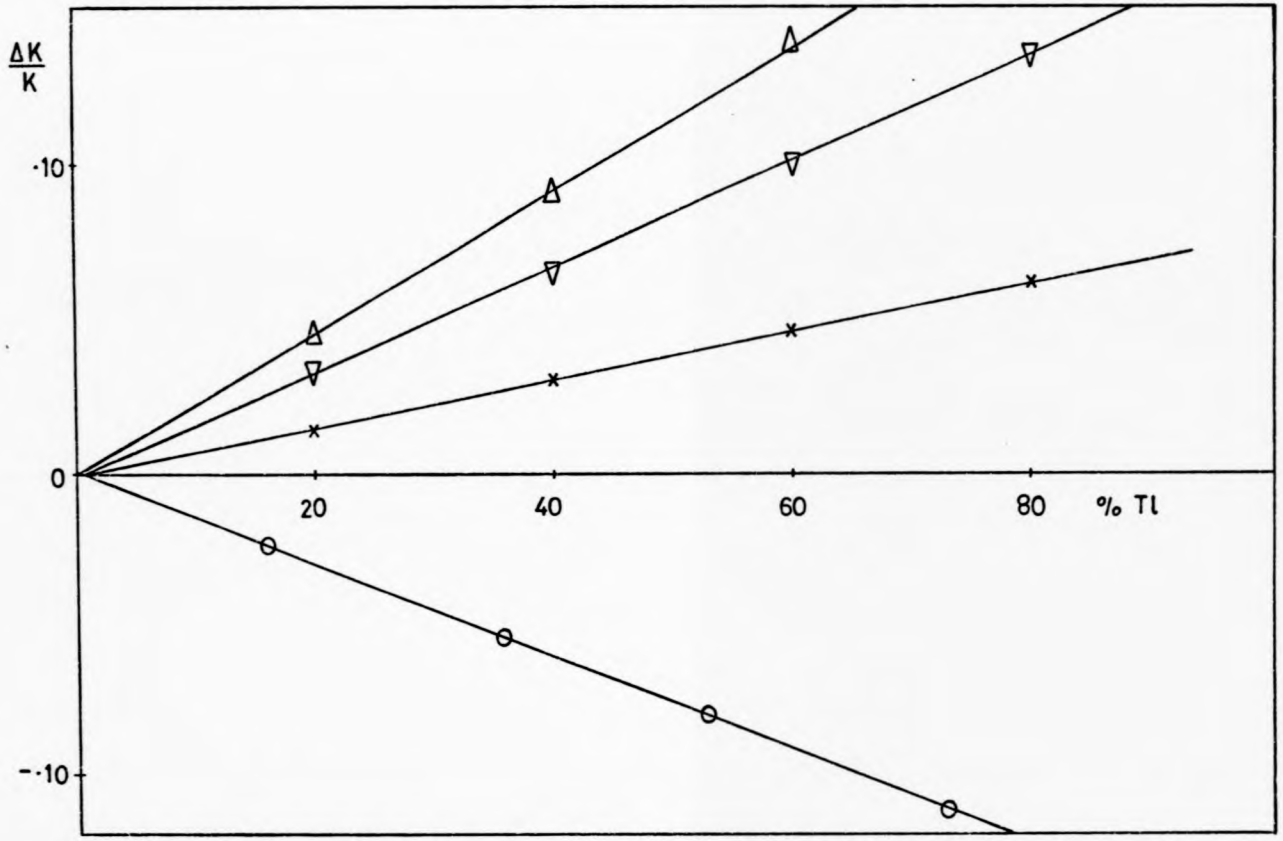

Fig. 5.28. Relative Change of Indium Knight Shift in In-Tl Alloys.
Key page 82.

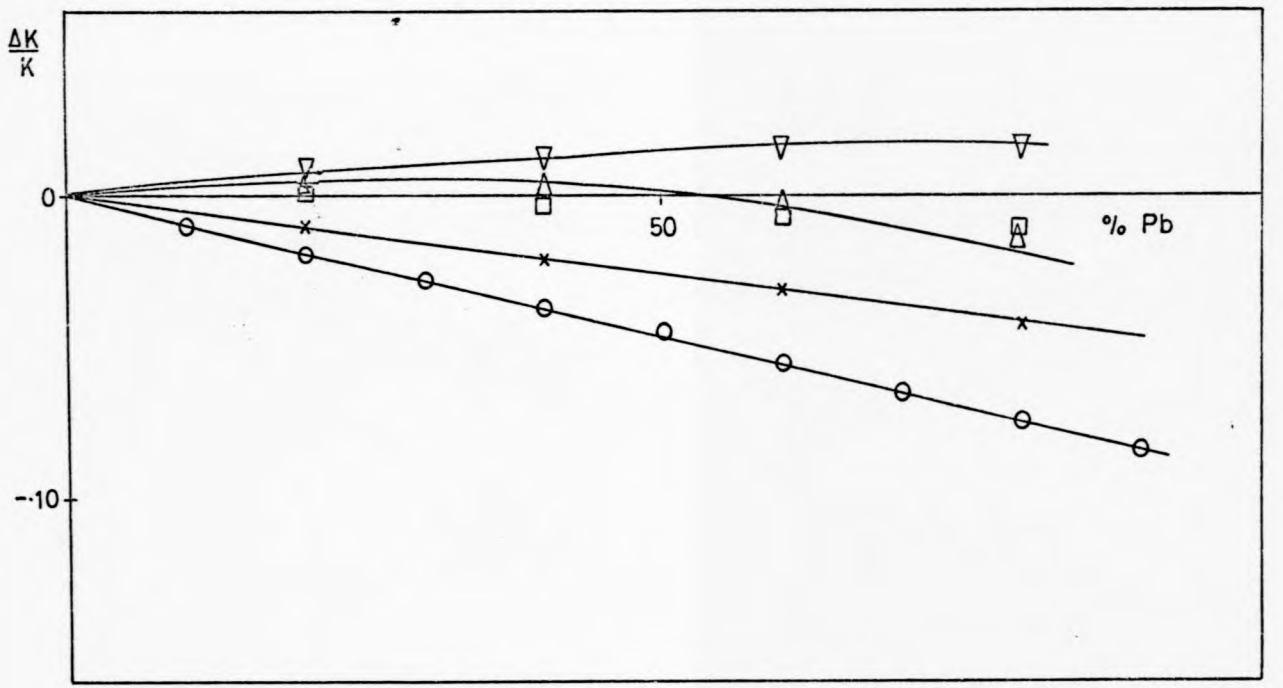

Fig. 5.29. Relative Change of Indium Knight Shift in In-Pb Alloys.
Key page 82.

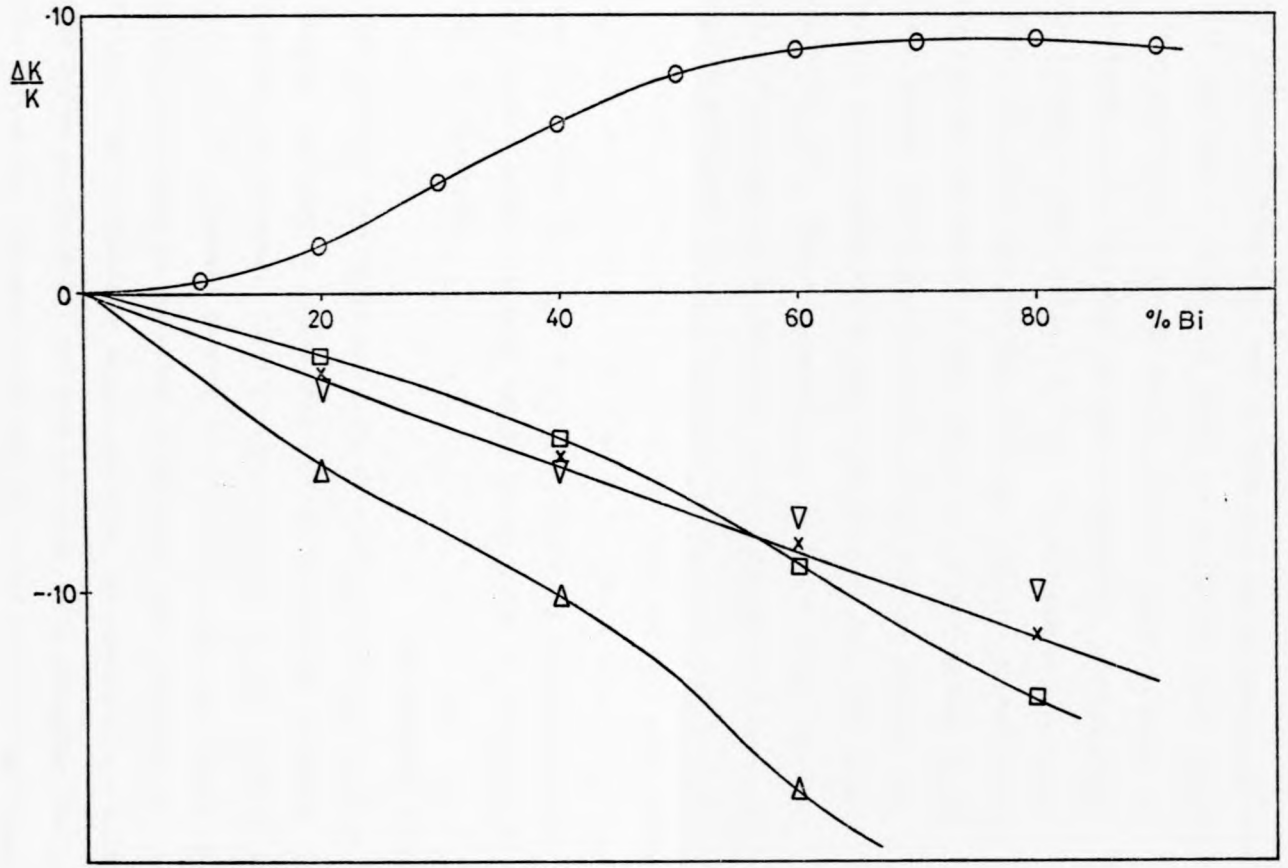

Fig. 5.30. Relative Change of Indium Knight Shift inIn-Bi Alloys.

Key page 82.

there are considerable differences between results obtained by the different methods and none of them give any systematic agreement with experiment. In gallium alloys the single OPW result provides a very good estimate of the Knight shift variation, although the corrected value, even when calculated nonlocally, overestimates the variation considerably. No value for the Ashcroft potential results are given here as this produces a negative contact density for pure gallium which is meaningless. In cadmium alloys the non-local results give a qualitatively correct picture although the results differ considerably from those obtained using the local approximations. Most disappointingly, in indium alloys there are only two systems, In-Cd and In-Pb, where a variation of even correct sign is predicted.

However it should be realised that these are very small changes of Knight shift, compared with those in the alkali metal alloys for example, so that even small errors in calculating the Knight shift will produce relatively large errors in the change of this quantity with concentration.

One possible source of error may be uncertainties in the spin susceptibilities of these elements. In order to investigate this possibility the following procedure was employed. Firstly values of χ for the pure elements were chosen to give agreement between the theoretical and experimental values of $\Delta K/K_o$ of cadmium in the alloy systems with these elements. To do this it was necessary to assume the value for cadmium of $\chi = 1.375$ (from Dupree and Geldhart) and then the values of χ throughout the alloy system were evaluated using the calculated values of the contact density and the experimental values for $\Delta K/K_o$. The resulting values of χ were then plotted against concentration and extrapolated to give the values of χ for the second elements in the alloys. This was only

possible for the metals zinc, indium and tin where the variation of χ calculated this way, was found to be linear and the results are compared with other calculations of χ for these metals in Table 5.9. In the other alloy systems the variation of χ was not linear and the lack of experimental results for low concentrations of cadmium made this process impossible.

The values of spin susceptibilities obtained in this way were then used to predict the variation of Knight shift of the second element in the Cd-In and Cd-Sn alloys and that for both metals in In-Sn. The results are presented in Figs.5.31 to 34, where they are compared with the results using the Dupree and Geldhart values for the susceptibilities. In all cases an improvement in agreement with experiment is obtained, however there are still considerable discrepancies so it can be seen there must be a variation of the correction factor for at least one, and probably both elements in these alloys. As with the alkali metals, the values of χ obtained by this method do not agree with those obtained by other metals. No calculations have been done for zinc alloys as there are no experimental results for comparison.

The correction factor, Λ, may vary because the core polarisation term is not constant, however, unlike the alkali metal alloys, these results depend strongly on the choice of pseudopotential, so it seems likely that the small inaccurracies in the potentials give rise to the final error. In particular in the gallium alloys the excellent agreement between the OPW results and experiments suggest that the correction term is calculated wrongly.

possible for the metals zinc, indium and tin where the variation of χ calculated this way, was found to be linear and the results are compared with other calculations of χ for these metals in Table 5.9. In the other alloy systems the variation of χ was not linear and the lack of experimental results for low concentrations of cadmium made this process impossible.

The values of spin susceptibilities obtained in this way were then used to predict the variation of Knight shift of the second element in the Cd-In and Cd-Sn alloys and that for both metals in In-Sn. The results are presented in Figs.5.31 to 34, where they are compared with the results using the Dupree and Geldhart values for the susceptibilities. In all cases an improvement in agreement with experiment is obtained, however there are still considerable discrepancies so it can be seen there must be a variation of the correction factor for at least one, and probably both elements in these alloys. As with the alkali metals, the values of χ obtained by this method do not agree with those obtained by other metals. No calculations have been done for zinc alloys as there are no experimental results for comparison.

The correction factor, Λ, may vary because the core polarisation term is not constant, however, unlike the alkali metal alloys, these results depend strongly on the choice of pseudopotential, so it seems likely that the small inaccurracies in the potentials give rise to the final error. In particular in the gallium alloys the excellent agreement between the OPW results and experiments suggest that the correction term is calculated wrongly.

Source ref.	Zn	In	Sn
Present	1.64	1.59	1.79
(22)	1.525	1.456	1.556
(24)	1.45	1.40	1.51
(8)		1.52	1.56

Table 5.9. Spin Susceptibility of Pure Metals.

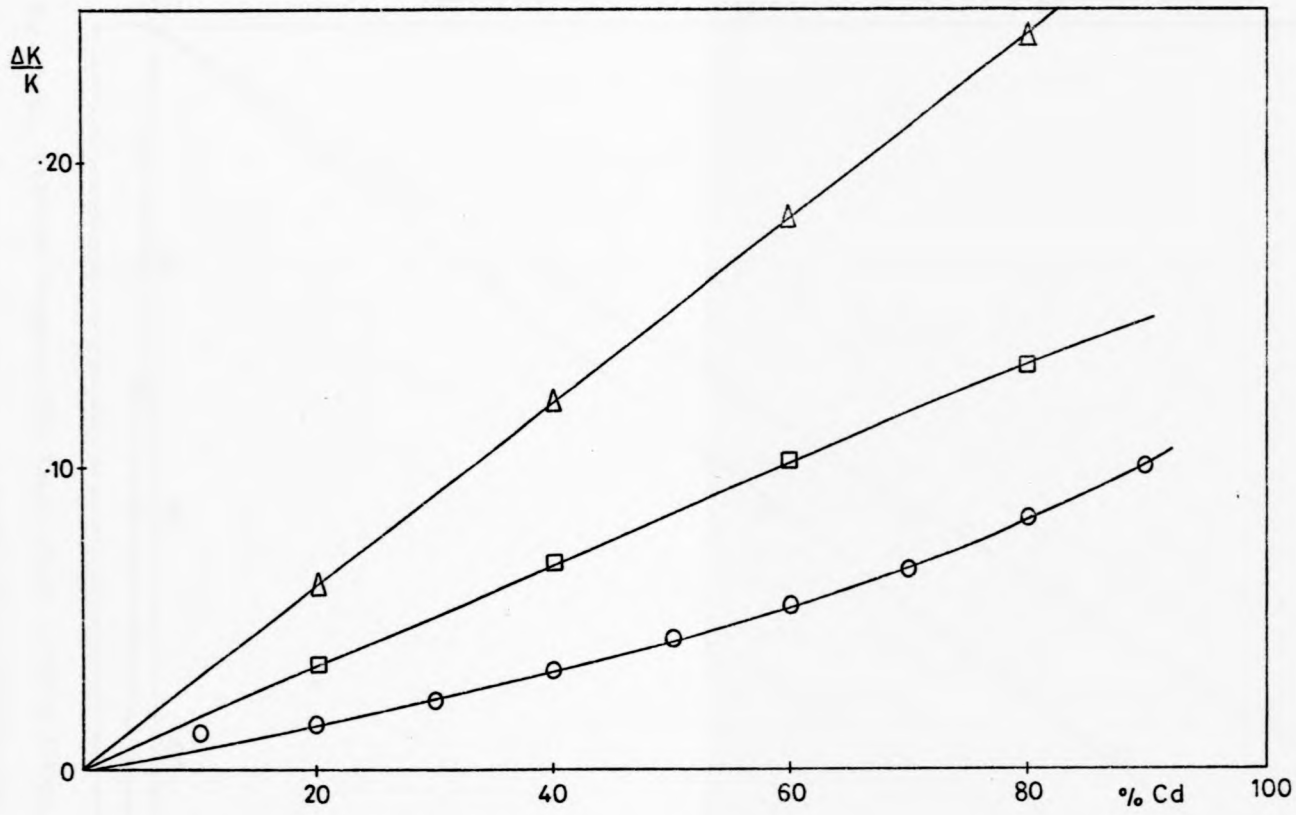

Fig. 5.31. Relative Change of Indium Knight Shift in In-Cd Alloys.

Experimental results are denoted by o . Theoretical results are given by Δ where χ_s is taken from Dupree and Geldhart, and by □ where χ_s is deduced from NMR.

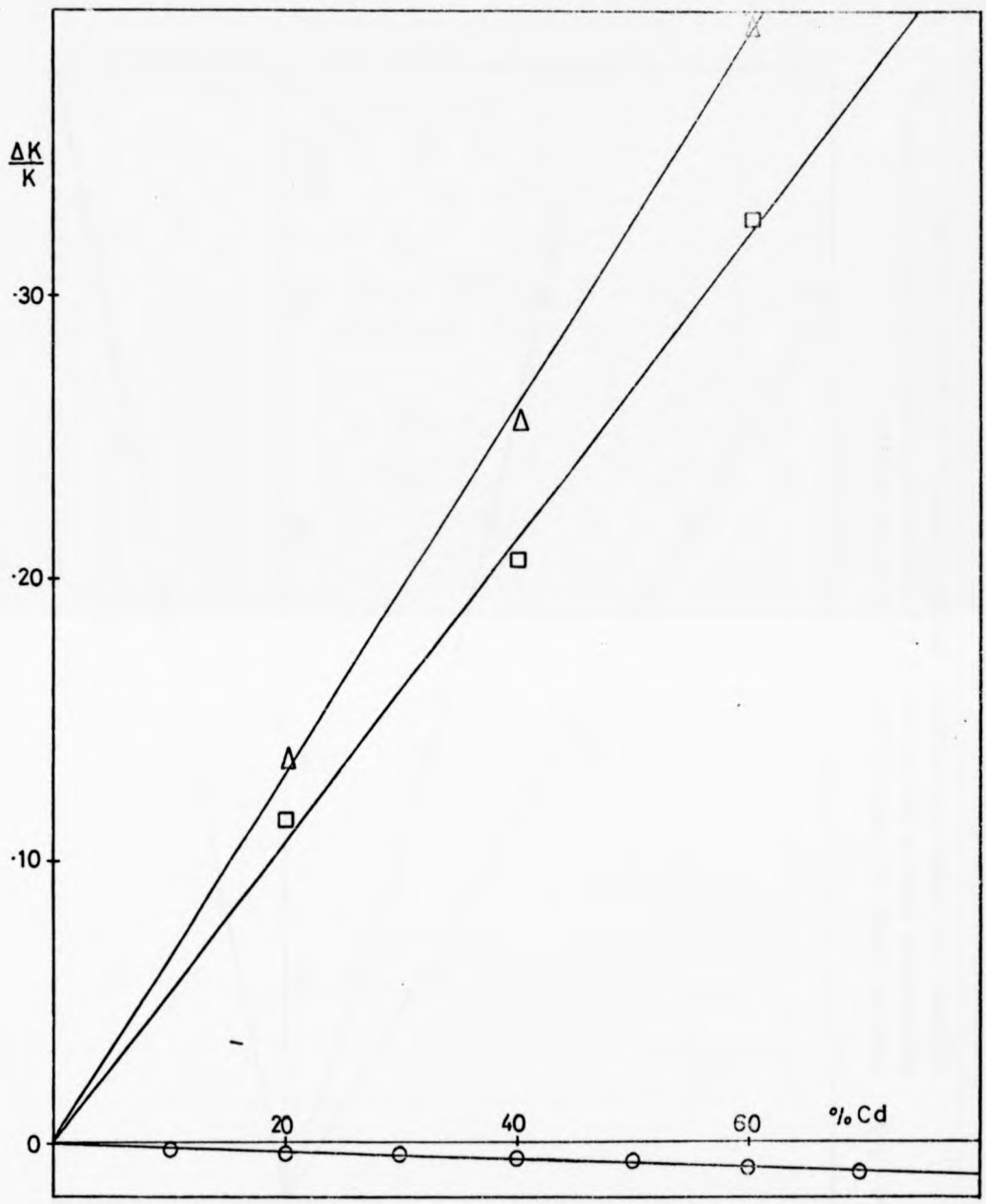

Fig. 5.32. Relative Change of Tin Knight Shift in Sn-Cd Alloys. Experimental results are denoted by o . Theoretical results are given by Δ where χ_s is taken from Dupree and Geldhart, and by □ where χ_s is deduced from NMR.

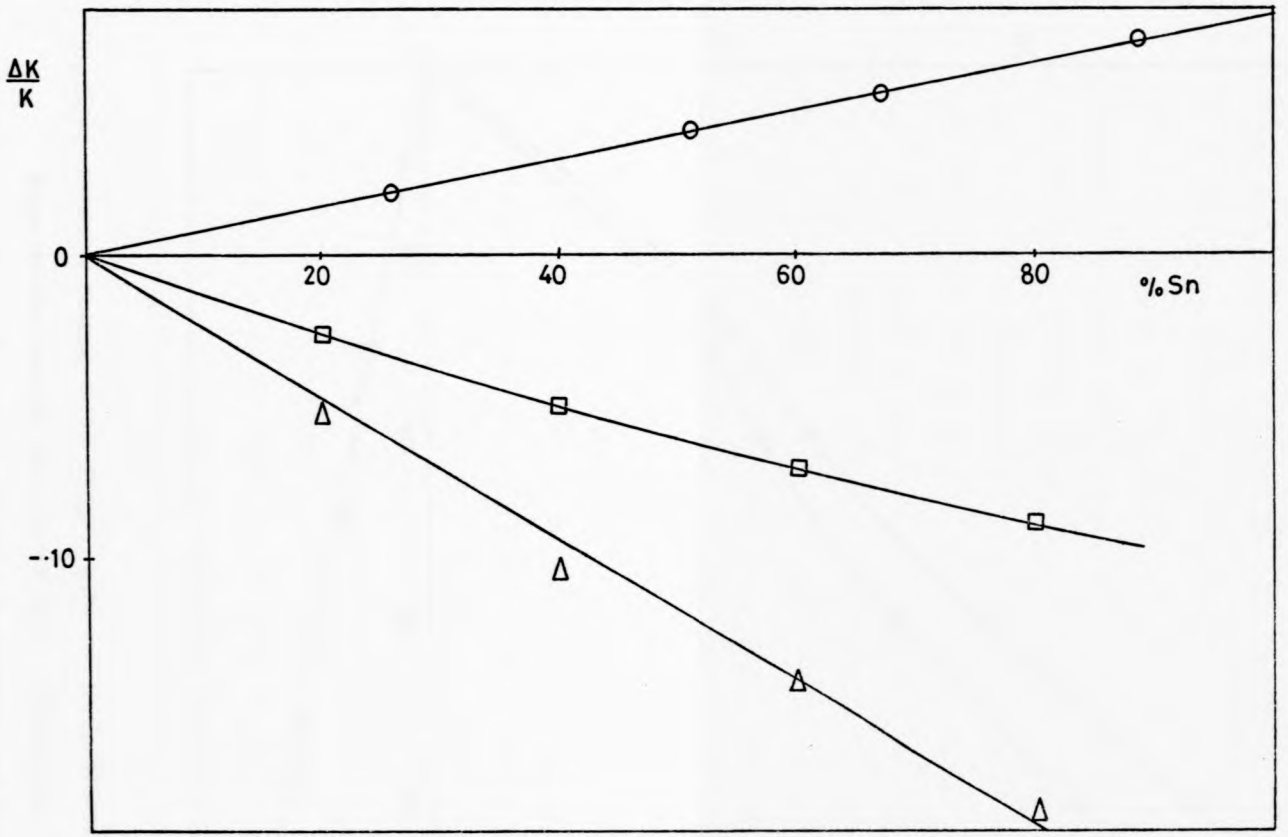

Fig. 5.33. Relative Change of Indium Knight Shift in In-Sn Alloys.
Experimental results are denoted by o . Theoretical results are given by Δ where χ_s is taken from Dupree and Geldhart, and by □ where χ_s is deduced from NMR.

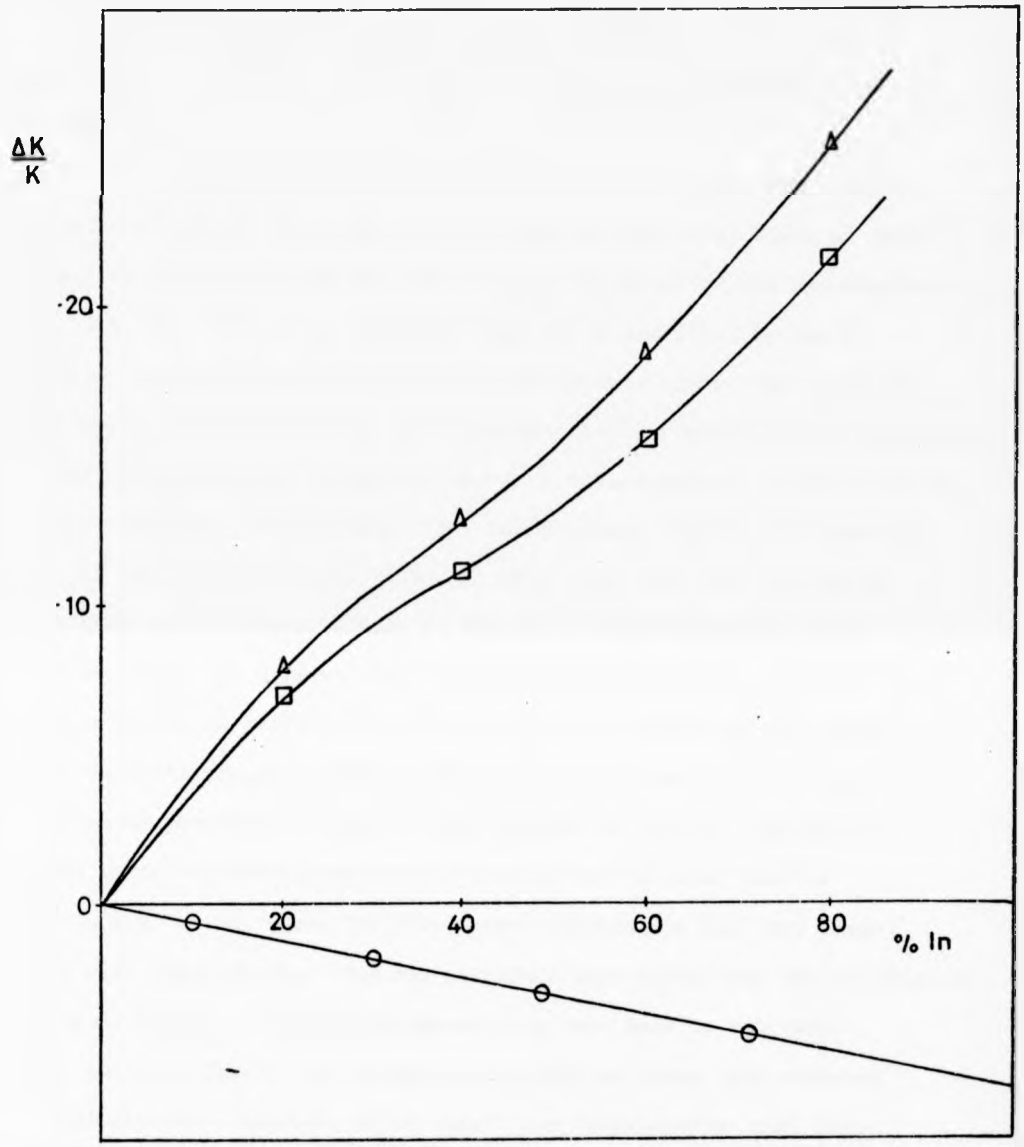

Fig.5.34. Relative Change of Tin Knight Shift in Sn-In Alloys. Experimental results are denoted by o . Theoretical results are given by Δ where χ_s is taken from Dupree and Geldhart, and by □ where χ_s is deduced from NMR.

5.3. Conclusion.

In this chapter, a nonlocal pseudopotential has been used to calculate the Knight shifts of liquid metals and alloys. The results are in good agreement with experiment.

In general there is an improvement on the single OPW results, and a considerable improvement on previous calculations, based on this formalism, which have ignored the nonlocal character of the pseudopotential (1, 5, 6, 7). Thus it is concluded that it is essential to use a nonlocal pseudopotential in a calculation of this kind. The remaining discrepencies between theory and experiment are due partly to uncertainties in the pseudopotential parameters,and to a lesser extent to inaccuracies in the structure factors used. For heavy metals, mainly for those in the 5th row of the periodic table, a large error has been introduced into these calculations because of the use of nonrelativistic core wavefunctions. It appears that ths spin susceptibilities of these elements are known sufficiently accurately to introduce no significant error into the present results. The present calculation only uses first order perturbation theory, and ignores the higher terms which almost certainly introduces large errors in the calculations for mercury and barium, where the first order corrections are very large. It is also possible that this may introduce some error into the calculation for other metals. Finally, no attempt has been made to calculate other contributions to the Knight shift, such as those from exchange polarization, however, it is clear from these results that these effects never produce a major contribution to the Knight shift.

The magnitude of the Knight Shift in alloys is calculated to a similar accuracy to that in the pure metals. In the alkali metal

alloys, where there are large changes of Knight shift with concentration, this means that the relative change of this quantity is quite accurately predicted. For other alloy systems, the Knight shift variation is very small and these calculations are insufficiently accurate to predict the details of these variations. The causes of the discrepencies are the same as for the pure metals, although the use of a single structure factor to describe the alloy structure is an additional approximation.

Contrary to the conclusions of Perdew and Wilkins (1), it is found that it is not possible to use the measured Knight shift and the calculated contact densities to evaluate the spin susceptibility accurately, even for the alkali metals.

In general these results must be regarded as being consistent with the NFE theory, although they are of insufficient accuracy to provide a stringent test of this theory. The calculations could be improved firstly by the use of relativistic wave functions and secondly by the use of the improved OMP given by Appapillai and Williams (13). For the alloys, it would be interesting to see how the use of experimentally determined partial structure factors effect the result. Other work that would also contribute to the understanding of the Knight shift would be the investigation of the high order correction terms and the accurate evaluation of exchange core polarization.

References

1. Perdew J.P. and Wilkins J.W., Phys.Rev.B., 7, 2461, (1973) and Solid State Comm., 8, 2041, (1970).
2. Liquid Metals Handbook., U.S. Atomic Energy Commission, (1950).
3. Ese O. and Reissland J.A., J.Phys.F., 3, 2066, (1973).
4. Evans R., J.Phys.C:Metal Phys.Supp., 2, 5137, (1970).
5. Jena P.et al., Phys.Rev.B., 1, 432, (1972).
6. Ford C.J. and Styles G.A., Props. of Liquid Metals:Proc.Int.Conf. at Tokyo (1972), Taylor and Francis,189.
7. Ritter A.L. and Gardner J.A., Phys.Rev.B., 3, 46, (1971).
8. Jena P.et al., Phys.Rev.B., 3, 2158, (1971).
9. Ashcroft N.W., J.Phys.C., 1, 232, (1968).
10. Shaw R.W. and Smith N.V., Phys.Rev., 178, 985, (1969).
11. Shaw R.W., Ph.D.Thesis Univ. of Stanford (1968).
12. Ashcroft N.W. and Lekner I., Phys.Rev., 145, 83, (1966).
13. Mann J.B., Los Alamos Scientific Lab. of the Univ. of California, Report (1967).
14. Hermann F. and Skillmann S., Atomic Structure Calculations (Englewood Cliffs, N.J.:Prentice Hall) 1963.
15. Bagus P.S., Phys.Rev., 139, 619, (1965).
16. Watson R.E. and Freeman A.J., Phys.Rev., 124, 1117, (1961).
17. Mahanti S.P. et al., Magnetic Resonance (ed Coogan et al) Plenum 1970.
18. Enderby J.E. et al., Phil.Mag., 10, 633, (1964).
19. Devine R.A.B. and Dupree R., Phil.Mag., 22, 1069, (1970).
20. Rice T.M., Phys.Rev., 175, 858, (1968).
21. Silverstein D., Phys.Rev., 130, 912, (1963).
22. Dupree R. and Geldhart D.J.W., Solid State Comm., 9, 145, (1971).
23. Halder N.C. and Jena P., Phys.Rev.B., 4, 2385, (1971).
24. Dupree R. and Seymour E.F.W., Phys.Kondens Mater. 12, 97, (1970).
25. Dupree R., To be published.
26. Liberman D. et al., Phys.Rev., 137, A27, (1965).

27. Mann J.B., Private Comm.

28. Van der Molen S.B. et al., Physica, 40, 1, (1968).

CHAPTER 6

Knight Shifts in Mercury-Indium Alloys

6.1. Introduction

The NMR properties of liquid mercury and of certain liquid alloys involving this metal are rather unusual. For many years it has been known that the pure metal has a Knight shift of 2.4% which is very large compared with the other elements in the 5th row of the periodic table, as shown in Table 6.1. More recently some interesting measurements have been obtained for the alloys Hg-In and Hg-Cd. The ^{115}In Knight shift in Hg-In alloys shows a complicated concentration dependence (see Fig.6.1), which is to be contrasted with the monotonic, often linear, behaviour observed in most other alloy systems. While the concentration dependence of the ^{113}Cd Knight shift in Cd-Hg alloys is indeed monotonic, the variation is larger than in other cadmium alloys.

Mercury and its alloys also differ from other simple liquid metals in many other properties. The resistivity is large and about three times that predicted from the Ziman formula(11) using the Heine-Animalu (12) pseudopotential. The temperature and volume coefficients of the resistivity are much larger than for other simple metals and most remarkable of all, mercury shows an initial drop in resistivity on alloying with divalent and polyvalent metals which is unlike any other simple metal. The thermoelectric parameter is very much larger than for the other simple metals and is again very different to the results obtained from calculations using the Heine and Animalu potential. The Lorentz number and Hall coefficient are, however, in agreement with the predictions of the Nearly Free Electron theory, although the Hall coefficients of many mercury alloys are not. Finally, there

CHAPTER 6

Knight Shifts in Mercury-Indium Alloys

6.1. Introduction

The NMR properties of liquid mercury and of certain liquid alloys involving this metal are rather unusual. For many years it has been known that the pure metal has a Knight shift of 2.4% which is very large compared with the other elements in the 5th row of the periodic table, as shown in Table 6.1. More recently some interesting measurements have been obtained for the alloys Hg-In and Hg-Cd. The ^{115}In Knight shift in Hg-In alloys shows a complicated concentration dependence (see Fig.6.1), which is to be contrasted with the monotonic, often linear, behaviour observed in most other alloy systems. While the concentration dependence of the ^{113}Cd Knight shift in Cd-Hg alloys is indeed monotonic, the variation is larger than in other cadmium alloys.

Mercury and its alloys also differ from other simple liquid metals in many other properties. The resistivity is large and about three times that predicted from the Ziman formula(11) using the Heine-Animalu (12) pseudopotential. The temperature and volume coefficients of the resistivity are much larger than for other simple metals and most remarkable of all, mercury shows an initial drop in resistivity on alloying with divalent and polyvalent metals which is unlike any other simple metal. The thermoelectric parameter is very much larger than for the other simple metals and is again very different to the results obtained from calculations using the Heine and Animalu potential. The Lorentz number and Hall coefficient are, however, in agreement with the predictions of the Nearly Free Electron theory, although the Hall coefficients of many mercury alloys are not. Finally, there

Metal	Cs	Ba	Hg	Tℓ	Pb	Bi
K%	1.44	0.403	2.42	1.48	1.49	1.41

Table 6.1. Knight Shift of Metals in 5th Row of Periodic Table.

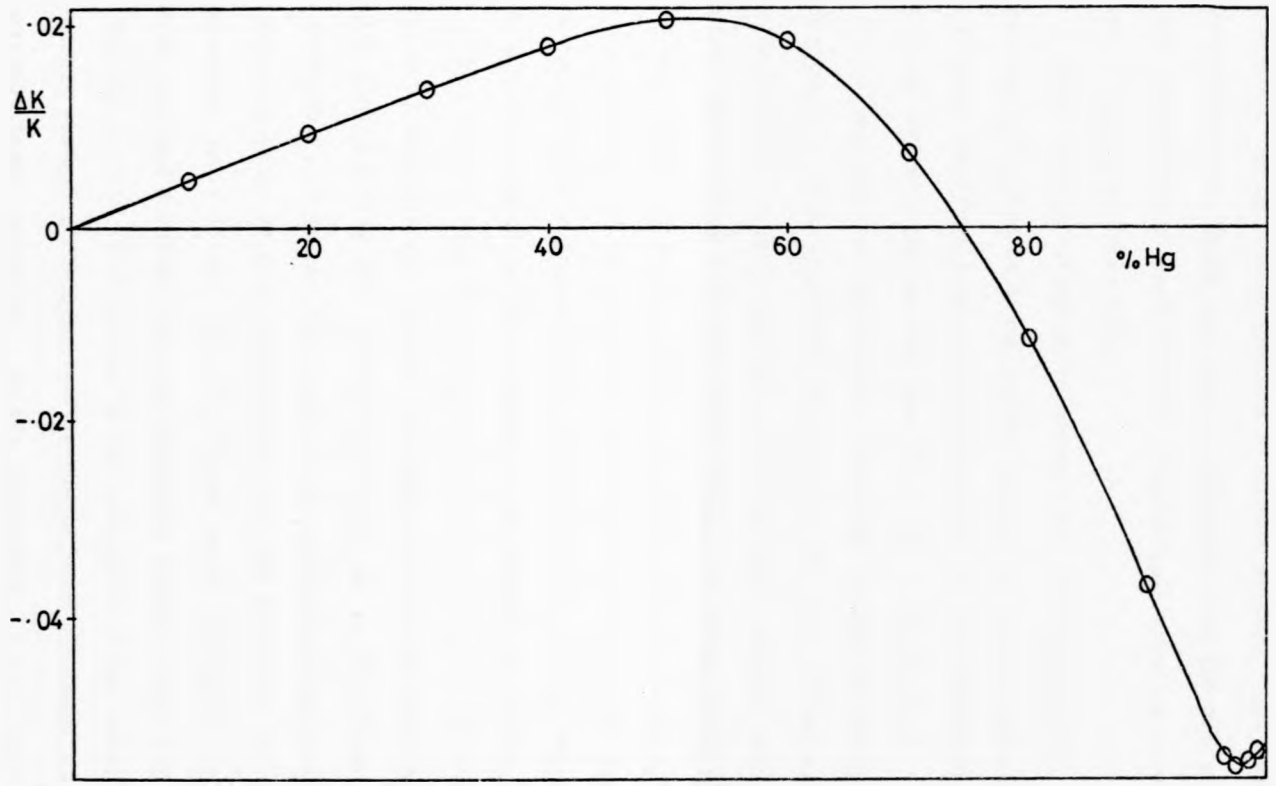

Fig. 6.1. ^{115}In Knight Shift in In-Hg Alloys at 20°C.

These results were obtained by Styles (5). The values for 10% and 20% Hg alloys were obtained by extrapolation from measurements made at higher temperatures.

has been a considerable controversy over the results of experiments to measure the optical properties of liquid mercury. However it is now believed that these are also in agreement with the NFE theory. A full discussion of each of these properties, including numerical data, is given by Faber (14).

Mott (1) has attempted to account for these properties by assuming that there is a dip in the density of states versus energy curve near the Fermi level, which he refers to as a pseudogap. Thus the large resistivity results from the lack of electrons at the Fermi level to take part in conduction. The large volume dependence of the resistivity is also explained because any change in volume will cause the Fermi level to move and thus alter the Fermi surface density of states. On alloying with polyvalent metals, the Fermi level will also rise to a region of higher density of states and so the anomalous increase in conductivity can be explained. Mott has also suggested that the minimum in the ^{115}In Knight shift in Hg-In alloys, at the mercury rich end, will correspond to the minimum in the density of states.

Two reasons have been suggested for the existence of the pseudogap. Firstly it has been put forward that some short range order may exist in the liquid giving rise to band structure, as in the solid. Alternatively, it may be the onset of the semiconducting behaviour that is known to occur at high temperatures and low densities (2). The temperature variation of the ^{115}In Knight shift throughout the alloy system provides a method for distinguishing between these two theories. If the dip in this curve is due to the retention of the solid band structure, it should gradually disappear as the temperature increases due to the increased thermal agitation. On the other hand, if it is due to the onset of semiconducting behaviour, the minimum will become deeper as the temperature rises. Experiments have therefore been carried out to measure the Knight shifts of both the constituents in Hg-In allo

over a range of temperatures and the results are presented in Sec.6.2.

It is, however, far from certain that a pseudogap really exists, and if so, if it is the cause of the anomalies in the properties of mercury and its alloys. Adams (3) has argued that the resistivity does not depend on the density of states in a liquid metal as the decrease in the number of current carriers is exactly compensated by a decrease in scattering. He has also shown that the change of resistivity in Hg-Au alloys is not commensurate with this model by comparing the resistivity of pure mercury at high temperatures with that of Hg-Au alloys of the same electron density and hence the same Fermi wave vector.

Most significantly, Evans (4), has been able to calculate the resistivity of pure mercury and several of its alloys by using a strongly nonlocal and energy-dependent model potential. The unusual characteristics of this potential, and hence the unusual properties of mercury, are thought to be due to the existence of a d-core state just below the Fermi level. Chan and Ballantine (10) have used this potential to evaluate the density of states in liquid mercury. They do find a slight dip in the density of states curves near the Fermi level, however this much smaller than the one suggested by Mott and incapable of having a significant effect on the electrical properties of this metal. Calculations have therefore been carried out to evaluate the Knight shift using this potential and the results are discussed in section 6.3.

6.2. Temperature Dependence of the Knight Shifts in Hg-In Alloys

Measurements have been made of both ^{115}In and ^{199}Hg Knight shifts in a number of Hg-In alloys in temperature range 20° to 300°C. The experiments were carried out as described in Chapter 2 and the results are presented in Tables 6.2 and 6.3 and Figs.6.2. and 6.3.

Sample Hg	Sample In	20°C	166°C	220°C	270°C	300°C	Typical error
0	100		.7918	.7872	.7851	(7835)	.0002
10	90		.7963	.7909	.7883	.7872	.0002
20	80		.8010	.7952	.7917	.7909	.0002
30	70	.8225	.8053	.7979	.7954		.0002
40	60	.8280	.8085	.8028	.7981	.7967	.0002
50	50	.8310	.8105	.8046	.7987	.7967	.0002
60	40	.8299	.8086	.8021	.7961	.7951	.0002
70	30	.8230	.8020	.7947	.7880	.7862	.0002
80	20	.8047	.7865	.7775	.7723	.7688	.0002
90	10	.7858	.7654	.7579	.7518	.7467	.0002
95	5	.7701	.7506	.7427	.7351	.7311	.0002
98	2	.7662	.7448	.7367	.7284	.7233	.0002
98.5	1.5	.7659	.7456	.7358	.7281	.7233	.0002
99	1	.7654	.7442	.7353	.7265	.7196	.0005
99.5	0.5	.7648	.7444	.7348			.0005

Table 6.2. ^{115}In Knight Shift in In-Hg Alloys.

The first column gives the alloy concentration and the Knight shifts are given in the other columns for the temperatures shown at the top. All Knight shifts and concentrations are expressed in %.

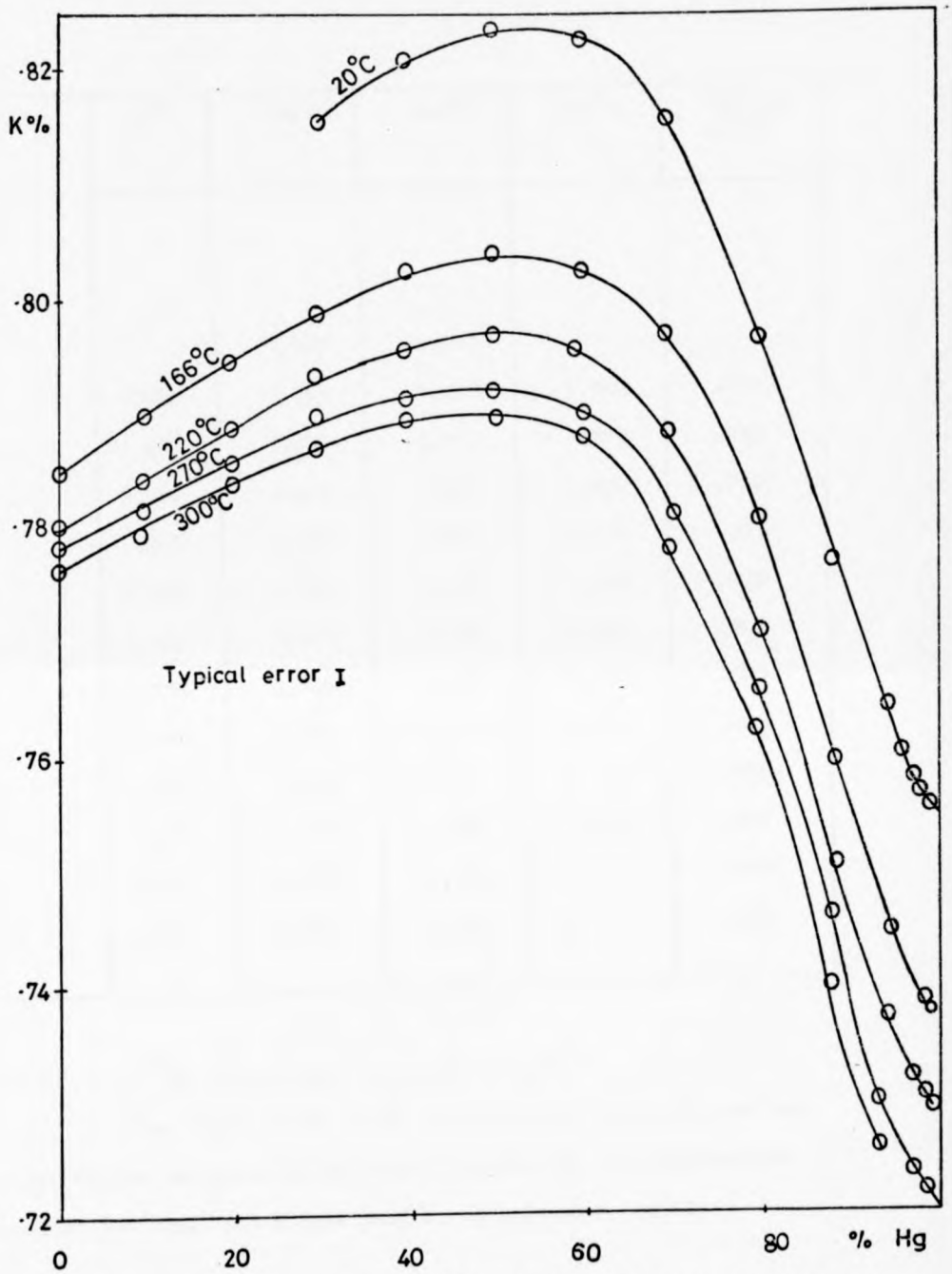

Fig. 6.2. The Variation of the ^{115}In Knight Shift with Concentration in In-Hg Alloys at Various Temperatures.The temperatures are indicated on the graph.

Temp. / Alloy	20°C	170°C	220°C	270°C	Typical error
Hg %					
10					
20		1.947	1.948		
30	1.967	1.963	1.958	1.944	.010
40	1.987	1.989	1.971	1.973	.010
50	2.020	2.009	1.996	1.990	.010
60	2.060	2.042	2.024	2.015	.005
70	2.109	2.078	2.057	2.052	.005
80	2.173	2.131	2.109	2.092	.005
90	2.239	2.180	2.157	2.131	.005
95	2.307	2.240	2.213	2.181	.005
98	2.366	2.299			.005
98.5	2.377	2.311	2.282	2.244	.005
99	2.400	2.333	2.303		.005
99.5	2.412	2.344	2.313		.005

Table 6.3. ^{199}Hg Knight Shift in Hg-In alloys.

The first column gives the alloy concentration and the Knight shifts are given in the other columns for the temperatures shown at the top. All Knight shifts are expressed in %.

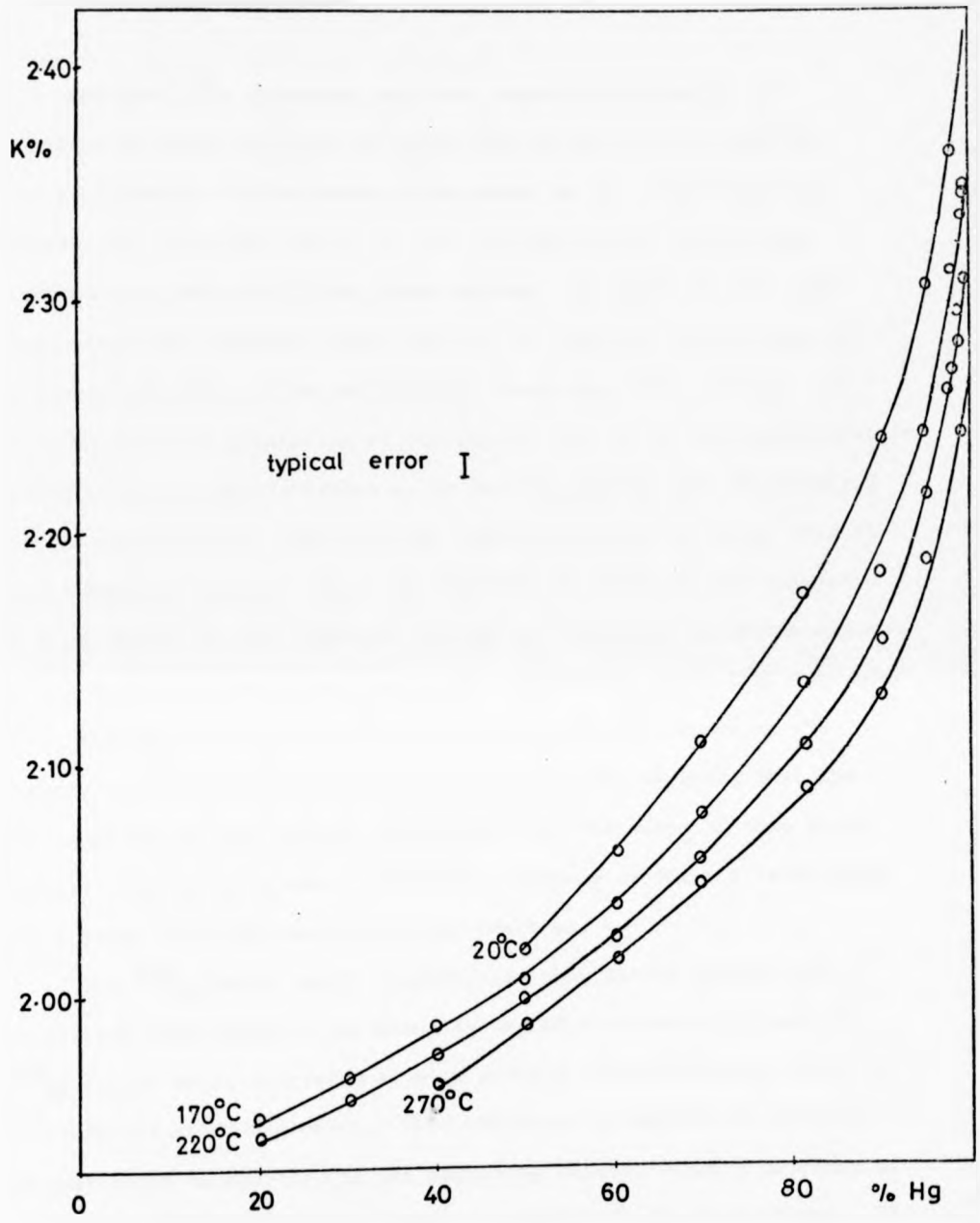

Fig.6.3. The Variation of the ^{199}Hg Knight Shift with Concentration in Hg-In Alloys at various Temperatures.

The temperatures are indicated on the graph.

For the ^{115}In resonance the room temperature results are identical to those obtained by Styles (5) and in general there is little alteration in the shape of the curve as the temperature is raised. The principal change is that the minimum at the mercury rich end disappears at higher temperatures. On repeating the room temperature measurements, after heating the samples, the minimum was no longer present. It is not entirely clear why this occurred. It could be due to a clustering of the indium ions in the low concentration alloys which is finally broken up by heating for the periods required for the measurements. Whatever the cause, it is now believed that the true behaviour does not show a minimum and the case for the existence of a pseudogap is thus weakened (though not ruled out since the minimum in the density of states may occur at a value of k above that for pure Hg). However, the fact that the general dip in this curve at the mercury end does not change with temperature also suggests that the pseudogap is not the correct explanation for the shape of this curve. However this is by no means conclusive evidence as only a relatively small range of temperatures has been explored.

The ^{199}Hg Knight shift results also show little change with increasing temperature. The main feature of this curve is that the ^{199}Hg Knight shift increases at high mercury concentrations, where the ^{115}In Knight shift decreases. This behaviour is surely the opposite of what would be expected if the pseudogap existed since a decrease of the density of states should cause both Knight shifts to decrease. It is possible that the observed behaviour arises because the contact density for mercury varies with concentration more rapidly and in the opposite direction to the Fermi surface density of states but this does not seem very likely. Thus, there seems to be very little concrete evidence for

the existence of a significant pseudogap and it seems more appropriate to assume that the shape of the Knight shift curves for both elements in Hg-In alloys are due principally to the variation of the contact density, and the next section investigates the possibility of calculating this quantity.

6.3. Pseudopotential Calculation of Knight Shifts

In view of the success of Evans (4) in calculating the resistivity of Hg and its amalgams it is interesting to see if his pseudopotential can be used to predict the Knight shifts in Hg-In and that for pure mercury using the theory outlined in chapter 4.

Evans' potential is based on the OMP and differs principally in the method of determing the parameters. As explained in Chapter 4 OMP parameters are obtained by interpolation or extrapolation of the parameters determined at the free ion term values. Animalu (6) originally suggested that this could be done by a linear interpolation simply because he noted that these values appeared to lie on a straight line, rather than for any fundamental reason. This process appears to be quite adequate for most metals. In mercury, however, there is an ionic d-level near the Fermi surface and the assumption of linear extrapolation appears to be no longer valid for the $\ell=2$ component. Evans uses a procedure based on the quantum defect method (7) for obtaining this parameter, A_2 (see Chapter 4 page 47). Here a quantity, the quantum defect, is defined which is related to the scattering properties of the ion but which is only a slowly varying function of energy, so that a reliable extrapolation can be made and A_2 determined accurately. Unfortunately, for the divalent metals for which he calculates the parameters,(zinc, cadmium and mercury) the radius of the $\ell=2$ component of the potential, R_2, is larger than the Wigner-Seitz

radius which makes the model nonphysical. In these cases he sets R_2 equal to the Wigner-Seitz radius and deduces A_2 according to the quantum defect method but ignoring the optimisation condition. For mercury, the potential form factors calculated in this way are very different from previous calculations, in that the first maximum occurs at a negative value as can be seen in Fig.6.4.

This potential was easily incorporated into the contact density program with a slight modification to the procedures for calculating the non-local contributions to the scattering matrix elements. The direct contribution to the Knight shifts have thus been determined for mercury, cadmium and indium. The results are given in Table 6.4. where they are compared with experiment and with the results obtained using the potential of Ese and Reissland (8). For indium the two calculations give the same results, but the Evans result for cadmium is further from the experimental value, possibly because this potential is not properly 'optimised'.

The result for mercury, obtained using the Evans potential, is considerably smaller than that obtained using the Ese and Reissland potential and much less than the experimental value. It is in fact much more in line with the results for the other metals in this row of the periodic table. The problem thus remains of why mercury has such a large Knight shift. This result will be affected by corrections to the core wavefunctions to include relativistic effects, but there seems no reason to suppose that these corrections would be any larger for mercury than for other metals in this row of the periodic table. One effect that could occur, however, is hybridisation of the conduction states with the unfilled core d-state close to the Fermi level. This is discussed in the next chapter with reference to barium, where it is found that this mechanism can only reduce the direct contribution to the Knight shift.

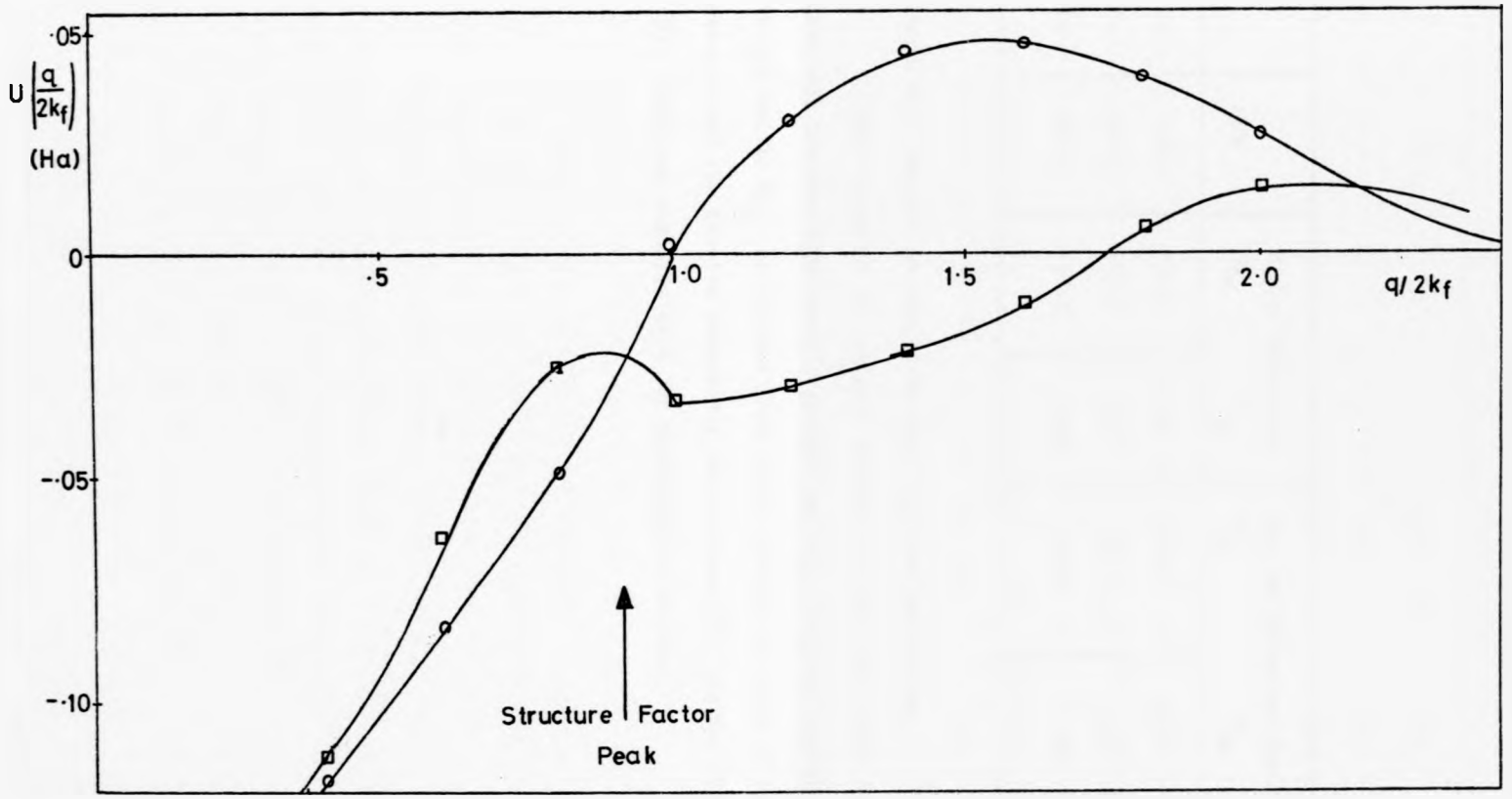

Fig 6.4. Form Factors for Mercury. Values given by o from Ese and Reissland(8).

Values given by □ from Evans(4).

	OPW	Evans Parameters		Ese and Reissland Par.		Expt.
		ΩP_F	K_{TH}	ΩP_F	K_{TH}	K_{expt}
Hg	1185	1510	1.70	2353	2.65	2.42
Cd	551.3	579.3	.667	664.2	.765	0.795
In	476.2	577.6	.709	567.6	.697	0.786

Table 6.4. Knight Shifts of Mercury, Cadmium and Indium.

The values of the contact density for the zero order calculation, OPW, and for the first order calculation, ΩP_F, is given together with Knight shifts K_{TH}, calculated from these results for each of these metals, and for the two potentials due to Evans (4) and Ese and Reissland (8). They are compared with the experimental values.

It is not entirely clear how hybridisation would effect the core polarisation, but Mahanti et al (9) find that for the alkali metals only s-electrons make a significant contribution to the core polarisation, and it is most unlikely that this is the cause of any major effect.

It therefore seems that this large Knight shift must come from the effect that this unusual potential has on the conduction electron states. The first order correction is large and it is therefore likely that the second and higher order contributions to the contact density are not negligible and provide an additional positive contribution to the Knight shift which ought to be taken into account.

The relative change of the Knight shifts in Hg-In have also been calculated using the Evans potential and that of Ese and Reissland. The results are given in Table 6.5. and are compared with experiment in Figs.6.5. and 6.6. It can be seen that for the ^{115}In resonance agreement between theory and experiment using the Evans potential is very much better than using the Ese and Reissland potential. The same is true for the ^{199}Hg Knight shift where the agreement obtained using Evans potential must be considered very satisfactory.

The results confirm the suggestion made earlier that it is possible to predict large changes of Knight shift by this method with reasonable certainty. This success is not in conflict with the rather poor agreement for the pure metal and merely suggests that other contributions vary at a similar rate to the direct, first order contributions and are therefore successfully included in the correction term Λ.

Alloy		$\frac{\Delta\chi}{\chi}$	Evans Potential		Ese and Reissland Potential	
Hg	In		$\Delta\mathcal{P}_F/\mathcal{P}_F$	$\Delta K/K$	$\Delta\mathcal{P}_F/\mathcal{P}_F$	$\Delta K/K$
^{115}In Resonance						
100	0					
80	20	-.061	.137	.076	.711	.650
60	40	-.046	.052	.008	.495	.449
40	60	-.030	.011	-.019	.304	.274
20	80	-.015	-.011	-.026	.139	.124
0	100	0	0	0	0	0
^{199}Hg Resonance						
100	0	0	0	0	0	0
80	20	.016	-.094	-.078	-.109	-.093
60	40	.033	-.148	-.115	-.210	-.117
40	60	.049	-.177	-.128	-.300	-.251
20	50	.066	-.198	-.132	-.382	-.316
0	100					

Table 6.5. Calculation of Knight Shifts in Hg-In.

$\Delta\chi/\chi$ gives the fractional change of spin susceptibility in these alloys from Dupree and Geldhart and the change of the contact density $\Delta\mathcal{P}_F/\mathcal{P}_F$ is obtained by first order perturbation theory using the Evans potential (4) or the Ese and Reissland potential (8). These values are combined to obtain two sets of values for relative change of Knight shift.

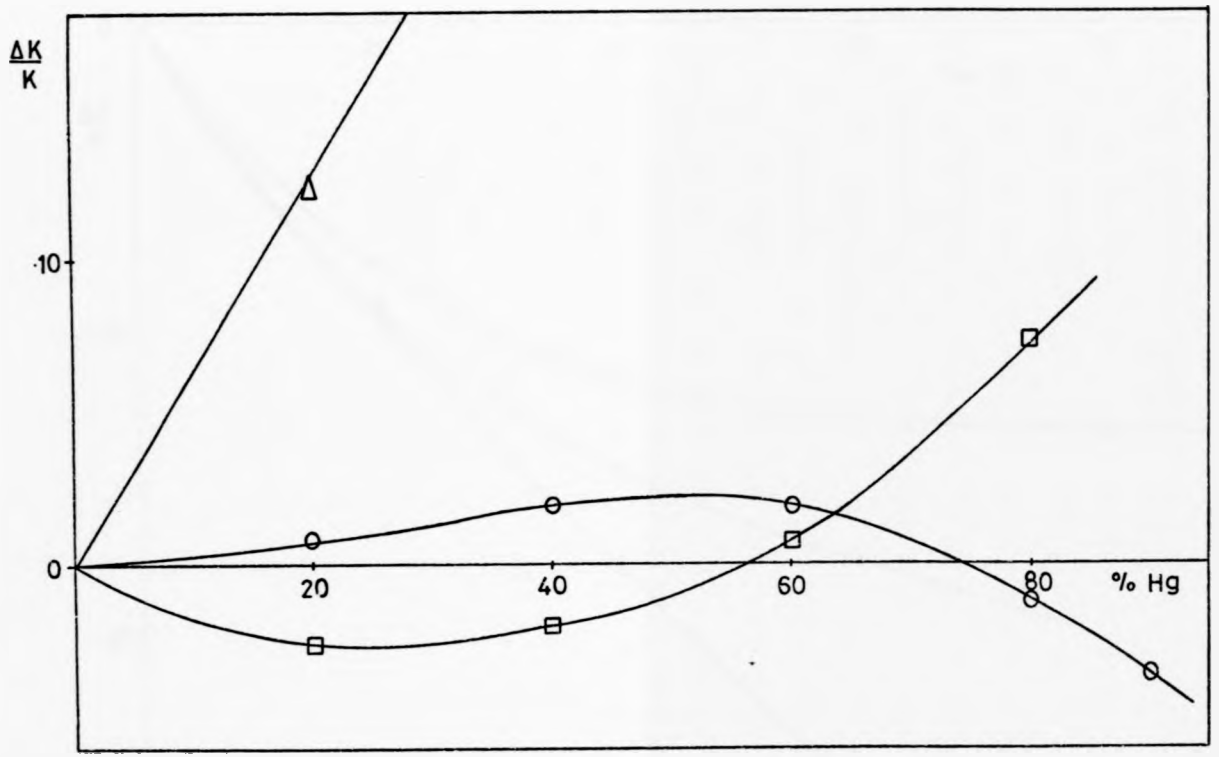

Fig.6.5. The Relative Change of the ^{115}In Knight Shift in In-Hg Alloys.

Experimental values are given by o . Values were obtained by calculation using parameters given by a) Ese & Reissland Δ , and b) Evans □ .

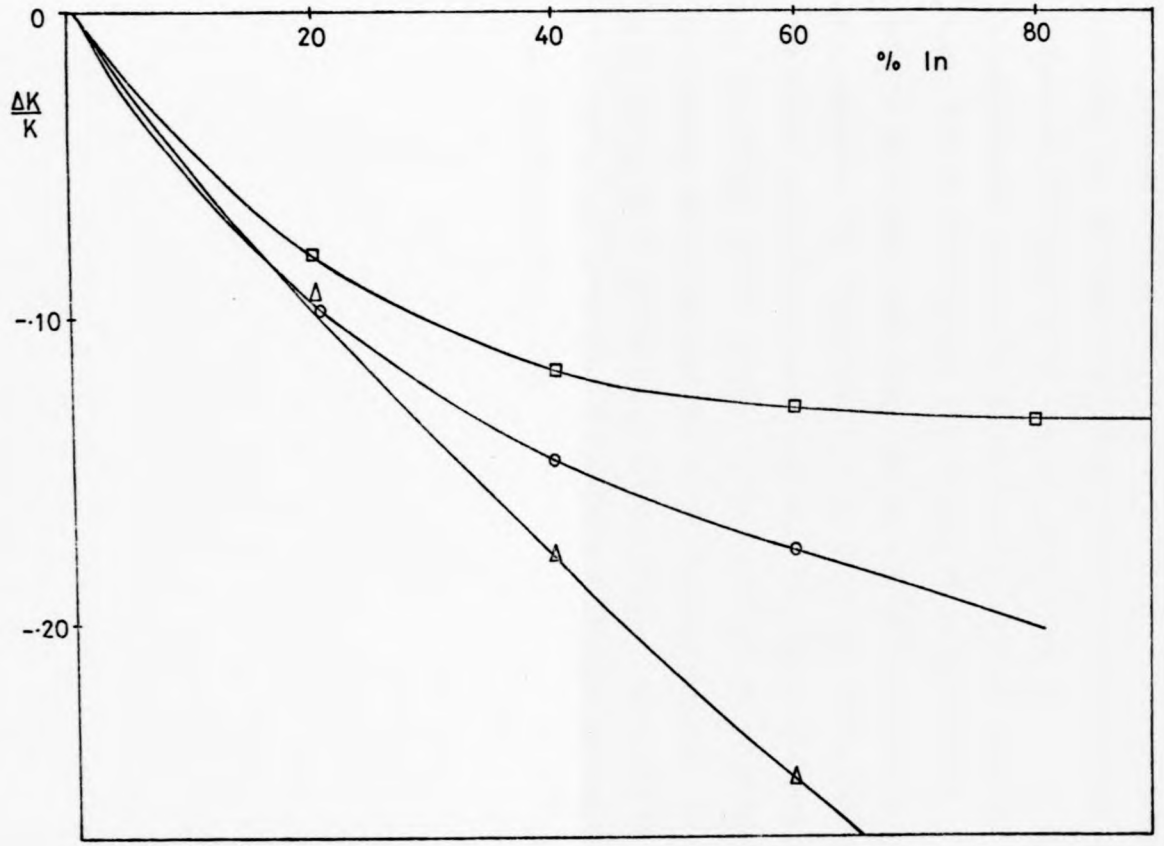

Fig.6.6. Relative Change of Mercury Knight Shift in Hg-In Alloys.
The experimental results are represented by o. Values were obtained from calculations using paremeters from a) Ese & Reissland Δ, and b) Evans □.

6.4. Summary

Although the properties of mercury and its alloys are rather different from the other simple metals, it is now believed that the differences are caused by the unusual character of the mercury pseudopotential, rather than any fundamental deviation from the Nearly Free Electron theory. The calculation of the absolute value of the Knight shift, using the Evans potential is not in very good agreement with experiment, although there are expected to be significant relativistic corrections which may improve the agreement, and the strength of the pseudopotential means that the first order perturbation theory used here may not be entirely adequate. In Hg-In alloys the Knight shifts of both mercury and indium can be predicted as well as in other simple metal alloys provided the Evans pseudopotential is used.

References

1. Mott N.F., Phil.Mag., 13, 989, (1966).
2. Even V. and Jortner S., Phys.Rev.Lett., 28, 31, (1972).
3. Adams P.D., Phys.Rev.Lett., 20, 537, (1968).
4. Evans R., J.Phys.C:Met.Phys.Supp., 2, 137, (1970).
5. Styles G.A., Ph.D.Thesis. University of Leeds., (1964).
6. Animulu A.O.E., Tech.Report 4. Cavendish Lab. Cambridge, U.K.
7. Ham F.S.,Solid St.Phys., 1, 127, (1955).
8. Ese O. and Reissland I.A., J.Phys.F., 3, 2066, (1973).
9. Mahanti P., et al., Magnetic Resonance (ed Coogen et al) Plenum, (1970).
10. Chan T. and Ballentine L.E.,Phys.Lett., 35A, 385, (1971).
11. Ziman J.M., Phil.Mag., 6, 1013, (1961).
12. Heine V. and Animalu A.O.E., Phil.Mag., 12, 1249, (1965).
13. Dupree R. and Geldhart D., Solid State Comm., 9, 145, (1971).
14. Faber T.E., Theory of Liquid Metal, C.U.P., (1972).

CHAPTER 7

The Knight Shift of Barium

7.1. Introduction

The Knight shift of barium is unusual in that it is very much smaller than the Knight shifts of the other metals in the fifth row of the periodic table. As can be seen in Table 7.1. the value of .403% in the solid at room temperature (1) is less than one-third of the Knight shift of any of the other fifth row elements. No measurements have been made on liquid barium because of its high melting point, great reactivity and poor NMR signal strength. Other electrical properties of barium are also rather different from those of the other simple metals. The resistivity of the solid shows a marked deviation from the Wiedermann-Franz law (2), which is more characteristic of the transition metals, while the resistivity of the liquid (3) is three times that of mercury or lead.

There is growing evidence that this unusual behaviour is due to the influence of a d-band just above the Fermi level (9). Moriarty (4) has made a theoretical investigation of the effects of this d-level using the formalism of the transition metal pseudopotential, where the zero order approximation to the wave function is taken to be a mixture of OPW and atomic d-state. He has found a high degree of hybridisation between the two and has thus been able to account for the large resistivity of the liquid. A somewhat different approach has been made by Ratti and Evans (5) who have calculated the resistivity using the T-matrix formulation and they find that the large resistivity is due to a very large d-contribution to the electron ion scattering cross section.

Metal	Cs	Ba	Hg	Tℓ	Pb	Bi
K%	1.44	0.403	2.42	1.48	1.49	1.41

Table 7.1. Knight Shift of Metals in 5th Row of Periodic Table.

The object of the present investigation of the Knight shift in barium and its variation with temperature was to see to what extent the unusual NMR behaviour may be accounted for by the presence of the d-level near the Fermi surface.

7.2. Experimental Results

The methods used for the preparation of samples and for measurements of the ^{137}Ba Knight shift are described in Chapter 2. Fig.7.1. shows a typical recording of the first-derivative signal obtained after averaging 16 sweeps, through the resonance using a sweep range of 25 gauss in 30 seconds. The resonance line is unusual in three respects. Firstly it is not symmetrical, the low field peak being 1.2 times larger than the high field peak. Secondly the resonance width of 2 gauss peak to peak (after correction for modulation broadening) is much greater than expected. The contributions to the linewidth from,the life time broadening due to the contact interaction,from the nuclear dipoler interaction and from indirect exchange,are each about 0.1 gauss giving a predicted width of only 0.3 gauss. Finally the signal is of very low intensity. Comparison with signals obtained from the ^{113}Cd nucleus in pure cadmium show that the signal is some 3 times smaller than expected.

It is believed that these anomalies are due to the presence of a nuclear quadrupole interaction in barium. The structure of barium is body-centred cubic and for a perfect lattice the quadrupole interaction would be expected to be zero. However, imperfections must be expected in barium for two reasons. Firstly, the filing of the samples is likely to produce a large number of dislocations and other lattice defects; and secondly the barium used was only of 99.5% purity. Impurities in the metal will in themselves produce distortions in the

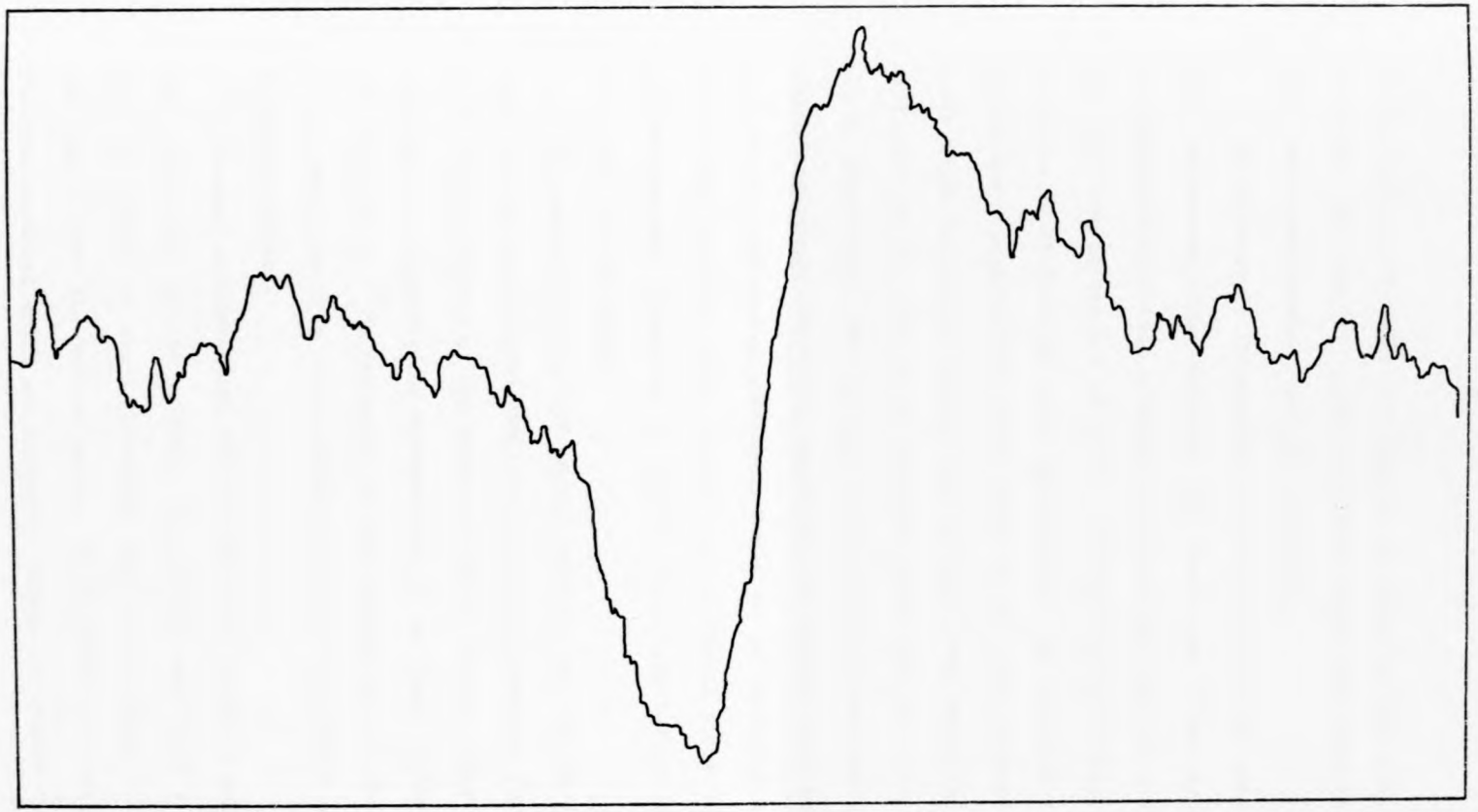

Fig. 7.1. NMR of ^{137}Ba in Pure Metallic Barium at 20 C, after averaging for 16 sweeps with a sweep range of 25 gauss and sweep time of 30 s.

in the lattice and will also help to pin existing dislocations in place. Consequently local deviations from cubic symmetry will occur and a quadrupole interaction results.

The quadrupole interaction is usually divided up into the first and second order effects. The first order effect splits the resonance line into a central line, at the original field position, due to the $m = +\frac{1}{2}$ to $m = -\frac{1}{2}$ transition plus several satellite lines from the other transitions. The position of the satellites depends on the local values of the field gradient, so where these are due to lattice imperfections, the satellites from different nuclei will be at different positions, and thus will not be observable. This process is observable in cold worked copper and impure aluminium, which like barium are cubic metals with nuclei processing quadrupole moments. It therefore seems likely that the poor signal intensity in barium is due to the fact that we are only observing the central transition for the majority of nuclei in the sample.

The second order effect causes a distortion of the central line in a polycrystalline sample and may be responsible for the width and assymmetry of the observed line in barium. This hypothesis is supported by measurements of the field dependence of the position of ^{137}Ba resonance at room temperature (6) which show a very small positive value characteristic of this second order quadrupole effect.

Several attempts were made to anneal the powdered samples and thus remove the lattice defects. The powders were mixed with finely powdered quartz, to avoid sintering, placed in an argon filled phial and heat to near the melting point. Unfortunately, a violent chemical reaction occurred which was initially thought to involve the quartz

powder. However, samples which were heated without quartz powder also reacted, possibly with the glass of the container, and it was found only possible to heat sample immersed in oil if they were not to be destroyed. This meant they could only be heated to 530K and annealing was therefore impossible. It should be pointed out however that these shifts caused by quadrupole effect are very small compared with the very large changes of position with temperature that were observed and so do not affect the accuracy of the Knight shift measurements.

The results for the Knight shift measured over the temperature range 4.2K to 530K are given in Table 7.2. and Fig. 7.2. All readings were taken at a field of 14,000 gauss. The room temperature measurements were repeated after the high temperature measurements to ensure that the latter were not due to any chemical changes in the samples. As can be seen the variation with temperature is both very large and remarkably non-linear. The value of $\frac{dK}{dT} = 2.3 \times 10^{-6} K^{-1}$ at 300K is already larger than any other simple metal (except cadmium where there is considerable influence from p-bands) so that the much larger value of $12 \times 10^{-6} K^{-1}$ at higher temperatures is exceptional. At the field used, this represents a change in the resonance position of 25 gauss which is very much larger than the effect of the line shift due to second-order quadrupole effects.

7.3. Calculation of the Barium Knight Shift

As seen in Chapter 5, the Knight shift of most metals may be predicted to within 20% using the single OPW approach. This is not the case for barium where the Knight shift calculated in this way is 0.885% instead of 0.403%. It is therefore clear that a single OPW is not suitable as a zero order approximation to the conduction electron

Temp. (K)	Knight Shift %	Error %
4.2	0.356	1
77	0.362	1
134	0.368	1
171	0.373	1
211	0.375	1
248	0.392	1
267	0.396	1
295	0.401	1
335	0.413	1
353	0.414	1
372	0.426	1
408	0.434	1
413	0.436	1
463	0.458	1
503	0.497	2
538	0.531	2.5

Table 7.2. Knight Shift of ^{137}Barium as a Function of Temperature

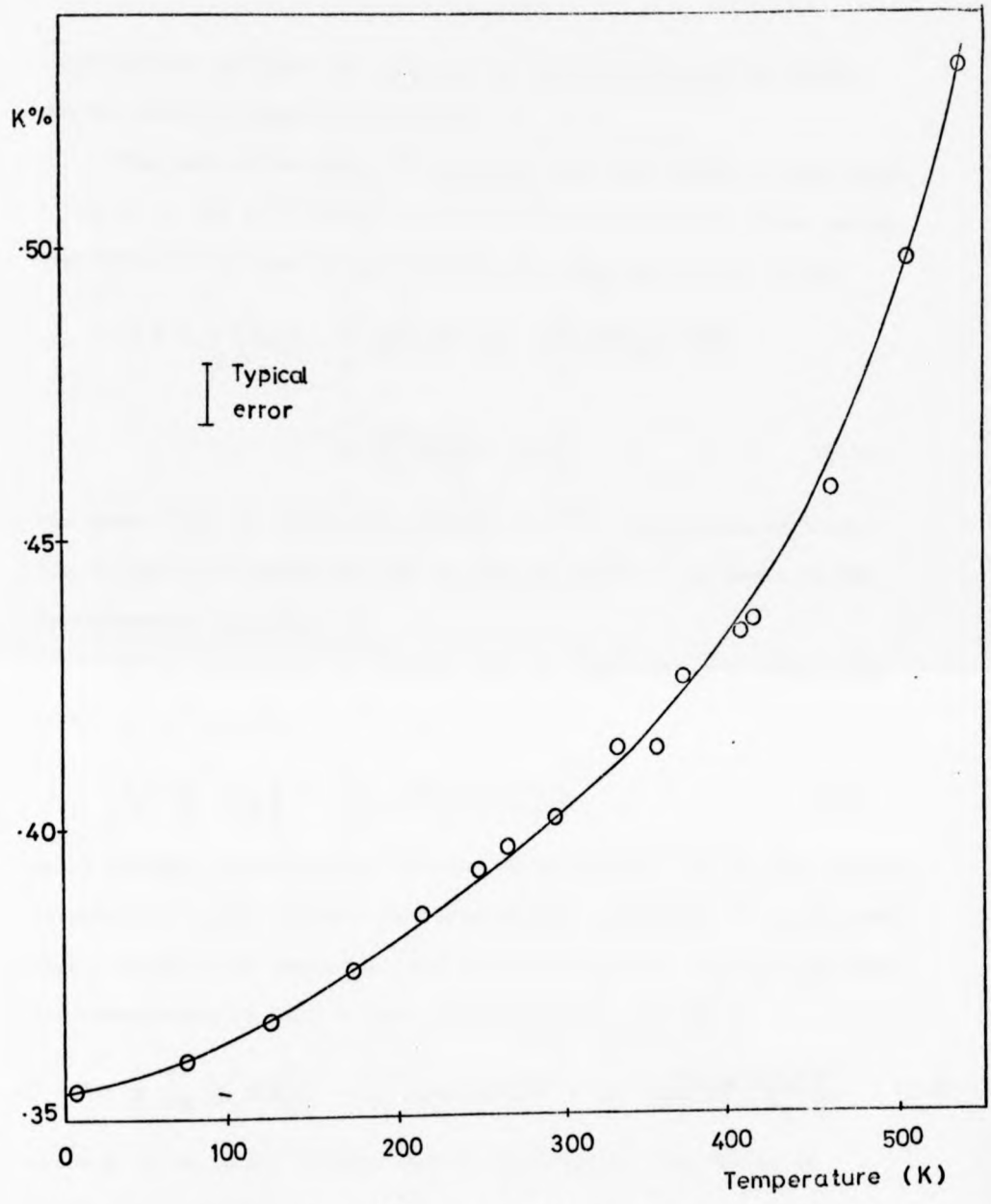

Fig. 7.2. Knight Shift of ^{137}Ba in Metallic Barium as a Function of Temperature.

wavefunction and that the influence of the d-level near the Fermi surface must be taken into account.

The work of Moriarty (4) suggests that this may be accomplished by using an OPW hybridised with an ionic 5d core state. Thus, using the formalism of the transition metal pseudopotential, we obtain

$$|\Psi\rangle = \frac{1}{N^{\frac{1}{2}}}\left(|\underline{k}\rangle - \sum_{\alpha}\langle\alpha|\underline{k}\rangle|\alpha\rangle - \sum_{d}\langle d|\underline{k}\rangle|d\rangle + \sum_{d}\frac{\langle d|\Delta|\underline{k}\rangle}{E_d - E_{\underline{k}}}|d\rangle\right) . \qquad (7.1)$$

The state $|\underline{k}\rangle$ is defined by $\langle r|\underline{k}\rangle = e^{i\underline{k}\cdot\underline{r}}$. The states $|\alpha\rangle$ are the filled core states and $|d\rangle$ is the 5d state. Δ is known as the hybridisation operator.

If the derivation is carried out the same way as in Chap.4 the Fermi contact density is then given by

$$\left|\Psi_F(0)\right|^2 = \frac{1}{N}\left|1 - \sum_{\alpha}\langle\alpha^A|\underline{k}\rangle\,\Psi_\alpha(0)\right|^2 \qquad (7.2)$$

which appears to be exactly the same as expression 4.6 for the contact density of a simple metal. The nomenclature of Chapter 4 is also used here. However the expression for the normalisation, is very different and normalising to unit volume, as in Chapter 4 we obtain

$$N = 1 - \frac{1}{\Omega}\sum_{\alpha}|\langle\alpha|\underline{k}\rangle|^2 - \frac{1}{\Omega}\sum_{d}|\langle d|\underline{k}\rangle|^2 + \frac{1}{\Omega}\sum_{d}\left|\frac{\langle\underline{k}|\Delta|d\rangle}{E_d - E_{\underline{k}}}\right|^2 \qquad (7.3)$$

where Ω is the ionic volume. Again following the derivation in Chapter 4 we obtain

$$\Omega P_F = \frac{1 - \frac{1}{4\pi}\sum_{n}\chi_s(A)\,B(n,o)}{1 - \frac{1}{\Omega}\sum_{n\ell}\left(\frac{2\ell+1}{4\pi}B^2(n,\ell) - \frac{1}{\Omega}\frac{5}{4\pi}B^2(n,2) + \frac{1}{\Omega}\cdot\frac{5}{4\pi}\frac{\Delta^2(k)}{E_d - E_{\underline{k}}}\right)} \qquad (7.4)$$

where $B(n,\ell) = \dfrac{\langle \alpha | k \rangle}{i^{\ell} Y^{*}_{\ell m}(\theta,\phi)}$

$$= 4\pi \int_{0}^{\infty} P(r).r.j_{\ell}(\underline{k}.\underline{r})\, dr.$$

Y is a Legendre polynomial, P(r) is the radial wave function, as defined in Mann's tables (7), $j_{\ell}(\underline{k}.\underline{r})$ is a spherical Bessel function and the hybridisation $\Delta(k)$ is given by

$$\Delta(k) \;.\; Y_{\ell m}(\theta,\phi) = \langle k|\Delta|d\rangle \;. \tag{7.5}$$

The expression for ΩP_F can then be written

$$\Omega P_F = \frac{\gamma^2(k)}{N_o + \frac{A}{\Omega} + \frac{B}{\Omega}} \tag{7.6}$$

where $A = \frac{5}{4\pi} B^2(n,2)$,

$$B = \frac{5}{4\pi} \frac{\Delta^2(k)}{E_d - E_k} \;,$$

and γ and N_o have the same meaning as in Chapter 4.

The quantities γ, N_o, A, B and Ω have been evaluated and the results presented in Table 7.3. The values of γ and N_o are taken from the calculations of Chapter 5. To evaluate A it was necessary to calculate $B^2(n,2)$ which requires the knowledge of the 5d wave function for barium. This is not occupied in the neutral atom and is not tabulated by Mann and to be strictly consistent with the value of Δ used, Moriarty's 5d functions should have been used. However, as these were not available, it was decided that the 5d wave function for lanthanum, truncated at the Wigner-Seitz radius should be used. It was noted that the 3d wavefunction for calcium, given by Moriarty, was very similar to Mann's result for scandium 3d wavefunction and one would expect this difference to be of a similar nature to that between the barium and lanthanum functions. In any case the value of A/Ω was

$\gamma = 26.99$	$\Omega P_F = \dfrac{\gamma^2}{N_o + A/\Omega + B/\Omega}$
$N_o = 0.69$	$\Omega P_F = 541.5$
$A/\Omega = 0.053$	$K = 0.45\%$
$B/\Omega = 0.6$	

Table 7.3. Calculation of Knight Shift in Barium.

The symbols used are those discussed in sec.7.3.

only 0.053 and therefore negligible compared with N_o of 0.69.

The value of $\Delta(k_F)$ was taken from Moriarty, and it was found that $B/\Omega = 0.6$. The effect of this extra term in the denominator is to reduce the simple OPW result by a factor of nearly one-half. The result of the present calculation, is thus K = 0.45% which must be regarded as very satisfactory for a zero order approximation. No evaluation of the first order correction has been attempted here since the detailed knowledge of $\Delta(k)$ for all k which is required is not available. Furthermore, as seen from the mercury results, model potential parameters would be needed, which take account of the presence of the d-level. Despite this limitation on the calculation, however, it is clear that the existence of the d-level has a profound effect of the Knight shift of barium and it seems likely that when a model potential and a knowledge of $\Delta(k)$ become available it will be possible to make an accurate calculation of the shift.

7.4. Temperature Dependence of the Knight Shift

Since the zero order approximation is so successful in calculating the Knight shift of barium it is clearly worthwhile attempting to calculate the temperature dependence within the same approximation. In order to clarify the situation the calculation is set out in three stages. In sec.7.4.1. the temperature dependence of the contact density is calculated treating barium as a simple metal. In sec.7.4.2. this is corrected by the inclusion of the terms involving the d-states and finally in sec.7.4.3. the temperature dependence of the Knight shift is calculated by including the temperature dependence of the spin susceptibility.

7.4.1. Temperature Dependence of ΩP_F: Simple Metal Case

The increase in temperature affects the contact density of a simple metal in two ways within this approximation. Firstly the expansion directly affects the normalisation, and secondly, the resulting change of k_F affects the overlap integrals. In order to calculate this dependence, a computer program was written which consisted of those parts of the contact density program, described in Appendix B, which calculate the zero order results; i.e., cards 512-530 of the main program together with the procedures BLL and BINT. The contact density was thus calculated at temperatures between -250° and $+250^{\circ}$C by feeding in the appropriate values of Ω and k_F. The value of the linear coefficient of expansion was taken to be $8.9 \times 10^{-6} K^{-1}$ (8) and the volume coefficient is just 3 times this value. k_F was calculated according to the formula

$$k_F^3 = \frac{3\pi^2 Z}{\Omega} \quad . \tag{7.7}$$

The results are summarised in table 7.4. where it is seen that both γ and N_o vary linearly with

$$\frac{d\gamma}{dT} = 2.2 \times 10^{-4} K^{-1}$$

and $$\frac{dN_o}{dT} = 9.6 \times 10^{-6} K^{-1} \quad .$$

The relation

$$\Omega P_F = \frac{\gamma^2}{N_o} \tag{7.8}$$

can be differentiated to give

$$\frac{d\Omega P_F}{dT} = \frac{2\gamma}{N_o} \frac{d\gamma}{dT} - \frac{\gamma^2}{N_o^2} \frac{dN_o}{dT} \tag{7.9}$$

so using the values from Table 7.2. we obtain

$$\frac{1}{\Omega P_F}\frac{d\Omega P_F}{dT} = \frac{2}{\gamma}\frac{d\gamma}{dT} - \frac{1}{N}\left(\frac{dN_o}{dT} + \frac{d(A/\Omega)}{dT} + \frac{d(B/\Omega)}{dT}\right)$$

$$= \frac{2}{26.99}\ 2.2 \times 10^{-4} - \frac{1}{1.3}\left(9.6 \times 10^{-6} - 1.5 \times 10^{-6} - 5.4 \times 10^{-5}\right)$$

$$= 5.05 \times 10^{-5}\ K^{-1}$$

Table 7.4. Calculation of Temperature Dependence of Contact Density in Barium. The symbols used are those discussed in sec.7.4.

$$\frac{d\Omega P_F}{dT} = 2.38 \times 10^{-3} K^{-1} \qquad (7.10)$$

or

$$\frac{1}{\Omega P_F}\frac{d\Omega P_F}{dT} = \underline{\underline{2.28 \times 10^{-6} K^{-1}}} \qquad (7.11)$$

7.4.2. Temperature Dependence of ΩP_F: Inclusion of d-bands

The expression for the contact density of a metal with d-bands present is

$$\Omega P_F = \frac{\gamma^2}{N_o + \frac{A}{\Omega} + \frac{B}{\Omega}} = \frac{\gamma^2}{N} \qquad (7.12)$$

giving a temperature dependence of

$$\frac{1}{\Omega}\frac{d\Omega P_F}{dT} = \frac{2}{\gamma}\frac{d\gamma}{dT} - \frac{1}{N}\left(\frac{dN_o}{dT} + \frac{d(A/\Omega)}{dT} + \frac{d(B/\Omega)}{dT}\right) . \qquad (7.13)$$

The temperature dependence of γ and N_o have been evaluated in the previous section so it remains to evaluate $\frac{d}{dT}(A/\Omega)$ and $\frac{d}{dT}(B/\Omega)$. Firstly $\frac{d}{dT}(A/\Omega)$ is evaluated

$$\frac{d(A/\Omega)}{dT} = \frac{1}{\Omega}\frac{dA}{dT} - \frac{A}{\Omega^2}\frac{d\Omega}{dT} . \qquad (7.14)$$

This second term can be written $-\frac{A}{\Omega} \times \frac{1}{\Omega}\frac{d\Omega}{dT}$, both quantities already evaluated giving

$$-\frac{A}{\Omega} \times \frac{1}{\Omega}\frac{d\Omega}{dT} = -0.053 \times 30 \times 10^{-6} = \underline{\underline{1.5 \times 10^{-6}}} \qquad (7.15)$$

It was not possible to evaluate the first term of equation 7.14 as here again the 5d wave function was not available. However it is almost certain that this is a negligible contribution. The temperature dependence of N_o, which involves very similar terms to those in $\frac{d(A/\Omega)}{dT}$, comes alost entirely (95%) from terms involving the change of Ω directly.

The term $\frac{d(B/\Omega)}{dT}$ is more complicated. Firstly we must write

$$\frac{d(B/\Omega)}{dT} = \frac{d}{dT}\left(\frac{5}{4\pi}\frac{\Delta^2(k_F)}{(E_d-E_k)^2}\cdot\frac{1}{\Omega}\right)$$

$$= -\frac{5}{4\pi}\cdot\frac{\Delta^2(k_F)}{(E_d-E_k)^2}\cdot\frac{1}{\Omega^2}\cdot\frac{d\Omega}{dT}$$

$$+\frac{5}{4\pi}\cdot\frac{2\Delta^2(k_F)}{(E_d-E_k)^3}\cdot\frac{1}{\Omega}\cdot\frac{dE_k}{dT}$$

$$+\frac{5}{4\pi}\cdot\frac{2\Delta(k_F)}{(E_d-E_k)^2}\cdot\frac{1}{\Omega}\cdot\frac{d\Delta}{dT}\cdot \qquad (7.16)$$

Of these three terms the first reduces to

$$-\frac{B}{\Omega}\cdot\frac{1}{\Omega}\frac{d\Omega}{dT}. \qquad (7.17)$$

If the free electron expression

$$E_k = \frac{\hbar^2k^2}{2m} \qquad (7.18)$$

is used the second term reduces to

$$-\frac{2}{3}\frac{B}{\Omega}\cdot\frac{1}{\Omega}\frac{d\Omega}{dT}\cdot \qquad (7.19)$$

A rigorous treatment of the third term requires a detailed knowledge of $\Delta(k)$ as a function of k. Moriarty does not provide this for barium but for calcium it is clear that

$$\frac{d\Delta}{dk} = \frac{\Delta}{k} \qquad (7.20)$$

is a reasonable approximation and, assuming this, the third term of equation 7.16 reduces to

$$\left(1+\frac{4}{3}\frac{E_F}{E_d-E_F}\right)\cdot\frac{B}{\Omega}\cdot\frac{1}{\Omega}\frac{d\Omega}{dT}, \qquad (7.21)$$

thus producing the final expression

$$\frac{d}{dT}(B/\Omega) = -\frac{B}{\Omega}\left(\frac{5}{3} + \frac{4}{3}\cdot\frac{E_F}{E_d - E_F}\right)\cdot\frac{1}{\Omega}\frac{d\Omega}{dT}$$

$$= -0.6\left(\frac{5}{3} + \frac{4}{3} \times \frac{0.27}{0.26}\right) \times 30 \times 10^{-6} K^{-1}$$

$$= \underline{-5.49 \times 10^{-5}} \quad K^{-1}. \qquad (7.22)$$

These various contributions are brought together in Table 7.4 to give the final result of

$$\frac{1}{\Omega P_F}\frac{d(\Omega P_F)}{dT} = \underline{5.05 \times 10^{-5} K^{-1}} \qquad (7.23)$$

This result is an order of magnitude larger than the result ignoring the d-levels and shows that these have a very significant effect on this temperature dependence.

7.4.3. Comparison with Experiment

Before the above result is compared with experiment the temperature dependence of the spin susceptibility, χ, must be evaluated. According to the free electron theory

$$\chi = \frac{\mu^2 m k_F}{\pi\hbar^2}, \qquad (7.24)$$

where μ is the Bohr magneton. This gives

$$\frac{1}{\chi}\frac{d\chi}{dT} = \frac{1}{k_F}\frac{dk_F}{dT} = \frac{-1}{3}\frac{1}{\Omega}\frac{d\Omega}{dT}$$

$$= \underline{-1 \times 10^{-5}} \quad K^{-1}. \qquad (7.25)$$

The temperature dependence of the Knight shift is then given by

$$\frac{1}{K}\frac{dK}{dT} = \frac{1}{\Omega P_F}\frac{d\Omega P_F}{dT} + \frac{1}{\chi}\frac{d\chi}{dT} = \underline{4.05 \times 10^{-5}} \quad K^{-1}. \qquad (7.26)$$

The experimental value at $0^{o}C$ is $5 \times 10^{-4} K^{-1}$ which is ten times the above result. Thus, this approach does not provide an adequate explanation of this dependence, although the fact is that it is a considerable improvement on the result from the OPW, ignoring the d-band effects. This discrepency cannot be blamed on the rather crude approximation for χ. In reality one would expect an increase in the density of states around the region of the d-level, above the free electron value. This would mean that as the temperature rises, and the Fermi level drops away from the d-level, the density of states, and hence the susceptibility, should decrease more rapidly than given by the free electron approximation.

It seems therefore that the increase in the contact density with temperature must be very much greater than calculated here. This could be due to a number of reasons. Firstly the first-order and higher order effects, where the wavefunction is considered to be a sum of OPW's, have been ignored. Normally these give a large part of the temperature dependence in simple metals and the effect would be amplified in barium, where the d-levels will cause the pseudopotential to be highly energy dependent. The so called intrinsic temperature dependence, which is caused by the increased lattice vibrations, normally does not give such a large contribution but again the effect may be amplified by the d-bands, since it may effect the hybidisation.

To summarize, the excellent agreement between theory and experiment obtained in the calculation of the absolute Knight shift of barium provides strong evidence that the low value of the shift observed is due to the presence of a 5d level just above the Fermi surface. The agreement between theory and experiment for the temperature dependence is less satisfactory. The calculation to zero-order incorporating the effect of the d-band gives a temperature coefficient which, while it is some ten times greater than that predicted for simple

The experimental value at 0°C is $5 \times 10^{-4} K^{-1}$ which is ten times the above result. Thus, this approach does not provide an adequate explanation of this dependence, although the fact is that it is a considerable improvement on the result from the OPW, ignoring the d-band effects. This discrepency cannot be blamed on the rather crude approximation for χ. In reality one would expect an increase in the density of states around the region of the d-level, above the free electron value. This would mean that as the temperature rises, and the Fermi level drops away from the d-level, the density of states, and hence the susceptibility, should decrease more rapidly than given by the free electron approximation.

It seems therefore that the increase in the contact density with temperature must be very much greater than calculated here. This could be due to a number of reasons. Firstly the first-order and higher order effects, where the wavefunction is considered to be a sum of OPW's, have been ignored. Normally these give a large part of the temperature dependence in simple metals and the effect would be amplified in barium, where the d-levels will cause the pseudopotential to be highly energy dependent. The so called intrinsic temperature dependence, which is caused by the increased lattice vibrations, normally does not give such a large contribution but again the effect may be amplified by the d-bands, since it may effect the hybidisation.

To summarize, the excellent agreement between theory and experiment obtained in the calculation of the absolute Knight shift of barium provides strong evidence that the low value of the shift observed is due to the presence of a 5d level just above the Fermi surface. The agreement between theory and experiment for the temperature dependence is less satisfactory. The calculation to zero-order incorporating the effect of the d-band gives a temperature coefficient which, while it is some ten times greater than that predicted for simple

The experimental value at 0°C is $5 \times 10^{-4} K^{-1}$ which is ten times the above result. Thus, this approach does not provide an adequate explanation of this dependence, although the fact is that it is a considerable improvement on the result from the OPW, ignoring the d-band effects. This discrepency cannot be blamed on the rather crude approximation for χ. In reality one would expect an increase in the density of states around the region of the d-level, above the free electron value. This would mean that as the temperature rises, and the Fermi level drops away from the d-level, the density of states, and hence the susceptibility, should decrease more rapidly than given by the free electron approximation.

It seems therefore that the increase in the contact density with temperature must be very much greater than calculated here. This could be due to a number of reasons. Firstly the first-order and higher order effects, where the wavefunction is considered to be a sum of OPW's, have been ignored. Normally these give a large part of the temperature dependence in simple metals and the effect would be amplified in barium, where the d-levels will cause the pseudopotential to be highly energy dependent. The so called intrinsic temperature dependence, which is caused by the increased lattice vibrations, normally does not give such a large contribution but again the effect may be amplified by the d-bands, since it may effect the hybidisation.

To summarize, the excellent agreement between theory and experiment obtained in the calculation of the absolute Knight shift of barium provides strong evidence that the low value of the shift observed is due to the presence of a 5d level just above the Fermi surface. The agreement between theory and experiment for the temperature dependence is less satisfactory. The calculation to zero-order incorporating the effect of the d-band gives a temperature coefficient which, while it is some ten times greater than that predicted for simple

metals, is still an order of magnitude less than that observed experimentally at room temperature. The discrepancy is believed to be due to the neglect of first-order corrections but calculations to first-order are impossible at the present time due to the lack of detailed knowledge of $\Delta(k)$ and of a suitable model potential.

References

1. Drain L.E., Metallurgical Rev., 12, 195, (1967).

2. Cook G. and Van der Meer M.P., J.Phys.F., 3, L130, (1973).

3. Van Zytveld et al., J.Phys.F., 2, 73, (1972).

4. Moriarty J.A., Phys.Rev.B., 6, 4445, (1972).

and Phys.Rev.B., 10, 3075, (1974).

5. Ratti V.K. and Evans R., J.Phys.F., 3, L238, (1973).

6. Styles G.A., Private Comm.

7. Mann J.B., Los Alamos Scientific Lab.Report LA-3690, (1967).

8. Pearson W.B., Handbook of Lattice Spacings and Structures of Metals: Pergamon Press (1967).

9. Johansen G., Solid State Comm. 7, 731, (1969).

CHAPTER 8

Knight Shift in Thallium

8.1. Introduction

In most metals the Knight shift is a linear function of temperature. Schratter (1) has found that this is not the case for thallium and has shown that the rather rapid decrease in the ^{205}Tl Knight shift in the range 20-100K (see Fig.8.1.) is due to an irregularity in the density of states curve in the region of the Fermi surface. It is believed that at higher temperatures the Fermi surface moves to a region where the density of states equals the free-electron value and Schratter has used the observation (2) that the Knight shift does not change on melting to substantiate this conclusion. However the results of ref.2 only compare the Knight shift in the low temperature α-phase with results for the liquid. No measurements have been made on the high temperature β-phase.

Accurate measurement of the Knight shift in thallium is made difficult for two reasons. Firstly the resonance line is exceptionally broad due to an indirect interaction between the nuclei (3) and secondly in the α-phase, which is not cubic, there is an anisotropic Knight shift which causes an asymmetric line shape. It is believed that no attempt was made to account for this asymmetry in the measurements of ref.2.

It was therefore decided to measure the isotropic component of the Knight shift in thallium in the temperature range 295K to 750K paying special attention to changes of the Knight shift at the two phase boundaries (solid α-thallium to solid β-thallium at 505K, and solid β-thallium to liquid at 575K), and taking into account the

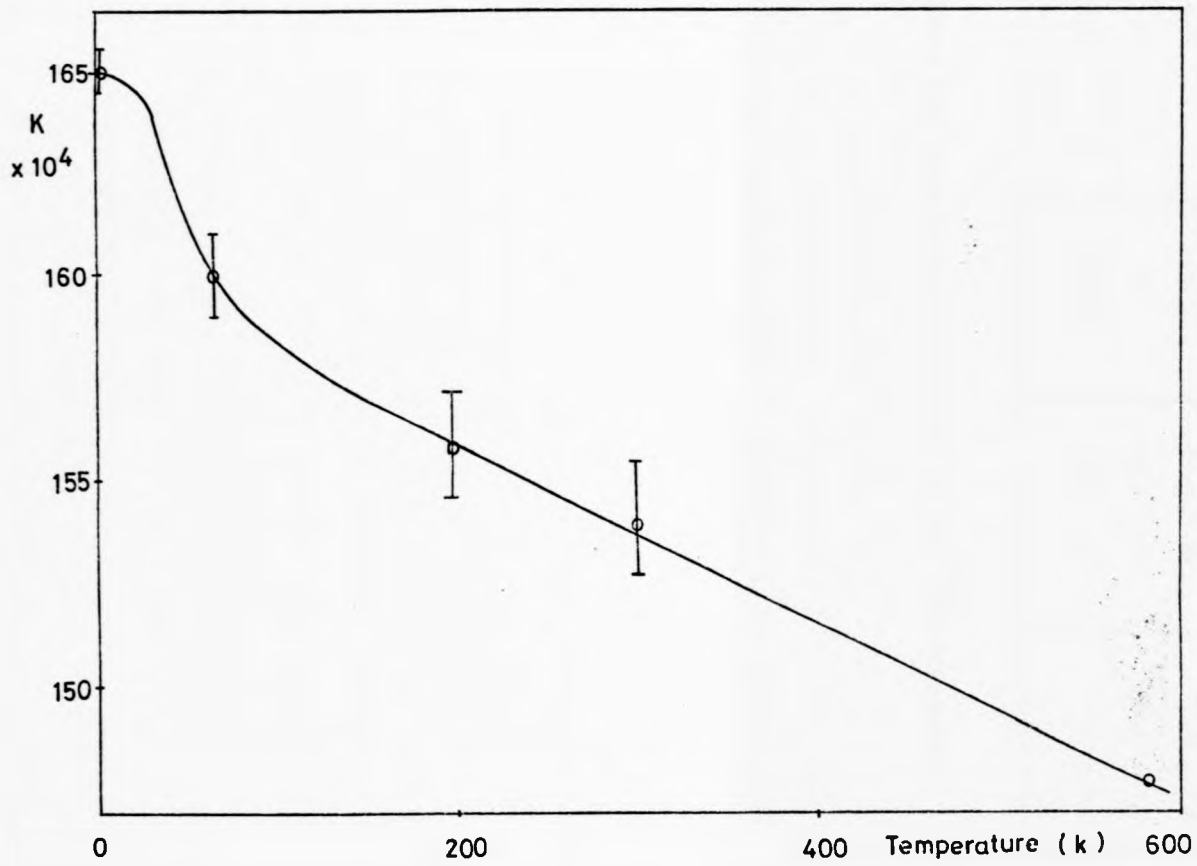

Fig.8.1. The Temperature Dependance of the Isotropic Knight Shift in Thallium from Schratter (1).

Temperature (K)	Phase	Line width (Gauss)	Line width (kHz)
295	α	$14.8 \pm .8$	37.0 ± 2.0
533	β	$15.5 \pm .7$	39.0 ± 1.7
623	Liquid	$16.5 \pm .9$	41.1 ± 2.3

Table 8.1. Peak to Peak Line Widths of the ^{205}Tl Resonance.

asymmetry of the line in the α-phase. In the course of these measurements it was noted that the line width of ^{205}Tl resonance in liquid thallium was large, despite the fact that the indirect nuclear interactions are motionally narrowed. The line widths were then measured in each phase. These results are presented in the next section, before the Knight shift results, since it is necessary to use the measured line widths in order to evaluate corrections to the Knight shift measurements in α-thallium.

8.2. The Line Width of ^{205}Tl resonance

In order to measure the peak to peak line width of this resonance, the line was observed using a relatively small modulation width (7.4. gauss), in a magnetic field of 5.5 KG. The measured width was then corrected for modulation broadening according to the method given by Andrew (4). Measurements were taken at 295K, 533K and 623K to observe the resonance in the α, β and liquid phases of the metal and the results are presented in Table 8.1. Each value is the average of six measurements.

The line width of α-thallium at 77K has been investigated thoroughly by Bloembergen and Rowland (3). By a phenomenological analysis of the line shape of samples of different isotopic abundances, and in various magnetic fields they show that the line shape has 3 main contributions:-

1) An indirect exhange interaction
2) A dipolar and pseudodipolar interaction whose effects cannot be separated phenomenologically
3) An anisotropy of the Knight shift.

The contribution of each of these interactions to the second moment of the ^{205}Tl resonance line at 77K is given in the first column of

Table 8.2. The r.m.s value of the line width is obtained by taking the square root and Bloembergen and Rowland observed that at 77K the peak to peak width was 1.4 times the r.m.s width. In the calculations of this chapter it is assumed that this ratio is maintained at all temperatures for solid thallium.

There is only a very small increase in the lattice parameters by 300K so it is reasonable to assume that all three contributions are essentially constant in the α-phase.

In the β-phase, however, the lattic is considerably different, as it changes from hexagonal close-packed to body-centred cubic. There can be no anisotropic component to the Knight shift in β-thallium because of the cubic symmetry of the lattice and the other contributions will change with the change of atomic separation. In order to evaluate the contributions from the indirect exchange and pseudo-dipolar interaction, corrections were made to the values deduced by Bloembergen and Rowland by using the theoretical radial dependence of their parameters which are also given in (3). The details of these calculations are given in Appendix E and the results are presented in the third column of Table 8.2. In the liquid phase, because of motional narrowing, there is no contribution from these interactions.

Except at very low temperatures, the line width is, however, affected by life-time broadening. In order to evaluate this contribution, T_1 was estimated from the Korringa relation (5)

$$T_1 K^2 = \frac{\hbar}{4\pi kT} \frac{\gamma_e^2}{\gamma_n^2} \alpha. \qquad (8.1)$$

K is the Knight shift, T_1 is the spin-lattice relaxation time, $\hbar$ is Planck's constant devided by 2π, k is Boltzmann's constant, T is the absolute temperature, γ_e and γ_n are the electron and nuclear gyromagnetic ratios respectively, and α is the Korringa enhancement factor which

Temperature	77	295	550	623
Phase	α	α	β	liquid
Indirect Exchange Contribution to M_2	312	312	124	0
Pseudodipolar and dipolar Contributions to M_2	170	170	165	0
Anistropic Knight shift contribution to M_2	100	100	0	0
Total M_2	582	582	289	0
r.m.s. width	24.1	24.1	17.0	0
peak to peak width	33.7	33.7	23.8	0
T_1 width	4.7	18.4	33.7	41.9
Total Theoretical PTP width	33.9	38.4	41.3	41.9
EXPT. PTP width	33.7	37.0	39.0	41.1

Table 8.2. Second Moments and Line Widths of ^{205}Tl Resonance. All second moments in $(kHz)^2$ and all line width in kHz.

takes account of the frequency dependence of the electronic spin susceptibility. In general for other metals this quantity is 1.2 to 1.3 and a value of 1.3 was assumed in this calculation. Since T_1 broadening of the line results in a Lorentzian shape the p.t.p width is related to T_1 by

$$\Delta\nu_{ptp} = \frac{1}{\sqrt{3}\pi T_1} \quad . \tag{8.2}$$

The linewidths calculated using equations 8.1 and 8.2 are given in Table 8.2. in the row labelled T_1 width. In order to combine this linewidth $\Delta\nu_L$ with the other sources of linewidth $\Delta\nu_o$, the relation

$$\Delta\nu_{ptp}^2 = \Delta\nu_o^2 + \Delta\nu_L^2 \tag{8.3}$$

was used and these results are compared with the experimental results in the final rows of Table 8.2.

Very good agreement with experiment is obtained throughout. It is somewhat surprising that Bloembergen and Rowland report no difference between the linewidths at 77K and room temperature. The present measurements show that the linewidth at 295K is larger than the value given by Bloembergen and Rowland, which is consistent with an additional contribution from the lifetime broadening. The exceptionally large line width in the liquid was at first thought to be due to the persistence of the indirect exchange interaction in the liquid but the present calculations make it clear that the linewidth results from the very rapid relaxation processes in liquid thallium. This occurs because this metal has a very large gyromagnetic ratio and a large Knight shift which will give a very small T_1 as shown by eq.8.1.

8.3. The Knight Shift

The Knight shift of ^{205}Tl has been measured at a number of

temperatures in the range 295 to 760K. The experimental method used was that described in Chapter 2 and, in order to obtain the line position from the resonance curve, the pen-recorder base-line was assumed to lie half way between the derivative peaks and the centre of the line taken as the intersection of the resonance with this baseline. For the measurements on α-thallium this introduces a significant error because the line was not symmetrical. The correction to these results could have been evaluated exactly if the exact form of the resonance curve was known, however, this was not the case. The contributions to the linewidths are discussed in the previous section. The shape function for anisotropic broadening is well known (6) and the value of the anisotropic component of the thallium Knight shift given by Schratter (1). However, there is no analytic form of the shape resulting from the other contributions, although the ratio of the p.t.p width to the r.m.s width, as given by Bloembergen and Rowland, shows that this shape is intermediate between a Gaussian and a Lorentzian curve.

The following method was therefore adopted in order to make an estimate of the correction to the Knight shift in α-thallium. Firstly a theoretical line shape was calculated by computer that was the convolution of the anisotropic line shape function and a Gaussian curve, whose width was chosen so that the final curve had the experimentally observed peak to peak width. The derivative of this final curve was then plotted. This derivative was treated in exactly the same way as the experimental curve. A base line was drawn equidistant between the peaks and the centre found from where this crossed the curve. The error in this procedure was then found by reference to the graph axes.
A similar procedure was then employed using a theoretical line that was constructed from a Lorentzian curve and the anisotropic line shape.

The details of these computer programs are given in Appendix F and

	Lorentzian Curve	Gaussian Curve
Error in Position (kHz)	4.2	2.2
Error in Knight Shift	3.2×10^{-4}	1.7×10^{-4}
% Error in Knight Shift	2.1	1.1

Table 8.3. Errors in Knight Shift Measurements in α- Thallium Calculated Using Line Shape based on a)Lorentzian b) Gaussian Curves.

their results are presented in Table 8.3. As the experimental error is somewhere intermediate between these values it was decided to use a simple average which gave a value of 1.545% for the Knight shift of pure thallium at 300K. This is in excellent agreement with the results of Schratter (1) made on single crystals.

The complete Knight shift results are given in Table 8.4. and they are also plotted in Fig.8.2. It should be noted that there is very little change of Knight shift on melting although there is a somewhate larger change at the α to β phase transition.

A discontinuous change of Knight shift at a phase transition is to be expected even if both the solid and the liquid are free electron like, because there is a discontinuous change of volume at this temperature. In order to examine whether the results do suggest that α-thallium is free electron like at room temperature, it was decided to plot a graph of Knight shift as a function of atomic volume. Values of the atomic volume, and linear coefficient of expansion are given byPearson (7) for α-thallium, and the atomic volume in the liquid was obtained from the Liquid Metals Handbook (8). The results are plotted in Fig.8.3.

As can be seen, the values for the solid and the liquid do not lie on a single straight line. If the values for the solid are extrapolated to the liquid volumes, the Knight shifts differ by about 5% of the value of 300K. However, this is a very small difference which is easily accounted for by slight differences between the details of the electronic wavefunctions in the solid and liquid phases. These results are therefore consistent with Schratter's assumption that the density of states in α-thallium above 100K is free electron like, although this is not definite proof of this hypothesis.

Temp °K		Knight Shift % as measure	Knight Shift with anisotropic correction	$\frac{\Delta K}{K}$ %	Atomic Volume u.u.
291		1.569 ± .003	1.545	0 ± 0.2	191.7
383	α-phase	1.551 ± .005	1.528	-1.2	
453		1.537 ± .005	1.513	-2.1 ± 0.3	
473		1.539 ± .005	1.516	-1.9	195.2
483*		1.550 ± .005	1.550	+0.3	
501		1.541 ± .005	1.541	-0.2	
513		1.538 ± .005	1.538	-0.4	
518	β-phase	1.538 ± .005	1.538	-0.4 ± 0.3	
543		1.524 ± .005	1.524	-1.4	196.2
561		1.512 ± .005	1.512	-2.1	
565		1.520 ± .005	1.520	-1.6	
573*		1.526 ± .005	1.526	-1.2 ± 0.3	202.8
601	Liquid phase	1.519 ± .005	1.519	-1.7 ± 0.3	203.4
638		1.517 ± .008	1.517	-1.8 ± 0.5	
683		1.509 ± .008	1.509	-2.3 ± 0.5	
758		1.504 ± .010	1.504	-2.7 ± 0.8	

Table 3.4. Knight Shift Thallium

* measurements on supercooled material.

+ error quoted does not include inaccuracies in evaluating the effect of the anistropic shift or measuring the α-phase.

Temp °K	Knight Shift % as measure	Knight Shift with anisotropic correction	$\frac{\Delta K^+}{K}$ %	Atomic Volume u.u.
291	1.569 ± .003	1.545	0 ± 0.2	191.7
383 α-phase	1.551 ± .005	1.528	-1.2	
453 α-phase	1.537 ± .005	1.513	-2.1 ± 0.3	
473 α-phase	1.539 ± .005	1.516	-1.9	195.2
483*	1.550 ± .005	1.550	+0.3	
501	1.541 ± .005	1.541	-0.2	
513 β-phase	1.538 ± .005	1.538	-0.4	
518 β-phase	1.538 ± .005	1.538	-0.4 ± 0.3	
543 β-phase	1.524 ± .005	1.524	-1.4	196.2
561 β-phase	1.512 ± .005	1.512	-2.1	
565 β-phase	1.520 ± .005	1.520	-1.6	
573*	1.526 ± .005	1.526	-1.2 ± 0.3	202.8
601 Liquid phase	1.519 ± .005	1.519	-1.7 ± 0.3	203.4
638 Liquid phase	1.517 ± .008	1.517	-1.8 ± 0.5	
683 Liquid phase	1.509 ± .008	1.509	-2.3 ± 0.5	
758 Liquid phase	1.504 ± .010	1.504	-2.7 ± 0.8	

Table 3.4. Knight Shift Thallium

* measurements on supercooled material.

\+ error quoted does not include inaccuracies in evaluating the effect of the anistropic shift or measuring the α-phase.

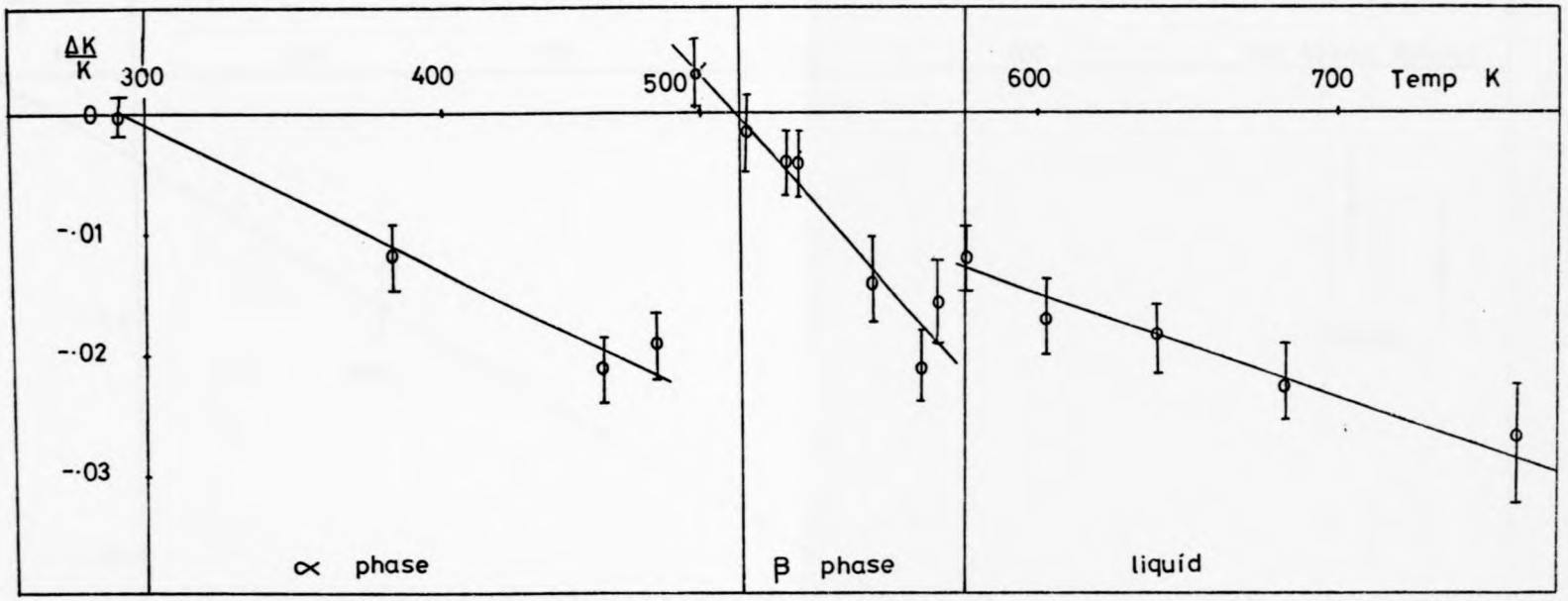

Fig.8.2. The Relative Change of the ^{205}Tl Knight Shift as a Function of Temperature.

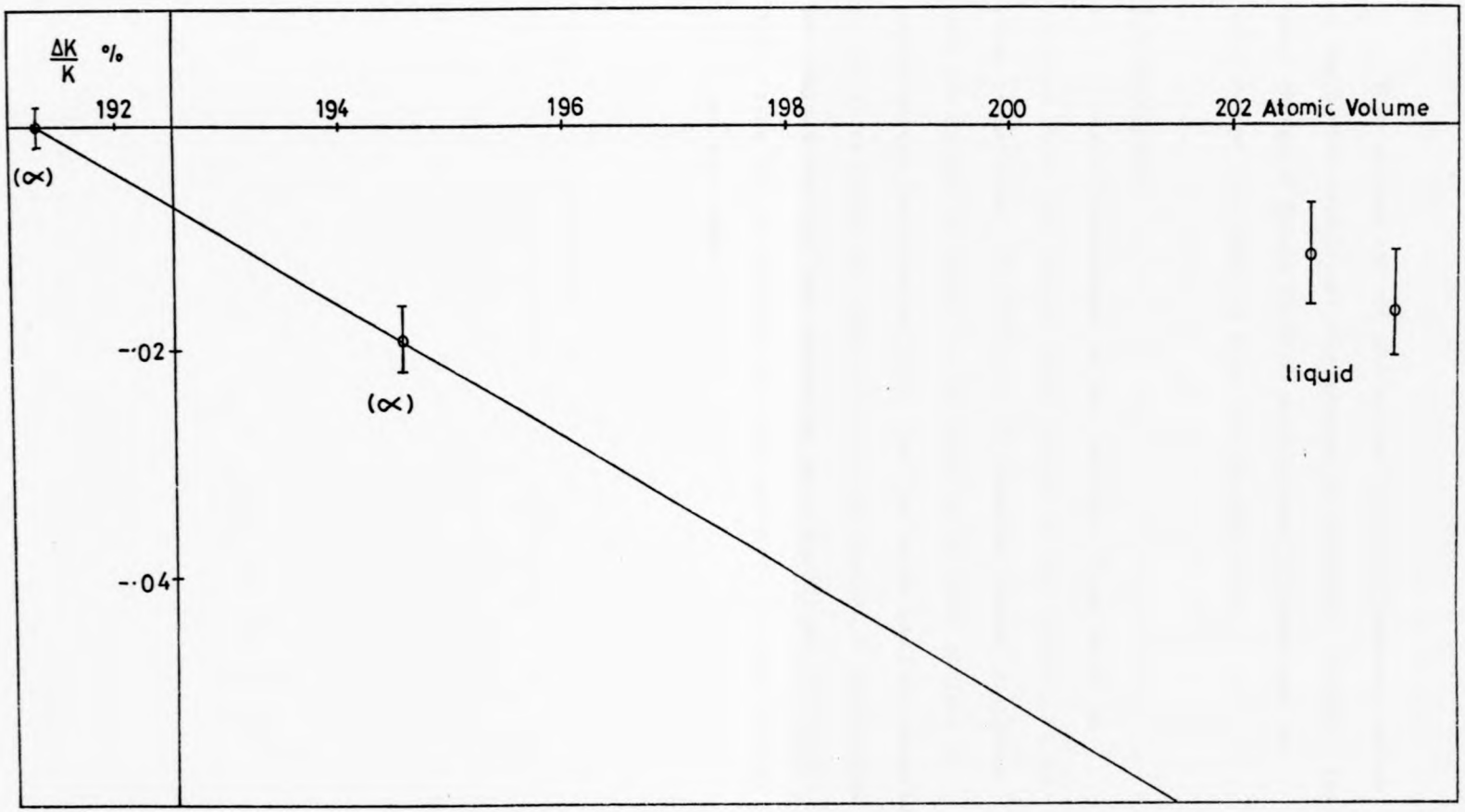

Fig.8.3. The Relative Change of the ^{205}Tl Knight Shift as a Function of Atomic Volume.

This process was not carried out for β-thallium as no value of the linear coefficient of expansion is available. However, the small change of Knight shift on melting does indicate that the behaviour of this phase is also free electron like.

8.4. Conclusion

A careful measurement of the isotropic Knight shift in thallium above 295K reveals small changes in this quantity at the phase transitions. As there is no substantial change it appears that the density of states in the solid at the Fermi surface is approximately free electron like. The line width has been measured in all three phases and contrary to the conclusions of Bloembergen and Rowland the life time broadening has a significant effect by 300K. When this is included very good agreement is found between theory and experiment.

References

1. Schratter J., Ph.D. Thesis, Univ. of British Columbia, (1973).

2. Moulson D.J., Ph.D. Thesis, Univ. of Leeds, (1966).

3. Bloembergen N. and Rowland T.J., Phys.Rev., 97, 1679, (1955).

4. Andrew E.P., Phys.Rev., 91, 425, (1953).

5. Schlicter P., Principles of Magnetic Resonance, Harper and Row, (1963).

6. Abragam A., Principles of Nuclear Magnetism, O.U.P, (1961).

7. Pearson W.B., Handbook of Lattice Spacings, Pergamon Press, (1967).

8. Liquid Metals Handbook, U.S. Atomic Commission, (1950).

Appendix A

Programs Used to Calculate Form Factors

Four programs were written in Algol 60 to evaluate the screened form factors for the cases where ℓ_o = 0, 1 or 2 and where the ℓ = 2 component could not be optimised as discussed in Chapter 6. Since the programs are all organised in the same way, only the ℓ = 2 case is discussed below. In the programs where ℓ_o = 0 and 1, the terms relating to higher angular momentum components are merely omitted, but for the case where the ℓ = 2 component is not optimised some of the expressions are different, so this program is listed together with the ℓ_o = 2 program at the end of this appendix.

Outline of Program

There are 10 procedures used frequently in the main program and these will be discussed first.

Procedures I0, I1 and I2

These three procedures evaluate the integrals I_o, I_1 and I_2, used in the calculation of the depletion hole, by means of a 10 point Simpson's rule integration. When the Bessel functions are written out in terms of their arguments the integrals can be expressed as

$$I_o = \int_o^1 dx \left[k_F R_o - \frac{\sin(2k_F R_o x)}{2x} \right] \qquad \text{(A1)}$$

$$I_1 = \int_o^1 dx \left[k_F R_1 + \frac{\sin(2k_F R_1 x)}{2x} - \frac{2\sin^2(k_F R_1 x)}{k_F R_1 x^2} \right] \qquad \text{(A2)}$$

$$I_2 = \int_o^1 dx \left[k_F R_2 - \frac{\sin(2k_F R_2 x)}{2x} - \frac{6}{k_F R_2 x^2} \left(\cos(k_F R_2 x) - \frac{\sin(k_F R_2 x)}{k_F R_2 x} \right)^2 \right]. \qquad \text{(A3)}$$

The R_ℓ are themselves dependent on x and are calculated using the optimisation condition

$$R_\ell(x) = Z \Big/ \left(A_\ell(E_F) + \frac{k_F^2}{2} (x^2 - 1) \frac{\partial A_\ell}{\partial E} \right) \qquad (A4)$$

except for the case where the $\ell = 2$ component is not optimised. Here R_2 is kept constant.

Procedure F

This evaluates the function F(k,q) defined in equation 4.115, again, using a 10 point Simpson's rule integration. The full expression for this function is

$$F(\underline{k},\underline{q}) = \frac{Z}{kk'} \int_0^1 dx \; \frac{x - 1}{x} \cdot \Bigg\{ \mathrm{Sin}(k'R_o x)\, \mathrm{Sin}(kR_o x) + 3\mathrm{Cos}\theta \left[\frac{\sin(k'R_1 x)}{k'R_1 x} - \mathrm{Cos}(k'R_1 x) \right] \times \left[\frac{\mathrm{Sin}(kR_1 x)}{kR_1 x} - \mathrm{Cos}(kR_1 x) \right]$$

$$+ \frac{S}{2} (3\mathrm{Cos}^2\theta - 1) \left[\left(\frac{3}{k'R_2 x^2} - 1 \right) \cdot \sin(k'R_2 x) - \frac{3\mathrm{Cos}(k'R_2 x)}{k'R_2 x} \right] - \times \left[\left(\frac{3}{kR_2 x^2} - 1 \right) \mathrm{Sin}(kR_2 x) - \frac{3\mathrm{Cos}(kR_2 x)}{kR_2 x} \right] \Bigg\} . \qquad (A5)$$

Here the integration does not involve an integral over energy so we write,

$$R_\ell(E) = Z/A_\ell(E) \qquad (A6)$$

where the A_ℓ is found from

$$A_\ell(E) = A_\ell(E_F) + \frac{k^2 - k_F^2}{2} \frac{\partial A_\ell}{\partial E} . \qquad (A7)$$

The effect of non-optimisation is that the initial multiplying factor $(x - 1)/x$ must be changed to $(1 - Z/A_2R_2x)$ for the third term, and that R_2 is no longer dependant on A_2.

Procedures FA and FKF

Procedure FA evaluates the integral $F(\underline{k},\underline{q})$ in the simplified ease of back scattering i.e. for $\text{Cos}\,\theta = 0$, while FKF evaluates $F(\underline{k},\underline{q})$ for Fermi shell scattering for which $k = k = k_F$.

Procedure DFDZ

This evaluates $\frac{\partial}{\partial z} F(k,q)$ for $k = k'$, which is required when evaluating the value of the integral $g(q)$ through the singularity. The derivative of R_ℓ gives no contribution since

$$R_\ell = \frac{Z}{A_\ell} \tag{A8}$$

and A_ℓ is independent of z. Thus the integrals can be performed analytically yielding

$$\frac{\partial F}{\partial z} = -\frac{k_F q}{2} \sum_{\ell=0}^{\ell_o} (2\ell + 1)\, P_\ell(\text{Cos}\theta)\, R_\ell^3 \frac{\partial A_\ell}{\partial E} \int_o^1 dx\, x^2\, j_\ell^2\,(kR_\ell x)$$

$$= -\frac{k_F q}{4} R_o^3 \frac{\partial A_o}{\partial E} \left[\frac{1}{(kR_o)^2} - \frac{\sin(2kR_o)}{2(kR_o)^3}\right]$$

$$+ 3\,\text{Cos}\theta\, R_1^3 \frac{\partial A_1}{\partial E} \left[\frac{1}{(kR_1)^2} + \frac{\text{Sin}(2kR_1)}{2(kR_1)^3} - \frac{2\,\text{Sin}^2(kR_1)}{(kR_1)^4}\right]$$

$$+ \frac{S}{2}(3\,\text{Cos}^2\theta - 1) \times R_2^3 \frac{\partial A_2}{\partial E} \left[\frac{1}{(kR_2)^2} - \frac{6\,\text{Cos}^2(kR_2)}{(kR_2)^4}\right.$$

$$\left. - \frac{6\,\text{Sin}^2(kR_2)}{(kR_2)^6} + \left(\frac{6}{(kR_2)^5} - \frac{1}{2(kR_2)^3}\right) \text{Sin}(2kR_2)\right] \tag{A9}$$

This result also applies in the non-optimised case where R_2 is a constant.

Procedure GZ

This performs the integral over u given by equation 4.119. Again Simpson's rule is used but the number of steps depends on the range of the integral. Where $k' = 0$ $F(u,z,\eta)$ is singular at $k' = 0$ but it can be shown that the limit of this function as $k' \to 0$ and is given by

$$\lim_{k' \to 0} F(\underline{k},\underline{q}) = \frac{A_o \mathrm{Sin}(qR_o)}{q^3} - \frac{Z}{q^2} \qquad \text{(A10)}$$

This limiting value is used in the procedure for $k' = 0$.

Procedure DGZ

This evaluates the integral over u of $\frac{\partial F}{\partial z}$ which is required when evaluating the principal part integral of $G(\eta)$. The integration method of the previous procedure is used.

Procedure G

This performs the final integration over z given in equation 4.118, and the integration range is divided into three regions each of which is dealt with differently. For $q > 2k_F$ this function is singular and an 80 point Simpson's rule integration method used with integrand at the singular point replaced by the function

$$F(1 - \eta_{/2}{}^2, -\eta_{/2}, \eta) \int_0^{1-(\eta/2)^2} du \; \frac{\partial F}{\partial z}(u, -\eta_{/2}, \eta)$$

as discussed in section 4.3.7. For $q = 2k_F$ the integrand has a limiting value at $z = -1$ of $2F(k_F,q^*)$ where q^* is such that $k = k' = k_F$ and a

40 point Simpson's rule integral is performed. A 40 point integration is also used for $q > 2k_F$, since there are no singularities in the function.

Main Program

Firstly the depletion hole is calculated and then the screened form factor is evaluated at various values of q as required, using the results from the above procedures substituted into equation 4.106. The non-local contributions are stored on disc file for use in the contact density and normalisation programs but the complete form factors for on-Fermi-shell scattering ($q < 2k_F$) and back scattering ($q > 2k$) are printed out for comparison with other work.

Key to Identifiers

AO, A1, A2		model potential well depths
DAO, DA1, DA2		Derivatives of above w.r.t. energy
KF	-	k_F (a.u.)
VO	-	ionic volume (a.u.)
PI	-	π
Z	-	valency
RHO	-	ρ
ZSTAR	-	z^*
ETA	-	$q/2k_F$
EPS	-	dielectric constant $\epsilon(q)$
WQ	-	$U(\underline{q})$
FW	-	non-local contribution to $U(\underline{q})$
KFT	-	Fermi Thomas wave vector
KI	-	χ
EPSS	-	$\epsilon^*(q)$
PU	-	u
PZ	-	z } as defined by equation 4.127
PETA	-	η
K	-	k
K1	-	k'
CS	-	Cos θ
RO, R1, R2		Model potential well radii
PK	-	k
X, M, N		Integors used variously in Simpson's rule integrations.
KRO	-	kR_o
KR1	-	kR_1

KR2 - kR_2

K1RO - $k'R_o$

K1R1 - $k'R_1$

K1R2 - $k'R_2$

ARG, ARG1, FUNC, FL, FLA, FAO, FA1, FA2, DFDZ1, FKFL, FN, are used variously as intermediate sums in integrations.

```
** ICL 4130 DES2 SYSTEM  :  SLAVE BACK      :  CORE 46K  :  VOL  4

&JOB;    PH/R060/F2;

&TIME;75;

 &ALGOL;L;
LIBRARY
ALGOL

&LIST;

    1   EVANS PSEUDOPOTENTIAL 02;
    2   "BEGIN""REAL"A0,A1,A2,DA0,DA1,DA2,   KF,V0,PI,Z,PHO,ZSTAR,ETA,EPS,WQ,FH,*
    3         KFT,KI,EPSS;
    4   "COMMENT""I0,I1,I2, ARE PROCEDURES FOR EVALUATING INTEGRALS USED IN THE
    5   DEPLETION HOLE CALC;
    6
    7   "REAL""PROCEDURE"I0(PK);      "VALUE"PK;
    8         "REAL"PK;
    9         "BEGIN""REAL"I,KR;      "INTEGER"X;    "REAL""ARRAY"FUNC[0:10];
   10                   "FOR"X:=1"STEP"1"UNTIL"9"DO"
   11                   "BEGIN"KR:=PK*Z/(A0*((X*2)/100-1)*(PK*2)*DA0/2);
   12                              FUNC[X]:=2*(KR-5*SIN(2*KR*X/10)/X)
   13                        "END";
   14                   KR:=PK*Z/A0;
   15                 FUNC[10]:=KR-SIN(2*KR)/2;
   16                 FUNC[0]:=0;
   17                 I:=0;
   18                 "FOR"X:=0"STEP"1"UNTIL"10"DO"
   19                    I:=I+FUNC[X];
   20                 "FOR"X:=1"STEP"2"UNTIL"9"DO"
   21                    I:=I+FUNC[X];
   22                 I0:=I/30;
   23         "END";
   24   "REAL""PROCEDURE"I1(PK); "VALUE"PK; "REAL"PK;
   25
   26         "BEGIN""REAL"KR,I;  "INTEGER"X;  "REAL""ARRAY"FUNC[0:10];
   27                "FOR"X:=1"STEP"1"UNTIL"9"DO"
   28                "BEGIN"KR:=PK*Z/(A1*(X*2/100-1)*PK*2*DA1/2);
   29                FUNC[X]:=2*(KR+5*SIN(2*KR*X/10)/X
   30                          =200*(SIN(KR*X/10))*2/(KR*X*2));
   31                "END";
   32                KR:=PK*Z/A1;
   33                FUNC[10]:=KR*SIN(2*KR)/2-2*(SIN(KR))*2/KR;
   34                FUNC[0]:=0;
   35                I:=0;
   36                "FOR"X:=0"STEP"1"UNTIL"10"DO"
   37                   I:=I+FUNC[X];
   38                 "FOR"X:=1"STEP"2"UNTIL"9"DO"
   39                   I:=I+FUNC[X];
   40                I1:=I/30;
```

```
41          "END";
42
43      "REAL""PROCEDURE"I1(PK);  "VALUE"PK;  "REAL"PK;
44          "BEGIN""REAL"KK,I;  "INTEGER"X;  "REAL""ARRAY"FUNC[0:10];
45                  "FOR"X:=1"STEP"1"UNTIL"9"DO"
46                  "BEGIN"KR:=KK*Z/(A2*X*2/100-1)*(PK*2)*DA2/2);
47                          FUNC[X]:=2*(KR-5*SIN(2*KR*X/10)/X-600*(COS(
48                                  KR*X/10)-10*SIN(KR*X/10)/(KR*X)**2/(KR*
49                                  X*2));
50                  "END";
51                  KR:="K*Z/A2;
52                  FUNC[10]:=KK*SIN(2*KR)/2-6*(COS(KR)*SIN(KR)/KR**2/KR;
53                  FUNC[0]:=0;              I:=0;
54                  "FOR"X:=0"STEP"1"UNTIL"10"DO"
55                     I:=I+FUNC[X];
56                  "FOR"X:=1"STEP"2"UNTIL"9"DO"
57                     I:=I+FUNC[X];
58                  I2:=I/30;
59          "END";
60
61      "COMMENT"F IS THE PROCEDURE FOR EVALUATING THE GENERAL NONLOCAL MATRIX
62      ELEMENTS F(K,Q), USED IN GZ DGZ AND GJ;
63      "REAL""PROCEDURE"F(PU,PZ,PETA);"VALUE"PU,PZ,PETA;  "REAL"PU,PZ,PETA;
64          "BEGIN""REAL"K,K1,KKF,R0,KR0,K1R0,CS,R1,KR1,K1R1,K1R2,KR2,R2
65                  ,ARG,ARG1,I;
66                  "INTEGER"N,M;    "REAL""ARRAY"FL[0:2,0:10];
67                  K:=KP*SQRT(PU*PZ*2);    KKF:=K*2*KF*2;
68                  K1:=KF*SQRT(PU*(PZ-PETA)*2);
69                  R0:=Z/(A0*KKF*DA0/2);    KR0:=K*R0;
70                  K1R0:=K1*R0;
71                  CS:=(PU*PZ*(PZ-PETA))/SQRT((PU*PZ*2)*
72                     (PU*(PZ-PETA)*2));
73                  R1:=Z/(A1*KKF*DA1/2);  R2:=Z/(A2*KKF*DA2/2);
74                  KR1:=K*R1;    K1R1:=K1*R1;
75                  KR2:=K*R2;    K1R2:=K1*R2;
76                  "FOR"N:=1"STEP"1"UNTIL"9"DO"
77                  "BEGIN"FL[0,N]:=2*((N-10)/N)*SIN(KR0*N/10)
78                                 *SIN(K1R0*N/10);
79                          ARG:=KR1*N/10;    ARG1:=K1R1*N/10;
80                          FL[1,N]:=2*((N-10)/N)*(SIN(ARG)/ARG-COS(ARG))
81                                  *(SIN(ARG1)/ARG1-COS(ARG1));
82                          ARG:=KR2*N/10;  ARG1:=K1R2*N/10;
83                          FL[2,N]:=2*((N-10)/N)          *((3/ARG*2-1)
84                                 *SIN(ARG)-3*COS(ARG)/ARG)*((3/ARG1*2-1)
85                                 *SIN(ARG1)-3*COS(ARG1)/ARG1);
86                  "END";
87                  "COMMENT"FOR N=0 OR 10   FL[X,N]=0;
88                  I:=0;
89                  "FOR"M:=1"STEP"1"UNTIL"2"DO"
90                  "FOR"N:=1"STEP"M"UNTIL"9"DO"
91                     I:=I+(Z/(K*K1))*(FL[0,N]+3*CS*FL[1,N]
92                        +2.5*(3*CS*2-1)*FL[2,N]);
93                  F:=I/30;
94          "END";
95          "COMMENT"FA EVALUATES F(K,Q) FOR K=KF  AND Q>2KF AND ANTIPARRALLEL**
96                  TO K;
97          "REAL""PROCEDURE"FA(PETA);  "VALUE"PETA;  "REAL"PETA;
98          "BEGIN""REAL"K,K1,KR0,KR1,KP2,K1R0,K1R1,K1R2,FAS,ARG,ARG1;
99                  "INTEGER"N,M;    "REAL""ARRAY"FA0,FA1,FA2[1:9];
100                 K:=KP;   K1:=KF*(PETA-1);
```

```
101                 KR0:=Z*K/A0;    K1R0:=Z*K1/A0;
102                 KR1:=Z*K/A1;    K1R1:=Z*K1/A1;
103                 KR2:=Z*K/A2;    K1R2:=Z*K1/A2;
104                 FOR"N:=1"STEP"1"UNTIL"9"DO"
105                 "BEGIN"FA0[N]:=2*((N-10)/N)*SIN(KR0*N/10)*SIN(K1R0*N/10);
106                       ARG:=KR1*N/10;    ARG1:=K1R1*N/10;
107                        FA1[N]:=2*((N-10)/N)*(SIN(ARG)/ARG-COS(ARG))*
108                              (SIN(ARG1)/ARG1-COS(ARG1));
109                       ARG:=KR2*N/10;    ARG1:=K1R2*N/10;
110                       FA2[N]:=2*((N-10)/N)*((3/ARG↑2-1)*SIN(ARG)-
111                              3*COS(ARG)/ARG)*((3/ARG1↑2-1)*SIN(ARG1)
112                              -3*COS(ARG1)/ARG1);
113                 END";
114                 FAS:=0;
115                 "COMMENT"FA0,FA1,FA2[0 OR 10] = 0;
116                 FOR"N:=1"STEP"1"UNTIL"2"DO"
117                 FOR"N:=1"STEP"M"UNTIL"9"DO"
118                 FAS:=FAS+(Z/(K*K1))*(FA0[N]+3*FA1[N]+5*FA2[N]);
119                 FA:=FAS/30;
120           "END";
121     "COMMENT"DFDZ IS A PROCEDURE FOR CALCULATING THE DERIVATIVE OF
122     F[K,J] W.R.T.PZ AT PZVQ/2 IT IS  REQUIRED FOR  PROC, DOZ;
123
124     "REAL""PROCEDURE"DFDZ(PU,PETA);  "VALUE"PU,PETA;  "REAL"PU,PETA;
125           "BEGIN"REAL"K,   A0,KR0,DFDZ1,R1,KR1,KR2,CS,KKF,R2;
126                 K:=KF*SQRT(PU↑(PETA/2)↑2);
127                 KKF:=K↑2-KF↑2;
128                  R0:=Z/(A0*KKF↑(DA0/2)); KR0:=K*R0;
129                 DFDZ1:=-(KF↑2*PETA/4)*D0↑3*DA0*(1/KR0↑2
130                       -SIN(2*KR0)/(2*KR0↑3));
131                 R1:=Z/(A1*KKF↑(DA1/2)); KR1:=K*R1;
132                       CS:=(PU-(PETA/2)↑2)/(PU↑(PETA/2)↑2);
133                       DFDZ1:=DFDZ1-(KF↑2*PETA/4)*3*CS*R1↑3*DA1*(1/KR1
134                             ↑2+SIN(2*KR1)/(2*KR1↑3)-2*(SIN(KR1))↑2
135                             /KR1↑4);
136                 R2:=Z/(A2*KKF↑(DA2/2));
137                 KR2:=K*R2;
138                 DFDZ1:=DFDZ1-(KF↑2*PETA/4)*(2,5*(3*CS↑2-1)*R2↑3*DA2
139                       *(1/KR2↑2-9*COS(KR2)↑2/KR2↑4-6*SIN(KR2)↑2/KR2↑6
140                       *(6/KR2↑5-1/(2*KR2↑3))*SIN(2*KR2)));
141                 DFDZ:=DFDZ1;
142           "END";
143
144     "COMMENT"PROCEDURE FKF IS TO EVALUATE F(K,0) WHEN K=K1=KF;
145     "REAL""PROCEDURE"FKF(PETA);  "VALUE"PETA;  "REAL"PETA;
146           "BEGIN"REAL"CS,KR0,KR1,ARG,KR2,I;    "INTEGER"N,M;
147                 "REAL""ARRAY"FKFL[0:2,0:10];
148                 CS:=1-PETA*2/2;
149                 FOR"N:=1"STEP"1"UNTIL"9"DO"
150                 "BEGIN"KR0:=Z*KF/A0;
151                       FKFL[0,N]:=2*((N-10)/N)*(SIN(KR0*N/10))↑2;
152                       KR1:=KF*Z/A1;  ARG:=KR1*N/10;
153                      FKFL[1,N]:=2*((N-10)/N)*(SIN(ARG)/ARG-COS(ARG))↑2;
154                        KR2:=KF*Z/A2; ARG:=KR2*N/10;
155                       FKFL[2,N]:=2*((N-10)/N)      *  ((3/ARG↑2-1)
156                                   *SIN(ARG)-3*COS(ARG)/ARG)↑2;
157                 END";
158           "COMMENT"ALL TERMS FKFL[M,0] AND FKFL[M,10]=0;
159                 I:=0;
160                 FOR"N:=1"STEP"1"UNTIL"2"DO"
```

```
                FOR N1:=1 STEP H UNTIL 9 DO
                   I1:=I+(Z/KF+2)*(FKFL[0,N]+3*CS*FKFL[1,N]
                      +2,5*(3*CS+2-1)*FKFL[2,N]);
                FKF:=I/30;
        END;

"COMMENT" GZ INTEGRATES F[K,Q] OVER THE RANGE U=0 TO 1=Z+2 ,USED IN G
   N;PZ IS USED FOR CO-ORD Z,ZIS KEPT FOR CHARGE;
REAL PROCEDURE GZ(PZ,PETA); VALUE PZ,PETA; REAL PZ,PETA;
        BEGIN REAL A,H,AL0,R0,I;     INTEGER N,M;

                A:=1+PZ+2;      H:=2*ENTIER(10*A)+1;
            BEGIN REAL ARRAY FN[0:M];
                H:=A/M;
                FOR N1:=1 STEP 2 UNTIL M-1 DO
                   FN[N]:=4*F(N*H,PZ,PETA);
                IF M>2 THEN
                FOR N1:=2 STEP 2 UNTIL M-2 DO
                   FN[N]:=2*F(N*H,PZ,PETA);
                FN[M]:=F(A,PZ,PETA);
                 IF ABS(PZ)<10*(-3)
                 THEN BEGIN AL0:=A0+KF+2*DA0/2;  R0:=Z/AL0;
                                FN[0]:=AL0*SIN(KF*PETA*R0)/(KF*PETA)+3
                                      -Z/(KF*PETA)+2;
                      END
                 ELSE BEGIN IF ABS(PZ*PETA)<10*(-3)
                           THEN BEGIN AL0:=A0+(PETA+2-1)*KF+2*DA0/2;
                                      R0:=Z/AL0;
                                   FN[0]:=AL0*SIN(KF*PETA*R0)
                                        /(KF*PETA)+3
                                        -Z/(KF*PETA)+2;
                                END
                           ELSE  FN[0]:=F(0,PZ,PETA);
                      END;
                I:=0;
                FOR N1:=0 STEP 1 UNTIL M DO
                   I1:=I+FN[N];
            END;
                GZ:=I*H/3;
        END;

"COMMENT"DGZ INTEGRATES DF(K,Q)/DZ REQUIRED IN PROC,G;
REAL PROCEDURE DGZ(PETA); VALUE PETA;  REAL PETA;
        BEGIN REAL A,H,I;    INTEGER N,M;
                A:=1+(PETA/2)+2;
                M:=2*ENTIER(10*A)+1;
            BEGIN REAL ARRAY FN[0:M];
                H:=A/M;
                FOR N1:=1 STEP 2 UNTIL M-1 DO
                   FN[N]:=4*DFDZ(N*H,PETA);
                IF M>2 THEN
                FOR N1:=2 STEP 2 UNTIL M-2 DO
                   FN[N]:=2*DFDZ(N*H,PETA);
                FN[M]:=DFDZ(A,PETA);
                FN[0]:=DFDZ(0,PETA);      I1:=0;
                FOR N1:=0 STEP 1 UNTIL M DO
                   I1:=I+FN[N];
            END;
              DGZ:=I*H/3;
        END;
```

```
221
222   "COMMENT" CINTEGRATES THE FN, GZ/(Z+ETA/2) FROM ZV=1 TO ZV+1;
223   "REAL""PROCEDURE"G(PETA);  "VALUE"PETA;  "REAL"PETA;
224         "BEGIN""REAL"I;     "INTEGER"N,M;
225               "IF"ABS(PETA-2)<10↑(-3)"THEN""GOTO"CASE 2;
226               "IF"PETA>2↑10↑(-3)"THEN""GOTO"CASE 3;
227          CASE 1;"BEGIN""REAL""ARRAY"FN[-40:40];
228                         "FOR"N:=-39"STEP"1"UNTIL"39"DO"
229                               "IF"ABS(N↑20↑PETA)>10↑(-3)
230                               "THEN"FN[N]:=2↑GZ(,025↑N,PETA)
231                                           /(,025↑N↑PETA/2 )
232                               "ELSE"FN[N]:=2↑PETA↑FKF(PETA)↑2↑DGZ(PETA);
233                         FN[40]:=0;  FN[-40]:=0;  I:=0;
234                         "FOR"M:=1"STEP"1"UNTIL"2"DO"
235                         "FOR"N:=-39"STEP"M"UNTIL"39"DO"
236                            I:=I↑FN[N];
237                         G:=(KF/(4↑PETA))↑(,025/3)↑I;
238                   "END";
239                   "GOTO"ENDG;
240         CASE 2;"BEGIN""REAL""ARRAY"FN[-20:20];
241                         "FOR"N:=-19"STEP"1"UNTIL"19"DO"
242                            FN[N]:=2↑GZ(,05↑N,2)/(,05↑N↑1);
243                         FN[-20]:=0;  FN[20]:=2↑FKF(2);  I:=0;
244                         "FOR"M:=1"STEP"1"UNTIL"2"DO"
245                         "FOR"N:=-19"STEP"M"UNTIL"19"DO"
246                            I:=I↑FN[N];
247                         I:=I↑FN[20];
248                         G:=(KF/8)↑(,05/3)↑I;
249                   "END";
250                   "GOTO"ENDG;
251         CASE 3;"BEGIN""REAL""ARRAY"FN[-20:20];
252                      "FOR"N:=-19"STEP"1"UNTIL"19"DO"
253                      FN[N]:=2↑GZ(,05↑N,PETA)/(,05↑N↑PETA/2);
254                      I:=0;
255                      "FOR"M:=1"STEP"1"UNTIL"2"DO"
256                      "FOR"N:=-19"STEP"M"UNTIL"19"DO"
257                         I:=I↑FN[N];
258                      G:=(KF/(4↑PETA))↑(,05/3)↑I;
259                   "END";
260   ENDG;"END";
261
262   "COMMENT"MAIN PROG TO CALC W(Q);
263         "READ"A0,A1,A2,DA0,DA1,DA2,   KF,V0,PI,Z;
264         RHO:=(2/PI)↑(DA0↑I0(KF)↑3↑DA1↑I1(KF)↑5↑DA2↑I2(KF));
265         "PRINT"/'L',SAMELINE,/'S4',/'ETA'S6'W[Q]'S7'NLF'S7'LF'S6'X';
266     LOOP;"READ"ETA;
267         "IF"ETA>100"THEN""GOTO"FIN;
268         "IF"ABS(ETA-2)<10↑(-3)
269         "THEN"EPS:=1+1/(2↑PI↑KF)
270        "ELSE"EPS:=1+(2/(PI↑KF↑ETA↑2))↑(((1-(ETA/2)↑2)/ETA)↑
271                     LN(ABS((1+ETA/2)/(1-ETA/2)))+1);
272         "IF"ETA<LE>4"THEN"FW:=FKF(ETA)
273         "ELSE"FW:=F\(ETA);
274         KFT:=12↑PI↑Z/(V0↑KF↑2);
275         KI:=-2↑PI/((ETA↑KF)↑2+KF↑2+KFT);
276         EPSS:=(EPS-1)↑(1+(ETA↑KF)↑2↑KI/(4↑PI))+1;
277         ZSTAR:=Z-(1+(ETA↑KF)↑2↑KI/(4↑PI))↑RHO;
278         WQ:=-4↑PI↑ZSTAR/(V0↑(KF↑ETA)↑2↑EPSS)  ↑(4↑PI/V0)↑FW
279             +(1+(ETA↑KF)↑2↑KI/(4↑PI↑EPSS))↑(32/(V0↑(ETA↑KF)↑2))↑G(ETA)
280             /EPS;
```

```
** ICL 4130 DES2 SYSTEM  :  SLAVE BIG        :  CORE 70K  :  VOL  3

&JOB(PH/R060/GT)

&ALGOL(          L)

$LIST)

    1   EVANS MERCURY PSEUDOPOTENTIAL   01)
    2   "BEGIN""REAL"A0,A1,A2,DA0,DA1,DA2,R2,KF,V0,PI,Z,RHO,ZSTAR,ETA,EPS,W0,FW
    3             ,KFT,KI,EPS)
    4   "COMMENT"IO,I1,I2, ARE PROCEDURES FOR EVALUATING INTEGRALS USED IN THE
    5   DEPLETION HOLE CALC)
    6
    7   "REAL""PROCEDURE"I0(PK))      "VALUE"PK)
    8         "REAL"PK)
    9         "BEGIN""REAL"I,KR)      "INTEGER"X)    "REAL""ARRAY"FUNC[0:10])
   10                   "JUMP"X:=1"STEP"1"UNTIL"9"DO"
   11                   "BEGIN"KR:=PK*Z/(A0+((X+2)/100-1)*(PK+2)*DA0/2))
   12                                FUNC[X]:=2*(KR-5*SIN(2*KR*X/10)/X))
   13                        "END")
   14                   KR:=PK*Z/A0)
   15                 FUNC[10]:=KR-SIN(2*KR)/2)
   16                 FUNC[0]:=0)
   17                 I:=0)
   18                 "FOR"X:=0"STEP"1"UNTIL"10"DO"
   19                    I:=I+FUNC[X])
   20                 "FOR"X:=1"STEP"2"UNTIL"9"DO"
   21                    I:=I+FUNC[X])
   22                 I0:=I/30)
   23         "END")
   24
   25   "REAL""PROCEDURE"I1(PK)); "VALUE"PK) "REAL"PK)
   26         "BEGIN""REAL"KR,I)   "INTEGER"X)   "REAL""ARRAY"FUNC[0:10])
   27                 "FOR"X:=1"STEP"1"UNTIL"9"DO"
   28                 "BEGIN"KR:=PK*Z/(A1+(X+2/100-1)*PK+2*DA1/2))
   29                 FUNC[X]:=2*(KR+5*SIN(2*KR*X/10)/X
   30                           -200*(SIN(KR*X/10))+2/(KR*X+2))
   31                 "END")
   32                 KR:=PK*Z/A1)
   33                 FUNC[10]:=KR+SIN(2*KR)/2-2*(SIN(KR))+2/KR)
   34                 FUNC[0]:=0)
   35                 I:=0)
   36                 "FOR"X:=0"STEP"1"UNTIL"10"DO"
   37                    I:=I+FUNC[X])
   38                 "FOR"X:=1"STEP"2"UNTIL"9"DO"
   39                    I:=I+FUNC[X])
   40                 I1:=I/30)
   41         "END")
   42
   43   "REAL""PROCEDURE"I2(PK)); "VALUE"PK)  "REAL"PK)
   44         "BEGIN""REAL"KR,I)   "INTEGER"X)   "REAL""ARRAY"FUNC[0:10])
   45                 "FOR"X:=1"STEP"1"UNTIL"9"DO"
```

```
46                  "BEGIN"KR:=PK*P2;
47                        FUNCLX]:=2*(KR-5*SIN(2*KR*X/10)/X-6*0*(COS(
48                              K*X/10)-10*SIN(KR*X/10)/(KR*X)**2/(KR*
49                              X*2));
50                  "END";
51                  KR:=PK*P2;
52                  FUNCL10]:=KR-SIN(2*KR)/2-6*(COS(KR)-SIN(KR)/KR)**2/KR;
53                  FUNCL0]:=0;          I:=0;
54                  "FOR"X:=0"STEP"1"UNTIL"10"DO"
55                     I:=I+FUNCCX];
56                  "FOR"X:=1"STEP"2"UNTIL"9"DO"
57                     I:=I+FUNCCX];
58                  I2:=I/30;
59            "END";
60
61      "COMMENT"F IS THE PROCEDURE FOR EVALUATING THE GENERAL NONLOCAL MATRIX
62      ELEMENTS F(K,G), USED IN GZ DGZ AND G;
63      "REAL""PROCEDURE"F(FL,PZ,PETA);"VALUE"PU,PZ,PETA; "REAL"PU,PZ,PETA;
64            "BEGIN""REAL"K,K1,KKF,P0,KR0,K1R0,CS,R1,KR1,K1R1,K1R2,KR2
65                        ,ARG,ARG1,T,AL2;
66                  "INTEGER"N,M;   "REAL""ARRAY"FL[0:2,0:10];
67            "BEGIN"K1:=KF*SQRT(PU*PZ*2);   KKF:=K*2-KF*2;
68                  K1:=KF*SQRT(PU*(PZ+PETA)*2);
69                  P0:=Z/(A0+KKF*DA0/2);   KR0:=K*R0;
70                  K1R0:=K1*R0;
71                  CS:=(PU+PZ*(PZ+PETA))/SQRT((PU+PZ*2)*
72                      (PU*(PZ+PETA)*2));
73                  P1:=Z/(A1+KKF*DA1/2);
74                  KR1:=K*R1;   K1R1:=K1*R1;
75                  KR2:=K*P2;   K1R2:=K1*P2;
76                  AL2:=A2+KKF*DA2/2;
77            "END";
78                  "FOR"N:=1"STEP"1"UNTIL"9"DO"
79                  "BEGIN"FL[0,N]:=2*((N-10)/N)*SIN(KR0*N/10)
80                              *SIN(K1R0*N/10);
81                        ARG:=KR1*N/10;   ARG1:=K1R1*N/10;
82                        FL[1,N]:=2*((N-10)/N)*(SIN(ARG)/ARG-COS(ARG))
83                              *(SIN(ARG1)/ARG1-COS(ARG1));
84                        ARG:=KR2*N/10;  ARG1:=K1R2*N/10;
85                        FL[2,N]:=2*(1-10*Z/(AL2*R2*N))*((3/ARG**2-1)
86                              *SIN(ARG)-3*COS(ARG)/ARG)*((3/ARG1**2-1)
87                              *SIN(ARG1)-3*COS(ARG1)/ARG1);
88                  "END";
89                  "COMMENT"FOR N=0 OR 10   FL[X,N]=0EXCEPT FL[2,10]
90                        DUE TO ADD OPTIMIZATION OF POTENTIAL;
91                  FL[2,10]:=(1-Z/(AL2*P2))*((3/KR2**2-1)*SIN(KR2)
92                        -3*COS(KR2)/KR2)*((3/K1R2**2-1)*SIN(K1R2)
93                        -3*COS(K1R2)/K1R2);
94                  I:=0;
95                  "FOR"N:=1"STEP"1"UNTIL"2"DO"
96                  "FOR"M:=1"STEP"1"UNTIL"9"DO"
97                     I:=I+(Z/(K*R1))*(FL[0,M]+3*CS*FL[1,M]
98                        +2.5*(3*CS**2-1)*FL[2,M]);
99                  I:=I+(Z/(K*K1))*2.5*(3*CS**2-1)*FL[2,10];
100                 F:=I/30;
101           "END";
102
103     "COMMENT"DGZ IS A PROCEDURE FOR CALCULATING THE DERIVATIVE OF
104     F(K,A) A,R,T,PZ AT PZV0/2 IT IS  REQUIRED FOR  PPOC, DGZ;
105
```

```
"REAL""PROCEDURE"DFDZ(PU,PETA);  "VALUE"PU,PETA;  "REAL"PU,PETA;
        "BEGIN""REAL"K,    R0,KR0,DFDZ1,R1,KR1,KR2,CS,KKF;
                KF:=KF*SQRT(PU*(PETA/2)*2);
                KKF:=K*2-KF*2;
                 RJ:=Z/(A0*KKF*(DA0/2)); KR0:=K*R0;
                DFDZ1:=-(KF*2*PETA/4)*PU*3*DA0*(1/KR0*2
                       -SIN(2*KR0)/(2*KR0*3));
                R1:=Z/(A1*KF*(DA1/2)); KR1:=K*R1;
                       CS:=(PU-(PETA/2)*2)/(PU*(PETA/2)*2);
                       DFDZ1:=DFDZ1-(KF*2*PETA/4)*3*CS*P1*3*DA1*(1/KR1
                              *2*SIN(2*KR1)/(2*KR1*3)-2*(SIN(KR1))*2
                              /KR1*4);
                KR2:=K*R2;
                DFDZ1:=DFDZ1-(KF*2*PETA/4)*(2,5*(3*CS*2-1)*R2*3*DA2
                       *(1/KR2*2-6*COS(KR2)*2/KR2*4-6*SIN(KR2)*2/KR2*6
                       *(6/KR2*5-1/(2*KR2*3))*SIN(2*KR2))));
                DFDZ:=DFDZ1;
        "END";

"COMMENT"PROCEDURE FKF IS TO EVALUATE F(K,0) WHERE K=K1=KF;
"REAL""PROCEDURE"FKF(PETA);  "VALUE"PETA;  "REAL"PETA;
        "BEGIN""REAL"CS,KR0,KR1,ARG,KR2,I;    "INTEGER"N,M;
                "REAL""ARRAY"FKFLL0:2,0:10];
                CS:=1-PETA*2/2;
                KR0:=Z*KF/AJ;    KR1:=KF*Z/A1;    KR2:=KF*R2;
                "FOR"N:=1"STEP"1"UNTIL"9"DO"
                "BEGIN"FKFLL0,N]:=2*((N-10)/N)*(SIN(KR0*N/10))*2;
                                        ARG:=KR1*N/10;
                      FKFLL1,N]:=2*((N-10)/N)*(SIN(ARG)/ARG-COS(ARG))*2;
                                        ARG:=KR2*N/10;
                       FKFLL2,N]:=2* (1-Z*:0/(A2*R2*K))*((3/ARG*2-1)
                                  *SIN(ARG)-3*COS(ARG)/ARG)*2;
                "END";
        "COMMENT"ALL TERMS FKFLL*,0] AND FKFLL*,10]=0
                 EXCEPT FLL2,10] DUE TO NONOPTIMISATION OF POTENTIAL;
             FKFLL2,10]:=(1-Z/(A2*R2))*((3/KR2*2-1)*SIN(KR2)
                        -3*COS(KR2)/KR2)*2;
                I:=0;
                "FOR"M:=1"STEP"1"UNTIL"2"DO"
                "FOR"N:=1"STEP"9"UNTIL"9"DO"
                   I:=I+(Z/KF*2)*(FKFLL0,N]+3*CS*FKFLL1,N]
                        +2,5*(3*CS*2-1)*FKFLL2,N]);
                I:=I+(Z/KF*2)*2,5*(3*CS*2-1)*FKFLL2,10];
                FKF:=I/30;
        "END";

"COMMENT" CZ INTEGRATES F(K,0] OVER THE RANGE U=0 TO 1-Z*2 ,USED IN G
    -IIPZ IS USED FOR GO-GRID Z,AIS KEPT FOR CHARGE;
"REAL""PROCEDURE"CZ(PZ,PETA);  "VALUE"PZ,PETA;  "REAL"PZ,PETA;
        "BEGIN""REAL"A,H,ALO,PO,I;    "INTEGER"N,M;

                A:=1-PZ*2;     M:=2*(ENTIER(10*A)+1);
            "BEGIN""REAL""ARRAY"F(0:M];
                H:=A/M;
                "FOR"N:=1"STEP"2"UNTIL"M-1"DO"
                   F[N]:=4*F(H*N,PZ,PETA);
                "IF"1>2"THEN"
                "FOR"N:=2"STEP"2"UNTIL"M-2"DO"
                   F[N]:=2*F(H*N,PZ,PETA);
                END I:=F(A,PZ,PETA);
```

```
166                 "IF"ABS(PZ)<10*(-3)
167                 "THEN""BEGIN" ALO:=A0-PF*2*DA0/2;  RO:=Z/ALO;
168                                 FN[0]:=ALO*SIN(KF*PETA*R0)/(KF*PETA)*3
169                                       -Z/(KF*PETA)*2;
170                       "END"
171                 "ELSE""BEGIN""IF"ABS(PZ*PETA)<10*(-3)
172                             "THEN""BEGIN"ALO:=A0+(PETA*2-1)*KF*2*DA0/2;
173                                        RO:=Z/ALO;
174                                   FN[0]:=ALO*SIN(KF*PETA*R0)
175                                        /(KF*PETA)*3
176                                        -Z/(KF*PETA)*2;
177                                 "END"
178                             "ELSE"  FN[0]:=F(0,PZ,PETA);
179                       "END";
180               I:=0;
181               "FOR"N:=0"STEP"1"UNTIL"H"DO"
182                  I:=I+FN[N];
183            "END";
184               QZ:=I*H/3;
185         "END";
186
187   "COMMENT"DQZ INTEGRATES DF(M,Z)/DZ REQUIRED IN PROC.3;
188   "REAL""PROCEDURE"DQZ(PETA);  "VALUE"PETA;  "REAL"PETA;
189         "BEGIN""REAL"A,H,I;   "INTEGER"N,M;
190               A:=3-(PETA/2)*2;
191               H:=2*(ENTIER(10*A)+1);
192            "BEGIN""REAL""ARRAY"FN[0:H];
193               H:=A/H;
194               "FOR"N:=1"STEP"2"UNTIL"H-1"DO"
195                  FN[N]:=4*DFDZ(N*H,PETA);
196               "IF"H>2"THEN"
197               "FOR"N:=2"STEP"2"UNTIL"H-2"DO"
198                  FN[N]:=2*DFDZ(N*H,PETA);
199               FN[0]:=DFDZ(A,PETA);
200               FN[H]:=DFDZ(0,PETA);       I:=0;
201               "FOR"N:=0"STEP"1"UNTIL"H"DO"
202                  I:=I+FN[N];
203            "END";
204               DQZ:=I*H/3;
205         "END";
206
207   "COMMENT" INTEGRATES THE FN, QZ/(Z+ETA/2) FROM ZV=1 TO ZV+1;
208   "REAL""PROCEDURE"G(PETA);  "VALUE"PETA;  "REAL"PETA;
209         "BEGIN""REAL"I;     "INTEGER"N,M;
210               "IF"ABS(PETA-2)<10*(-3)"THEN""GOTO"CASE 2;
211               "IF"PETA>2+10*(-3)"THEN""GOTO"CASE 3;
212          CASE 1:"BEGIN""REAL""ARRAY"FN[-40:40];
213                     "FOR"N:=-39"STEP"1"UNTIL"39"DO"
214                          "IF"ABS(N+2L*PETA)>10*(-3)
215                          "THEN"FN[N]:=2*QZ(.025*N,PETA)
216                                       /(.025*N+PETA/2 )
217                          "ELSE"FN[N]:=2*PETA*FKF(PETA)*2*DQZ(PETA);
218                     FN[40]:=0;  FN[-40]:=0;  I:=0;
219                     "FOR"N:=1"STEP"1"UNTIL"2"DO"
220                     "FOR"N:=-39"STEP"1"UNTIL"39"DO"
221                        I:=I+FN[N];
222                     G:=(KF/(4*PETA))*(.025/3)*I;
223               "END";
224               "GOTO"ENDG;
225         CASE 2:"BEGIN""REAL""ARRAY"FN[-20:20];
```

```
226                         "FOR"N1:=-19"STEP"1"UNTIL"19"DO"
227                            FNE"I1:=2*GZ(,05*I,2)/(,05*I+1);
228                         FNE[-20]:=0;  FNE[20]:=2*FKF(C);  I:=0;
229                         "FOR"N:=1"STEP"1"UNTIL"2"DO"
230                         "FOR"N1:=-19"STEP"1"UNTIL"19"DO"
231                            I:=I+20[I];
232                         I:=I+FNE[20];
233                         G:=(KF/4)*(.05/3)*I;
234                   "END";
235                   "GOTO"ENDG;
236            CASE 3:"BEGIN""REAL""ARRAY"FNE[-20:20];
237                      "FOR"I:=-19"STEP"1"UNTIL"19"DO"
238                      FNE[I]:=2*GZ(,05*I,BETA)/(,05*I+2*BETA/2);
239                      I:=0;
240                      "FOR"N:=1"STEP"1"UNTIL"2"DO"
241                      "FOR"N1:=-19"STEP"1"UNTIL"19"DO"
242                         I:=I+FNE[I];
243                      G:=(KF/(4*BETA))*(,05/3)*I;
244                   "END";
245      ENDG:"END";
246
247      "COMMENT"MAIN PROG TO CALC 2(I);
248            "READ"A0,A1,A2,DA0,DA1,DA2,R2,KF,V0,PI,Z;
249            R1:=(2/PI)*(DA0*I0(KF)+3*DA1*I1(KF)+5*DA2*I2(KF));
250            "PRINT"/'L'',SAMELINE,''S4'','BETA'S6'RE0I'37'LF'37'LF'S6'X';
251        LOOP:"READ"BETA;
252            "IF"BETA>1.0"THEN""GOTO"FIN;
253            "IF"ABS(BETA-2)<10*(-7)
254            "THEN"EPS:=1+1/(2*PI*KF)
255           "ELSE"EPS:=1+(2/(PI*KF*BETA*2))*(((1-(BETA/2)*2)/BETA)*
256                        LN(ABS((1+BETA/2)/(1-BETA/2)))+1);
257            "IF"BETA"LE"2"THEN"FNE:=FKF(BETA)
258            "ELSE"FNE:=F(0,-1,BETA);
259            KFT:=2*PI*Z/(V0*KF*2);
260            KI:=2*PI/((BETA*KF)*2+KF*2+KFT);
261            EPSS:=(EPS-1)*(1+(BETA*KF)*2*KI/(4*PI))+1;
262            ZSTAR:=Z*(1+(BETA*KF)*2*KI/(4*PI)))*RHO;
263            JC:=4*PI*ZSTAR/(V0*(KF*BETA)*2*EPSS)  -(4*PI/V0)*FW
264                *(1+(BETA*KF)*2*KI/(4*PI*EPSS)))*(3C/(V0*(BETA*KF)*2))*G(BETA)
265                /EPSS;
266            "PRINT"/'L'',SAMELINE,FREEPOINT(5),BETA,'    ',J0,'    ',FW,
267                   '    ',J0*4*PI*FW/V0,'    ',BETA/2;
268            "GOTO"LOOP;
269   FIN:"PRINT"/'L'',FREEPOINT(4),AC,A1,A2,DA0,DA1,DA2,R2,KF,V0,PI,Z;
270    "END";
  786      NS
 3350   CODE
 4130 TOTAL


&END;
```

Appendix B

Contact Density Program

Outline of Program

There are eight procedures used in the main program which are described first.

Procedure NF

This evaluates the function F, the non-local contribution to the form factors, which is defined by equation 4.115. A ten point Simpson's rule integration is performed in the sections labelled CASE0, CASE1 AND CASE2, for metals with ℓ_o = 0, 1 or 2 respectively. When the ℓ = 2 component of the potential is not optimised as discussed in Chapter 6 the modified integral is evaluated in the section labelled CASE3. The expression is finally multiplied by $3Z^*/k_F^2$ to make it dimensionless in the sense of equation 4.61 and stored in the array FLA to avoid calculation of the same function twice.

Procedure CO

The angular integral C_o defined by equation 4.85 is evaluated in this procedure. Here we are faced with a principal part integral of the type

$$I = P \int_{-1}^{+1} \frac{dy\ A(y)}{\alpha y - 1} \qquad \text{(B1)}$$

where A does not have an analytic form, but is a sufficiently slowly varying function of y to be represented by a linear interpolation between calculated points. We can thus write

$$A(y) = a_n y + b_n,\ Y_n < y < Y_{n+1} \qquad \text{(B2)}$$

where the value of A is found at the points Y_n and the values of a_n

and b_n chosen so A(y) goes through these points. The integral then reduces to a sum of integrals, each of which can be performed analytically.

$$I = \sum_n P \int_{Y_n}^{Y_{n+1}} \frac{a_n y + b_n}{\alpha y - 1} \, dy \tag{B3}$$

$$= \sum_n \left(\frac{a_n}{\alpha^2} \left(Y_{n+1} - Y_n \right) + \left(\frac{a_n}{\alpha^2} + \frac{b_n}{\alpha} \right) \ell n \left| \frac{\alpha Y_{n+1} - 1}{\alpha Y_n - 1} \right| \right). \tag{B4}$$

The procedure scans through the calculated values of $B(\underline{k}')$, $(\underline{k}' = \underline{k} + \underline{q})$ to find those involved in the integral and evaluates the expression B4 with $B(\underline{k}') \equiv A(y)$. This expression becomes infinite if any Y_n lies on the point of the singularity. If this is the case Y_n is replaced by $0.9\ Y_n + 0.1\ Y_{n+1} = Y_n^1$ and an appropriate value of A calculated according to

$$A(y') = 0.9\ A(Y_n) + 0.1\ A(Y_{n+1}) \tag{B5}$$

Procedure GO

Is used to evaluate G_o, the second of the non-local angular integrals defined in section 4.3.4. The contribution V_A^{NL} can be written as a function of k' and q, and is evaluated, using the current value of q, for each k' at which there exists a calculated value of $B(k')$. This is sufficiently frequent to allow the linear interpolation approximation described in the last section to be used, and the procedure thus follows the method of procedure CO.

Procedure DO

This evaluates D_o, the other non-local angular integral. It uses the same values of $V_A^{NL}(q,k')$ as GO which are stored in the array FLA.

Procedure S

This calculates the structure factor by evaluating the final expression of section 4.3.7. using the current value of q.

Procedure W

Local contributions to the matrix elements are evaluated for only a limited number of values of q and this procedure interpolates the values for intermediate q. A 3 point Newtonian interpolation technique is used (1). The procedure requires at least 6 calculated values and it also terminates the q integration of the main program when q equals the highest value for which a calculated value of $V^L(q)$ exists.

Procedure BINT

This procedure evaluates the integrand, $P_{n\ell}(r).4\pi r.j_\ell(kr)$, used in determing $B(k)$. In order to avoid divergence of the j_ℓs for small arguments, if $kr < 0.01$ it is set equal to 0.01.

Procedure BLL

This uses the integrand formed in procedure BINT to evaluate the integrals $B_{n\ell}(k)$. The radial wave functions $P_{n\ell}(r)$, as given by Mann (2), are tabulated in sets of 10 with the interval in r doubling between each set and so a Simpson's rule integration is carried out for each set separately.

Main Program

This starts on line 361 (See program list), after the procedure declarations. The program firstly reads in the data relevant to the two pure elements making up the alloys to be considered. This includes the radial wavefunction (which enable the overlap integrals to be calculated

for 150 values of k up to 13 a.u. and stored in the array BLK, lines 387-390), the atomic volumes, Fermi wave vectors and model potential parameters. In line 441 the program enters the concentration loop and all subsequent instruction refer to an alloy whose concentration is defined here. The mean atomic and electronic volumes, Fermi wave vector, and model potential parameters of the alloy are calculated in lines 443-463. Next, the local contributions to the form factors are read in and arrays of differences set up in lines 464-470 for use in the interpolation procedure.

There is now sufficient information to calculate the contact density and lines 512-526 do this calculation for a single O.P.W. The correction terms each require an integration over $x(= q/2k_F)$ which has a singularity at x=1, so an integration mesh is set up in lines 531-538. Here values of x are divided into groups within which there is an equal spacing between the x's. The spacing varies between groups so as to be finest near the singularity. Simpson's rule is applied to the integration within each group. In lines 545-566 the integrand of each correction term is calculated and the integral for each group calculated in lines 566-591. A running total is kept in the terms PST, PDT, PNLST, and PNLDT, of each of these results.

When the value of x is greater than the maximum value for which there is a calculated value of $V^L(q)$, the program goes to the label CONTINUE on line 594 where the current values of the correction terms are used to evaluate the contact density for alloys of each required concentration.

Key to Identifiers

In algol an identifier may be used simultaneously to represent a parameter within a procedure, and a quite different parameter in the main program. A complete list of the identifiers used in the main program is given below, and a list of those used in each procedure is given only for those identifiers that refer to a different parameter.

Main Program

R - r (atomic units) distance from nucleus.

RZERO - starting value of Simpson's rule integration in Procedure BLL before conversion to a.u.

BL - Value of overlap integral

F - Simpsons rule interval

B1,B2,B3,B4 -

- Intermediate sums in Simpson's rule integration

HCON - Simpson's rule interval in Procedure BLL

RZEROCON - Staring value in above

KF - k_F (Fermi wave number)

X - $q/2k_F$

K2 - k_F^2

Q - q

PNLS, PNLD, PS, PD - Final sums in Simpson's rule integration of Σ_{NL}, Δ_{NL}, Σ_L and Δ_L

PNLST, PNLDT, PST, PDT - Running totals of above

KFA - k_F for pure element A

KFB - k_F for pure element B

RG1, RG2, RD1, RD2 — Running totals of contributions to Λ

LA - Λ_A

LB - Λ_B

NL1 - Integrand of Σ_{NL}

NL2 and NL3 - Contributions to integrand of Δ_{NL}

GS - Integrand of Σ_L

GD - Integrand of Δ_L

PI - π

GAMMA - $\gamma(k_F)$

TERMA, TERMB — Contributions to the normalisation

H3 - Simpson's rule interval in q integration divided by 3.

SIG - Hard sphere diameter

STR - Structure factor as a function of current q.

OMEGAA - Atomic volume of pure element A

OMEGAB - Atomic volume of pure element B

NOA - $(k_F^2 - k_F^{A2})/2$

NOB - $(k_F^2 - k_F^{B2})/2$

FL - $\ell n \left| \frac{1 - q/2k_F}{1 + q/2k_F} \right|$

XFL - X x FL

CAPGAM - Γ

RB, RC — intermediate sums in evaluating Γ

VA, VB — Local contribution to form factors

VAL - Average valency of alloy

N - Principal quantum number of core states

L - Angular momentum quantum number of core states

RAD - Abscissa integer for core states

M - Integer used in integration over A

KINT - k value integer

RADZERO - integer labeling value of RZEROCON

I -
C - integers used in BLL

A -
B - integers used in CO

E - integer labelling element (A = 0, B = 1)

NJI -
T - used in q integration

K - labels concentration of alloy

TEMP - labels temperature

BLA(E,L,N,KINT) - Array of Overlap integrals

I(L) - Array of Bessel functions

P(E,L,N,RAD) - Array holding radial wave functions

AO(E)
A1(E)
A2(E) } Model potential parameter for pure elements

AAO(E)
AA1(E)
AA2(E)
ADAO(E)
ADA1(E)
ADA2(E)
AR2(E) } Model potential parameter for elements in alloys

FLA(KINT,E) - Array of non-local contributions to form factors

CA(K) - concentration of element A

CB(K) - concentration of element B

OMEGAE(K) - electronic volume

BETA(K) - $N(k_F)$

OPW(K) - $\gamma(k_F)^2/N(k_F)$

H(T) - Simpson's rule interval q-intergration

AJ(T) - Starting value for Simpson's rule q-intergration

NJ(T) - Number of intervals in Simpson's rule q-intergration

PT(K) - $1 + \Sigma + \Delta$

OMEGAI(K) - Average ionic volume in alloy

XS(N) - $R_{no}(0)$ for s-core functions

BLK(N) - BLL for $k = k_F$

CON(E) - Conversion factor for core wave function

NMAX(E) - Maximum n value for core function

LMAX(E,N) - maximum ℓ value for core function

NRAD(E,L,N) - number of wave function ordinates for given core states

NWF(E) - number of core states

QT(E) - Number of values given for local contribution to form factor

LO(E) - ℓ_o

Z(E) - valency of elements

TITLE(E) - names of elements in alloy

Procedure NF

K - k_F

K1 - k

KKF - $k^2 - k_F^2$

RO -
R1 - } Model potential well radii
R2 -

PU - u

PZ - z

PETA - η

CS - Cos θ

AO -
A1 -
A2 -
DAO - } model potential parameters
DA1 -
DA2 -
R2 -

Other identifiers, KRO, KR1, KR2, KIRO, KIR1, KIR2, ARG1, ARG, FLA, I, F,

PT(K) - $1 + \Sigma + \Delta$

OMEGAI(K) - Average ionic volume in alloy

XS(N) - $R_{no}(O)$ for s-core functions

BLK(N) - BLL for $k = k_F$

CON(E) - Conversion factor for core wave function

NMAX(E) - Maximum n value for core function

LMAX(E,N) - maximum ℓ value for core function

NRAD(E,L,N) - number of wave function ordinates for given core states

NWF(E) - number of core states

QT(E) - Number of values given for local contribution to form factor

LO(E) - ℓ_o

Z(E) - valency of elements

TITLE(E) - names of elements in alloy

Procedure NF

K - k_F

K1 - k

KKF - $k^2 - k_F^2$

RO -
R1 - } Model potential well radii
R2 -

PU - u

PZ - z

PETA - η

CS - Cos θ

AO -
A1 -
A2 -
DAO - } model potential parameters
DA1 -
DA2 -
R2 -

Other identifiers, KRO, KR1, KR2, KIRO, KIR1, KIR2, ARG1, ARG, FLA, I, F,

are used as intermediate terms in the evaluation of this integral.

Procedures CO, DO and GO

W - $2k_F/q$

NO - k_F^2/q^2

I - running total integral

B1 - Slope of $B(k')$

KINTO
KINTP - Values of KINT on either side of range of integration

P - Number of calculated points in range of integration plus one

X(M) - k' at points where $B(k')$ is calculated

B(M) - $B(k')$ in procedure CO

- $V_{NL}^A(k',q)$ in procedure DO

- $B(k') \times V_{NL}^A(k,q)$ in procedure GO.

```
** ICL 4130 DES2 SYSTEM  :  SLAVE BIG        :  CORE 70K  :  VOL  2

$JOB;PH/R060/GT;

$LINES;7000;

$ASSIGN;5;DC;10;PERDEWAN,PH/R060/;

$DELETE;5;
DELETE

$ALGOL;L;
LIBRARY
ALGOL

    1   "PERDEW AND WILKINS CALCULATION OF KNIGHT SHIFTS IN LIQUID ALLOYS;
    2   "BEGIN""REAL"  R,RZERO,BL,F,B1,B2,B3,B4,HCON,RZEROCON,          X,
    3                KF,K2,U,   PHLS,PNLD,PNLST,PNLDT,                KFA,KFB,
    4   RG1,RG2,RGS1,RGS2,RD1,RD2,LA,LB,              NL1,NL2,NL3,
    5   OMEGAA,OMEGAB,    FUA,NOB,                    PI,    GAMMA,TERMA,TERMB,
    6   RS,PD,M3,SIG,STR,FL,XFL,CAPGAM,KB,RC,VA,VB,GS,GD,PST,PDT,DENS,PF,
    7       VAL;
    8   "COMMENT"CALCULATES PF IN LIQUID ALLOYS AT SPECIFIC CONCENTRATIONS;USES
    9   ASHCROFT AND LEKNER STRUCTURE FACTORS,      NON LOCAL PSEUDOPOTENTIAL
   10    AND HERMAN AND SKILLMAN CORE WAVE FUNCTIONS;
   11          "REAL""ARRAY"FLA[1:2,0:3,1:5,0:130],JC[0:4],P[1:2,0:3,1:5,0:110],
   12                AU,A1,A2[1:2],
   13               AAU,AA1,AA2,ADA0,ADA1,ADA2,AR2,NFSING[1:2],FLA[0:154,1:2],
   14                CA,CB,OMEGAB,BETA,OPH,H,AJ,NJ,PT,OMEGAI[1:111],XS,BLK[1:6],
   15               CON[1:2],XT,FT,F1,F2,F3[1:60,1:2],XMAX[1:2];
   16          "INTEGER"N,L,RAD,M,KINT,RADZERO,I,C,A,B,E,NJ1,T,D,G,U,K,TEMP;
   17          "INTEGER""ARRAY"NMAX[1:2],LMAX[1:2,1:5],NRAD[1:2,0:3,1:5],
   18                NWF,QT[1:2],TITLE[1:21],LO,Z[1:2];

ITEM INSERTED
   19          "LIBRARY"TIMEA;
   31          "COMMENT"   PROCEDURES NF    DO    GO   EVALUATE THE ANGULAR
   32                INTEGRALS  REQUIRED FOR NON LOCAL CALCULATIONS;
   33          "REAL""PROCEDURE"NF(PU,PZ,PETA,E);   "VALUE"PU,PZ,PETA,E;
   34          "REAL"PU,PZ,PETA;   "INTEGER"E;
   35          "BEGIN""REAL"K,K1,KKF,R0,KR0,K1P0,CS,R1,KR1,K1P1,KR2,K1P2,R2,ARG,
   36                ARG1,I,F,AL2, AD,A1,A2,DA1,DA2,DA0;
   37                "INTEGER"N,M;      "REAL""ARRAY"FLC[2,0:10];
   38                "IF"LO[E]=1"THEN""GO"TO"CASE1;
   39                "IF"LO[E]=2"THEN""GO"TO"CASE2;
   40                "IF"LO[E]=3"THEN""GO"TO"CASE3;
   41           CASE0;A0:=AA0[E];     DA0:=ADA0[E];
   42                K1:=F*SQRT(PU*PZ*2);    KKF:=K*2*KF*2;
   43                K1:=KF*SQRT(PU*(PZ*PETA)*2);
```

```
44              R0I=Z[E]/(AJ*KKF*DA0/2); KR0I=K*R0;
45              K1R0I=K1*R0;
46              "FOR"NI=1"STEP"1"UNTIL"9"DO"
47              "BEGIN"FL[0,NJ]I=2*((N-10)/N)*SIN(KR0*N/10)
48                                  *SIN(K1R0*N/10);
49              "END";
50              "COMMENT"FOR N=0 OR 10   FL[X,N]=0;
51              II=0;
52              "FOR"MI=1"STEP"1"UNTIL"2"DO"
53              "FOR"NI=1"STEP"M"UNTIL"9"DO"
54                 II=I+(ZEE]/(K*K1))*FL[0,N];
55              FI=I/30;
56                    "GOTO"ENDCASE;
57      CASE1[AU]=AA0[E]; DAU]=ADA0[E];
58              A1]=AA1[E]; DA1]=ADA1[E];
59              K]=KF;
60              K1]=KF*SQRT(PU+(PZ*PETA)*2);
61              R0]=Z[E]/A0]  KR0]=K*R0;
62              K1R0]=K1*R0;
63              CS]=(PU+PZ*(PZ+PETA))*KF/K1;
64              R1]=Z[E]/A1;
65              KR1]=K*R1];  K1R1]=K1*R1;
66              "FOR"NI=1"STEP"1"UNTIL"9"DO"
67              "BEGIN"FL[0,NJ]I=2*((N-10)/N)*SIN(KR0*N/10)
68                                  *SIN(K1R0*N/10);
69                     ARG]=KR1*N/10;  ARG1]=K1R1*N/10;
70                     FL[1,NJ]I=2*((N-10)/N)*(SIN(ARG)/ARG-COS(ARG))
71                                  *(SIN(ARG1)/ARG1-COS(ARG1));
72              "END";
73              "COMMENT"FOR N=0 OR 10   FL[X,N]=0;
74              II=0;
75              "FOR"MI=1"STEP"1"UNTIL"2"DO"
76              "FOR"NI=1"STEP"M"UNTIL"9"DO"
77                 II=I+(ZEE]/(K*K1))*(FL[0,N]+3*CS*FL[1,N]);
78              FI=I/30;
79                    "GOTO"ENDCASE;
80      CASE2[AU]=AA0[E];      DA0]=ADA0[E];
81              A1]=AA1[E];      DA1]=ADA1[E];
82              A2]=AA2[E];      DA2]=ADA2[E];
83              K]=KF;
84              K1]=KF*SQRT(PU+(PZ+PETA)*2);
85              R0]=Z[E]/A0]  KR0]=K*R0;
86              K1R0]=K1*R0;
87              CS]=(PU+PZ*(PZ+PETA))*KF/K1;
88              R1]=Z[E]/A1]  R2]=Z[E]/A2;
89              KR1]=K*R1];  K1R1]=K1*R1;
90              KR2]=K*R2];  K1R2]=K1*R2;
91              "FOR"NI=1"STEP"1"UNTIL"9"DO"
92              "BEGIN"FL[0,NJ]I=2*((N-10)/N)*SIN(KR0*N/10)
93                                  *SIN(K1R0*N/10);
94                     ARG]=KR1*N/10;  ARG1]=K1R1*N/10;
95                     FL[1,NJ]I=2*((N-10)/N)*(SIN(ARG)/ARG-COS(ARG))
96                                  *(SIN(ARG1)/ARG1-COS(ARG1));
97                     ARG]=KR2*N/10;  ARG1]=K1R2*N/10;
98                     FL[2,NJ]I=2*((N-10)/N)        *((3/ARG*2-1)
99                                  *SIN(ARG)-3*COS(ARG)/ARG)*((3/ARG1*2-1)
100                                 *SIN(ARG1)-3*COS(ARG1)/ARG1);
101             "END";
102             "COMMENT"FOR N=0 OR 10   FL[X,N]=0;
103             II=0;
```

```
104                "FOR"M1:=1"STEP"1"UNTIL"2"DO"
105                "FOR"N1:=1"STEP"M"UNTIL"9"DO"
106                   I1:=I+(ZCE]/(K*K1))*(FL[0,N]+3*CS*FL[1,N]
107                      +2,5*(3*CS*2-1)*FL[2,N]);
108                F:=I/30;
109                   "GOTO"ENDCASE;
110             CASE3:A01:=AA0[E];       DA0:=ADA0[E];
111                A1:=AA1[E];       DA1:=ADA1[E];
112                A2:=AA2[E];        DA2:=ADA2[E];    R2:=AR2[E];
113                K:=KF;
114                K1:=KF*SQRT(PU*(PZ*PETA)*2);
115                PU:=Z[E]/A0;   KR0:=K*R0;
116                K1R0:=K1*R0;
117                CS:=KF*(PU+PZ*(PZ*PETA))/K1;
118                P1:=Z[E]/A1;
119                KR1:=K*R1;   K1R1:=K1*P1;
120                KR2:=K*R2;   K1R2:=K1*R2;
121                AL2:=A2+KKF*DA2/2;
122                "FOR"N1:=1"STEP"1"UNTIL"9"DO"
123                "BEGIN"FL[0,N]:=2*((N-10)/N)*SIN(KR0*N/10)
124                                *SIN(K1R0*N/10);
125                      ARG:=KR1*N/10;   ARG1:=K1R1*N/10;
126                      FL[1,N]:=2*((N-10)/N)*(SIN(ARG)/ARG-COS(ARG))
127                                *(SIN(ARG1)/ARG1-COS(ARG1));
128                      ARG:=KR2*N/10;  ARG1:=K1R2*N/10;
129                      FL[2,N]:=2*(1-10*Z[E]/(AL2*R2*N))*((3/ARG*2-1)
130                                *SIN(ARG)-3*COS(ARG)/ARG)*((3/ARG1*2-1)
131                                *SIN(ARG1)-3*COS(ARG1)/ARG1);
132                "END";
133                "COMMENT"FOR N=0 OR 10   FL[X,N]=0EXCEPT FL[2,10]
134                      DUE TO NON OPTIMISATION OF POTENTIAL;
135                FL[2,10]:=(1-Z[E]/(AL2*R2))*((3/KR2*2-1)*SIN(KR2)
136                   -3*COS(KR2)/KR2)*((3/K1R2*2-1)*SIN(K1R2)
137                    -3*COS(K1R2)/K1R2);
138                I1:=0;
139                "FOR"M1:=1"STEP"1"UNTIL"2"DO"
140                "FOR"N1:=1"STEP"M"UNTIL"9"DO"
141                   I1:=I+(Z[E]/(K*K1))*(FL[0,N]+3*CS*FL[1,N]
142                      +2,5*(3*CS*2-1)*FL[2,N]);
143                   I1:=I+(Z[E]/(K*K1))*2,5*(3*CS*2-1)*FL[2,10];
144                F:=I/30;
145             ENDCASE:
146                NF:=          -3*VAL *F/(KF*KF);
147                FLACKINT,E]:=-3*VAL *F/(KF*KF);
148             "END"OF PROCEDURE  NF;
149             "REAL""PROCEDURE"G0(N);   "VALUE"N;   "INTEGER"N;
150             "BEGIN""REAL"U,NO,I,B1;
151                "INTEGER"KINT0,KINTP,P,M;
152                "REAL""ARRAY"B,X[0:130];
153                KINT0:=ENTIER(10*(KF-0))+1;
154                KINTP:=ENTIER(10*ABS(KF-0));
155                P:=KINT0-KINTP+1;
156                U:=2*KF/0; NO:=(KF/0)*(KF/0);
157                "FOR"N1:=0"STEP"1"UNTIL"P+1"DO"
158                "BEGIN"KINT:=KINT0-N;
159                      X[N]:=NO-(KINT/10)*(KINT/10)/(0*0);
160                      "IF"ABS(X[N])<0,00001"THEN"
161                            "BEGIN"B[N]:=0,9*BLA[1,0,N,KINT]*
162                                        0,1*BLA[1,0,N,KINT+1];
163                                  X[N]:=0,1*(NO-((KINT+1)/10)
```

```
                                  *((KINT+1)/10)/(Q*Q));
                         "END"
                         "ELSE"B[M]:=BLA[1,0,N,KINT];
         "END";
         I:=0;
         "IF"P>1"THEN"
         "BEGIN""FOR"M:=1"STEP"1"UNTIL"P-1"DO"
               "BEGIN"B1:=(B[M+1]-B[M])/(X[M+1]-X[M]);
                     I:=I+B1*(X[M+1]-X[M])+(B[M]-B1*X[M])
                         *LN(ABS(X[M+1]/X[M]));
               "END";
         "END";
         "IF"P>0"THEN"
         "BEGIN"B1:=(B[1]-B[0])/(X[1]-X[0]);
               I:=I+B1*(X[1]-1+W)+(B[0]-B1*X[0])
                   *LN(ABS(X[1]/(1+W)));
               B1:=(B[P+1]-B[P])/(X[P+1]-X[P]);
               I:=I+B1*(W-1-X[P])+(B[P]-B1*X[P])
                  *LN(ABS((W-1)/X[P]));
         "END"
         "ELSE"
         "BEGIN"B1:=(B[1]-B[0])/(X[1]-X[0]);
               I:=B1*2*W+(B[0]-B1*X[0])*LN(ABS((W-1)/(W+1)));
         "END";
         CO:=I*C/(2*KF);
"END" OF PROCEDURE CO;
"REAL""PROCEDURE"GO(N,E);   "VALUE"N,E;  "INTEGER"N,E;
"BEGIN""REAL"Y,W,NO,I,B1;
      "INTEGER"KINTO,KINTP,P,M;
      "REAL""ARRAY"B,X[0:130];
      KINTO:=ENTIER(10*(KF+Q))+1;
      KINTP:=ENTIER(10*ABS(KF-Q));
      P:=KINTO-KINTP-1;
      W:=2*KF/Q;    NO:=KF*KF/(Q*Q);
      "FOR"M:=0"STEP"1"UNTIL"P+1"DO"
      "BEGIN"KINT:=KINTO-M;
            "IF"KINT=0"THEN"X[M]:=NO-,0001/(Q*Q)
            "ELSE"
            X[M]:=NO-(KINT*KINT/(100*Q*Q));
      "IF"ABS(X[M])<,00001"THEN"
            "BEGIN"X[M]:=,1*(NO-(KINT+1)*(KINT+1)/(100*Q*Q));
                  B[M]:=(,9*BLA[1,0,N,KINT]+
                        ,1*BLA[1,0,N,KINT+1])*FLA[KINT,E]
                        *4*PI/OMEGAI[K];
            "END"
            "ELSE"     B[M]:=BLA[1,0,N,KINT]*FLA[KINT,E]
                         *4*PI/OMEGAI[K];
      "END";
      I:=0;
      "IF"P>1"THEN"
      "BEGIN""FOR"M:=1"STEP"1"UNTIL"P-1"DO"
            "BEGIN"B1:=(B[M+1]-B[M])/(X[M+1]-X[M]);
                  I:=I+B1*(X[M+1]-X[M])+(B[M]-B1*X[M])
                      *LN(ABS(X[M+1]/X[M]));
            "END";
      "END";
      "IF"P>0"THEN"
      "BEGIN"B1:=(B[1]-B[0])/(X[1]-X[0]);
            I:=I+B1*(X[1]-1+W)+(B[0]-B1*X[0])
```

```
224                         *LN(ABS(X[1]/(1+W)))
225                     B1:=(B[P+1]-B[P])/(X[P+1]-X[P]);
226                     I:=I+B1*(W-1-X[P])+(B[P]-B1*X[P])
227                        *LN(ABS((W-1)/X[P]))
228             "END"
229             "ELSE"
230             "BEGIN"B1:=(B[1]-B[0])/(X[1]-X[0]);
231                     I:=B1*2*W+(B[0]-B1*X[0])*LN(ABS((W-1)/(W+1)))
232             "END";
233             DO1:=I*C/(2*KF);
234         "END" OF PROCEDURE DO1;
235         "REAL""PROCEDURE"DO(E);     "VALUE"E;    "INTEGER"E;
236         "BEGIN""REAL"Y,W,NO,I,B1;
237             "INTEGER"KINTO,KINTP,P,M;
238             "REAL""ARRAY"B,X[0:130];
239             KINTO:=ENTIER(10*(KF+Q))+1;
240             KINTP:=ENTIER(10*ABS(KF-Q));
241             P:=KINTO-KINTP+1;
242             M:=2*KF/Q;    NO:=KF*KF/(Q*Q);
243             "FOR"M:=0"STEP"1"UNTIL"P+1"DO"
244             "BEGIN"KINT:=KINTO-M;
245                     "IF"KINT=0"THEN"X[M]:=NO-.0001/(Q*Q)
246                     "ELSE"
247                     X[M]:=NO-(KINT*KINT/(100*Q*Q));
248                     "IF"ABS(X[M])<.00001"THEN"
249                        X[M]:=.1*(NO-((KINT+1)*(KINT+1)/(100*Q*Q)));
250                     Y:=(X[M]+1)/W;
251                     B[M]:=NF(1-Y*Y,Y*(-1),Q/KF,E)*4*PI/OMEGA[K];
252             "END";
253             I:=0;
254             "IF"M>1"THEN"
255             "BEGIN""FOR"M:=1"STEP"1"UNTIL"P-1"DO"
256                     "BEGIN"B1:=(B[M+1]-B[M])/(X[M+1]-X[M]);
257                        I:=I+B1*(X[M+1]-X[M])+(B[M]-B1*X[M])
258                           *LN(ABS(X[M+1]/X[M]));
259                     "END";
260             "END";
261             "IF"W>0"THEN"
262             "BEGIN"B1:=(B[1]-B[0])/(X[1]-X[0]);
263                     I:=I+B1*(X[1]+1+W)+(B[0]-B1*X[0])
264                        *LN(ABS(X[1]/(1+W)));
265                     B1:=(B[P+1]-B[P])/(X[P+1]-X[P]);
266                     I:=I+B1*(W-1-X[P])+(B[P]-B1*X[P])
267                        *LN(ABS((W-1)/X[P]));
268             "END"
269             "ELSE"
270             "BEGIN"B1:=(B[1]-B[0])/(X[1]-X[0]);
271                     I:=B1*2*W+(B[0]-B1*X[0])*LN(ABS((W-1)/(W+1)));
272             "END";
273             DO1:=I*C/(2*KF);
274         "END" OF PROCEDURE DO1;
275         "COMMENT"PROCEDURE S CALCULATES STRUCTURE FACTOR USING CURRENT
276         ALLOY VALUES OF KF AND SIGMA,THE PACKING FRACTION ETA IS 0,45
277         THROUGHOUT;
278         "REAL""PROCEDURE"S(Z,ETA);
279         "REAL"Z,ETA;
280         "BEGIN""REAL"ZZ,ZZZ,R1,R2,R3,R4,R5,T1,T2,T3;
281             "IF"Z<0,5"THEN"S:=0,025"ELSE"
282             "BEGIN"
283             ZZ:=Z*Z;
```

```
                        *LN(ABS(X[1]/(1+W)));
                    B1:=(B[P+1]-B[P])/(Y[P+1]-X[P]);
                    I:=I+B1*(W-1-X[P])+(B[P]-B1*X[P])
                        *LN(ABS((W-1)/X[P]));
            "END"
            "ELSE"
            "BEGIN"B1:=(B[1]-B[0])/(X[1]-X[0]);
                    I:=B1*2.4+(B[0]-B1*X[0])*LN(ABS((W-1)/(W+1)));
            "END";
            DO1:=I*C/(2*KF);
"END" OF PROCEDURE GO1;
"REAL""PROCEDURE"DO(E);    "VALUE"E;    "INTEGER"E;
"BEGIN""REAL"Y,W,NO,I,B1;
        "INTEGER"KINTO,KINTP,P,M;
        "REAL""ARRAY"B,X[0:130];
        KINTO:=ENTIER(150*(KF+Q))+1;
        KINTM:=ENTIER(10*ABS(KF-Q));
        P:=KINTO-KINTP+1;
        W:=2*KF/Q;    NO:=KF*KF/(Q*Q);
        "FOR"M:=0"STEP"1"UNTIL"P+1"DO"
        "BEGIN"KINT:=KINTO-M;
                "IF"KINT=0"THEN"X[M]:=NO-.0001/(Q*Q)
                "ELSE"
                X[M]:=NO-(KINT*KINT/(100.0*Q));
                "IF"ABS(X[M])<.00001"THEN"
                    X[M]:=.1*(NO-((KINT+1)*(KINT+1)/(100.0*Q)));
                Y:=(X[M]+1)/W;
                B[M]:=NF(1-Y*Y,Y*(-1),Q/KF,E)*4*PI/OMEGA[K];
        "END";
        I:=0;
        "IF"P>1"THEN"
        "BEGIN""FOR"M:=1"STEP"1"UNTIL"P-1"DO"
                "BEGIN"B1:=(B[M+1]-B[M])/(X[M+1]-X[M]);
                    I:=I+B1*(X[M+1]-X[M])+(B[M]-B1*X[M])
                        *LN(ABS(X[M+1]/X[M]));
                "END";
        "END";
        "IF"M>0"THEN"
        "BEGIN"B1:=(B[1]-B[0])/(X[1]-X[0]);
            I:=I+B1*(X[1]+1+W)*(B[0]-B1*X[0])
                *LN(ABS(X[1]/(1+W)));
            B1:=(B[M+1]-B[P])/(Y[P+1]-X[P]);
            I:=I+B1*(W-1-X[P])+(B[P]-B1*X[P])
                *LN(ABS((W-1)/X[P]));
        "END"
        "ELSE"
        "BEGIN"B1:=(B[1]-B[0])/(X[1]-X[0]);
                I:=B1*2.4+(B[0]-B1*X[0])*LN(ABS((W-1)/(W+1)));
        "END";
        DO1:=I*C/(2*KF);
"END" OF PROCEDURE DO;
"COMMENT"PROCEDURE S CALCULATES STRUCTURE FACTOR USING CURRENT
ALLOY VALUES OF KF AND SIGMA,THE PACKING FRACTION ETA IS 0.45
THROUGHOUT;
"REAL""PROCEDURE"S(Z,ETA);
"REAL"Z,ETA;
"BEGIN""REAL"ZZ,ZZZ,R1,R2,R3,R4,RR,T1,T2,T3;
        "IF"Z<0.5"THEN"S:=0.025"ELSE"
        "BEGIN"
        ZZ:=Z*Z;
```

```
284             ZZZ:=Z*Z*Z;
285         T1:=(1+2*ETA)+2/(1-ETA)*4;
286         T2:=6*ETA*(1+ETA/2)+2/(1-ETA)+4;
287         T3:=1/2*ETA*(1+2*ETA)*2/(1-ETA)*4;
288         R1:=T1+2*T2+4*T3-24*T3/ZZ;
289         R2:=-(T1+T2+T3)*Z+(2*T2+12*T3)/Z-24*T3/ZZZ;
290         R3:=-2*T2/Z+24*T3/ZZZ;
291         R4:=24*ETA/ZZZ;
292             R5:=R4*(R1*SIN(Z)+R2*COS(Z)+R3);
293             S:=1/(1+R5);
294             "END";
295         "END"OF PROCEDURE S;
296 "COMMENT" INTERPOLATION OF NUMERICAL FORM FACTORS;
297         "REAL""PROCEDURE"W(Y,P);
298         "REAL"Y;     "INTEGER"P;
299         "BEGIN""REAL"FY;    "INTEGER" N,M;
300             "IF"Y>XMAX[P]"THEN""GOTO"CONTINUE;
301             "FOR"N:=1"STEP"1"UNTIL"QT[P]"DO"
302                "IF"Y=XT[N,P]"THEN""BEGIN"FY:=FT[N,P];
303                                        "GOTO"AN;
304                                    "END";
305             "FOR"N:=2"STEP"1"UNTIL"QT[P]-3"DO"
306                "IF"Y<XT[N+1,P]"THEN""BEGIN"M:=N;
307                                        "GOTO"CALC;
308                                    "END";
309             N:=QT[P]-2;
310          CALC:FY:=FT[M-1,P]*(Y-XT[M-1,P])*(Y-XT[M,P])*F1[M-1,P]
311                 +(Y-XT[M-1,P])*(Y-XT[M,P])*F2[M-1,P]
312                 +(Y-XT[M-1,P])*(Y-XT[M,P])*(Y-XT[M+1,P])*F3[M-1,P];
313          AN:W:=FY;
314         "END" OF PROCEDURE W;
315         "REAL""PROCEDURE"BINT(N,L,RAD,E);
316         "INTEGER"N,L,RAD,E;
317         "BEGIN""REAL"XKR;
318             XKR:=KF*R;
319             "IF"XKR<0,01"THEN"XKR:=0,01;
320             JC0]:=SIN(XKR)/XKR;
321             "IF"L>0"THEN"JC1]:=JC0]/XKR-COS(XKR)/XKR;
322             "IF"L>1"THEN"JC2]:=3*JC1]/XKR-JC0];
323             "IF"L>2"THEN"JC3]:=5*JC2]/XKR-JC1];
324             "IF"L>3"THEN"JC4]:=7*JC3]/XKR-JC2];
325             BINT:=4*3,14159*R*POE(L,N,PAD]*JCL];
326         "END"OF PROCEDURE BINT;
327         "REAL""PROCEDURE"BLL(N,L,KF,E);
328         "REAL"KF;
329         "INTEGER"N,L,E;
330         "BEGIN"RZERO:=0,05;
331                                 BL:=0;
332                                 "FOR"C:=1"STEP"1"UNTIL"(NRADCE,L,N]-1)"DIV"
333                                     10"DO"
334                                 "BEGIN"F:=0,01*(2*C)/2;
335                                     B1:=B2:=0;
336                                     RADZERO:=10*(C-1);
337                                     RZERO:=RZERO+5*F;
338                                                 HCON:=F*CONCE];
339                                     RZEROCON:=RZERO*CONCE];
340                                     "FOR"I:=1"STEP"2"UNTIL"9"DO"
341                                     "BEGIN"RAD:=RADZERO+I;
342                                             R:=RZEROCON+HCON*I;
343                                             B1:=B1+BINT(N,L,RAD,E);
```

```
344                                     "END";
345                                     "FOR"I:=2"STEP"2"UNTIL"8"DO"
346                                     "BEGIN"RAD:=RADZERO+I;
347                                             R1:=RZEROCON+HCON*I;
348                                             B2:=B2+BINT(N,L,RAD,E))
349                                     "END";
350                                     RAD:=RADZERO;
351                                     R1:=RZEROCON;
352                                     B3:=BINT(N,L,RAD,E);
353                                     RAD:=RADZERO+10;
354                                     R1:=RZEROCON+10*HCON;
355                                     B4:=BINT(N,L,RAD,E);
356                                     BL:=BL+(HCON/3)*(B3+B4)+4*(HCON/3)*B1+
357                                             +2*(HCON/3)*B2;
358                             "END";
359                             BLL:=BL;
360             "END" OF PROCEDURE BLL;
361             DIGITS(2);
362             "FOR"E:=1"STEP"1"UNTIL"2"DO"
363             "BEGIN""READER((E+1)*10);
364                     NI:=1;INSTRING(TITLE,N);
365                     NI:=1;OUTSTRING(TITLE,N);
366                     "READ"CORE[,NUFCE],NMAXCE];
367                     "FOR"N:=1"STEP"1"UNTIL"NMAXCE]"DO""READ"LMAXCE,N];
368                     "FOR"NI:=1"STEP"1"UNTIL"NUFCE]"DO"
369                     "BEGIN""READ"N,L,NRADCE,L,N];  "PRINT"/'L'',N,L;
370                             "FOR"RAD:=0"STEP"1"UNTIL"NRADCE,L,N]=1"DO"
371                             "BEGIN"
372                                     "READ"PCE,L,N,RAD];
373                                     "PRINT"SAMELINE,FREEPOINT(4),'  ',
374                                             PCE,L,N,RAD];
375                             "END";
376                     "END";
377             READER(6);
378                     "FOR"NI:=1"STEP"1"UNTIL"NMAXCE]"DO"
379                     "BEGIN""FOR"KFI:=0"STEP"0.1"UNTIL"13.0"DO"
380                             "BEGIN"KINT:=ENTIER(10*(KF+0.0001));
381                                     BLACE,0,N,KINT]:=BLL(N,0,KF,E);
382                             "END";
383                     "END";
384             "END";
385             E:=1;
386     "BEGIN""PRINT"/'L'ELEMENT='',SAMELINE,E;
387             "FOR"NI:=1"STEP"1"UNTIL"NMAXCE]"DO"
388             "BEGIN""PRINT"/'L'N='',SAMELINE,N;
389     "FOR"KINT:=0"STEP"1"UNTIL"130"DO"
390                             "PRINT"PREFIX(/'S2''),SAMELINE,FREEPOINT(4),
391                             BLACE,0,N,KINT];
392             "END";
393     "END";
394             "FOR"NI:=1"STEP"1"UNTIL"NMAXC1]"DO""READ"XSCN];
395             "FOR"NI:=1"STEP"1"UNTIL"NMAXC1]"DO""PRINT"SAMELINE,FREEPOINT(5),
396                                                     /'L'XS = '',XSCN];
397     "PRINT"/'L'TIME TO CALC OVERLAP INTEGRALS ',    TIMEA;
398             "COMMENT"INPUT PARAMETERS FOR EACH ELEMENT ARE NOW READ IN;
399             READER(100);
400             "BEGIN"SAMELINE;FREEPOINT(4);
401             "READ"KFA,OMEGAA,ZC1],LOC1];
402             "PRINT"/'L'KFA = '',KFA,'  OMEGA ='',OMEGAA,' Z = '',ZC1],
403                     '  LO = '',LOC1];
```

```
404           "IF"L0[1]=1"THEN""GOTO"L11;
405           "IF"L0[1]=2"THEN""GOTO"L12;
406           "IF"L0[1]=3"THEN""GOTO"L13;
407           "PRINT"/'L'"MODEL POT PARAMETERS = ';
408        L10;"READ"A0[1],ADA0[1];
409           "PRINT"A0[1],ADA0[1];
410           "GOTO"ENDL1;
411        L11;"READ"A0[1],A1[1],ADA0[1],ADA1[1];
412           "PRINT"A0[1],A1[1],ADA0[1],ADA1[1];
413           "GOTO"ENDL1;
414        L12;"READ"A0[1],A1[1],A2[1],ADA0[1],ADA1[1],ADA2[1];
415           "PRINT"A0[1],A1[1],A2[1],ADA0[1],ADA1[1],ADA2[1];
416           "GOTO"ENDL1;
417        L13;"READ"A0[1],A1[1],A2[1],ADA0[1],ADA1[1],ADA2[1],AR2[1];
418           "PRINT"A0[1],A1[1],A2[1],ADA0[1],ADA1[1],ADA2[1],AR2[1];
419     ENDL1;
420           "READ"KFB,OMEGAB,Z[2],L0[2];
421           "PRINT"/'L'KFB = ',KFB,'  OMEGA = ',OMEGAB,'  Z = ',Z[2],
422                  '  L0 = ',L0[2];
423           "IF"L0[2]=1"THEN""GOTO"L21;
424           "IF"L0[2]=2"THEN""GOTO"L22;
425           "IF"L0[2]=3"THEN""GOTO"L23;
426           "PRINT"/'L'"MODEL POT PARAMETERS B =';
427        L20;"READ"A0[2],ADA0[2];
428           "PRINT"A0[2],ADA0[2];
429           "GOTO"ENDL2;
430        L21;"READ"A0[2],A1[2],ADA0[2],ADA1[2];
431           "PRINT"A0[2],A1[2],ADA0[2],ADA1[2];
432           "GOTO"ENDL2;
433        L22;"READ"A0[2],A1[2],A2[2],ADA0[2],ADA1[2],ADA2[2];
434           "PRINT"A0[2],A1[2],A2[2],ADA0[2],ADA1[2],ADA2[2];
435           "GOTO"ENDL2;
436        L23;"READ"A0[2],A1[2],A2[2],ADA0[2],ADA1[2],ADA2[2],AR2[2];
437           "PRINT"A0[2],A1[2],A2[2],ADA0[2],ADA1[2],ADA2[2],AR2[2];
438     ENDL2;
439           "END";
440           PI:=3.14159;
441           "COMMENT"THE NEXT INSTRUCTION MUST BE CHANGED TO CHANGE
442           COMPOSITIONS;
443           "FOR"K:=3"STEP"2"UNTIL"9"DO"
444           "BEGIN"CA[K]:=1-0.1*(K-1);
445                  CB[K]:=1-CA[K];
446                  OMEGAB[K]:=3*PI*PI*((CA[K]/KFA*3+CB[K]/KFB*3));
447                  OMEGAA[K]:=CA[K]*OMEGAA*CB[K]*OMEGAB;
448                  VAL:=(CA[K]*OMEGAA*KFA*3+CB[K]*OMEGAB*KFB*3)/(3*PI*PI);
449                  KF:=(3*PI*PI/OMEGAA[K])*(1/3);
450                  KINT:=ENTIER(10*(KF+0.0001));
451                  NOA:=(KF*KF-KFA*KFA)/2;
452                  NOB:=(KF*KF-KFB*KFB)/2;
453                  AA0[1]:=A0[1]*NOA*ADA0[1];
454                  "IF"L0[1]=0"THEN""GOTO"SKIPA;
455                  AA1[1]:=A1[1]*NOA*ADA1[1];
456                  "IF"L0[1]=1"THEN""GOTO"SKIPA;
457                  AA2[1]:=A2[1]*NOA*ADA2[1];
458           SKIPA;
459                  AA0[2]:=A0[2]*NOB*ADA0[2];
460                  "IF"L0[2]=0"THEN""GOTO"SKIPB;
461                  AA1[2]:=A1[2]*NOB*ADA1[2];
462                  "IF"L0[2]=1"THEN""GOTO"SKIPB;
463                  AA2[2]:=A2[2]*NOB*ADA2[2];
```

```
464             SKIPB;
465     "PRINT""'L'CA=',SAMELINE,FREEPOINT(4),CA[K],''S2'KF=',KF;
466           "COMMENT"  THE LOCAL PART OF THE PSEUDOPOTENTIAL IS NOW READ
467                    IN FOR EACH ELEMENT TOGETHER WITH THE MODEL POTENTIAL
468             PARAMETERS TO CALC THE NON LOCAL PART;
469           "FOR"U:=1"STEP"1"UNTIL"2"DO"
470           "BEGIN"
471           "READ"QT[U];
472           "IF"QT[U]<5"THEN""BEGIN""PRINT""'INSUFFICIENT DATA';
473                                    "GOTO"FIN;
474                        "END";
475           "IF"QT[U]>60"THEN""BEGIN""PRINT""'TOO MANY POINTS';
476                                    "GOTO"FIN;
477                        "END";
478                 "FOR"N:=1"STEP"1"UNTIL"QT[U]"DO"
479              "BEGIN""READ"XT[N,U],FT[N,U]; FT[N,U]:=FT[N,U]*3/(KF*KF);
480              "END";"PRINT""'L''S10'    Q          W                W(HA)';
481                 "PRINT""'L'ELEMENT',U;
482                 "FOR"N:=1"STEP"1"UNTIL"QT[U]"DO"
483                     "PRINT""'L'',SAMELINE,FREEPOINT(4),''S10'',
484                              PREFIX(''S3''),XT[N,U],
485                              FT[N,U],FT[N,U]*KF*KF/3;
486           XMAX[U]:=XT[QT[U],U];
487                 "FOR"N:=1"STEP"1"UNTIL"QT[U]-1"DO"
488                    F1[N,U]:=(FT[N,U]-FT[N+1,U])/(XT[N,U]-XT[N+1,U]);
489                 "FOR"N:=1"STEP"1"UNTIL"QT[U]-2"DO"
490                    F2[N,U]:=(F1[N,U]-F1[N+1,U])/(XT[N,U]-XT[N+2,U]);
491                 "FOR"N:=1"STEP"1"UNTIL"QT[U]-3"DO"
492                    F3[N,U]:=(F2[N,U]-F2[N+1,U])/(XT[N,U]-XT[N+3,U]);
493                 "PRINT""'L'Z = ',SAMELINE,DIGITS(1),Z[U];
494                 "IF"LO[U]=1"THEN""GOTO" L01;
495                 "IF"LO[U]=2"THEN""GOTO"L02;
496                 "IF"LO[U]=3"THEN""GOTO"L03;
497           L00;  "PRINT""'L'A0 = ',SAMELINE,FREEPOINT(4),AA0[U],
498                        ''L'DA0= ',ADA0[U];
499                 "GOTO"ENDLO;
500           L01;  "PRINT""'L'A0=',SAMELINE,FREEPOINT(4),AA0[U],
501                        ''L'A1= ',AA1[U],''L'DA0 =',ADA0[U],
502                        ''L'DA1= ',ADA1[U];
503                 "GOTO"ENDLO;
504           L02;  "PRINT""'L'A0=',SAMELINE,FREEPOINT(4),AA0[U],
505                        ''L'A1 =',AA1[U],''L'A2 =',AA2[U],
506                        ''L'DA2=',ADA2[U];
507                 "GOTO"ENDLO;
508           L03;  "PRINT""'L'A0=',SAMELINE,FREEPOINT(4),AA0[U],
509                        ''L'A1 =',AA1[U],''L'A2 =',AA2[U],
510                        ''L'DA0=',ADA0[U],''L'DA1=',ADA1[U],
511                        ''L'DA2=',ADA2[U],''L'R2 =',AR2[U];
512
513           ENDLO;
514           "END";
515                 GAMMA1:=1;
516                 TERMA1:=0;
517                 "FOR"N:=1"STEP"1"UNTIL"NMAX[1]"DO"
518                 "BEGIN"GAMMA1:=GAMMA-(1/(4*PI))*XS[N]*BLL(N,0,KF,1);
519                        BLK[N]:=BLL(N,0,KF,1);
520                 "FOR"L:=0"STEP"1"UNTIL"LMAX[1,N]"DO"
521                 TERMA1:=TERMA+((2*L+1)/(4*PI))*BLL(N,L,KF,1)↑2;
522                 "END";
523                 TERM1:=0;
524                 "FOR"N:=1"STEP"1"UNTIL"NMAX[2]"DO"
```

```
524                 "BEGIN""FOR"L:=0"STEP"1"UNTIL"LMAX[2,N]"DO"
525                 TERM:=TERMB*((2*L+1)/(4*PI))*PLL(U,L,KF,2)**2;
526                 "END";
527                 BETA[K]:=1-(CA[K]*TERMA+CB[K]*TERMB)/OMEGA[K];
528                 OP[K]:=GAMMA*GAMMA/BETA[K];
529     PRINT"//L'GAMMA=',SAMELINE,FREEPOINT(4),GAMMA,''S2'BETA=',BETA[K],
530     ''S2'OPW=',OP*[K];
531                 "PRINT"//L'   0          LST          LDT'
532                       ,SAMELINE,'        PNLST        PNLDT';
533                 PS:=1;PD:=0;      PNLS:=0;  PNLD:=0;
534                 H[1]:=H[10]:=0,05;H[2]:=H[9]:=0,025;H[3]:=H[8]:=0,01;
535                 H[4]:=H[7]:=0,00475;H[5]:=H[6]:=0,00045;H[11]:=0,10;
536                 AJ[1]:=0,05;AJ[2]:=0,5;AJ[3]:=0,9;AJ[4]:=0,98;
537                 AJ[5]:=0,999;AJ[6]:=1,0001;AJ[7]:=1,001; AJ[8]:=1,02;
538                 AJ[9]:=1,40;AJ[10]:=2,50;AJ[11]:=3,40;
539                 NJ[1]:=9;NJ[2]:=16;NJ[3]:=8; NJ[4]:=NJ[7]:=4;
540                 NJ[5]:=NJ[6]:=2;NJ[8]:=36;NJ[9]:=44;NJ[10]:=18;NJ[11]:=26;"
541           "COMMENT"PROGRAMME NOW ENTERS Q LOOP,INTEGRATION MESH
542                 FINEST CLOSE TO SINGULARITY(Q=2*KF);
543                 "FOR"T:=1"STEP"1"UNTIL"11"DO"
544                 "BEGIN"NJ1:"NJ[T]+1;
545                       H3:=H[T]/3;
546                       "FOR"M:=1"STEP"1"UNTIL"NJ1"DO"
547                       "BEGIN"X:=AJ[T]+(M-1)*H[T];
548                             Q:=X*2*KF;
549                       SIG:=((18*PI*,450*VAL)+(1/3))/KF;
550                             STR:=S'0*SIG,,450)-1;
551                             FL:=LN(ABS((1-X)/(1+X)));
552                             XFL:=X*FL;
553                             RB:=RC:=0; RG1:=RG2:=RGS1:=RGS2:=0;
554                             RD1:=DQ(1);   RD2:=DQ(2);
555                             "FOR"N:=1"STEP"1"UNTIL"KMAX[1]"DO"
556                             "BEGIN"RC:=RC+XS[N]*CQ(N);
557                                   RG1:=RG1+GQ(N,1)*XS[N];
558                                   RG2:=RG2+GQ(N,2)*XS[N];
559                             "END";
560                       CAPGAM:=(XFL-(1/(4*PI)*RC))/GAMMA;
561                       LA:=(RD1-(1/(4*PI)*RG1))/GAMMA;
562                       LB:=(RD2-(1/(4*PI)*RG2))/GAMMA;
563                                   VA:=VAL*W(X,1);  VB:=VAL*W(X,2);
564                                   QS:=2*CAPGAM*VA;
565                                   QD:=2*CAPGAM*(CA[K]*STR*VA+CB[K]*STR*VB);
566                                   NL1:=2*LA;
567                                   NL2:=2*CA[K]*STR*LA;
568                                   NL3:=2*CB[K]*STR*LB;
569                                   "COMMENT"INTEGRATION OF SELF  AND DISTINCT
570                                   TERM INTEGRANDS OVER Q WILL NOW BE DONE
571                                   USING SIMPSONS RULE;
572                                   "IF"M=1"THEN""GOTO"FIRSTANDLAST;
573                                   "IF"M=NJ1"THEN""GOTO"FIRSTANDLAST;
574                                   "IF"M=ENTIER(M/2)*2"THEN""GOTO"EVEN"ELSE"
575                                   "GOTO"ODD;
576                       FIRSTANDLAST: PS:=PS+H3*QS;
577                                   PNLS:=PNLS+NL1*H3;
578                                   PNLD:=PNLD+(NL2+NL3)*H3;
579                                   PD:=PD+H3*QD;PST:=PS;PDT:=PD;
580                                   PNLST:=PNLS;   PNLDT:=PNLD;
581     PRINT"//L'',SAMELINE,FREEPOINT(6),Q,'   ',PST,'  ',PDT,'  ',PNLST,
582                       '   ',PNLDT;
583                                   "GOTO"EXIT;
```

```
584                             EVEN1   PS1=PS+4*H3*QS1
585                                     PNLS1=PNLS+4*NL1*H31
586                                     PNLD1=PNLD+(NL2+NL3)*4*H31
587                                     PD1=PD+4*H3*QD1
588                                     "GOTO"EXIT1
589                             ODD1    PS1=PS+2*H3*QS1
590                                     PNLS1=PNLS+2*NL1*H31
591                                     PNLD1=PNLD+(NL2+NL3)*H3*21
592                                     PD1=PD+2*H3*QD1
593                             EXIT1   PT[K]1=PST+PDT+PNLST+PNLDT1
594                             "END"1
595                     "END"1
596     CONTINUE1DENS1=OPR[K]*PT[K]1
597                     PF1=DENS/OMEGA1[K]1
598     "PRINT"/'L'',SAMELINE,FREEPOINT(5),'SELF TERMS =',PST,' + ',PNLST,
599             ' = ',PST+PNLST,'   DISTINCT TERM = ',PDT,' + ',PNLDT,' = ',
600             PDT+PNLDT,/'L'TOTAL TERM = ',PT[K],'   DENS = ',DENS1
601             "END"OF K LOOP1
602     FIN1
603     "END"OF PROGRAMME1
 1128       MC
 6964   CODE
 8092 TOTAL


eEND1
```

Appendix C

Normalisation Correction Program

Outline of Program

This program contains a lot of expressions which occur in the contact density program and have been discussed already, furthermore the same identifiers have been used where possible so no further key is given her. Again the procedures are described before the main program.

Procedures NF, BLL, BINT. W. STR

Same as in contact density program.

Procedure PP

This evaluates the angular integral Π of section 4.3.6 given by

$$\Pi = \frac{1}{\Omega} \sum_{n\ell} \frac{2\ell+1}{4\pi} B_{n\ell}(k_F)\ C_{n\ell}(k,q)$$

where

$$C_{n\ell}(k,q) = P \int_{-1}^{+1} \frac{dy\ P_\ell(x).B_{n\ell}(k').V(k')}{\frac{2k}{q}y - 1} ,$$

$$x = \frac{k - qy}{\sqrt{(k^2+q^2-2kq}}$$

and

$$k' = \sqrt{k^2+q^2-2kq} .$$

As when evaluating the angular integral G_o, we note that $B_{n\ell}(k').V(k')$ is a slowly varying function of k' and write

$$A_{n\ell}(k') = B_{n\ell}(k').V(k') .$$

No ion has core states with $\ell > 3$ so we need only consider 4

Appendix C

Normalisation Correction Program

Outline of Program

This program contains a lot of expressions which occur in the contact density program and have been discussed already, furthermore the same identifiers have been used where possible so no further key is given her. Again the procedures are described before the main program.

Procedures NF, BLL, BINT. W. STR

Same as in contact density program.

Procedure PP

This evaluates the angular integral Π of section 4.3.6 given by

$$\Pi = \frac{1}{\Omega} \sum_{n\ell} \frac{2\ell+1}{4\pi} B_{n\ell}(k_F)\, C_{n\ell}(k,q)$$

where

$$C_{n\ell}(k,q) = P \int_{-1}^{+1} \frac{dy\, P_\ell(x).B_{n\ell}(k').V(k')}{\frac{2k}{q}y - 1} ,$$

$$x = \frac{k - qy}{\sqrt{(k^2+q^2-2kq}}$$

and

$$k' = \sqrt{k^2+q^2-2kq} .$$

As when evaluating the angular integral G_o, we note that $B_{n\ell}(k').V(k')$ is a slowly varying function of k' and write

$$A_{n\ell}(k') = B_{n\ell}(k').V(k') .$$

No ion has core states with $\ell > 3$ so we need only consider 4

expressions for $C_{n\ell}$

i.e. $$C_{no} = P \int_{-1}^{+1} \frac{dy\ A_{no}(k')}{\frac{2k}{q} y - 1} ,$$

$$C_{n1} = P \int_{-1}^{+1} \frac{dy\ x\ A_{n1}(k')}{\frac{2k}{q} y - 1} ,$$

$$C_{n2} = P \int_{-1}^{+1} \frac{dy\ (\frac{3}{2} x^2 - \frac{1}{2}) A_{n2}(k')}{\frac{2k}{q} y - 1} ,$$

and

$$C_{n3} = P \int_{-1}^{+1} \frac{dy\ (\frac{5}{2} x^3 - 3x)\ A_{n3}(k')}{\frac{2k}{q} y - 1} .$$

where the Legendre polynomials have been written cut as a function of x. C_{n2} and C_{n3} can both be split up into two parts so if we define 4 new functions by

$$C_o^1(n,\ell) = P \int_{-1}^{+1} \frac{dy\ A_{n\ell}(k')}{\frac{2k}{q} y - 1} ,$$

$$C_1^1(n,\ell) = P \int_{-1}^{+1} \frac{dy\ x\ A_{n\ell}(k')}{\frac{2k}{q} y - 1} ,$$

$$C_2^1(n,\ell) = \frac{3}{2} P \int_{-1}^{+1} \frac{dy\ x^2\ A_{n\ell}(k')}{\frac{2k}{q} y - 1} ,$$

and

$$C_3^1(n,\ell) = \frac{5}{2} P \int_{-1}^{+1} \frac{dy\ x^3\ A_{n\ell}(k')}{\frac{2k}{q} y - 1} .$$

They are related to the original functions by

$$C_{no} = C_o^1 (n,o) \ ,$$

$$C_{n1} = C_1^1 (n,1) \ ,$$

$$C_{n2} = C_2^1 (n,2) - \tfrac{1}{2} C_o^1(n,2) \ ,$$

$$C_{n3} = C_3^1 (n,3) - \tfrac{z}{2} C_1^1(n,3) .$$

Each of the C^1 integrals can now be found by the method used for C_o in the contact density program, although the integrals in the regions between the calculated points are of a somewhat complex form. The integral in $C_o^1(n,\ell)$ is precisely of the same form as given in the previous appendix but for the more complicated integrals it is useful to write A as a function of z where $z = k^2$,

so that $A(z) = A(Z_m) + A^1(Z_m)\ (z - Z_m)$ where A is calculated at the points were $z = Z_m$

and
$$A^1(Z_m) = \frac{A\ (Z_{m+1}) - A\ (Z_m)}{Z_{m+1} - Z_m} \ .$$

The expressions for each of the integrals is then

$$C^1(n,\ell) = \sum_m \left[P\ell n \left| \frac{k+z^{\frac{1}{2}}}{k-z^{\frac{1}{2}}} \right| + Qz^{\frac{1}{2}} + Rz^{\frac{3}{2}} \right]_{Z_m}^{Z_{m+1}} \ ,$$

where
$$P = - \alpha \frac{q}{4k^3} - \beta \frac{q}{4k} - \gamma \frac{qk}{4} \ ,$$

$$Q = \frac{q}{2}\left(\frac{\beta}{k^2} + \gamma\right) \ ,$$

$$R = \frac{2}{3} \frac{q\gamma}{(2k)^2} \ ,$$

and
$$\alpha = (k^2 - q^2) \left[A(Z_m) - A^1(Z_m).Z_m\right] \ ,$$

$$\beta = (k^2 - q^2)\ A^1(Z_m) + A(Z_m) - A^1(Z_m).Z_m \ ,$$

$$\gamma = A^1(Z_m) \ .$$

$$C_2^1(n,\ell) = \sum_m \frac{-3q}{16k^3} \left[N\ell nz + P\ell n\left| k^2 - z \right| + Qz + Rz^2 \right]_{Z_m}^{Z_{m+1}} ,$$

with

$$N = \alpha/k^2 - \beta - \gamma k^2 - \delta k^4 ,$$

$$Q = -\gamma - \delta k^2 ,$$

$$R = -\delta/2 ,$$

and

$$\alpha = (k^2 - q^2)^2 \left(A(Z_m) - A^1(Z_m).Z_m\right) ,$$

$$\beta = (k^2 - q^2)^2 A^1(Z_m) + 2(k^2 - q^2)\left(A(Z_m) - A^1(Z_m).Z_m\right) ,$$

$$\gamma = 2(k^2 - q^2) A^1(Z_m) + \left(A(Z_m) - A^1(Z_m).Z_m\right) ,$$

$$\delta = A^1(Z_m) .$$

Finally

$$C_3^1(n,\ell) = \frac{-5q}{2(2k)^4} \sum_m \left[N z^{-\frac{1}{2}} + P\ell n \left| \frac{k+z^{\frac{1}{2}}}{k-z^{\frac{1}{2}}} \right| + Qz^{\frac{1}{2}} + Rz^{\frac{3}{2}} + Sz^{\frac{5}{2}} \right]_{Z_m}^{Z_{m+1}} ,$$

where

$$N = \frac{-2\alpha}{k^2} ,$$

$$P = \frac{\alpha}{k^3} + \frac{\beta}{k} + \gamma k + \delta k^3 + \epsilon k^5 ,$$

$$Q = -2\gamma - 2\delta k^2 - 2\epsilon k^4 ,$$

$$R = \frac{-2\delta}{3} - \frac{2}{3}\epsilon k^2 ,$$

$$S = \frac{-2}{5}\epsilon ,$$

and

$$\alpha = (k^2 - q^2)^3 .\left(A(Z_m) - A^1(Z_m).Z_m\right) ,$$

$$\beta = 3(k^2 - q^2)^2 .\left(A(Z_m) - A^1(Z_m).Z_m\right) + (k^2 - q^2).A^1(Z_m) ,$$

$$\gamma = 3(k^2 - q^2)\left(A(Z_m) - A^1(Z_m)Z_m\right) + 3(k^2 - q^2)^2 A^1(Z_m) ,$$

$$\delta = (A(Z_m) - A^1(Z_m).Z_m) + 3(k^2 - q^2)A^1(Z_m) ,$$

$$\epsilon = A^1(Z_m) .$$

In the program these various integrals are calculated in the interior procedures. C0, C1, C2 and C3 and the summation over all n and ℓ performed in the main part of procedure PP.

Main Program

The core wave functions are firstly fed in and the overlap integrals calculated by line 771 (see program list). The program then collects the remainder of the information required for the calculation, Fermi wave vector, atomic volume, packing fraction, local part of form factors and model potential parameters in lines 772-759. Finally the integral over q is performed using exactly the same integration mesh as in the contact density program. To check this was sufficiently fine, the calculated points of the integrand were plotted out using the procedure GRAPH 1.

```
** ICL 4130 DES2 SYSTEM  :  SLAVE DIG        :  CORE 62K  :  VOL  2

&JOB;PH/R060/XX;


&LINES;2000;
*OP
TW 2600
ATCH


&ALGOL/L;
;BINARY
&GOL

   1   NORMALISATION CORRECTION;
   2   "BEGIN""REAL"KF,OMEGA,NETA,     PI,PS,ORA,VAL,SIG,VA,GS,PST,PT,DN,Q,X,H3,**
   3               STP,U,FL,CON;
   4           "INTEGER"U,L,RAD,N,  NWF,NMAX,KINT,GN,I,M,NJ1,Z,T;
   5           "REAL""ARRAY"FLC[3,1:6,0:100],CLAC0:3,1:6,0:125],AJ,HF[1:11],
   6                        FLA[0:130],F1,F2,F3,YT,FT[1:60,1:2]  ,
   7                        AA0,AA1,AA2,ADA0,ADA1,ADA2,AD2[1:2],
   8                        GX,GY[1:200];
   9           "INTEGER""ARRAY"UPAD[0:3,1:6],LINAY[1:6],TITLEC0:20],NJ[1:11],
  10                         L0,QT,XMAX[1:2];
  11           "COMMENT"PROCEDURE S CALCULATES STRUCTURE FACTOR USING CURRENT
  12           ALLOY VALUES OF KF AND SIGMA,THE PACKING FRACTION ETA IS 0,45
  13           THROUGHOUT;
  14           "REAL""PROCEDURE"S(Z,ETA);
  15           "REAL"Z,ETA;
  16           "BEGIN""REAL"ZZ,ZZZ,R1,R2,R3,R4,R5,T1,T2,T3;
  17                   "IF"Z<0,5"THEN"S:=0,025"ELSE"
  18                   "BEGIN"
  19                   ZZ:=Z*Z;
  20                   ZZZ:=Z*Z*Z;
  21           T1:=(1+2*ETA)**2/(1-ETA)**4;
  22           T2:=-6*ETA*(1+ETA/2)**2/(1-ETA)**4;
  23           T3:=1/2*ETA*(1+2*ETA)**2/(1-ETA)**4;
  24           R1:=T1+2*T2+4*T3-24*T3/ZZ;
  25           R2:=-(T1+T2+T3)*Z+(2*T2+12*T3)/Z-24*T3/ZZZ;
  26           R3:=-2*T2/Z+24*T3/ZZZ;
  27           R4:=24*ETA/ZZZ;
  28                   R5:=R4*(R1*SIN(Z)+R2*COS(Z)+R3);
  29                   S:=1/(1+R5);
  30                   "END";
  31           "END"OF PROCEDURE S;
  32           "REAL""PROCEDURE"NF(PU,PZ,PETA,E);    "VALUE"PU,PZ,PETA,E;
  33           "REAL"PU,PZ,PETA;    "INTEGER"E;
  34           "BEGIN""REAL"K,K1,KKF,RU,KR0,K1R0,CS,R1,KR1,K1R1,KR2,K1R2,R2,ARG,**
  35                   ARG1,I,F,AL2, A0,A1,A2,DA1,DA2,DA0;
  36                   "INTEGER"N,M;        "REAL""ARRAY"FLC0:2,0:10];
  37                   "IF"LOCE]=1"THEN""GOTO"CASE1;
  38                   "IF"LOCE]=2"THEN""GOTO"CASE2;
  39                   "IF"LOCE]=3"THEN""GOTO"CASE3;
  40            CASE0;A0:=AA0CE];      DA0:=ADA0CE];
  41                   K1:=KF*SQRT(PU*PZ*2);    NEF1=K*2-KF*2;
  42                   K1:=KF*SQRT(PU*(PZ*PETA)*2);
```

```
43              RU:=Z/(A0+KKF*DA0/2))    KR0:=K*R0;
44              K1R0:=K1*R0;
45              "FOR"N:=1"STEP"1"UNTIL"9"DO"
46              "BEGIN"FL[0,N]:=2*((N-10)/N)*SIN(KR0*N/10)
47                                 *SIN(K1R0*N/10);
48              "END";
49              "COMMENT"FOR N=0 OR 10    FL[X,N]=0;
50              I:=0;
51              "FOR"N:=1"STEP"1"UNTIL"2"DO"
52              "FOR"N:=1"STEP"1"UNTIL"9"DO"
53                 I:=I+(Z/(K*K1))*(FL[0,N]);
54              F:=I/30;
55                    "GOTO"ENDCASE;
56      CASE1:A0:=AA0[F];    DA0:=ADA0[F];
57              A1:=AA1[F];       DA1:=ADA1[F];
58              K:=KF*SQRT(PU*PZ*2);    KKF:=K*2-KF*2;
59              K1:=KF*SQRT(PU*(PZ+PETA)*2);
60              RU:=Z/(A0+KKF*DA0/2);    KR0:=K*R0;
61              K1R0:=K1*R0;
62              CS:=(PU*PZ*(PZ+PETA))/SQRT((PU*PZ*2)*
63                  (PU*(PZ+PETA)*2));
64              R1:=Z/(A1+KKF*DA1/2);
65              KK1:=K*R1;    K1R1:=K1*R1;
66              "FOR"N:=1"STEP"1"UNTIL"9"DO"
67              "BEGIN"FL[0,N]:=2*((N-10)/N)*SIN(KR0*N/10)
68                                 *SIN(K1R0*N/10);
69                     ARG:=KR1*N/10;    ARG1:=K1R1*N/10;
70                     FL[1,N]:=2*((N-10)/N)*(SIN(ARG)/ARG-COS(ARG))
71                                 *(SIN(ARG1)/ARG1-COS(ARG1));
72
73              "END";
74              "COMMENT"FOR N=0 OR 10    FL[X,N]=0;
75              I:=0;
76              "FOR"N:=1"STEP"1"UNTIL"2"DO"
77              "FOR"N:=1"STEP"1"UNTIL"9"DO"
78                 I:=I+(Z/(K*K1))*(FL[0,N]+3*CS*FL[1,N]);
79              F:=I/30;
80                    "GOTO"ENDCASE;
81      CASE2:A0:=AA0[F];       DA0:=ADA0[F];
82              A1:=AA1[F];       DA1:=ADA1[F];
83              A2:=AA2[F];       DA2:=ADA2[F];
84              K:=KF*SQRT(PU*PZ*2);    KKF:=K*2-KF*2;
85              K1:=KF*SQRT(PU*(PZ+PETA)*2);
86              RU:=Z/(A0+KKF*DA0/2);    KR0:=K*R0;
87              K1R0:=K1*R0;
88              CS:=(PU*PZ*(PZ+PETA))/SQRT((PU*PZ*2)*
89                  (PU*(PZ+PETA)*2));
90              R1:=Z/(A1+KKF*DA1/2);  R2:=Z/(A2+KKF*DA2/2);
91              KK1:=K*R1;    K1R1:=K1*R1;
92              KK2:=K*R2;    K1R2:=K1*R2;
93              "FOR"N:=1"STEP"1"UNTIL"9"DO"
94              "BEGIN"FL[0,N]:=2*((N-10)/N)*SIN(KR0*N/10)
95                                 *SIN(K1R0*N/10);
96                     ARG:=KR1*N/10;    ARG1:=K1R1*N/10;
97                     FL[1,N]:=2*((N-10)/N)*(SIN(ARG)/ARG-COS(ARG))
98                                 *(SIN(ARG1)/ARG1-COS(ARG1));
99                     ARG:=KR2*N/10;    ARG1:=K1R2*N/10;
100                    FL[2,N]:=2*((N-10)/N)          *((3/ARG*2-1)
101                                *SIN(ARG)-3*COS(ARG)/ARG)*((3/ARG1*2-1)
102                                *SIN(ARG1)-3*COS(ARG1)/ARG1);
103
104             "END";
```

```
103                 "COMMENT"FOR N=0 OR 10   FL[X,N]=0;
104                 I:=0;
105                 "FOR"M:=1"STEP"1"UNTIL"2"DO"
106                 "FOR"N:=1"STEP"1"UNTIL"9"DO"
107                    I:=I+(Z/(K*R1))*(FL[0,N]+3*CS*FL[1,N]
108                       +2,5*(3*CS*2-1)*FL[2,N]);
109                 F:=I/30;
110                    "GOTO"ENDCASE;
111           CASE3:A0:=AA0[E];       DA0:=ADA0[E];
112                 A1:=AA1[E];       DA1:=ADA1[E];
113                 A2:=AA2[E];       DA2:=ADA2[E];    R2:=AR2[E];
114           "BEGIN"K:=KF*SQRT(PU*PZ*2);   KKF:=K*2=KF*2;
115                 K1:=KF*SQRT(PU*(PZ+PETA)*2);
116                 R0:=Z/(A0*KKF*DA0/2);   KR0:=K*R0;
117                 K1R0:=K1*R0;
118                 CS:=(PU*PZ*(PZ+PETA))/SQRT((PU*PZ*2)*
119                     (PU*(PZ+PETA)*2));
120                 R1:=Z/(A1*KKF*DA1/2);
121                 KR1:=K*R1;   K1R1:=K1*R1;
122                 KR2:=K*R2;   K1R2:=K1*R2;
123                 AL2:=A2*KKF*DA2/2;
124           "END";
125                 "FOR"N:=1"STEP"1"UNTIL"9"DO"
126                 "BEGIN"FL[0,N]:=2*((N-10)/N)*SIN(KR0*N/10)
127                                *SIN(K1R0*N/10);
128                        ARG:=KR1*N/10;   ARG1:=K1R1*N/10;
129                        FL[1,N]:=2*((N-10)/N)*(SIN(ARG)/ARG-COS(ARG))
130                                 *(SIN(ARG1)/ARG1-COS(ARG1));
131                        ARG:=KR2*N/10;   ARG1:=K1R2*N/10;
132                        FL[2,N]:=2*(1-10*Z/(AL2*R2*N))*((3/ARG*2=1)
133                                *SIN(ARG)-3*COS(ARG)/ARG)*((3/ARG1*2-1)
134                                *SIN(ARG1)-3*COS(ARG1)/ARG1);
135                 "END";
136                 "COMMENT"FOR N=0 OR 10   FL[X,N]=0EXCEPT FL[2,10]
137                          DUE TO NON OPTIMISATION OF POTENTIAL;
138                 FL[2,10]:=(1-Z/(AL2*R2))*((3/KR2*2-1)*SIN(KR2)
139                           -3*COS(KR2)/KR2)*((3/K1R2*2-1)*SIN(K1R2)
140                            +3*COS(K1R2)/K1R2);
141                 I:=0;
142                 "FOR"M:=1"STEP"1"UNTIL"2"DO"
143                 "FOR"N:=1"STEP"1"UNTIL"9"DO"
144                    I:=I+(Z/(K*R1))*(FL[0,N]+3*CS*FL[1,N]
145                       +2,5*(3*CS*2-1)*FL[2,N]);
146                 I:=I+(Z/(K*K1))*2,5*(3*CS*2-1)*FL[2,10];
147                 F:=I/30;
148           ENDCASE:
149                 FLACK[NT]:=-12*PI*F*Z/(KF*KF*OMEGA);
150                 NF:=FLACK[NT];
151           "END"OF PROCEDURE  NF;
152     "COMMENT" INTERPOLATION OF NUMERICAL FORM FACTORS;
153           "REAL""PROCEDURE"FY(Y,P);
154           "REAL"Y;     "INTEGER"P;
155           "BEGIN""REAL"FY;     "INTEGER"  N,M;
156                 "IF"Y>XMAX[P]"THEN""GOTO"CONTINUE;
157                 "FOR"N:=1"STEP"1"UNTIL"QT[P]"DO"
158                    "IF"Y=XT[N,P]"THEN""BEGIN"FY:=FT[N,P]
159                                          "GOTO"AN;
160                                       "END";
161                 "FOR"N:=2"STEP"1"UNTIL"QT[P]-3"DO"
162                    "IF"Y<XT[N+1,P]"THEN""BEGIN"M:=N;
```

```
                                        "GOTO"CALC;
                                    "END";
          N:=CT[P]-2;
      CALC:FY:=FT[N-1,P]+(Y-XT[N-1,P])*F1[N-1,P]
                +(Y-XT[N-1,P])*(Y-XT[N,P])*F2[N-1,P]
                +(Y-XT[N-1,P])*(Y-XT[N,P])*(Y-XT[N+1,P])*F3[N-1,P];
      AUX:=FY;
"END" OF PROCEDURE W;
"REAL""PROCEDURE"BINT(N,L,RAD,R); "VALUE"N,L,RAD,R;
    "REAL"R;  "INTEGER"N,L,RAD;
"BEGIN""REAL"XKR;      "REAL""ARRAY"JC0:4];
        XKR:=KF*R;
        "IF"XKR<0,01"THEN"XKR:=0,01;
        JC0]:=SIN(XKR)/XKR;
        "IF"L>0"THEN"JC1]:=JC0]/XKR-COS(XKR)/XKR;
        "IF"L>1"THEN"JC2]:=3*JC1]/XKR-JC0];
        "IF"L>2"THEN"JC3]:=5*JC2]/XKR-JC1];
        "IF"L>3"THEN"JC4]:=7*JC3]/XKR-JC2];
        BINT:=4*3,1415*R*PC[L,N,RAD]*JC[L];
"END"OF PROCEDURE BINT;
"REAL""PROCEDURE"BLL(N,L,KF); "VALUE"N,L,KF;
"REAL"KF;
"INTEGER"N,L;
"BEGIN""REAL"RZERO,F,R1,B2,B3,B4,HCON,R,BL,RZEROCON;
        "INTEGER"C,RADZERO,I;
        RZERO:=,08;
                        BL:=0;
                        "FOR"C:=1"STEP"1"UNTIL"(NRADCL,N]-1)"DIV"
                            10"DO"
                        "BEGIN"F:=0,01*(2*C)/2;
                               B1:=B2:=0;
                               RADZERO:=10*(C-1);
                               RZERO:=RZERO+5*F;
                                        HCON:=F*CON;
                               RZEROCON:=RZERO*CON;
                               "FOR"I:=1"STEP"2"UNTIL"9"DO"
                               "BEGIN"RAD:=RADZERO+I;
                                      R:=RZEROCON+HCON*I;
                                      B1:=B1+BINT(N,L,RAD,R);
                               "END";
                               "FOR"I:=2"STEP"2"UNTIL"8"DO"
                               "BEGIN"RAD:=RADZERO+I;
                                      R:=RZEROCON+HCON*I;
                                      B2:=B2+BINT(N,L,RAD,R);
                               "END";
                               RAD:=RADZERO;
                               R:=RZEROCON;
                               B3:=BINT(N,L,RAD,R);
                               RAD:=RADZERO+10;
                               R:=RZEROCON+10*HCON;
                               B4:=BINT(N,L,RAD,R);
                               BL:=BL+(HCON/3)*(B3+B4)+4*(HCON/3)*B1+
                                   +2*(HCON/3)*B2;
                        "END";
                        BLL:=BL;
"END" OF PROCEDURE BLL;
"REAL""PROCEDURE"PP(D); "VALUE"D; "REAL"D;
"BEGIN""REAL"RTL,RTN;
"REAL""PROCEDURE"CO(N,L); "VALUE"N,L;"INTEGER"N,L;
"BEGIN""REAL"W,HO,I,B1,Y;
```

```
223             "INTEGER"KINTO,KINTP,P,M;
224             "REAL""ARRAY"B,X[0:130];
225             KINTO:=ENTIER(10*(KF+Q))+1;
226             KINTP:=ENTIER(10*ABS(KF-Q));
227             P:=KINTO-KINTP+1;
228             W:=2*KF/Q;     W0:=(KF/Q)*(KF/Q);
229             "FOR"M:=0"STEP"1"UNTIL"P+1"DO"
230             "BEGIN"KINT:=KINTO-M;
231                     X[M]:=W0-(KINT/10)*(KINT/10)/(Q*Q);
232             Y:=(X[M]+1)/W;
233             "COMMENT" TO AVOID FPOFLO IN WHEN K1 = 0;
234             "IF"ABS(1-Y*Y+(Q/KF-Y)*2)<.0001"THEN" Y:=Y-.0001;
235             B[M]:=BLAKE(N,FINT)*(WF(1-Y*Y,-Y,1/KF,1)+VA);
236             "END";
237             "FOR"M:=0"STEP"1"UNTIL"P"DO"
238               "IF"ABS(X[M])<.00001"THEN"
239             "BEGIN"B[M]:=0.9*B[M]+0.1*B[M+1];
240                     X[M]:=0.1*X[M+1];
241             "END";
242             I:=0;
243             "IF"P>1"THEN"
244             "BEGIN""FOR"M:=1"STEP"1"UNTIL"P-1"DO"
245                     "BEGIN"B1:=(B[M+1]-B[M])/(X[M+1]-X[M]);
246                             I:=I+B1*(X[M+1]-X[M])*(B[M]-B1*X[M])
247                                     *LN(ABS(X[M+1]/X[M]));
248                     "END" ;
249             "END" ;
250             "IF"P>0"THEN"
251             "BEGIN"B1:=(B[1]-B[0])/(X[1]-X[0]);
252                     I:=I+B1*(X[1]+1+W)*(B[0]-B1*X[0])
253                             *LN(ABS(X[1]/(1+W)));
254                     B1:=(B[P+1]-B[P])/(X[P+1]-X[P]);
255                     I:=I+B1*(W-1-X[P])*(B[P]-B1*X[P])
256                             *LN(ABS((W-1)/X[P]));
257             "END"
258             "ELSE"
259             "BEGIN"B1:=(B[1]-B[0])/(X[1]-X[0]);
260                     I:=B1+2*W*(B[0]-B1*X[0])*LN(ABS((W-1)/(W+1)));
261             "END";
262             CO:=1+C/(2*KF);
263     "END"OF PROCEDURE CO;
264     "REAL""PROCEDURE"C1(NN,LL); "VALUE"NN,LL;"INTEGER"NN,LL;
265     "BEGIN""REAL"I0,A,B,C,SZ,SZ1,PI,P1;
266             "INTEGER"KINTO,KINTR,R,G;
267             "REAL""ARRAY"Z,H,L,N,M[0:125];
268             "REAL""PROCEDURE"IG(G,SZ); "VALUE"G,SZ;
269                     "REAL"SZ;      "INTEGER"G;
270             "BEGIN"IG:=L[G]*LN(ABS((KF+SZ)/(KF-SZ)))+M[G]*SZ
271                             +N[G]*SZ*3;
272             "END"OF PROCEDURE IG;
273             KINTO:=ENTIER(10*(KF+Q))+1;
274             KINTR:=ENTIER(10*ABS(KF-Q));
275             R:=KINTO-KINTR+1;
276             W0:=KF*KF-Q*Q;
277             "FOR"G:=0"STEP"1"UNTIL"R+1"DO"
278             "BEGIN"KINT:=KINTO-G;
279                     Z[G]:=KINT*KINT/100;
280                     H[G]:=BLAKE(LL,NN,KINT)*(FLAC[KINT]+VA);
281             "END";
282             "FOR"G:=1"STEP"1"UNTIL"R"DO"
```

```
                "IF"ABS(KF-SQRT(Z[G]))<0.00001"THEN"
                "BEGIN"Z[G]:=0.9*Z[G]+0.1*Z[G+1];
                       H[G]:=0.9*H[G]+0.1*H[G+1];
                "END";
                "FOR"G:=G"STEP"1"UNTIL"R"DO"
                "BEGIN"H1:=(H[G]-H[G+1])/(Z[G]-Z[G+1]);
                       A:=H0*(H[G]-H1*Z[G]);
                       B:=NG*B1*H[G]-B1*Z[G];
                       C:=G1;
                       L[G]:=-(A/(KF*3)+B/KF+C*KF)*Q/4;
                       M[G]:=(B/(KF*KF)+C)*Q/2;
                       N[G]:=Q*C/(4*KF*KF);
                "END";
                P:=0;
                "IF"R>1"THEN"
                "FOR"G:=1"STEP"1"UNTIL"R-1"DO"
                "BEGIN"SZ:=SQRT(Z[G]);   SZ1:=SQRT(Z[G+1]);
                       A:=IG(G,SZ);
                       B:=IG(G,SZ1);
                       RT:=RT+B-A;
                "END";
                "IF"<>0"THEN"
                "BEGIN"SZ:=KF*Q; SZ1:=SQRT(Z[1]);
                       A:=IG(0,SZ);
                       B:=IG(0,SZ1);
                       RT:=RT+B-A;
                       SZ:=SQRT(Z[R]); SZ1:=ABS(KF-Q);
                       A:=IG(R,SZ);
                       B:=IG(R,SZ1);
                       RT:=RT+B-A;
                "END"
                "ELSE"
                "BEGIN"SZ:=KF*Q;   SZ1:=ABS(KF-Q);
                       A:=IG(0,SZ);
                       B:=IG(0,SZ);
                       RT:=RT+B-A;
                "END";
                C1:=RT;
        "END"OF PROCEDURE C1;
        "REAL""PROCEDURE"C2(NN);"VALUE"NN; "INTEGER"NN;
        "REAL""PROCEDURE"IG(G,TZ); "VALUE"G,TZ;
                "INTEGER"KINTO,KINTR,R,G;
                "REAL""ARRAY"Z,H,L,M,N,P[0:125];
                "REAL"TZ;   "INTEGER"G;
                "BEGIN"IG:=(L[G]*LN(ABS(TZ))+H[G]*LN(ABS(KF*KF-TZ))
                          +M[G]*TZ+P[G]*TZ*TZ)*3*Q/(-16*KF*3);
                "END"OF PROCEDURE IG;
                KINT:=ENTIER(10*(KF*Q))+1;
                KINTR:=ENTIER(10*ABS(KF-Q));
                R:=(KINTO-KINTR)*1;
                NO:=KF*KF-Q*Q;          N2:=NO*NO;
                "FOR"G:=0"STEP"1"UNTIL"R+1"DO"
                "BEGIN"KINT:=KINTO+G;
                   Z[G]:=KINT*KINT/100;
                H[G]:=BLAC  2,"N"+KINT]*(FLA[KINT]+"A");
                "END";
                "FOR"G:=1"STEP"1"UNTIL"R"DO"
                "IF"ABS(KF-SQRT(Z[G]))<0.00001"THEN"
                "BEGIN"Z[G]:=0.9*Z[G]+0.1*Z[G+1];
```

```
343                     H[G]:=0,9*H[G]+0,1*H[G+1];
344                 "END";
345                 "FOR"G:=0"STEP"1"UNTIL"R"DO"
346                 "BEGIN"B1:=(H[G]-H[G+1])/(Z[G]-Z[G+1]);
347                         A:=N2*(H[G]-B1*Z[G]);
348                         B:=N2*B1+2*N0*(H[G]-B1*Z[G]);
349                         C:=2*N0*B1+H[G]-B1*Z[G];
350                         D:=B1;
351                         L[G]:=A/(KF*KF);
352                         H[G]:=-A/(KF*KF)-D-C*KF*KF-D*KF*4;
353                         N[G]:=-C-D*KF*KF;
354                         P[G]:=-D/2;
355                 "END";
356                 RT:=0;
357                 "IF"R>1"THEN"
358                 "FOR"G:=1"STEP"1"UNTIL"R-1"DO"
359                 "BEGIN"TZ:=Z[G];      TZ1:=Z[G+1];
360                         A:=IG(G,TZ);
361                         B:=IG(G,TZ1);
362                         RT:=RT+B-A;
363                 "END";
364                 "IF"R>0"THEN"
365                 "BEGIN"TZ:=(KF+Q)*(KF+Q);    TZ1:=Z[1];
366                         A:=IG(0,TZ);
367                         B:=IG(0,TZ1);
368                         RT:=RT+B-A;
369                         TZ:=Z[R];      TZ1:=(KF-Q)*(KF-Q);
370                         A:=IG(R,TZ);
371                         B:=IG(R,TZ1);
372                         RT:=RT+B-A;
373                 "END"
374                 "ELSE"
375                 "BEGIN"TZ:=(KF+Q)*(KF+Q);    TZ1:=(KF-Q)*(KF-Q);
376                         A:=IG(0,TZ);
377                         B:=IG(0,TZ1);
378                         RT:=RT+B-A;
379                 "END";
380                 C2:=RT-C0(NN,2)/2;
381         "END"OF PROCEDURE C2;
382         "REAL""PROCEDURE"C3(N);   "VALUE"N;"INTEGER"N;
383         "BEGIN""REAL"I0,N1,N2,A,B,C,D,E,SZ,SZ1,RT1,K3,K2,K3,K4,B1;
384                 "INTEGER"KINTO,KINTR,G,K;
385                 "REAL""ARRAY"Z,H,L,M,N,P,Q0[0:125];
386                 "REAL""PROCEDURE"IG(G,SZ);   "VALUE"G,SZ;
387                         "REAL"SZ;   "INTEGER"G;
388                 "BEGIN""COMMENT"L[G] IS PROPORTIONAL TO SZ*3;
389                         "IF"ABS(SZ)<.0001"THEN"IG:=0
390                         "ELSE"
391                         IG:=(L[G]/SZ+N[G]*LN(ABS((KF+SZ)/(KF-SZ)))
392                             +M[G]*SZ+P[G]*SZ*3+Q0[G]*SZ*5)*5*0/(-32*K4);
393                 "END"OF PROCEDURE IG;
394                 KINTU:=ENTIER(10*(KF+Q))+1;
395                 KINTR:=ENTIER(10*ABS(KF-Q));
396                 R:=KINTO-KINTR+1;
397                 NO:=KF*KF-Q*Q;   N21=NO*NO;   N3:=N2*NO;
398                 K2:=KF*KF;  K3:=K2*KF;   K4:=K2*K2;
399                 "FOR"G:=0"STEP"1"UNTIL"R+1"DO"
400                 "BEGIN"KINT:=KINTO-G;
401                         Z[G]:=KINT*KINT/100;
402                         H[G]:=BLAL  3,N1,KINT]*(FLA[KINT]+VA);
```

```
403                 "END";
404                 "FOR"G:=1"STEP"1"UNTIL"R"DO"
405                 "IF"ABS(KF-SQRT(Z[G]))<0.00001"THEN"
406                 "BEGIN"Z[G]:=0.9*Z[G]+0.1*Z[G+1];
407                       H[G]:=0.9*H[G]+0.1*H[G+1];
408                 "END";
409                 "FOR"G:=G"STEP"1"UNTIL"R"DO"
410                 "BEGIN"B1:=(H[G]-H[G+1])/(Z[G]-Z[G+1]);
411                       A:=H3*(H[G]-B1*Z[G]);
412                       B:=3*N2*(H[G]-B1*Z[G])+N3*B1;
413                       C:=3*N0*(H[G]-B1*Z[G])+3*N2*B1;
414                       D:=H[G]-B1*Z[G]+3*N0*P1;
415                       E:=B1;
416                       L[G]:=-2*A/K2;
417                       M[G]:=A/K3+D/KF+C*KF+D*K3+E*K2*K3;
418                       N[G]:=-2*C-2*D*K2-2*E*K4;
419                       P[G]:=-2*D/3-2*E*K2/3;
420                      Q[G]:=-2*E/5;
421                 "END";
422                 RTI:=0;
423                 "IF"K>1"THEN"
424                 "FOR"G:=1"STEP"1"UNTIL"K-1"DO"
425                 "BEGIN"SZ:=SQRT(ABS(Z[G])); SZ1:=SQRT(ABS(Z[G+1]));
426                       A:=IG(G,SZ);
427                       B:=IG(G,SZ1);
428                       RTI:=RTI+B-A;
429                 "END";
430                 "IF"K>0"THEN"
431                 "BEGIN"SZ:=KF+0;      SZ1:=SQRT(ABS(Z[1]));
432                       A:=IG(0,SZ);
433                       B:=IG(0,SZ1);
434                       RTI:=RTI+B-A;
435                       SZ:=SQRT(ABS(Z[P])); SZ1:=ABS(KF-Q);
436                       A:=IG(P,SZ);
437                       B:=IG(P,SZ1);
438                       RTI:=RTI+B-A;
439                 "END"
440                 "ELSE"
441                 "BEGIN"SZ:=KF+0;      SZ1:=ABS(KF-Q);
442                       A:=IG(0,SZ);
443                       B:=IG(0,SZ1);
444                       RTI:=B-A;
445                 "END";
446                 G3:=RTI=3*C1(N1,3)/2)
447           "END"OF PROCEDUREG3;
448                 RTI:=0;
449                 "FOR"N:=1"STEP"1"UNTIL"NMAX"DO"
450                 "BEGIN"SAVELINE(1);KEEPOINT(5);PREFIX('S2');
451                       RTL:=CO(N,0)*PLL(N,0,KF)/(4*PI);
452                       "PRINT"'L'  RTL =',RTL;
453                       "IF"LMAX[N]>0"THEN"
454                       RTL:=RTL+C1(N,1)*PLL(N,1,KF)*3/(4*PI);
455                       "PRINT"RTL;
456                       "IF"LMAX[N]>1"THEN"
457                       RTL:=RTL+C2(N)*PLL(N,2,KF)*5/(4*PI);
458                       "PRINT"RTL;
459                       "IF"LMAX[N]>2"THEN"
460                       RTL:=RTL+C3(N)*PLL(N,3,KF)*7/(4*PI);
461                       "PRINT"RTL;
462                       RTN:=RTN+RTL;
```

```
403                 "END";
404               PP:=RTN;
405           "END"OF PROCEDURE PP;


&UNLIST;


&ASSIGN:1;DC16;GRAPH2,P1/M071/;



&LIST;
      "READ"COM,'C,'MAX;
693         "FOR"N:=1"STEP"1"UNTIL"MAX"DO""READ"LMAX[N];
694         "FOR"N:=1"STEP"1"UNTIL"MAX"DO"
695         "BEGIN""READ"L,'NRADEL,N]; "PRINT"'/L'',SAMELINE,N,L,NRADEL,N];
696               "FOR"RAD:=0"STEP"1"UNTIL"NRADEL,N]-1"DO"
697               "BEGIN""READ"PEL,N,RAD];
698                     "PRINT"SAMELINE,FREEPOINT(5),'  ',PEL,N,RAD];
699               "END";
700               "FOR"KF:=0"STEP"0,1"UNTIL"12,5"DO"
701               "BEGIN"KINT:=ENTIER(10*(KF+0,0001));
702                     BLACL,N,KINT]:=BLL(N,L,KF);
703               "END";
704         "END";
705         "FOR"N:=1"STEP"1"UNTIL"NMAX"DO"
706         "BEGIN""PRINT"'/L'N=',SAMELINE,N;
707               "FOR"L:=0"STEP"1"UNTIL"LMAX[N]"DO"
708               "BEGIN""PRINT"'/L'L = ',SAMELINE,L;
709                     "FOR"KINT:=0"STEP"1"UNTIL"125"DO"
710                     "PRINT"SAMELINE,FREEPOINT(4),'  ',BLACL,N,KINT];
711               "END";
712         "END";
713         "READ"KF,OMEGA,META;          PI:=3,14159;
714         "PRINT"'/L'',SAMELINE,FREEPOINT(4),'KF = ',KF,'  OMEGA=',
715               OMEGA,'  META=',META;
716         "COMMENT"  THE LOCAL PART OF THE PSEUDOPOTENTIAL IS NOW READ
717                  IN FOR EACH ELEMENT TOGETHER WITH THE MODEL POTENTIAL
718           PARAMETERS TO CALC THE NON LOCAL PART;
719         UI:=1;
720         "REC"U"   SAMELINE,FREEPOINT(5)];
721         "READ"CTL U];
722        "IF"CTL[U]<0"THEN""BEGIN""PRINT"'/INSUFFICIENT DATA';
723                           "GOTO"FIN;
724                     "END";
725         "IF"CTL[U]>60"THEN""BEGIN""PRINT"'/TOO MANY POINTS';
726                           "GOTO"FIN;
727                     "END";
728               "FOR"NI:="STEP"1"UNTIL"OTC[U]"DO"
729            "BEGIN""READ"XTEN,U],FTEN,U]; FTEN,U]:=FTEN,U]*3/(KF*KF);
730            "END";"PRINT"'/L''S10'   0        W    IN HA';
731               "PRINT"'/L'ELEMENT',U;
732               "FOR"I:=1"STEP"1"UNTIL"OTC[U]"DO"
733                  "PRINT"'/L'',SAMELINE,FREEPOINT(4),''S10'',XTEN,U],
734                        FTEN,U],FTEN,U]*KF*KF/3;
735         XMAX[U]:=XTEOTC[U],U];
```

```
736                 "FOR"N1:=1"STEP"1"UNTIL"QT[U]-1"DO"
737                    F1[N,U]:=(FT[N,U]-FT[N+1,U])/(XT[N,U]-XT[N+1,U]);
738                 "FOR"N1:=1"STEP"1"UNTIL"QT[U]-2"DO"
739                    F2[N,U]:=(F1[N,U]-F1[N+1,U])/(XT[N,U]-XT[N+2,U]);
740                 "FOR"N1:=1"STEP"1"UNTIL"QT[U]-3"DO"
741                    F3[N,U]:=(F2[N,U]-F2[N+1,U])/(XT[N,U]-XT[N+3,U]);
742                 "READ"LO[U],Z;
743                 "PRINT"/,'LO =',LO[U],'  Z = ',Z,'
744                      MODEL POT PARAMETERS =';
745                 "IF"LO[U]=1"THEN""GOTO" L01;
746                 "IF"LO[U]=2"THEN""GOTO"L02;
747                 "IF"LO[U]=3"THEN""GOTO"L03;
748           L00:  "READ"AA0[U],ADA0[U];
749                 "PRINT"AA0[U],ADA0[U];
750                 "GOTO"ENDLO;
751           L01:  "READ"AA0[U],AA1[U],ADA0[U],ADA1[U];
752                 "PRINT"AA0[U],AA1[U],ADA0[U],ADA1[U];
753                 "GOTO"ENDLO;
754           L02:  "READ"AA0[U],AA1[U],AA2[U],ADA0[U],ADA1[U],ADA2[U];
755                 "PRINT"AA0[U],AA1[U],AA2[U],ADA0[U],ADA1[U],ADA2[U];
756                 "GOTO"ENDLO;
757           L03:  "READ"AA0[U],AA1[U],AA2[U],ADA0[U],ADA1[U],ADA2[U],AP2[U];
758                 "PRINT"AA0[U],AA1[U],AA2[U],ADA0[U],ADA1[U],ADA2[U],AP2[U];
759           ENDLO;
760           "END";
761           VAL:=OMEGA*KF*3/(3*PI*PI);
762           WI:=0.5161/KF;
763           PS:=0;          GM:=0;
764                 H[1]:=H[2]:=0.05;H[2]:=H[0]:=0.025;H[3]:=H[8]:=0.01;
765                 H[4]:=H[7]:=0.00475;H[5]:=H[6]:=0.00045;H[11]:=0.10;
766                 AJ[1]:=0.05;AJ[2]:=0.5;AJ[3]:=0.9;AJ[4]:=0.98;
767                 AJ[5]:=0.999;AJ[6]:=1.001;AJ[7]:=1.001; AJ[8]:=1.02;
768                 AJ[9]:=1.40;AJ[10]:=2.5;AJ[11]:=3.40;
769                 NJ[1]:=9;NJ[2]:=16;NJ[3]:=8;NJ[4]:=NJ[7]:=4;
770                 NJ[5]:=NJ[6]:=2;NJ[8]:=32;NJ[9]:=44;NJ[10]:=18;NJ[11]:=26;
771           "COMMENT"PROGRAMME NOW ENTERS Q LOOP,INTEGRATION MESH
772                 FINEST CLOSE TO SINGULARITY(Q=2*KF);
773                 "FOR"T:=1"STEP"1"UNTIL"11"DO"
774                 "BEGIN"NJ1:=NJ[T]+1;
775                       H3:=H[T]/3;
776                       "FOR"N1:=1"STEP"1"UNTIL"NJ1"DO"
777                       "BEGIN"X:=AJ[T]+(N-1)*H[T];
778                             Q:=X*2*KF;
779                             FL:=LN(ABS( (1-X)/(1+X)));
780                             SIG:=((1R*Q)*BETA*VAL)*(1/3))/KF;
781                             STR:=S(Q*SIG,BETA);
782                             WA:=2*W(X,3);
783                            GS:=-PP(Q)*2*STR/OMEGA;
784                             GN:=GN+1;
785                             GXEGN]:=X;
786                             GYLGN]:=GS;
787                             "COMMENT"INTEGRATION OF
788                                   INTEGRANDS OVER Q WILL NOW BE DONE
789                             USING SIMPSON'S RULE;
790                             "IF"N=1"THEN""GOTO"FIRSTANDLAST;
791                             "IF"N=NJ1"THEN""GOTO"FIRSTANDLAST;
792                             "IF"N-ENTIER(N/2)*2=0"THEN""GOTO"EVEN"ELSE"
793                             "GOTO"ODD;
794                       FIRSTANDLAST; PS:=PS+H3*GS;  PST:=PS;
795                             "GOTO"EXIT;
```

```
796                         EVEN:  PS:=PS+4+H3+PS;
797                                "GOTO"EXIT;
798                         ODD:   PS:=PS+2+H3+PS;
799                         EXIT:PT:=PST;
800                         "END";
801                   "END"OF D LOOP;
802           CONTINUE:D:=PT;
803           I:=1; "READ"INSTRING(TITLE,I);
804           I:=1;
805       "BEGIN"SAMELINE;
806           "PRINT"('L4'FIRST ORDER CORRECTION TO NORMALISATION FOR',
807           OUTSTRING(TITLE,I));
808           "PRINT"(=',FREEPOINT(4),DN;
809       "END";
810           GRAPH2(GX,GY,GN,TITLE,30,0,10,0,1,1);
811    FIN;
812    "END";
  1312     HC
  7112   CODE
  6424  TOTAL


&END;
```

Appendix D

Numerical Results

This appendix contains the calculated results for the contact density, $\mathcal{P}_F$, Knight Shift, K, and the change of these quantities relative to their values in the pure metal, $\frac{\Delta\mathcal{P}_F}{\mathcal{P}_F}$ and $\frac{\Delta K}{K}$, for a number of alloys. In all cases the calculations refer to the Knight shift of the first named element.

The columns labelled OPW give the results of single OPW calculations and others contain first order perturbations using the Ashcroft Model Potential (labelled ASHCROFT POT.), the optimised model potential (labelled OMP), or the optimised model potential used in the local approximation, (labelled OMP LOCAL) as discussed in Chapter 5. Ashcroft and Lekner structure factors are used thoughout except where the column is labelled EXPT. STR. Here the experimental structure factors described in Sec.5.2.1. are used. Table D.2. is an exception as $\mathcal{P}_F$ was obtained from Perdew and Wilkins (ref.1. Chap 5). The values of the spin susceptibility, χ, are a linear interpolation of the best values for the pure metals, as discussed in Section 5.1.4. in all tables.

Alloy Conc.	χ x 10^6	OPW		OMP:		OMP: EXPT.STR.	
		$\mathcal{P}_F$	$\Delta K/K$	$\mathcal{P}_F$	$\Delta K/K$	$\mathcal{P}_F$	$\Delta K/K$
Na-K							
100 0	1.056	152.4		133.8		141.6	
80 20	1.020	160.4	0.017	159.5	0.151	168.7	0.151
60 40	0.983	166.7	0.018	183.1	0.273	195.3	0.284
40 60	0.947	171.8	0.011	205.4	0.377	220.8	0.399
20 80	0.910	176.0	-0.004	226.5	0.460	244.3	0.487
Na-Rb							
100 0	1.056	152.4		133.8		141.6	
80 20	1.011	165.0	0.037	170.9	0.223	177.9	0.202
60 40	0.965	174.3	0.045	207.3	0.415	215.9	0.393
40 60	0.920	181.3	0.037	241.4	0.570	250.8	0.543
20 80	0.874	186.8	0.015	272.3	0.684	278.0	0.625
Na-Cs							
100 0	1.056	152.4		133.8		141.6	
80 20	1.000	172.8	0.074	192.0	0.359	195.2	0.305
60 40	0.944	186.2	0.093	250.0	0.670	252.6	0.595
40 60	0.888	192.7	0.063	302.5	0.910	304.5	0.809
20 80	0.832	202.6	0.048	350.5	1.071	348.3	0.938
K-Na							
100 0	0.874	441.1		451.6		488.2	
80 20	0.910	427.7	0.010	419.2	-0.033	453.5	-0.032
60 40	0.947	411.9	0.012	386.5	-0.073	415.3	-0.078
40 60	0.983	393.3	0.002	352.9	-0.121	374.4	-0.138
20 80	1.020	370.7	-0.019	318.2	-0.178	333.1	-0.204
Rb-Na							
100 0	0.829	803.4		848.3		847.4	
80 20	0.874	768.0	0.008	795.0	-0.049	987.7	-0.020
60 40	0.920	725.0	0.002	680.7	-0.109	712.5	-0.067
40 60	0.965	672.3	-0.026	596.7	-0.181	621.2	-0.147
20 80	1.011	606.3	-0.080	510.2	-0.266	524.6	-0.244

Table D.1. Calculations of Relative Change of Knight Shift in Alkali Metal Alloys.

Alloy Conc.	ΩP_F	$\chi \times 10^6$	$\frac{\Delta K}{K}$
Na-K			
100 0	102.0	1.056	
72 28	125.9	1.005	0.174
16 84	170.6	0.903	0.431
Na-Rb			
100 0	102.0	1.056	
58 42	159.5	0.961	0.423
30 70	195.1	0.897	0.625
2 98	227.8	0.833	0.762
K-Na			
100 0	261.9	0.874	
90 10	250.9	0.892	-0.022
40 60	197.6	0.983	-0.157
Rb-Na			
100 0	775.0	0.829	
96 4	758.5	0.838	-0.008
44 56	580.1	0.956	-0.198
Na-Cs			
100 0	102.0	1.056	
92 8	118.6	1.033	0.137
30 70	277.7	0.850	0.876

Table D.2. Relative Change of Knight Shift in Alkali Metal Alloys using Calculations by Perdew and Wilkins.

ALLOY	$\frac{\Delta x}{x}$	OPW		ASHCROFT POT.		OMP: LOCAL		OMP	
		$\Delta\wp_F/\wp_F$	$\Delta K/K$	$\Delta\wp_F/\wp_F$	$\Delta K/K$	$\Delta\wp_F/\wp_F$	$\Delta K/K$	$\Delta\wp_F/\wp_F$	$\Delta K/K$
Cd-Zn									
20	0.022	-.034	-.012	-.044	-.022	-.085	-.063	-.066	-.044
40	0.044	-.072	-.028	-.084	-.040	-.167	-.123	-.130	-.086
60	0.065	-.114	-.049	-.119	-.054	-.244	-.179	-.195	-.130
80	0.087	-.160	-.073	-.148	-.061	-.318	-.231	-.264	-.177
Cd-In									
20	0.012	-.032	-.020	0.036	0.048	0.017	0.039	-.017	-.005
40	0.024	-.062	-.038	0.056	0.080	0.020	0.044	-.047	-.023
60	0.035	-.093	-.058	0.062	0.097	0.012	0.047	-.082	-.047
80	0.047	-.123	-.076	0.051	0.098	-.002	0.045	-.123	-.076
Cd-Sn									
20	0.026	-.052	-.026	0.058	0.084	-.003	0.023	-.049	-.023
40	0.053	-.104	-.051	0.060	0.113	-.020	0.033	-.107	-.054
60	0.079	-.157	-.078	0.020	0.099	-.044	0.035	-.170	-.091
80	0.105	-.213	-.108	-.037	0.068	-.090	0.015	-.241	-.136
Cd-Hg									
20	-.004	0.019	0.015	0.191	0.187	0.074	0.070	0.095	0.091
40	-.009	0.036	0.027	0.400	0.391	0.147	0.138	0.193	0.184
60	-.013	0.056	0.043	0.629	0.616	0.223	0.210	0.294	0.281
80	-.017	0.070	0.053	0.879	0.862	0.299	0.282	0.398	0.381
Cd-Tℓ									
20	0.007	-.018	-.011			0.061	0.068	0.031	0.038
40	0.015	-.035	-.020			0.094	0.109	0.043	0.058
60	0.022	-.052	-.030			0.123	0.145	0.041	0.063
80	0.029	-.069	-.040			0.134	0.163	0.027	0.056
Cd-Pb									
20	0.021	-.041	-.020	0.050	0.071	0.043	0.064	0.017	0.038
40	0.043	-.081	-.038	0.068	0.111	0.060	0.103	0.000	0.043
60	0.064	-.120	-.056	0.054	0.108	0.052	0.116	-.039	0.025
80	0.086	-.161	-.075	0.017	0.103	0.028	0.114	-.094	-.008
Cd-Bi									
20	0.026	-.057	-.031	0.072	0.098	0.197	0.223	0.103	0.129
40	0.052	-.112	-.060	0.060	0.112	0.120	0.172	0.011	0.063
60	0.078	-.167	-.089	-.014	0.064	0.010	0.088	-.141	-.063
80	0.104	-.224	-.120	-.116	0.012	-.079	0.025	-.254	-.150

Table D.3. Calculations of the Cadmium Knight Shifts in Alloys.

ALLOY	$\frac{\Delta x}{x}$	OPW		ASHCROFT POT.		OMP: LOCAL		OMP	
		$\Delta\Omega P_F/\Omega P_F$	$\Delta K/K$	$\Delta\Omega P_F/\Omega P_F$	$\Delta K/K$	$\Delta\Omega P_F/\Omega P_F$	$\Delta K/K$	$\Delta\Omega P_F/\Omega P_F$	$\Delta K/K$
In-Ga									
20	0.018	-.034	-.016	-.048	-.030	-.059	-.041	-.069	-.051
40	0.036	-.071	-.035	-.091	-.055	-.134	-.098	-.155	-.119
60	0.054	-.111	-.067	-.125	-.071	-.194	-.140	-.225	-.171
80	0.073	-.156	-.083	-.153	-.080	-.251	-.179	-.292	-.219
In-Cd									
20	-.011	0.033	0.022	0.024	0.013	0.039	0.025	0.062	0.051
40	-.022	0.067	0.045	0.038	0.016	0.068	0.046	0.125	0.103
60	-.033	0.101	0.068	0.037	0.004	0.096	0.063	0.186	0.153
80	-.045	0.135	0.090	0.019	-.026	0.115	0.090	0.241	0.196
In-Sn									
20	0.014	-.024	-.010	-.026	-.012	-.042	-.028	-.053	-.039
40	0.027	-.049	-.022	-.057	-.030	-.078	-.051	-.102	-.075
60	0.041	-.075	-.034	-.092	-.051	-.110	-.069	-.145	-.104
80	0.055	-.102	-.047	-.127	-.072	-.140	-.085	-.185	-.130
In-Hg									
20	-.016	0.054	0.038	0.098	0.082	0.092	0.076	0.139	0.123
40	-.033	0.107	0.074	0.237	0.204	0.196	0.163	0.304	0.271
60	-.049	0.160	0.111	0.428	0.379	0.308	0.259	0.495	0.446
80	-.066	0.214	0.148	0.686	0.620	0.432	0.366	0.711	0.645
In-Tℓ									
20	-.004	0.016	0.012			0.037	0.033	0.046	0.042
40	-.009	0.031	0.022			0.074	0.065	0.092	0.083
60	-.013	0.047	0.034			0.113	0.100	0.141	0.128
80	-.017	0.062	0.045			0.153	0.137	0.192	0.175
In-Pb									
20	0.009	-.010	-.001	-.010	-.001	-.002	0.007	0.004	0.013
40	0.018	-.020	-.002	-.021	-.003	-.005	0.013	0.004	0.022
60	0.027	-.031	-.003	-.034	-.007	-.010	0.017	-.003	0.024
80	0.036	-.043	-.007	-.050	-.014	-.019	0.017	-.015	0.021
In-Br									
20	0.013	-.027	-.014	-.034	-.021	-.042	-.029	-.060	-.057
40	0.027	-.055	-.028	-.075	-.048	-.080	-.053	-.100	-.073
60	0.040	-.084	-.044	-.132	-.092	-.116	-.076	-.166	-.126
80	0.054	-.114	-.060	-.198	-.134	-.153	-.099	-.212	-.158

Table D.4. Calculations of the Indium Knight Shifts in Alloys.

ALLOY	$\Delta\chi/\chi_o$	OPW		OMP LOCAL		OMP		OMP: EXPT.STR	
		$\Delta\Omega P_F/\Omega P_F$	$\Delta K/K$	$\Delta\Omega P_F/\Omega P_F$	$\Delta K/K$	$\Delta\Omega P_F/\Omega P_F$	$\Delta K/K$	$\Delta\Omega P_F/\Omega P_F$	$\Delta K/K$
Ga-Zn									
20	-.008	0.023	0.015	0.024	0.016	0.058	0.050	0.047	0.039
40	-.016	0.046	0.030	0.040	0.024	0.116	0.100	0.099	0.089
60	-.024	0.070	0.046	0.043	0.019	0.175	0.151	0.160	0.136
80	-.032	0.094	0.062	0.011	-.021	0.225	0.193	0.228	0.196
Ga-In									
20	-.015	0.039	0.024	0.142	0.127	0.109	0.094	0.098	0.083
40	-.031	0.074	0.043	0.295	0.264	0.222	0.191	0.204	0.173
60	-.046	0.104	0.058	0.454	0.408	0.340	0.294	0.317	0.271
80	-.062	0.132	0.070	0.675	0.617	0.496	0.434	0.471	0.409
Ga-Sn									
20	-.004	0.014	0.010	0.077	0.073	0.049	0.045	0.034	0.130
40	-.008	0.027	0.019	0.145	0.137	0.095	0.087	0.066	0.058
60	-.012	0.038	0.026	0.208	0.196	0.135	0.123	0.100	0.088
80	-.016	0.049	0.033	0.260	0.244	0.178	0.162	0.134	0.118

Table D.5. Calculations of the Gallium Knight Shift in Alloys.

Appendix E

NMR Line Width in β-Thallium

Calculations of the second moment of the ^{205}Tl resonance in β-thallium due to a) Indirect Exchange and b) Dipolar and Pseudodipolar interactions are given below.

E.1. Indirect Exchange

Bloembergen and Rowland (1) have shown that a significant contribution to the line width in α-thallium comes from an interaction whose Hamiltonian has the same form as an exchange interaction i.e.

$$\mathcal{H} = A\, \underline{I}_i \cdot \underline{I}_j \qquad (E.1)$$

where I_i and I_j are two nuclear spins, and A is a parameter describing the strength of the interaction. Such an interaction (2) gives rise to a resonance line whose second moment, M_2, is given by

$$M_2 = \tfrac{1}{3}\, I_i\, (I_i + 1) \sum_j \left(\frac{A(R_{ij})}{h} \right)^2 . \qquad (E.2)$$

I_i is the spin of the nucleus being observed, and the summation is over all unlike nuclei in the specimen. Like nuclei do not contribute to the second moment. h is Planck s constant and A is a function of R_{ij}, the separation of two nuclei i and j.

Bloembergen and Rowland show that this interaction arises from an indirect exchange between nuclei via the conduction electrons and find that A is given by

$$A(R_{ij}) = -2^{-5} \left\langle |\Delta_{ij}|^2 \right\rangle m\, \hbar^2\, \pi^{-3} \times R_{ij}^{-4} \left(\sin(2k_F R_{ij}) - 2k_F \cos(2k_F R_{ij}) \right) , \qquad (E.3)$$

where m is the electron mass, k_F is the Fermi wave vector and $\left\langle |\Delta_{ij}|^2 \right\rangle$

Appendix E

NMR Line Width in β-Thallium

Calculations of the second moment of the ^{205}Tl resonance in β-thallium due to a) Indirect Exchange and b) Dipolar and Pseudodipolar interactions are given below.

E.1. Indirect Exchange

Bloembergen and Rowland (1) have shown that a significant contribution to the line width in α-thallium comes from an interaction whose Hamiltonian has the same form as an exchange interaction i.e.

$$\mathcal{H} = A \, \underline{I}_i \underline{I}_j \qquad \text{(E.1)}$$

where I_i and I_j are two nuclear spins, and A is a parameter describing the strength of the interaction. Such an interaction (2) gives rise to a resonance line whose second moment, M_2, is given by

$$M_2 = \tfrac{1}{3} I_i (I_i + 1) \sum_j \left(\frac{A(R_{ij})}{h} \right)^2 . \qquad \text{(E.2)}$$

I_i is the spin of the nucleus being observed, and the summation is over all unlike nuclei in the specimen. Like nuclei do not contribute to the second moment. h is Planck s constant and A is a function of R_{ij}, the separation of two nuclei i and j.

Bloembergen and Rowland show that this interaction arises from an indirect exchange between nuclei via the conduction electrons and find that A is given by

$$A(R_{ij}) = -2^{-5} \left\langle |\Delta_{ij}|^2 \right\rangle m \hbar^2 \pi^{-3} \times R_{ij}^{-4} \left(\mathrm{Sin}(2k_F R_{ij}) - 2k_F \, \mathrm{Cos}(2k_F R_{ij}) \right) , \qquad \text{(E.3)}$$

where m is the electron mass, k_F is the Fermi wave vector and $\left\langle |\Delta_{ij}|^2 \right\rangle$

is a matrix element for the electron-nuclear interaction. This interaction is clearly of very short range and Bloembergen and Rowland show that the majority of the contribution to the second moment comes from nearest neighbours. They therefore calculate the value for nearest neighbours only and then add an extra 20% to account for other contributions.

In α-thallium there are 12 nearest neighbours, 6 at 3.4496Å and 6 at 3.401Å, however, for this calculation these distances are assumed to be the same and equal to their average value of 3.425Å. Thus with 12 equidistant nearest neighbours of which a proportion f are unlike nuclei, this contribution to the second moment in α-thallium is given by

$$M_2 = 4\ I(I+1)\ f\ \frac{A^2}{\hbar^2} \quad . \tag{E.4}$$

Bloembergen and Rowland find that a value of $\frac{A}{\hbar}$ = 17kHz accounts for the observed second moment due to this interaction and that it corresponds to a realistic value for the matrix element in eq. E.3.

In β-thallium the situation cannot be simplified in this way since there is a much greater difference in the distances of the 8 nearest neighbours at R_1 = 3.355Å and the 6 next nearest neighbours at R_2 = 3.874Å. Thus equation E.2. becomes

$$M_2 = \tfrac{1}{3}\ I(I+1)\ f\ \left(8\left(\frac{A(R_1)}{\hbar}\right)^2 + 6\left(\frac{A(R_2)}{\hbar}\right)^2\right) . \tag{E.5}$$

It is not possible to evaluate $A(R_1)$ and $A(R_2)$ accurately from first principles, because of the difficulty in evaluating $\left\langle |\Delta_{ij}|^2 \right\rangle$, however they may be found by comparison with the results of Bloembergen and Rowland since $\left\langle |\Delta_{ij}|^2 \right\rangle$ is almost entirely independent of R_{ij}.

Thus we can write

$$\frac{A(R_{ij})}{h} = K \times F(R_{ij}) \qquad (E.6)$$

where $F(R_{ij}) = R_{ij}^{-4} \left(\mathrm{Sin}(2k_F R_{ij}) - 2k_F R_{ij} \mathrm{Cos}(2k_F R_{ij})\right)$.

In α-thallium $\frac{A(R_{ij})}{h}$ = 17kHz and using $k_F = 3.17\text{Å}^{-1}$ we find that $F(R_{ij}) = 0.154\text{Å}^{-4}$,

giving $K = 110.4\text{kHz Å}^4$.

In β-thallium it is found

$$F(R_1) = 0.083\text{Å}^{-4}$$

and $F(R_2) = 0.094\text{Å}^{-4}$,

giving $\frac{A(R_1)}{h} = 9.2\text{kHz}$

and $\frac{A(R_2)}{h} = 10.4\text{kHz}$.

Thus the contribution to the second moment as given by equation E.5. is $103(\text{kHz})^2$. Following the procedure of Bloembergen and Rowland a further 20% was added to take account of any other contributions thus the final calculated second moment, due to this interaction in β-thallium is $\underline{124(\text{kHz})^2}$.

E.2. Dipolar and Pseudodipolar Interactions

Although the pseudodipolar interaction arises out of the interaction between the nuclei and the conduction electrons, as does the indirect exchange interaction, its effect is very different in that the interaction between like nuclei is more effective in broadening the line than that between unlike nuclei. In fact its effect is identical to the classical dipolar interaction which has been treated by Van Vleck (2) and these two are here treated as one interaction with Hamiltonian

$$\mathcal{H} = B\left(\underline{I}_i \cdot \underline{I}_j + \frac{(\underline{I}_i \cdot \underline{R}_{ij})(\underline{I}_j \cdot \underline{R}_{ij})}{R_{ij}^2}\right). \qquad (E.7)$$

The second moment due to this interaction is then given by

$$M_2 = I_i(I_i + 1)\left(\frac{3}{5}\sum_j \frac{B^2(R_{ij})}{h^2} + \frac{4}{5}\sum_k \frac{B^2(R_{ik})}{h^2}\right), \qquad (E.8)$$

where the sum over j refers to like nuclei and the sum over k refers to unlike nuclei.

Again this is a short range interaction and making the assumptions of the previous section for α-thallium

$$M_2 = I(I + 1)\left(\frac{16}{5}f + \frac{36}{5}(1-f)\right)\frac{B^2}{h^2}(R_{ij}). \qquad (E.9)$$

The expression for the second moment in β-thallium is thus

$$M_2 = I(I + 1)\left(\frac{4}{5}f + \frac{3}{5}(1-f)\right)\left(8\,\frac{B^2(R_1)}{h^2} + 6\,\frac{B^2(R_2)}{h^2}\right). \qquad (E.10)$$

The value of B is again very difficult to evaluate from first principles but is has an R^{-3} dependence so we can write

$$\frac{B(R_{ij})}{h} = L \times R_{ij}^{-3}.$$

For α-thallium

$$\frac{B(R_{ij})}{h} = 5.5\text{kHz},$$

and therefore $L = 221.0\text{kHz}\text{Å}^3$.

Thus in β-thallium

$$\frac{B(R_1)}{h} = 5.9\text{kHz},$$

and

$$\frac{B(R_2)}{h} = 3.8\text{kHz}.$$

Thus the second moment given by eq.E.10. is $137.2(\text{kHz})^2$ and an additional

20% for the contribution of more distant atoms gives

$$\underline{\underline{M_2 = 165(\text{kHz})^2}} \ .$$

References

1. Bloembergen N. and Rowland T.J., Phys.Rev., 97, 1679, (1955).
2. Van Vleck J.H., Phys.Rev., 74, 1168, (1948).

Appendix F

Line Shape in α-Thallium

F.1. Theory

The line shape of two theoretical curves was calculated a) for a Gaussian line broadened by an anisotropic Knight shift b) for a Lorentzian line broadened by an anisotropic Knight shift.

Thus the line shape $G(\nu)$ is given by the convolution

$$G(\nu) = \int f(\nu' - \nu)\, g(\nu')\, d\nu' \qquad \text{(F.1)}$$

where $g(\nu)$ is the anisotropic broadening shape function given by

$$g(\nu) = \left(1 + \frac{2\nu}{K'\nu_o}\right)^{-\frac{1}{2}}, \quad \frac{-K'\nu_o}{2} < \nu < K'\nu_o \qquad \text{(F.2)}$$

where K' is the anisotropic component of the Knight shift and ν_o is the resonance frequency. $f(\nu)$ is the Gaussian or Lorentzian curve. Because $g(\nu)$ only exists for finite range of ν the limits of the integration in eq.F.1. are also $\frac{-K'\nu_o}{2}$ and $K'\nu_o$ so this appears to be relatively easy to evaluate by computer. Unfortunately the integrand of equation F.1. becomes infinite at the lower limit, although the integral remains finite. To evaluate this integral by computer the following procedure was adopted. An integration was performed over 9/10 of the region of integration, omitting the final 1/10 containing the singularity, using a 10 point Simpsons rule integration. The same procedure was then performed over 9/10 of the remaining region, repeatedly until the results of the final integral was less than 1/10,000 of the total integral. This process was then repeated at 100 points around the resonance frequency in order to make up the total curve.

F.2. Computer Program

The listing of the program in section F.3 is for the Gaussian curve, however, this is the same as for the Lorentizian line except for LINE.8 which evaluates the integrand of eq.F.1.

The program has three procedures: F(x) which evaluates the integrand of eq.F.1., GG(C) which performs this integral for any point, and GRAPH 2 which controls the graph plotting and is not listed. The main program then starts at line 263 and the parameters D, the Gaussian width, VO the resonance freq and K1 the anisotropic component of the Knight shift, are read. The value of the shape function G[C] is then calculated for 100 values of the frequency Y[C] measured from the resonance centre. This resulting curve is then differentiated, by subtracting consecutive values and the array Z[C] is introduced which gives the frequencies of the differentiated points. Finally the differentiated line shape is plotted using the procedure GRAPH 2.

```
** ICL 4130 DES2 SYSTEM  :  SLAVE DIG        :  CORE 70K  :  VOL  3


&JOB:PH/R060/GT:


&TIME:10:


&ALGOL:L:
LIBRARY
ALGOL

    1   ANISOTROPIC BROADENING OF A GAUSSIAN LINE:
    2   "BEGIN""REAL"D,V:,K1:
    3         "INTEGER"I,C:
    4         "REAL""ARRAY"Y,G,N,Z[1:100]:
    5         "INTEGER""ARRAY"TITLE[1:50]:
    6         "REAL""PROCEDURE"F(X): "VALUE"X: "REAL"X:
    7         F:=EXP(-(Y[C]-X)**2/(2*D**2))/SQRT(ABS( 1+2*X /(K1*V0))):
    8         "REAL""PROCEDURE"GG(C): "VALUE"C: "INTEGER"C:
    9         "BEGIN""REAL"XX,L,DD,V,X,RT: "INTEGER"N,A:
   10               "REAL""ARRAY"FF[0:10]:
   11               D:=0:
   12                     XX:=K1*V0:       DD:=-K1*V0/2:
   13               START:N:=D+1:          XX:=XX-L:
   14               L:=(XX-DD)*.9:
   15               "FOR"A:=0"STEP"1"UNTIL"10"DO"
   16               "BEGIN"X:=XX-A*.1*L:
   17                     FF[A]:=F(X):
   18               "END":
   19               V:=(0.1*L/3)*(FF[0]+4*FF[1]+2*FF[2]+4*FF[3]+2*FF[4]
   20                           +4*FF[5]+2*FF[6]+4*FF[7]+2*FF[8]
   21                           +4*FF[9]+FF[10]):
   22               "IF"I=100"THEN""BEGIN""PRINT"'XS INT'
   23                                "GOTO"CONT:
   24                           "END":
   25               "IF"N=1"THEN""BEGIN"RT:=V:      "GOTO"START:
   26                           "END":
   27              "IF"V>RT/10000"THEN""BEGIN"RT:=RT+V:   "GOTO"START:
   28                                "END":
   29               "PRINT"'L' C=',C,'N=',N:
   30               GG:=RT:
   31         "END":


&UNLIST:


&ASSIGN:1:DC16:GRAPH2:
```

```
&LIST;
"COMMENT"  PROG PLOTS A GRAPH OF THE LINE RESULTING FROM A GAUSSIAN OF H******I
           BROADENED BY AN ANISOTROPIC KNIGHT SHIFT K1 AT FREQUENCY V
  263                INPUT; TITLE,D,V0,K1;
  264          N:=1; INSTRING(TITLE,N);
  265          SAMPLINE;FREEPOINT(5);
  266          "READ"D,V0,K1;
  267          "PRINT"'D= ',D,'KHZ   V0= ',V0,' KHZ   K1= ',K1,''L';
  268          "FOR"C:=1"STEP"1"UNTIL"100"DO"
  269          "BEGIN"Y[C]:=(C-50)*.08*D;
  270                 G[C]:=GG(C);
  271            CONT;"PRINT"G[C];
  272          "END";
  273          "FOR"C:=1"STEP"1"UNTIL"99"DO"
  274          "BEGIN"H[C]:=G[C]-G[C+1];
  275                 Z[C]:=(Y[C]+Y[C+1])/2;
  276          "END";
  277          GRAPH2(Z,H,99,TITLE,30,10,1,1);
  278
  279    "END";
    538      IC
   1322   CODE
   1860  TOTAL


 ADIAG;
DIAG
```